Exploring a novel class of fluorophores: the 2,5-dihydro-1,2,3-triazines

by

Michelle Kyne, B.Sc.

Thesis presented for the degree of Ph.D.

Submitted September 2016

Supervisor: Prof. Alan Ryder

Head of School: Prof. Paul Murphy

School of Chemistry

National University of Ireland, Galway

Glossary of Symbols and Acronyms

α	empirical parameter of solvent hydrogen-bond donor acidity (Taft and Kamlet)
β	empirical parameter of solvent hydrogen-bond acceptor basicity (Taft and Kamlet)
ε	Molar extinction coefficient/Permittivity
ε	Permittivity
η	Viscosity
θ	Rotational correlation time
ν	Wavenumber
τ	Fluorescence lifetime
φ	Quantum yield
μ	Dipole moment
a	Radius of the cavity in which the fluorophore resides
c	Speed of light in a vacuum
D	Rotational diffusion coefficient
F	Fluorescence intensity in the presence of a quenching species
F_0	Unquenched fluorescence intensity
F_D	Wavelength dependent donor emission spectrum
G	Grating factor
h	Planck's constant
I_0	Fluorescence intensity in the absence of surfactant
I_∞	Fluorescence intensity under conditions of complete micellisation
I_t	Fluorescence intensity at intermediate surfactant concentrations
$J(\lambda)$	Area of spectral overlap
K_D	Dynamic quenching constant
K_{eq}	Equilibrium binding constant
k_{nr}	Non-radiative decay rate
k_q	Bimolecular quenching constant
k_r	Radiative decay rate
K_S	Static quenching association constant
K_{SV}	Stern-Volmer quenching constant
n	Refractive index
Q	Quenching species
r	Anisotropy
R	Gas constant
r_0	Fundamental anisotropy
R_0	Förster distance in resonance energy transfer

R_{DA}	Distance between a donor and acceptor pair in resonance energy transfer
s	Ellipsoid radius
v	Speed of light in a medium other than a vacuum
V_M	Molar volume
ε_A	Extinction coefficient spectrum of the acceptor in resonance energy transfer
θ_A	Angle between the vector joining the donor and acceptor and the transition dipole of the acceptor in resonance energy transfer
θ_D	Angle between the vector joining the donor and acceptor and the transition dipole of the donor in resonance energy transfer
κ^2	Orientation factor in resonance energy transfer
μ	Ellipsoid half-length
μ_E	Dipole moment of excited state
μ_G	Dipole moment of ground state
$\bar{\nu}_A - \bar{\nu}_F$	Stokes shift
τ_0	Fluorescence lifetime in the absence of quencher
τ_D	Fluorescence lifetime of donor in the absence of acceptor in resonance energy transfer
τ_{DA}	Fluorescence lifetime of donor in the presence of acceptor in resonance energy transfer
τ_n	Natural fluorescence lifetime
ϕ	Angle between the planes
2,5-DHT	2,5-dihydro-1,2,3-triazine
2-AN	2-anilinonaphthalene
5MPE-TDT	5-methoxycarbonyl-5-(N-phenylimino(ethyl))-2,4,6-triphenyl-2,5-dihydro-1,2,3-triazine
5MPFH-TDT	5-methoxycarbonyl-5-(N-phenylformimidoyl)-2,4,6-triphenyl-2,5-dihydro-1,2,3-triazine fluorophore
AO	Atomic orbital
$AgNO_3$	Silver nitrate
BODIPY	Family of dyes based on 1,3,5,7,8-pentamethyl pyrromethene-BF_2, or 4,4-difluoro-4-bora-3a,4a-diaza-s-indacene; BODIPY is a trademark of Molecular Probes Inc.
BP	Band position
BSA	Bovine serum albumin
C_{70}	Fullerene
CFD	Constant fraction discriminator
CMC	Critical micelle concentration
CrEL	Cremophor EL
CT	Charge transfer
CTAB	Cetyltrimethylammonium bromide
DCM	Dichloromethane

DMF	Dimethylformamide
DMH	2-(2’-hydroxyphenyl)-4,6-dimethoxy-1,3,5-triazine
DMSO	Dimethyl sulfoxide
DPH	1,6-diphenyl-1,3,5-hexatriene
DS1	1,4-Bis(5,6-diphenyl-1,2,4-triazin-3-yl)benzene
DS2	1,3-Bis(5,6-diphenyl-1,2,4-triazin-3-yl)benzene
ELISA	Enzyme-linked immunosorbent assay
EM	Electromagnetic
ESIPT	Excited-state intramolecular proton transfer
EthGly	Ethylene glycol
EtOH	Ethanol
FCS	Fluorescence correlation spectroscopy
FITC	Fluorescein isothiocyanate
FMR	Fluorescent molecular rotor
FRET	Förster resonance energy transfer
HEPES	4-(2-Hydroxyethyl)piperazine-1-ethanesulfonic acid
HOMO	Highest occupied molecular orbital
HPW	High purity water
HSA	Human serum albumin
IC	Internal conversion
ISC	Intersystem crossing
LCAO	Linear combination of atomic orbitals
LE	Locally excited
LOD	Limit of detection
LUMO	Lowest unoccupied molecular orbital
MO	Molecular orbital
MOPS	3-(N-Morpholino)propanesulfonic acid
M-OH-P	2-(2’Hydroxy-4’-methoxyphenyl)-4,6-diphenyl-1,3,5-triazine
NaOH	Sodium hydroxide
ND	Neutral density
P3P	1,3-dipyrenylpropane
PF	Prompt fluorescence
Py 2	Pyridine 2
$Ru(phen)_3$	Ruthenium tris-1,10-phenanthroline
SDS	Sodium dodecyl sulfate
SEC	Size-exclusion chromatography
SMD	Single molecule detection
SR101	Sulforhodamine 101
TADF	Thermally activated delayed fluorescence
TCSPC	Time correlated single photon counting

TDT	2,4,6-triphenyl-2,5-dihydro-1,2,3-triazine
TICT	Twisted intramolecular charge-transfer
TN	2-(2’-hydroxyphenyl)-4-(dimethylamino)-6-(4’’methylphenyl)-1,3,5-triazine
TRITC	Tetramethylrhodamine isothiocyanate

Acknowledgments

Firstly, I would like to thank my supervisor, Professor Alan Ryder, who encouraged me to undertake a doctorate when I was completing my undergraduate studies. I am very grateful for the advice and knowledge he provided throughout my Ph.D. and for his patience and enthusiasm. I have thoroughly enjoyed being part of his research group in the NBL.

Likewise, I have really enjoyed being part of the Chemistry department in NUIG for the past several years. Thanks to the lecturers and technical staff for helping when possible and the departmental secretaries, Karen and Judy, for the advice and chat. The many hours spent as a TA in labs were made shorter by the help offered and the friendly atmosphere. Getting to know all of the postgrads, who have come and gone during my time here, has been one of the best things about doing a Ph.D. in Galway. I'm so happy to have been part of such a funny, interesting, curious, and always awesome group of people! In particular I want to mention the members of my research group who were always there for countless chats over teas and coffees: Bridget, Cheryl, Amandine, Michelle, Boyan, Valerie, Przemyslaw, Yannick, Camila, Dzmitry, Augusto, Stephen, Ana, Kevin, Marina, Radu, and Muhammad. Thanks for being such great friends and work mates!

Thank you to my family, in particular my parents, Michael and Mai, for being a constant source of support and patience. I'm so lucky to have such amazing people as parents and I hope I turn out half as well someday. And to Gillian and Kathryn, I'm so grateful to have two older sisters to look up to. Thanks for all the conversations and debates – I hope we continue to challenge each other! I also want to mention some of my friends who have been there even when I wasn't much fun to be around! Maebh, Brian, Emma, and Dave, thanks for the many chats, laughs, craic and support. And to Sandra, Michelle, Rachel, Siobhán and Fiona, thanks for being there always.

Finally I'd like to acknowledge that this work was funded by the Irish Research Council.

Table of Contents

Abstract

The 1,2,3-triazines, also known as the v-triazines, are the least studied of the three classes of triazine. This is due to the ring's lower stability and more limited synthetic routes. A new class of fluorophores, based on a 1,2,3-triazine core with substituted aryl groups, has been synthesized [1]. Here we study the photophysical behaviour of one derivative, 5-methoxycarbonyl-5-(N-phenylformimidoyl)-2,4,6-triphenyl-2,5-dihydro-1,2,3-triazine (5MPFH-TDT). In most solvents, 5MPFH-TDT has a strong absorbance band at 310 nm (S_2 excitation) with a weaker band at ~400 nm associated with excitation into S_1. 5MPFH-TDT fluorescence is complex with three distinct emission bands centred at 520 nm when excited at 405 nm. These three fluorescence emission bands are a consequence of three conformers (g0, g1, and g2) that are vibrationally accessible. Inter-conversion between these conformers occurs in the excited state. The shape and position of these three emission bands have been shown to be fairly constant and no strong solvatochromism is observed for a wide range of organic solvents [2].

However, 5MPFH-TDT is very hydrophobic and has a high tendency to aggregate in aqueous solutions, which is problematic as we are exploring the use of 5MPFH-TDT as a protein label. To improve solubility in aqueous solutions we studied the use of a range of non-ionic, anionic, and cationic surfactants to solubilize 5MPFH-TDT. 5MPFH-TDT emission properties in the various micelles were studied in detail as a simple model for its behaviour in protein solutions. Its steady-state fluorescence emission was found to be very stable in all non-ionic and cationic surfactant solutions above the critical micelle concentration (CMC). Though the shape of each fluorescence emission band changed very little, the fluorescence intensity increased and the three fluorescence emission bands were slightly blue-shifted with higher surfactant concentration. The fluorescence anisotropy and fluorescence lifetime also increased significantly with increasing surfactant concentration indicating that the fluorophore had been incorporated within the micelle. Conversely, 5MPFH-TDT fluorescence was found to be quenched in anionic surfactants.

The hydrophobic effect seems to be the driving force behind the interaction between the triazine and the micelles and the strength of this interaction was found to be comparable with some much smaller, planar fluorophores. The strong interaction

between 5MPFH-TDT and the micelle aggregates meant it was a suitable fluorophore for the estimation of micelle size. 5MPFH-TDT and SR101 were used as a FRET pair for the estimation of the size of CTAB micelles and the donor-acceptor distance calculated corresponded closely to the radius of a CTAB micelle. The quenching effect of SR101 on 5MPFH-TDT fluorescence was modelled by a Perrin plot indicated that a quenching "sphere-of-action" was in operation.

Since 5MPFH-TDT interacted quite strongly with micelles it seemed likely that it would also interact well with BSA. A clear blue shift and high fluorescence anisotropy marked the interaction between fluorophore and protein. A BSA–5MPFH-TDT binding stoichiometry of 2:1 was determined from a Job plot analysis, suggesting that the triazine was initiating the formation of BSA dimers by conferring a greater degree of hydrophobicity to the protein surface. However, the rotational correlation time of the triazine (15.51 (±7.07%) ns) was considerably less than the value reported in the literature for BSA [3] indicating that the mobility of the triazine, as part of the BSA–5MPFH-TDT complex, was not overly restricted. The location of 5MPFH-TDT on the protein surface would explain the greater level of mobility indicated by the rotational correlation time calculated.

1 Introduction

1.1 Molecular orbitals and electronic transitions

Since the 1980s fluorescence spectroscopy has become a widely used analytical technique in a broad range of research and industrial applications, including; medical diagnostics, environmental analysis, and bioprocess quality control. Its high-sensitivity, non-destructive nature, and ease of implementation are some of the qualities that make fluorescence based analytical methodologies so appealing. The phenomenon of fluorescence can be ascribed to the organisation of a molecule's molecular orbitals and its electronic arrangement therein. An understanding of molecular orbital theory provides an initial foothold for the subject of fluorescence.

Molecular orbital theory was developed in the 1920s to explain the formation of electron-deficient compounds and to account for paramagnetic behaviour in compounds whose Lewis model would suggest diamagnetism [4]. Molecular orbitals, (MOs), are formed by the interaction of atomic orbitals (AOs) irrespective of the absence or presence of electrons. Therefore, according to MO theory, a molecular orbital defines a region of space that may be, but is not necessarily, occupied by up to two electrons [4]. The approximate shape of an MO wave function may be simply approximated (using the Schrodinger equation and other equations therein) by considering it to be the sum of the AO wave functions from which it is derived. One method is to consider a MO as a linear combination of atomic orbitals (LCAO).

A number of different types of MOs exist. A σ-orbital is formed when two s-orbitals, an s- and a p-orbital, or two p-orbitals, with a collinear axis of symmetry, overlap. The bond formed in this way is called a σ-bond. On the formation of a σ-orbital, an antibonding σ-orbital, σ^*, is also produced. This occurs along the nodal plane between the two atoms. Any electron located here has a higher energy than when located on the isolated atom. When two p-orbitals overlap in a 'side-on' conformation a π-orbital results and the atoms are said to be π-bonded. Once again, the formation of a π-orbital is coupled with the formation of an antibonding π-orbital, π^*, of higher energy. Heteroatoms may possess non-bonding electrons that exist in an

n-orbital [4, 5]. The energetic order of the transitions between these orbitals generally follows the pattern below:

$$n \rightarrow \pi^* < \pi \rightarrow \pi^* < n \rightarrow \sigma^* < \sigma \rightarrow \pi^* < \sigma \rightarrow \sigma^*$$

Hybrid MOs occur when the net energy change following bond formation is less than that achieved with non-hybridised orbitals. Hybrid orbitals of a particular energy level are identical to one another and the number of hybrid MOs is always the same as the number of original AOs. An sp^3 hybridised system consists of four identical MOs, which are a combination of one s-orbital and three p-orbitals. The delocalised electron cloud of a benzene molecule is a consequence of resonance structures of an sp^2 hybridised system. Three identical sp^2 orbitals form σ-bonds while the non-hybridised p-orbital forms a π-bond. These π-bonded electrons are described as two double donut-shaped clouds above and below the plane of the ring. An sp hybridised system results in a triply bonded species, *e.g.* ethyne [4].

The two most important MOs that are considered in absorption and fluorescence spectroscopy are the lowest unoccupied molecular orbital (LUMO) and the highest occupied molecular orbital (HOMO), both of which refer to the electronic arrangement of the ground state molecule. An electronic transition occurs when an electron in a ground state orbital is promoted to an excited state orbital by absorbing the correct quantity of energy. In the case of a photon of light, the energy of the photon absorbed corresponds to the difference in energy between the two states:

$$\boldsymbol{E = hf = E_e - E_g} \qquad \textbf{Equation 1}$$

where h is Planck's constant, f is the frequency of the photon of light, E_e is the energy of the excited state, and E_g is the energy of the ground state. In quantum chemistry, the multiplicity of an excited state refers to the number of electronic spin configurations that contribute to its wavefunction. It is determined using the equation, $2S + 1$, where S is the total spin quantum number [5]. When an electron is promoted to an MO of higher energy it generally retains its spin quantum number. In this case the transition occurs between two singlet states. A singlet state has a multiplicity of one, and arises when the electron in the excited orbital is paired (of opposite spin) to the electron in the ground state orbital. However, the spin state of the electron can change in the excited state to produce a triplet state.

There are two main selection rules that govern electronic transitions. Firstly, transitions between states of different multiplicity are forbidden. But since there is a weak interaction between the wavefunctions of different multiplicities, due to spin-orbit coupling (the interaction of the electron's spin magnetic moment with the magnetic moment due to the orbital motion of the electron [6]), these transitions may be observed. Secondly, the symmetry of the electronic wave function must change for a transition to be possible. However, since molecular vibrations result in a deviation from perfect symmetry, these transitions can sometimes occur [5].

1.2 Fundamental characteristics of fluorescence emission

"Luminescence is the spontaneous emission of radiation from an electronically or vibrationally excited species not in thermal equilibrium with its environment" [6]. Fluorescence and phosphorescence are particular cases of luminescence that may occur following the absorption of a photon of energy. Fluorescence emission is observed if the transition occurs between states of the same multiplicity. This is a quantum mechanically allowed transition, as it obeys the selection rules that govern electronic transitions, and occurs on a typical timescale of 10^{-10}–10^{-7} s. Phosphorescence is observed if the transition occurs between states of different multiplicity. Phosphorescence has a much longer timescale than fluorescence (10^{-6}–1 s) as it is quantum mechanically forbidden. These radiative transitions compete with various non-radiative transitions such as internal conversion (10^{-11}–10^{-9} s) and intersystem crossing (10^{-10}–10^{-8} s). The Jabłoński diagram (Figure 1), named after the Polish scientist Alexander Jabłoński, is a useful way in which to represent a number of processes that occur as a result of the absorption of light of a particular energy [7].

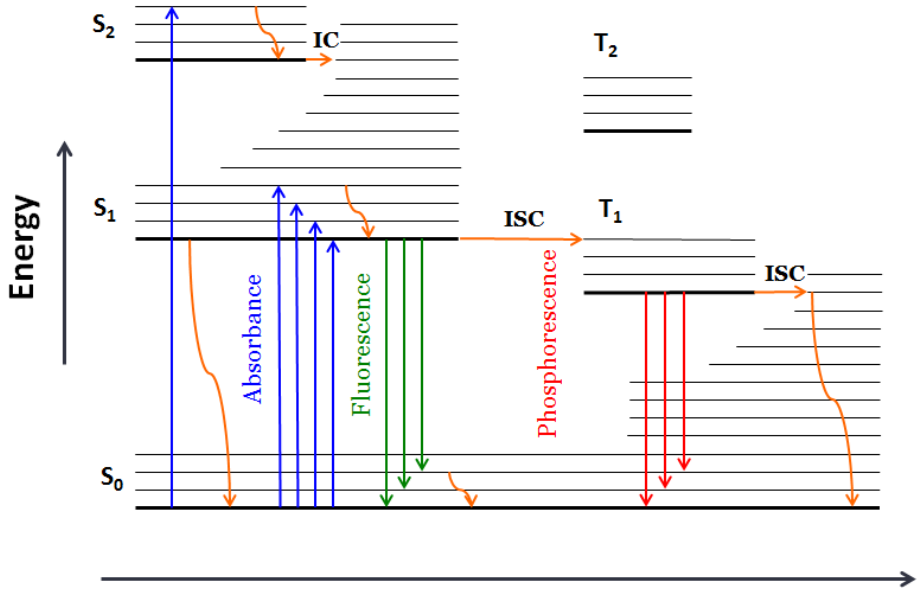

Figure 1: One form of a Jabłoński diagram. Radiative transitions of absorption, fluorescence, and phosphorescence are depicted as well as non-radiative transitions of internal conversion (IC) and intersystem crossing (ISC). Image reproduced with permission from reference [8].

A redistribution of electronic charge generally accompanies an electronic transition in a molecule. When electronic and vibrational transitions occur simultaneously in this way they are described as vibronic transitions. These vibronic transitions follow the Franck-Condon principle, which states that the initial and final nuclear geometries of a transition must be very similar [9]. This is because the mass of the electron is so much less than that of the nuclei and during the absorbance of light, which occurs on the femtosecond timescale, the nuclei are essentially stationary. When electrons have reached their final arrangement, adjustments are made at the nuclear level. This concept can be simply illustrated using molecular potential energy curves for two electronic states of a diatomic molecule (Figure 2). The upper curve is shifted slightly to the right because excitation of electrons generally produces more antibonding character. The transition, which is depicted as a vertical line between the ground state and the excited state, occurs between the vibrational ground state and the vibrational state that it most resembles in the excited state. Therefore, the vibrational wavefunction changes minimally on going from the ground state to the excited state [10]. The similarity between the wavefunctions in the ground and excited states explains why sometimes the absorption and emission spectra of a molecule are mirror images of one another. However, deviations from the 'mirror-image' rule exist when

the excited state species differs considerably from the ground state species [7]. For example, 1-hydroxypyrene-3,6,8-trisulfonate (HPTS), only obeys this rule at a pH of 13, when its hydroxyl group is ionised in the ground state as well as the excited state. At low pH values this hydroxyl group is protonated in the ground state and ionised in the excited state giving rise to an emission spectrum that differs considerably from its absorption spectrum [7].

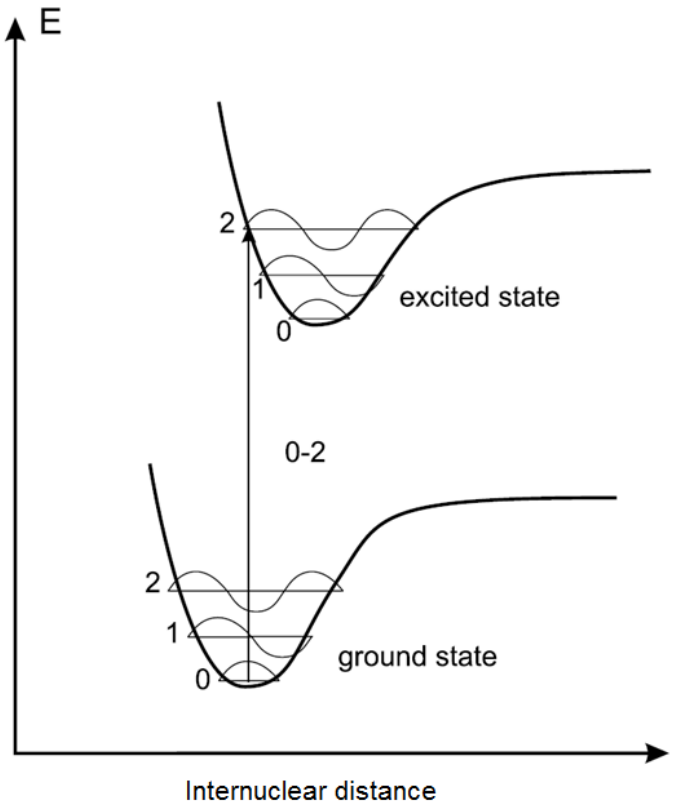

Figure 2: Molecular potential energy curves for two electronic states of a diatomic molecule. The illustration shows the transition of an electron from the lowest vibrational state of the ground state to the vibrational state that it most resembles in the excited state (Franck–Condon principle). Image reproduced with permission from reference [5].

Although the energy of the absorbed light may promote an electron to an excited vibrational state of S_1 or S_2, it is usually the transition from the lowest vibrational state of S_1 to the ground state, S_0, which gives rise to fluorescence. This is known as Kasha's rule, which states that polyatomic molecular species only exhibit luminescence with appreciable yield from the lowest vibrational state of the lowest excited state of a given multiplicity [6]. An apparent loss in energy is observed when

the energy supplied is greater than that required for the promotion of an electron to the S_1 excited state. This may be due to either vibrational relaxation or internal conversion, or a combination of the two. Both processes are faster than fluorescence, and result in the emitted photon being of lower energy and longer wavelength than that of the photon absorbed. This difference in energy is known as the Stokes shift; $\Delta\bar{\nu} = \bar{\nu}_a - \bar{\nu}_f$ [8].

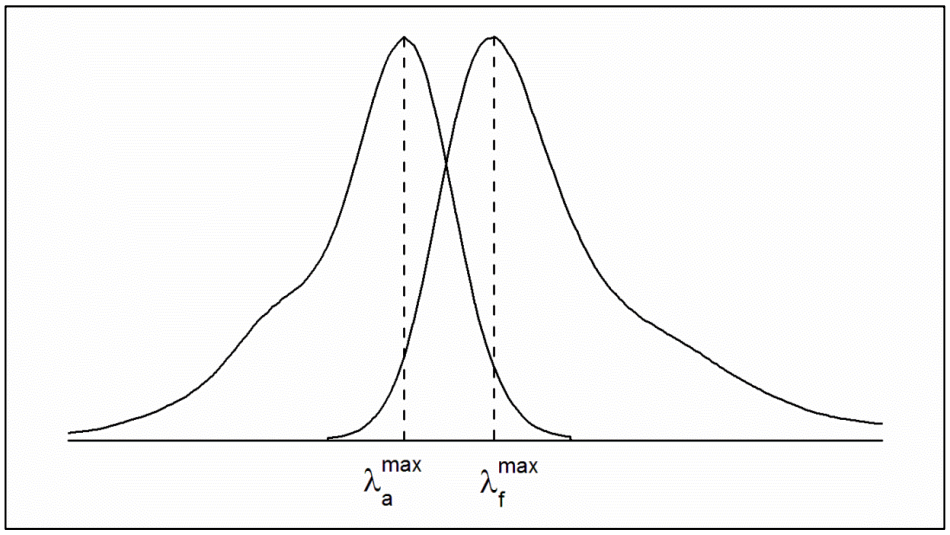

Figure 3: Graphical representation of the Stokes Shift, which is the difference between the spectral positions of the band maxima of the absorption and luminescence arising from the same electronic transition [6].

It is defined as the difference (usually in frequency units) between the spectral positions of the band maxima (or the band origin) of the absorption and luminescence arising from the same electronic transition [6]. The loss in energy is dependent upon the degree of overlap between the wavefunctions of the vibrationally excited states for the electronic states involved. A high degree of overlap leads to a high probability of a transition between states. In some instances the $S_2 \rightarrow S_1$ or $S_3 \rightarrow S_1$ energy gaps are relatively large and fluorescence may compete with the process of internal conversion. In these cases, emission spectra can result from transitions between higher singlet states and the ground state [11]. The Stokes shift may be additionally affected by factors such as solvent effects, excited-state reactions, complex formation, and/or energy transfer. Therefore, the extent of the Stokes shift can provide an insight into the molecular environment of the fluorophore.

1.3 Fluorescence parameters

The fluorescence process can be quantified and described using several important parameters. These parameters are listed and explained in the following sections.

1.3.1 Quantum yield

The quantum yield is the number of defined events occurring per photon absorbed by the system [6]. If we consider that all of the energy absorbed must revert to the ground state by radiative (k_r) or non-radiative (k_{nr}) decay the fluorescence quantum yield may be described as:

$$\varphi_F = \frac{k_r}{k_r + k_{nr}} \qquad \textbf{Equation 2}$$

1.3.2 Fluorescence lifetime

The fluorescence lifetime, τ, of a fluorophore is defined as the reciprocal of all radiative and non-radiative processes (Equation 3). It is the average time the fluorophore spends in the excited state before returning to the ground state [7]. The fluorescence lifetime also determines how far a fluorophore can diffuse in its environment before it reverts to the ground state. This may affect the number of encounters a fluorophore can have with other species during its excited state lifetime.

$$\tau = \frac{1}{k_r + k_{nr}} \qquad \textbf{Equation 3}$$

The radiative lifetime, or natural lifetime, τ_n, is the fluorescence lifetime that would be observed if de-excitation from S_1 to S_0 occurred by fluorescence emission alone [7].

$$\tau_n = \frac{1}{k_r} \qquad \textbf{Equation 4}$$

According to Strickler and Berg, the radiative decay of a fluorophore, or the reciprocal of the natural fluorescence lifetime of a fluorophore, is inversely proportional to the square of the refractive index [7, 12]. This is shown in the following equation:

$$k_r = \frac{1}{\tau_n} = 2.88 \times 10^9 n^2 \frac{\int F(\bar{\nu}) d\bar{\nu}}{\int F(\bar{\nu}) d\bar{\nu}/\bar{\nu}^3} \int \frac{\varepsilon(\bar{\nu}) d\bar{\nu}}{\bar{\nu}} \qquad \textbf{Equation 5}$$

where n is the refractive index, $F(\bar{\nu})$ is the emission spectrum plotted on the wavenumber scale, and $\varepsilon(\bar{\nu})$ is the extinction coefficient at wavenumber, $\bar{\nu}$.

1.3.3 Fluorescence anisotropy

Light is an electromagnetic (EM) wave consisting of an electric and a magnetic field that are perpendicular to one another and to the direction of propagation. For unpolarised light, these fields have no preferential direction of orientation. Linearly polarised light, however, oscillates along a defined direction. If a fluorophore is irradiated with polarised light the fluorescence emission may also be polarised. In this case the fluorescent sample is said to have a nonzero anisotropy. Anisotropy, r, occurs because fluorophores have defined transition moments for absorption and emission. When irradiated with polarised light, those fluorophores whose absorption dipole moments are orientated along the direction of polarisation are preferentially excited; this phenomenon is known as photoselection. The probability that a fluorophore will absorb a photon of light is proportional to $\cos^2\theta$, where θ is the angle the absorption dipole moment makes with the electric vector of the incident light [13]. Therefore, anisotropy is a measure of the average angular displacement of a fluorophore that occurs between absorption and emission [14].

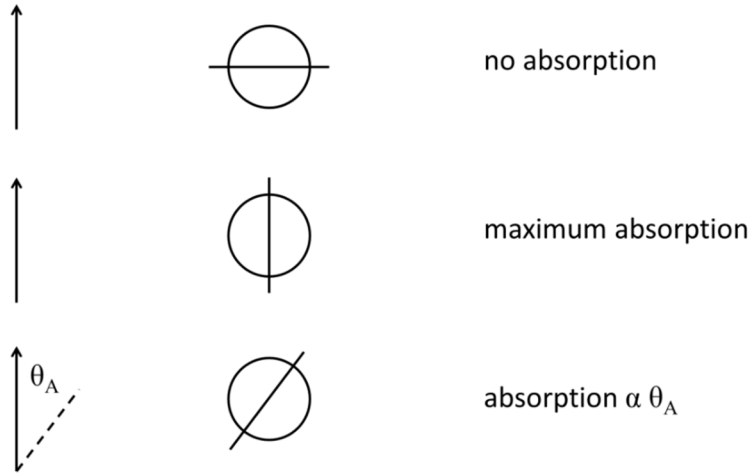

Figure 4: When a population of fluorophores is irradiated with linearly-polarised light, those fluorophores whose absorption dipole moments are aligned closely with the electric vector of the incident light are preferentially excited. This is known as photoselection. Image reproduced with permission from reference [8].

Anisotropy may also be defined as a measure of the extent of depolarisation that occurs between the absorption and emission of a photon of light. Depolarisation may occur for a number of reasons, including: non-parallel absorption and emission dipole moments; energy transfer to a molecule with a different orientation; and rotational diffusion [15]. Rotational diffusion is the most common mechanism by which the fluorescence anisotropy of a sample may be reduced (Figure 5). The rate of rotational diffusion during the lifetime of a fluorophore determines its effect on the anisotropy.

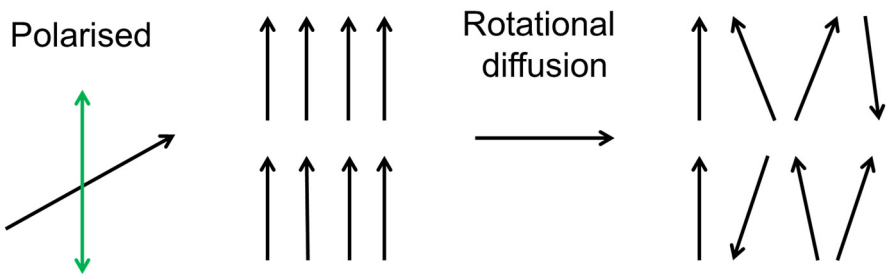

Figure 5: If a population of fluorophores, which has been selectively excited by plane-polarised light, undergoes rotational diffusion before returning to the ground state, the fluorescence emission is said to be depolarised.

Two main factors affect the rate of rotational diffusion: the size and shape of the fluorophore/macromolecule and the viscosity. Depolarisation of spherical rotors by rotational diffusion is described by the Perrin equation:

$$\frac{r_0}{r} = 1 + \frac{\tau}{\theta} = 1 + 6D\theta \qquad \textbf{Equation 6}$$

where r_0 is the fundamental anisotropy[1], r is the measured anisotropy, τ is the fluorescence lifetime, θ is the rotational correlation time, and D is the rotational diffusion coefficient. The rotational correlation time is a parameter that defines the average time it takes for a molecule to rotate through one radian [16]. Larger, bulkier molecules tumble more slowly in solution and have longer rotational correlation times. When the rotational correlation time is much longer than the fluorescence lifetime ($\theta >> \tau$), rotation of the fluorophore during its fluorescence lifetime is minimal and the anisotropy approaches the fundamental anisotropy [13]. This equation demonstrates the important relationship between the fluorescence lifetime and the anisotropy of a fluorophore. The lengthening of the fluorescence lifetime of a fluorophore leads to the apparent reduction of the fluorescence anisotropy and *vice versa*. The rotational correlation time of a fluorophore may be related to the volume of the rotating unit, V, or the molecular weight, M, by the following equation:

$$\theta = \frac{\eta V}{RT} = \frac{\eta M}{RT}(\bar{v} + h) \qquad \textbf{Equation 7}$$

where η is the viscosity, R is the gas constant, T is the temperature, $\bar{v}$ is the specific volume, and h is the hydration. A highly viscous solvent imposes a large viscous drag on a fluorophore and a large anisotropy results. Conversely, a fluorophore in a solvent with a very low viscosity will rotate freely in solution and its anisotropy will be close to zero [14].

The anisotropy is determined by experiment using the following equation:

$$r = \frac{I_{VV} - GI_{VH}}{I_{VV} + 2GI_{VH}} \qquad \textbf{Equation 8}$$

[1] The anisotropy recorded in the absence of rotational diffusion is the fundamental anisotropy.

where I_{VV} is the intensity recorded when both the excitation and emission polarisers are in the vertical position, I_{VH} is the intensity recorded when the excitation and emission polarisers are in the vertical and horizontal position, respectively, and G is a grating factor given by,

$$G = \frac{S_V}{S_H} = \frac{I_{HV}}{I_{HH}} \qquad \textbf{Equation 9}$$

where S_V and S_H are the sensitivities of the emission channel for the vertically and horizontally polarised components [13].

As stated previously, fluorescence anisotropy may be used to determine various physical properties of biological molecules or molecular assemblies. Zhang *et al.* have used fluorescence anisotropy measurements to determine the critical micelle concentration (CMC) of a number of surfactants by measuring the depolarisation of 1,6-diphenyl-1,3,5-hexatriene (DPH) above and below the CMC [17]. DPH was also used by Roy *et al.* for the investigation of micelles. In this case the microviscosity of the micelle units was determined by measuring the rotational correlation time of the fluorophore in the micelle assemblies.

1.4 Environmental effects

1.4.1 Quenching of fluorescence

Fluorescence quenching describes a broad range of processes by which fluorescence intensity may be diminished. Quenching may take place by an assortment of mechanisms and its effect on fluorescence spectra is likewise variable. Dynamic quenching affects fluorophores that have already been promoted to the excited state. An interaction between fluorophore and quencher results in the non-radiative deactivation of the excited species. Of course, this can only occur if the quencher diffuses to the excited fluorophore before emission takes place and is thus sensitive to fluorescence lifetime [7]. Dynamic quenching is described by the Stern-Volmer equation:

$$\frac{F_0}{F} = 1 + K_D[Q] = 1 + k_q\tau_0[Q] \qquad \textbf{Equation 10}$$

where F_0 is the unquenched fluorescence intensity, F is the fluorescence intensity in the presence of a quenching species, K_D is the Stern-Volmer quenching constant, [Q] is the quencher concentration, k_q is the bimolecular quenching constant, and τ_0 is the fluorescence lifetime in the absence of quencher. Static quenching describes fluorescence deactivation by the formation of a ground state complex. The complex, which comprises of fluorophore and quencher, is non-fluorescent. This means that fluorophores involved in the complex are prevented from reaching the excited state and so the overall fluorescence intensity is reduced. Static quenching may be described by a variation of the Stern-Volmer equation:

$$\frac{F_0}{F} = 1 + K_S[Q] \qquad \textbf{Equation 11}$$

where K_S is an association constant,

$$K_S = \frac{[F - Q]}{[F][Q]} \qquad \textbf{Equation 12}$$

The quenching mechanism may be identified by its effect on the fluorescence lifetime. The rate of static quenching determines the number of fluorophores that reach the excited state but once a fluorophore has been promoted to the excited state it is not sensitive to this form of quenching. The fluorescence lifetime is therefore unchanged. Dynamic quenching, conversely, involves another process that depopulates the excited state, thereby decreasing the fluorescence lifetime. Therefore, static and dynamic quenching can be differentiated by measuring the fluorescence lifetime in the presence and absence of quencher. Another way in which the mechanism may be elucidated involves an investigation of temperature effects. An increase in temperature inhibits the formation of a ground state complex and static quenching is thereby reduced. Dynamic quenching is enhanced as a consequence of the greater rate of diffusion that accompanies higher temperatures.

In some cases quenching takes place by both static and dynamic quenching mechanisms and a modified form of the Stern-Volmer equation must be used (Equation 13 and Equation 14). The Stern-Volmer plot in this case exhibits an upward curvature, concave towards the y-axis. The dynamic portion of the overall quenching mechanism can be determined using lifetime data *i.e.* $\tau_0/\tau = 1 + K_D[Q]$. However, K_D and K_S can also be determined graphically using steady-state

fluorescence emission data by plotting K_{app} against the quencher concentration (Equation 15).

$$\frac{\mathbf{F_0}}{\mathbf{F}} = (\mathbf{1} + \mathbf{K_D}[\boldsymbol{Q}])(\mathbf{1} + \mathbf{K_S}[\boldsymbol{Q}]) \qquad \textbf{Equation 13}$$

$$\frac{\boldsymbol{F_0}}{\boldsymbol{F}} = \mathbf{1} + (\boldsymbol{K_D} + \boldsymbol{K_S})[\boldsymbol{Q}] + \boldsymbol{K_D K_S}[\boldsymbol{Q}]^2 \qquad \textbf{Equation 14}$$

$$\boldsymbol{K_{app}} = \left[\frac{\boldsymbol{F_0}}{\boldsymbol{F}} - \mathbf{1}\right]\frac{\mathbf{1}}{[\boldsymbol{Q}]} = (\boldsymbol{K_D} + \boldsymbol{K_S}) + \boldsymbol{K_D K_S}[\boldsymbol{Q}] \qquad \textbf{Equation 15}$$

The phenomenon of fluorescence quenching is useful in the determination of the structural arrangement of proteins in aqueous solution. As the hydrophobic interior of a protein is impermeable to the quencher species, the location of a fluorescent moiety may be determined based on the quencher's influence on its fluorescence. In Figure 6, the fluorescence of tryptophan is quenched when it is located on the hydrophilic exterior of the protein molecule. However, when tryptophan is embedded in the hydrophobic protein interior it is shielded from the quenching species and its fluorescence is less affected by the quencher.

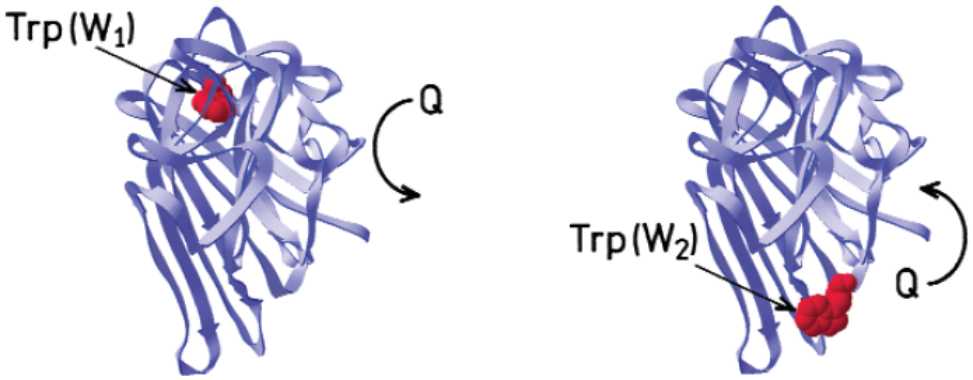

Figure 6: Protein structural determination by fluorescence quenching. Image reproduced with permission from reference [18].

1.4.2 Förster resonance energy transfer

Förster resonance energy transfer (FRET) is another way in which the emission intensity of a fluorophore may be reduced. In this case, energy is transferred non-radiatively between a donor molecule and an acceptor by long-range, dipole-dipole interactions. The emission of the donor typically overlaps with the absorption of the acceptor (Figure 7) [19]. The acceptor may be fluorescent or non-fluorescent but in any case the fluorescence signal of the donor fluorophore is diminished. FRET is a through-space interaction meaning there is no molecular contact between the donor and acceptor. This means that RET is less sensitive to steric or electrostatic factors [19].

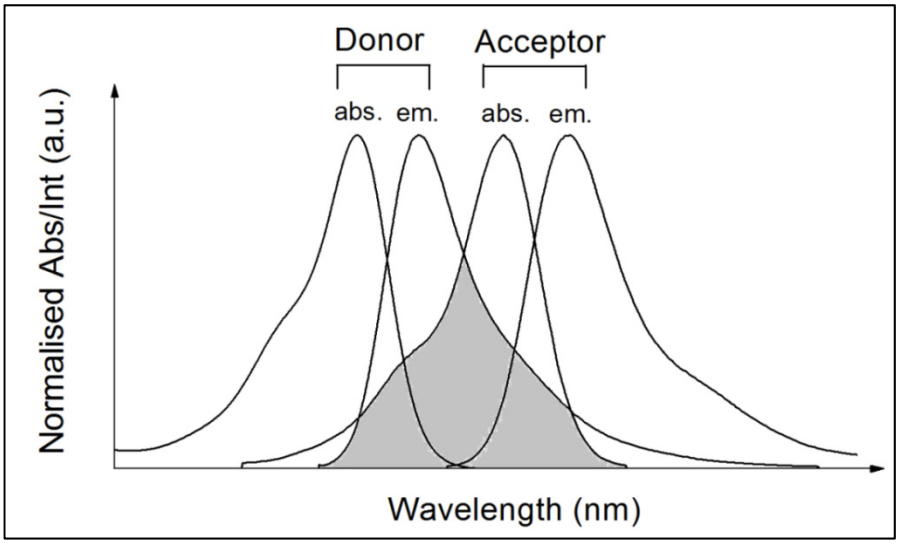

Figure 7: Absorption and fluorescence emission spectra of a RET pair. The shaded area indicates the spectral overlap of the FRET donor's fluorescence emission and the FRET acceptor's absorption. Image reproduced with permission from reference [20].

The Förster distance, R_0, is the separation between the donor and acceptor at which FRET is 50% efficient. It is this distance dependence that distinguishes FRET from other forms of fluorescence quenching. Förster distances vary for different donor-acceptor pairs but values generally lie in the 15–60 Å range [20]. Kosk-Kosicka *et al.* report a FITC-TRITC Förster distance of 53.8 Å [21]. This pair of fluorophores is sometimes considered the standard for high energy transfer efficiency [22]. Since this distance range is comparable to the size of biological molecules this technique is very

useful for the study of protein conformational changes. The Förster distance can be calculated using the following equation:

$$R_0 = 0.211 \left[\frac{\kappa^2 \varphi_D J(\lambda)}{n^4}\right]^{\frac{1}{6}} \qquad \textbf{Equation 16}$$

where κ^2 is an orientation factor between the donor and acceptor, n is the refractive index, φ_D is the fluorescence quantum yield of the donor in the absence of the acceptor, and $J(\lambda)$ is the area of spectral overlap between the fluorescence emission spectrum of the donor and the absorption spectrum of the acceptor. Here $J(\lambda)$ is in units of M^{-1} cm^{-1} nm^4 and is defined by:

$$J(\lambda) = \int_0^\infty \varepsilon_A(\lambda)\lambda^4 F_D(\lambda) d\lambda \qquad \textbf{Equation 17}$$

where ε_A is the extinction coefficient spectrum of the acceptor in units of M^{-1} cm^{-1}, λ is the wavelength in nm and F_D is the wavelength dependent donor emission spectrum normalised to an area of one.

The relative orientation factor, κ^2, if unknown, can introduce some inaccuracy in the determination of the donor-acceptor distance [23]. It is given by the following equation:

$$\kappa^2 = (sin\theta_D sin\theta_A cos_\phi - 2cos\theta_D cos\theta_A)^2 \qquad \textbf{Equation 18}$$

where θ_D and θ_A are the angles between the vector joining the donor and acceptor and the transition dipoles of the donor and acceptor, respectively, and ϕ is the angle between the planes. This value can range between zero and four. Head to tail parallel transition dipoles result in the maximum κ^2 value of four, parallel transition dipoles result in a κ^2 value equal to one, while for perpendicular transition dipoles κ^2 is equal to zero [19].

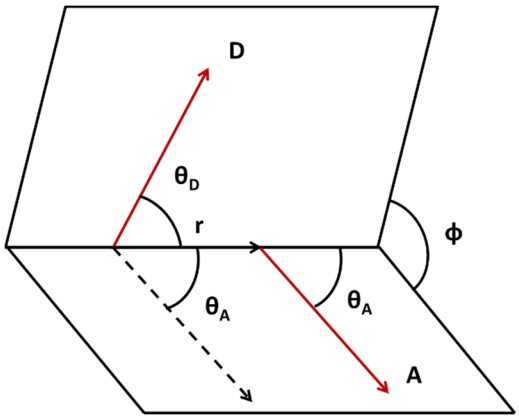

Figure 8: Dependence of the orientation factor, κ^2, on the direction of the emission dipole of the donor and the absorption dipole of the acceptor. Image reproduced with permission from reference [19].

The transfer efficiency (Equation 19) can be used to measure distances between sites on a protein. This is the ratio of the transfer rate to the total decay rate of the donor in the presence of the acceptor. It can be calculated by measuring the fluorescence lifetime of the donor in the presence and absence of the acceptor [19].

$$E = 1 - \frac{\tau_{DA}}{\tau_D} \qquad \textbf{Equation 19}$$

The distance between a donor-acceptor pair is calculated using the following equation:

$$\frac{R_{DA}}{R_0} = \left(\frac{1}{E} - 1\right)^{\frac{1}{6}} \qquad \textbf{Equation 20}$$

FRET studies are often carried out in micellar media because these organised assemblies can be considered as model membrane systems. Therefore, the donor-acceptor behaviour of a pair of fluorophores can be assessed in a simple, well-defined assembly that shares many of the same characteristics as complex biological systems. As well as providing information about the spectroscopic properties of the FRET pair, these investigations provide an insight into the physical parameters of the micelle assembly itself [24, 25].

FRET studies in micelles are particularly useful because it is possible to obtain high local concentrations of fluorophores in close enough proximity for energy transfer to

occur. The main motivations for FRET studies in micelle assemblies are to determine the micellisation sites of the fluorophores [24], to gain an insight into the structural changes of the micelles [26], and to determine the aggregation number of the micelle [27]. Aydin *et al.* carried out FRET studies between fluorescein and merocyanine 540 in aqueous solution and micellar solutions. The transfer efficiency was found to be greater in all micelle environments compared to deionised water with the greatest transfer efficiency recorded for cetyltrimethylammonium bromide (CTAB) micelles. This has been ascribed to the favourable electrostatic interactions between the fluorophores and the CTAB micelles [24]. Tummino *et al.* determined the aggregation number of several micelles using pyrene and coumarin 153. Since the degree of fluorescence quenching, or FRET, between the donor and acceptor is dependent on the micelle concentration, the aggregation number of the micelles may be calculated [28]. Sanchez *et al.* investigated the influence of NaOH additions on aggregation numbers using the same technique [29].

1.4.3 Solvent effects

Some of the factors that can affect a fluorophore's emission include: solvent polarity and viscosity, internal charge transfer (CT), proton transfer and excited-state reactions, rigidity of the local environment, and fluorophore conformational changes. Polarity sensitive fluorophores usually have a greater dipole moment (μ) in the excited state than in the ground state and reorientation of the solvent molecules around the fluorophore in the excited state acts to lower its energy. Fluorescence lifetimes (1−10 ns) are generally much longer than the time required for solvent reorientation (1−100 ps) and so fluorescence emission is representative of the solvent relaxed state. Generally, as the polarity of the solvent increases, the energy of the solvent-relaxed state decreases and the fluorescence emission is shifted increasingly to the red [30].

Since viscosity influences the rate of solvent relaxation it can also have a bearing on the extent of the solvatochromic shift observed. If the polarity sensitive fluorophore is solvated in a highly viscous medium the time required for solvent relaxation may be greater than the fluorescence lifetime and emission will arise from a state that closely resembles the Franck-Condon state [30]. Viscosity can also have a marked effect on fluorophores that undergo conformational changes in the excited state, since a highly

viscous environment inhibits rotation. This phenomenon is examined by Zhou *et al.* in the case of p-(Dialkylamino)benzylidene malononitriles; a family of fluorescent molecular rotors[2] (FMRs) whose excited state consists of a locally excited (LE) and a twisted intramolecular charge-transfer (TICT) state. Only the LE state is considered emissive and so the inhibition of the formation of the TICT state enhances the fluorescence of these FMRs. Highly viscous solvents prevent rotation in the excited state, which is necessary for the formation of the TICT state [32].

The sensitivity of a fluorophore to specific interactions with a solvent (hydrogen bonding, preferential solvation, charge-transfer interactions) may be considered to be either beneficial or problematical, depending on the application. If the fluorescence emission is affected by specific interactions it can reveal information about the fluorophore's locality. For example, if the fluorescence emission of a fluorophore is sensitive to hydrogen-bonding, protic solvents could be used to detect the accessibility of a macromolecule-bound fluorophore to the aqueous phase. However, this sensitivity to a specific solvent property could be a disadvantage for applications where the fluorophore's response to the bulk solution is of interest [33]. 2-anilinonaphthalene (2-AN) is an example of a fluorophore whose fluorescence emission is very sensitive to hydrogen bonding. The fluorescence emission of 2-AN in cyclohexane is shifted to the red upon the addition of trace quantities of ethanol (EtOH) (Figure 9). Despite the small concentration of EtOH, the shape of the fluorescence emission band and the position of its band maximum have changed considerably. In fact, 50% of the bathochromic shift is achieved for a 3% EtOH concentration. Therefore, the fluorescence emission of 2-AN in the presence of EtOH is not representative of the polarity of the bulk solution but rather indicates a specific interaction between the fluorophore and one or a few neighbouring solvent molecules. This shows that the sensitivity of a fluorophore to specific solvent effects can lead to the misinterpretation of results [34].

[2] Molecular rotors are a group of fluorophores that form twisted intramolecular charge transfer (TICT) states upon photoexcitation [31].

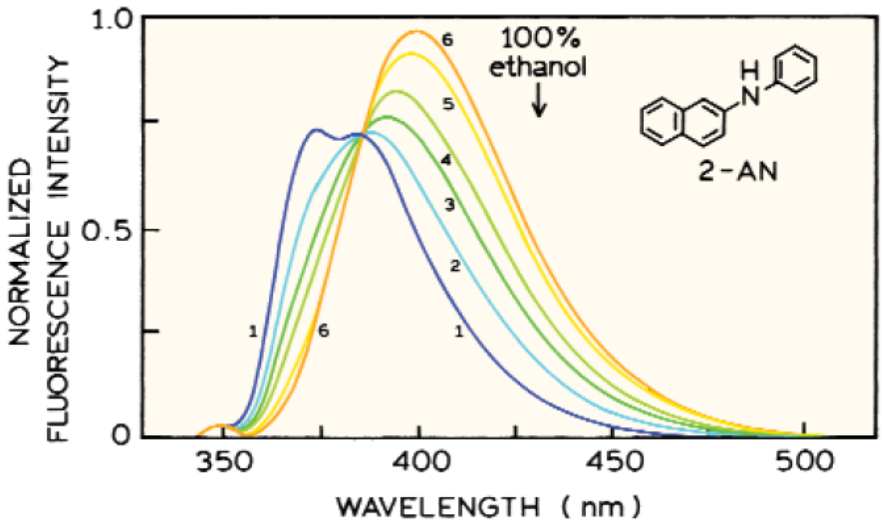

Figure 9: Fluorescence emission of 2-anilinonaphthalene in cyclohexane spiked with small quantities of EtOH. These quantities were (1) 0%, (2) 0.2%, (3) 0.4%, (4) 0.7%, (5) 1.7%, and (6) 2.7%. Image reproduced with permission from reference [33].

1.4.4 Refractive index

The refractive index must always be considered when evaluating the spectroscopic behaviour of a fluorophore. This is particularly true when it comes to electronic spectroscopy: since refractive index effects are most pronounced at high frequencies, it deserves particular attention when the spectra of the energetic transitions involved appear on the UV-visible region of the EM spectrum. The refractive index, n, is the ratio of the speed of light in a vacuum, c, to that in a given medium, v (Equation 21). Since the frequency remains unchanged while the speed decreases, the wavelength of the light is altered—this is known as dispersion.

$$n = \frac{c}{v} \qquad \textbf{Equation 21}$$

In other words, it is a measure of how the speed of light is affected by the medium in which it is travelling [6]. When an EM wave's phase velocity is slowed in a material it is because the electric field exerts a force on the electrons that causes them to oscillate at the same frequency as the incident wave. The oscillation of the electrons produces a secondary EM wave that is out of phase with the primary wave. This

secondary wave recombines with the primary wave to form the net transmitted wave [35, 36].

The effect of a medium's refractive index on the fluorescence emission of a fluorophore may be explained quantitatively by the Lippert-Mataga equation:

$$\bar{\nu}_A - \bar{\nu}_F = \frac{2}{hc}\left(\frac{\varepsilon - 1}{2\varepsilon + 1} - \frac{n^2 - 1}{2n^2 + 1}\right)\frac{(\mu_E - \mu_G)^2}{a^3} + constant \qquad \textbf{Equation 22}$$

where $\bar{\nu}_A - \bar{\nu}_F$ is the Stokes shift, h is Planck's constant, c is the speed of light, ε is the permittivity of the medium, n is the refractive index, *a* is the radius of the cavity in which the fluorophore resides, and μ_E and μ_G are the excited and ground state dipole moments, respectively. This model considers the fluorophore to be a dipole in a medium of uniform permittivity. The Stokes shift is shown to be affected by the permittivity and the refractive index of the medium[3]. Generally speaking, an increase in the refractive index results in a smaller Stokes shift. This depends on the motion of electrons within the solvent molecules, which is an instantaneous response that can occur at the same time as absorption. As the refractive index increases, the degree of stabilisation of the ground and excited states by an electronic rearrangement around each dipole is enhanced. However, each state is stabilised by this electronic rearrangement to a similar extent and so the refractive index has a minimal effect on the Stokes shift of the fluorophore. The permittivity, on the other hand, which depends on electronic and molecular rearrangements, causes an increase in the Stokes shift as it itself increases.

The measured fluorescence quantum yield is also dependent upon the refractive index of the sample medium. φ is usually determined experimentally for a compound by comparison with a fluorophore of known quantum yield.

$$\varphi = \varphi_R \frac{I}{I_R}\frac{OD_R}{OD}\frac{n}{n_R} \qquad \textbf{Equation 23}$$

[3] The relative permittivity and refractive index of water at 273.16 K is 87.90 and 1.3339, respectively [37].

where φ is the quantum yield, I is the integrated intensity, OD is the optical density, and n is the refractive index. Parameters pertaining to the reference standard are denoted by the subscript R [38]. The Strickler-Berg equation (Equation 5) shows how the radiative decay, Γ, of a fluorophore is also dependent upon the refractive index of the medium. However, this equation is not an expression of the radiative decay rate in terms of intrinsic properties of a fluorophore. Both the extinction coefficient and the radiative decay rate vary with refractive index. Therefore, a simple correlation between these parameters cannot be drawn from this equation [39].

1.5 Fluorophores

Fluorophores, whether natural or man-made, are at the core of the subject of fluorescence. It is the existence of these molecules which makes a myriad of luminescent analytical techniques possible. Typically, it is aromatic molecules which exhibit the phenomenon of fluorescence [7]. The natural product quinine, which was used as an antimalarial drug in the 17th century [40], was the first well–defined fluorescent small molecule [41]. In 1845, Herschel reported the visible emission from an aqueous quinine solution [42]. The actual term "fluorescence" was not used until G.G. Stokes observed that this occurrence was due to the absorption and emission of light by the quinine molecule [43].

1.5.1 Design criteria of fluorophores

Fluorophores are used for the investigation of physicochemical, biochemical, and biological microenvironments [8]. Since they may be used for a wide variety of applications there is a strong incentive to produce a large range of fluorophores with different photophysical properties and sensitivities. However, the main design criteria for the photophysical properties of a fluorophore remain unchanged. Firstly, it is most important that the fluorophore is stable in the presence of chemicals and light. Secondly, a bright fluorescence emission is essential and can be defined as the product of the extinction coefficient, ε(λ), at the wavelength of excitation and the fluorescence quantum yield, φ [41]. It is generally favourable that signalling takes place by a fluorescence enhancement process or shifts in excitation and/or emission wavelengths. Signalling by a turn-off process leads to a decrease in the signal-to-

noise ratio. Fluorophores that produce a ratiometric signal from multiple emission bands are superior as environmental indicators [44]. The wavelength of light absorbed and emitted by the fluorophore is also of critical importance. Fluorophores that absorb and emit light in the visible region of the EM spectrum have considerable advantages over fluorophores excited by UV-light. These fluorophores avoid the necessity for expensive lasers, detectors and optical components and are preferable as biological indicators. Longer wavelengths of excitation and emission minimise the risk of photodamage to biological cells and tissues. Further biological constraints include water solubility, membrane permeability and minimal toxicity to live samples [44]. No one fluorophore can satisfy all of these criteria.

1.5.2 Classes of fluorophores

Fluorophores may be broadly divided into two main classes—intrinsic and extrinsic. Intrinsic fluorophores are those which occur naturally within the sample, *e.g.* amino acids in proteins, cells, tissue. The aromatic amino acids, NADH, flavins, derivatives of pyridoxal, and chlorophyll are some examples of intrinsic fluorophores [45]. The fluorescent parameters of a number of natural fluorophores are presented in Table 1.

Table 1: Fluorescence parameters of naturally occuring fluorophores at neutral pH.

Fluorophore	λ_{ex} (nm)	λ_{em} (nm)	Bandwidth (nm)	φ	τ (ns)	Ref.
Phenylalanine	260	282	—	0.02	6.8	[45]
Tyrosine	275	304	34.0	0.14	3.6	[45]
Tryptophan	295	353	60.0	0.13	3.1 (mean)	[45]
NADH	340	470	58.0	—	0.4 (mean)	[46]
Pyridoxal-P hydrate (pH 7)	328	430	—	0.03	—	[47]
Pyridoxal-P free aldehyde (pH 7)	388	515	—	<0.005	—	[47]

The fluorescence of the aromatic amino acids—namely tryptophan, tyrosine, and phenylalanine (Figure 10)—was first described by Teale and Weber in 1957 [48]. Of the aromatic amino acids, tryptophan exhibits the most intense fluorescence.

Tryptophan is relatively rare in protein molecules but when present its fluorescence emission may be used to monitor conformational transitions, subunit association, substrate binding, or denaturation [18, 49]. In some cases the intrinsic fluorescence is not sufficient for the experiment of interest and it is necessary to introduce a brighter fluorophore [45]. Certain biological molecules including DNA and lipids possess no, or very weak, intrinsic fluorescence [7]. The introduction of an extrinsic fluorophore means the microenvironment of these molecules may also be monitored. Commonly, fluorophores with longer wavelengths of excitation and emission than the aromatic amino acids are employed. There are two main reasons for this: first, irradiation of live cells and biomolecules with UV radiation may have a damaging effect on the sample and second, energy transfer studies may be carried out if the fluorophore's absorption spectrum overlaps with the sample's intrinsic fluorescence emission.

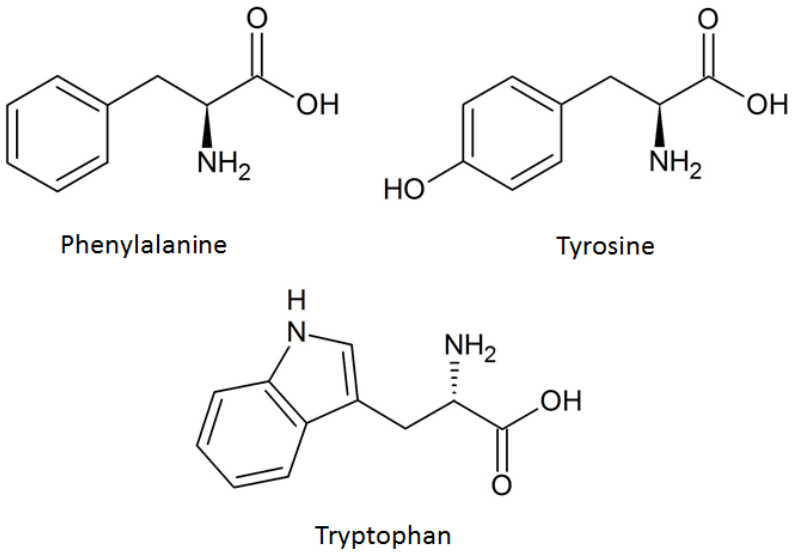

Figure 10: Structures of the aromatic amino acids.

Some common classes of fluorophores, some of which are shown in Figure 11, include; pyrene derivatives, coumarins, quinolines, indoles and imidizoles, fluorescein, rhodamine, BODIPY, cyanines, oxazines and many more. Fluoresceins and rhodamines are widely used fluorophores due to their long wavelength absorption and emission bands and exceptionally high molar extinction coefficients of approximately 80,000 M^{-1} cm^{-1}. When polarisation measurements are required, dansyl chloride (1-dimethylamino-5-naphthylsulfonyl chloride), is a popular choice. This fluorophore may be conjugated to free amino components of protein molecules.

λ_{max} occurs at 350 nm—too long a wavelength to excite the aromatic amino acids—and λ_{em} typically occurs at approximately 520 nm. Absorbance at 350 nm also means that this fluorophore may act as an acceptor of intrinsic tryptophan and tyrosine fluorescence [45].

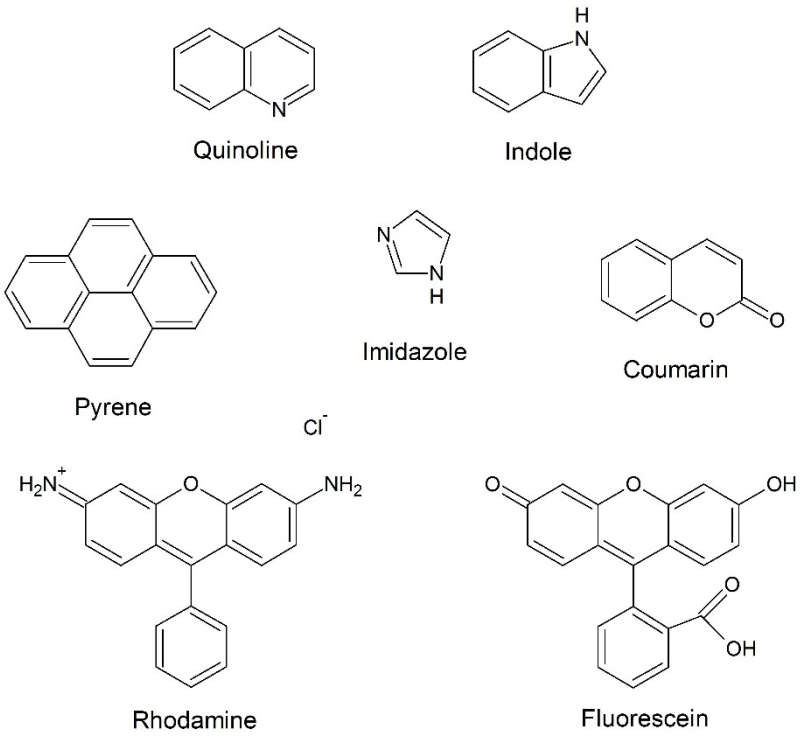

Figure 11: Common core structures of some important classes of fluorophores.

1.5.3 Fluorescence sensing

Fluorescence is seen as an attractive analytical methodology for the detection of chemical and biochemical analytes due to its rapid, non-invasive, and low cost characteristics. The technique is continuously being developed for clinical, bioprocess, and environmental applications. In many cases it eliminates the use of radiotracers which are expensive, hazardous, highly regulated, and expensive to discard [50]. In these instances, the fluorophore acts as a label as well as functioning as an indicator of non-fluorescent species such as oxygen and metal ions, and physiochemical properties like pH and polarity, among others. The detection of a particular analyte may be achieved by observing a change in a specific spectral property of the fluorophore in use. The intensity, excitation spectrum, emission

spectrum, anisotropy, and/or the lifetime of the fluorophore may be altered by its interaction with the analyte [51].

FRET is an example of a fluorescence sensing technique. If a donor and acceptor are in close enough proximity, the intensity of the donor's emission will be diminished. The efficiency of the transfer process and the donor-acceptor distance can subsequently be calculated. In some cases the donor and acceptor entities are encapsulated in a single species. If the component which acts as an acceptor is only activated under certain environmental conditions then these conditions may be monitored [7]. Mahato *et al.* describes a method for the detection of Cr^{3+} and Hg^{2+} in drinking water using a newly synthesised rhodamine derivative that exhibits intramolecular FRET upon Cr^{3+}/Hg^{2+} binding. The rhodamine fluorophore acts as a ratiometric sensor of the metal cations based on the FRET process. The naphthalimide fragment acts as the donor while the acceptor is the Cr^{3+}/Hg^{2+}-bound xanthene fragment [52]. Upon excitation at 455 nm, a steady decrease in fluorescence emission intensity at 533 nm with increasing $[Cr^{3+}]/[Hg^{2+}]$ was observed along with a concomitant increase in emission intensity at 583 nm.

Zhu *et al.* developed a method that has the potential to be used for the detection of trace quantities of anionic surfactants in drinking water. They detected trace quantities of sodium dodecyl sulfate (SDS) using a near-infrared fluorophore in the presence of Triton X-100 (TX-100) at a concentration above the CMC. This methodology is attractive as it avoids the process of solvent extraction, which employs large quantities of expensive and toxic solvents. Since the fluorophore was also quenched in aqueous solution, the non-ionic surfactant TX-100 was used to solvate the fluorophore. The fluorescence intensity of the fluorophore was monitored in the presence of varying quantities of SDS. The limit of detection (LOD) was found to be 8.3×10^{-8} M [53].

Anisotropy based sensing techniques are also very common, particularly for biological assays that involve analyte size changes, *e.g.* protein-protein interactions. One technique that pairs a reference fluorophore that is not sensitive to the analyte and a sensing fluorophore that is sensitive to the analyte is discussed in reference [54]. The intensity or concentration of the sensing fluorophore must change and its anisotropy must be different from the reference. Since a reference fluorophore with a

very low or a very high anisotropy may be chosen, an anisotropy assay with a very wide range can be developed. This method is based on the additivity property of anisotropies demonstrated by Jabłoński [55]. In this experiment, a pH-sensitive fluorophore, 6-carboxyfluorescein, was paired with the anisotropy reference, pyridine 2 (Py2). In this case, Py2 is immobilised in a stretched PVA film to produce an anisotropy of ~0.9. As the pH increases, the intensity of the freely diffusing, pH-sensing fluorophore increases relative to that of Py2 and the sum of the anisotropies decreases. Since anisotropy measurements are accurate to 0.002, pH measurements accurate to ±0.02 can be obtained using this methodology.

Lifetime based sensing is sometimes preferable to fluorescence intensity based sensing techniques. Fluorescence lifetime is independent of the total fluorescence intensity, which is susceptible to changes in excitation light intensity, to photobleaching, variation in light scattering and absorption of the sample [56]. Baleizão *et al.* describe a dual sensor based on fluorescence lifetime for the detection of both trace oxygen and temperatures up to 120 °C. The temperature sensitive fluorophore, ruthenium tris-1,10-phenanthroline ($Ru(phen)_3$), is incorporated in poly(acrylonitrile) to eliminate any sensitivity to oxygen while fullerene (C_{70}), the oxygen-sensing fluorophore, is incorporated in a highly oxygen-permeable polymer. The simultaneous detection of trace oxygen and temperature was found to be possible using this fluorophore combination through lifetime decay measurements. The cross-sensitivity of C_{70} to temperature was accounted for by means of the temperature sensor. Both of the fluorophores were excited at 488 nm. $Ru(phen)_3$ had an emission maximum at about 580 nm, while the emission maximum of C_{70} lay in the range 670–700 nm. The C_{70} decays by two mechanisms: prompt fluorescence (PF) and thermally activated delayed fluorescence (TADF). The TADF mechanism consists of a cycle from S_1 to T_1 and back to S_1. This $S_1 \rightarrow T_1 \rightarrow S_1$ cycle may occur several times before fluorescence takes place. The TADF of C_{70} has a high quantum yield and lifetimes fall in the millisecond range making it ideal as a trace oxygen sensor. It becomes more sensitive to oxygen with increasing temperature as it spends more time in the triplet state and therefore interacts more efficiently with triplet oxygen [57].

1.6 Triazine fluorophores

Triazines are six membered ring compounds containing three nitrogen atoms. Three different triazine systems are possible depending on the position of the three nitrogen atoms, namely: 1, 3, 5-triazine, 1, 2, 4-triazine, and 1, 2, 3-triazine (Figure 12) [58].

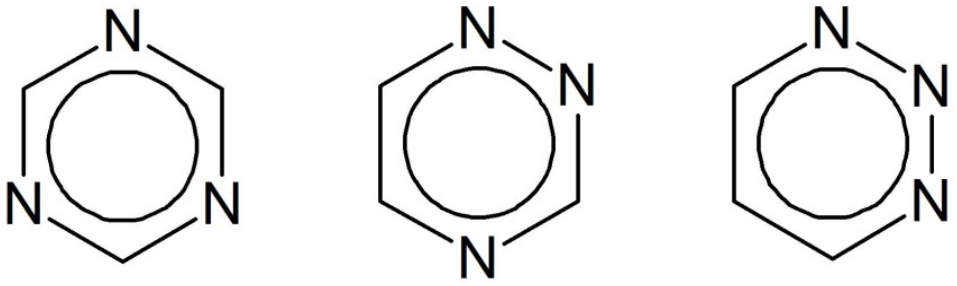

Figure 12: The three isomeric forms of triazine: 1,3,5-triazine, 1,2,4-triazine, and 1,2,3-triazine.

In a review by S.F. Mason, the electronic spectra of a number of N-heteroaromatic systems were compared. The electronic spectra of the azabenzenes (Figure 13) are very similar to the spectrum of benzene with three absorption bands located at around 248, 191, and 165 nm [59]. However, it was discovered that all of these compounds have an absorption band that has no corresponding band in the spectrum of benzene. Further solvent studies determined that this band arises due to the transition of a non-bonding electron from a lone-pair orbital on the nitrogen atom to one of the ring's π-orbitals. The n→π transitions of azabenzenes are quite weak with oscillator strengths varying between 0.003 and 0.021. This is because the lone-pair orbitals and π-orbitals are perpendicular to one another meaning the probability of a transition is quite low. Furthermore, only the s-component of the sp^2 hybridised lone-pair orbital can contribute to the transition moment, since the $p_\sigma \rightarrow p_\pi$ transition is forbidden [60].

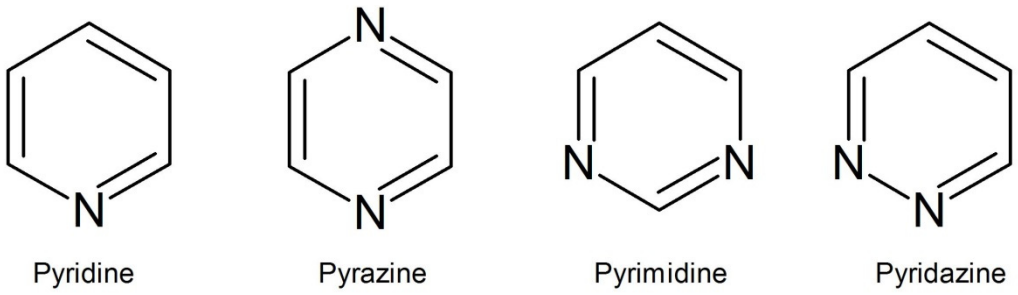

Figure 13: Structures of some of the azabenzenes examined by Mason.

Relative to pyridine, the n→π transition of the azabenzenes occurs at longer wavelengths. The position of the nitrogen substituents, rather than their number, has a significant bearing on this red shift. When nitrogen atoms are adjacent to one another within the ring structure, the lone pair orbitals interact strongly to form a bonding and an antibonding lone pair MO. The transition from the antibonding lone-pair MO to the π-orbital requires less energy and emission is thus shifted to the red relative to the transition from the non-bonding AO to the π-orbital [60, 61]. Mason also determined that when the azabenzenes are in a protic solvent, the lone pair electrons are often involved in hydrogen bonding. In this case, the promotion of such an electron to a π-orbital requires more energy because the hydrogen bonding interaction must first be overcome. The electron donating ability of the azabenzenes was inferred from the blue shift of the n→π transition on going from cyclohexane to aqueous solution [60].

1.6.1 1,3,5-triazine based fluorophores

The 1,3,5-triazine is a symmetrical, six-membered heterocycle, otherwise known as the s-triazine or sym-triazine. Derivatives of this species are quite easily prepared from cyanuric chloride using a temperature-dependant, stepwise nucleophilic substitution approach for the replacement of its three chlorine atoms [62]. In reference to 2,4,6-triphenyl-1,3,5-triazine, Stueber *et al.* explained that derivatives with a hydroxyl or an alkoxy group on one or more of the phenyl substituents have an additional longer-wavelength absorption band, as well as the ππ* band. This band arises due to an intramolecular CT from the electron rich hydroxyl/alkoxy moiety into the electron deficient triazine ring. This absorption band is most intense when the alkoxy substituent is in the para-position. This served as a reference point for the examination of the structural and spectroscopic character of 2-(2'-hydroxyphenyl)-

1,3,5-triazines and their methoxy derivatives (Figure 14) [63]. Elbe *et al.* noted that, with the introduction of additional para-alkoxy groups, the ππ* band is shifted to longer wavelengths and the CT band is shifted to shorter wavelengths. This is due to enhanced electron donation into the triazine π system [64].

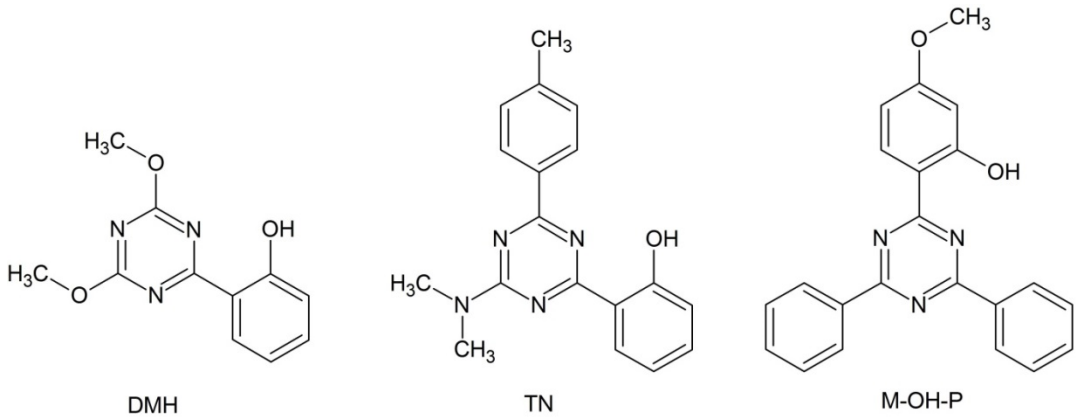

Figure 14: Structures of 1,3,5-triazines discussed by Stueber *et al.*in reference [63]. The number of aryl substituents on the 1,3,5-triazine ring was found to have a direct effect on the fluorescence of the molecules.

Stueber *et al.* found that derivatives with one aryl group only, *e.g.* 2-(2'-hydroxyphenyl)-4,6-dimethoxy-1,3,5-triazine (DMH), exhibit a proton-transferred fluorescence ($\lambda_{ex}/\lambda_{em}$ 313/510 nm) with large Stokes shift (9890 cm^{-1}) and high quantum yield (0.24). Introduction of another aryl substituent into the triazine system weakens the proton transferred fluorescence for 2-(2'-hydroxyphenyl)-4-(dimethylamino)-6-(4''methylphenyl)-1,3,5-triazine (TN). Fluorescence is completely quenched in compounds with three aryl substituents, *e.g.* 2-(2'Hydroxy-4'-methoxyphenyl)-4,6-diphenyl-1,3,5-triazine (M-OH-P) [63]. The absorbance spectrum of M-OH-P and the fluorescence emission spectrum of DMH are shown in Figure 15.

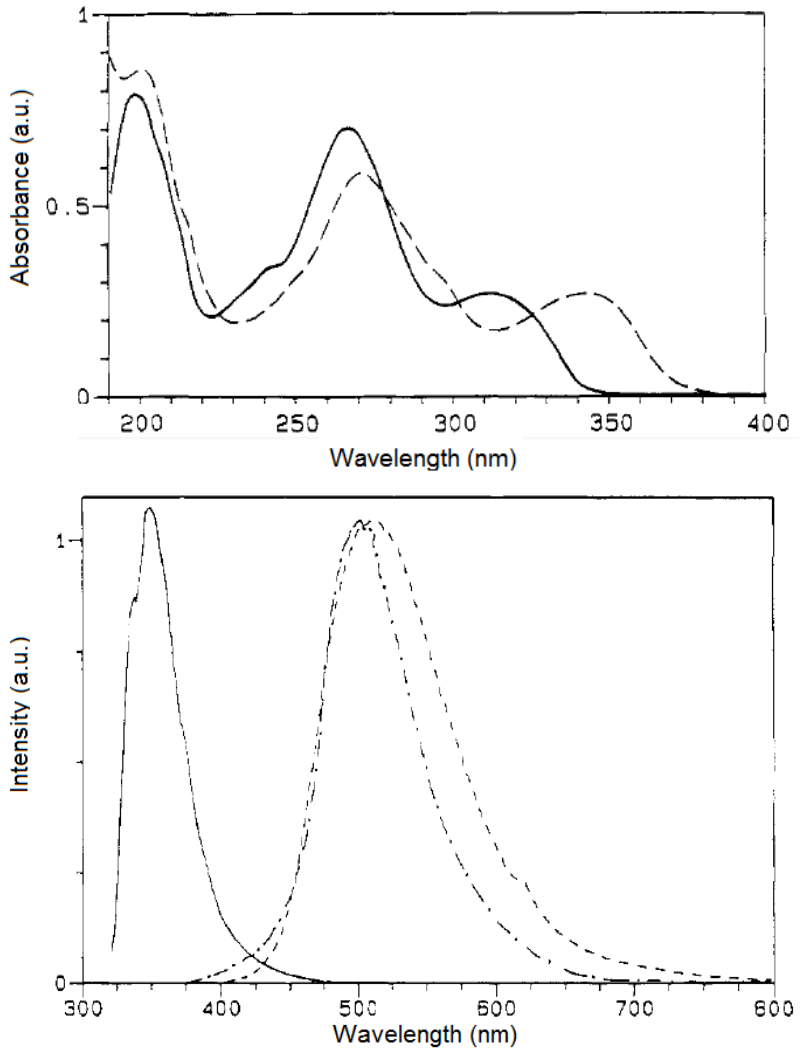

Figure 15: Absorption spectrum (above) of M-OH-P (- - -) in DMSO at 293 K and fluorescence emission spectrum (below) of DMH (- · - · -) in methylcyclohexane/2-methylbutane at 77 K. Images reproduced with permission from reference [63].

These compounds have been used for the absorption of UV light in optical lenses and photography [65]. In a similar fashion, these compounds may be used to protect a polymer matrix from damaging incident UV-light. Compounds such as 2-(2-hydroxyphenyl)-1,3,5-triazine can absorb UV-light and transform it into vibrational energy by highly efficient, radiationless deactivation pathways. An excited-state intramolecular proton transfer (ESIPT) reaction facilitates this deactivation process [66]. Additionally, collections of s-triazines have been screened to find derivatives with useful biological activities including: the enhancement of the production of biofuels in microorganisms [67]; the inhibition of secreting agents that promote

tumour proliferation [68]; insulin mimetics [69]; neuroblastoma inhibition [70]; antimicrobial peptide mimetics [71]; tyrosinase inhibition [72].

1.6.2 1,2,4-triazines based fluorophores

The 1,2,4-triazine is also known as the asymmetrical or as-triazine. Mason *et al.* compare the electronic spectrum of 3,5,6-trimethyl-1,2,4-triazine with that of the 1,3,5-triazine and some other azabenzenes. Since it is an alkyl derivative it is not directly comparable to the other azabenzenes. However, it is worth noting that, relative to pyridine, the n→π transition of 3,5,6-trimethyl-1,2,4-triazine is the second most red shifted of all the azabenzenes in cyclohexane (second to pyridazine). As stated in Section 1.6, this shift is more dependent on the position than the number of aza-substituents. In the case of 3,5,6-trimethyl-1,2,4-triazine the red-shift has two points of origin: the formation of bonding and antibonding lone pair MOs upon the interaction between adjacent nitrogen atoms and the steric effect of the alkyl groups, which shield the aromatic ring, to some extent, from any solvent interactions that might be present [60].

Sun *et al.* synthesised several nitrogen containing heterocyclic chromophores including two bis-1,2,4-triazine based fluorophores: 1,4-bis(5,6-diphenyl-1,2,4-triazin-3-yl)benzene (DS1) and 1,3-bis(5,6-diphenyl-1,2,4-triazin-3-yl)benzene (DS2) (Figure 16) [73]. The structures of these fluorophores only vary in their central unit: DS1 contains a 1,4-phenylene linker while DS2 contains 1,3-phenylene. The absorbance spectra show the effect of the linker on conjugation: two sharp bands are present at 276 nm and 331 nm in the absorbance spectrum of DS1, while a band at 275 nm with a weak shoulder on the longer wavelength side is present in the spectrum of DS2. Sun *et al.* inferred that conjugation in the 1,4-phenylene linker in DS1was greater than in the 1,3-phenylene linker in DS2. Fluorescence emission bands at 460 nm, 480 nm, and 530 nm were detected for DS1 and DS2, while the overall band maxima were located at 483 nm and 460 nm, respectively.

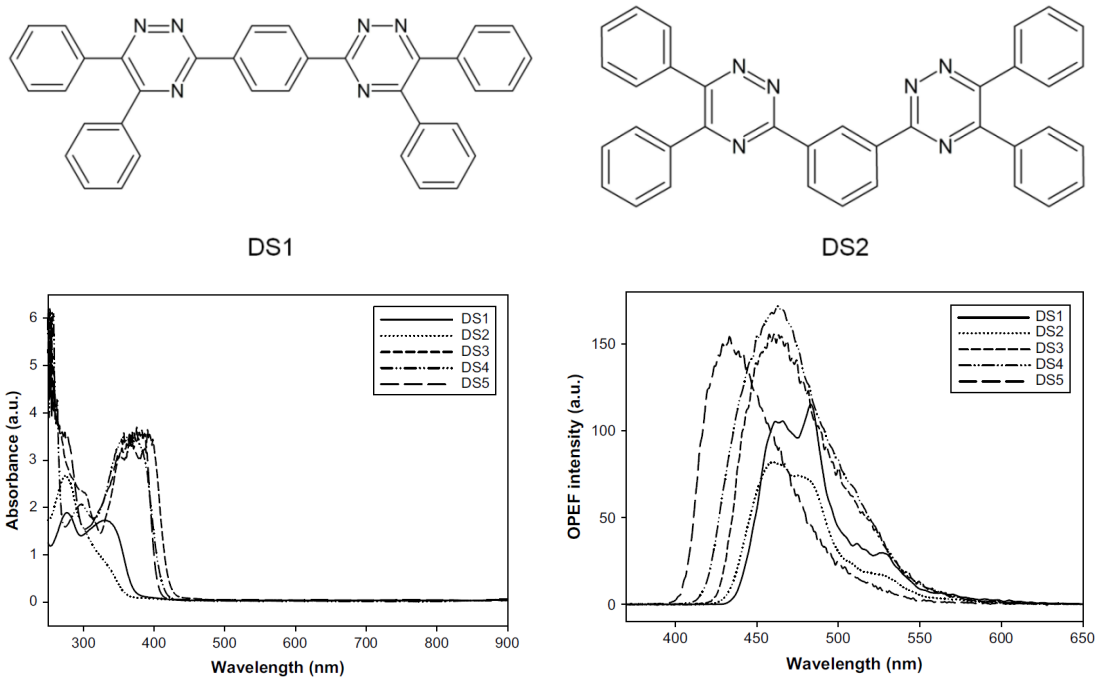

Figure 16: Structures (above) and absorbance (below left) and fluorescence emission (below right) spectra of 1,2,4-triazine based fluorophores, DS1 and DS2. Images reproduced with permission from reference [73].

1.6.3 1,2,3-triazine based fluorophores

The 1,2,3-triazines, also known as the v-triazines, are the least studied of the three classes of triazine [74]. This is due to the ring's lower stability and more limited synthetic routes. The unsubstituted 1,2,3-triazine construct was first synthesised by Ohsawa in 1981 [75]. The 1,2,3-triazine construct itself is not reported to exhibit any fluorescence. In 1972, Henriksen *et al.* reported the synthesis of two series of thieno-1,2,3-triazin-4-ones (Figure 17) [76]. The thieno-[3,4-e]-3,4-dihydro-1,2,3-triazin-4-ones were reported to have a long wavelength absorption band at around 390 nm and a strong yellow fluorescence, which made them observable at low concentrations. However, no fluorescence was detected upon examination of the thieno-[3,2-e]-3,4-dihydro-1,2,3-triazin-4-ones, and the absorption band was positioned at about 305 nm. In 2009, Zhu *et al.* carried out a comprehensive solvent study on the original molecules synthesised by Henriksen over thirty-five years previously. Spectral calculations revealed that the first electronic state of these molecules is due to a HOMO-LUMO transition. It was found that the fluorescence properties of 2-methyl-thio-5-(Z-carbonyl)-thieno-[3,4-e]-3,4-dihydro-1,2,3-triazin-4-ones could be altered

by changing the substitution pattern and/or the solvent. Increasing solvent polarity (and protic solvents) produced a decrease in the fluorescence quantum yield and a red-shift in the fluorescence emission band. This bathochromic shift was attributed to a higher-dipole moment in the excited state.

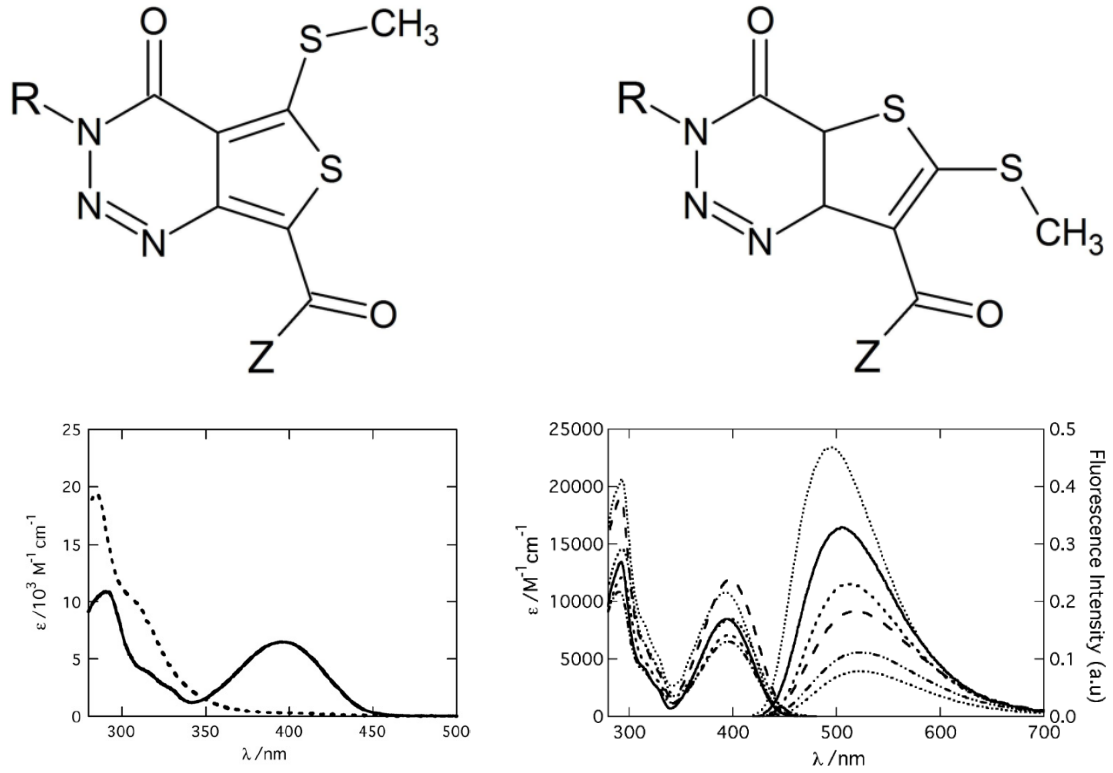

Figure 17: Fluorescent (above left) and non-fluorescent isomer (above right) of the thieno-1,2,3-triazin-4-ones synthesised by Henriksen *et al.* Absorbance spectra (bottom left) of the (Z=NH_2, R=Me) derivative (—) and its non-fluorescent isomer (- - -). Fluorescence emission spectra (bottom right) of the (Z=NH_2, R=Me) derivative in a variety of solvents. Images reproduced with permission from reference [77].

1.6.3.1 2,5-dihydro-1,2,3-triazines

A synthetic route for the first fluorophores of the 2,5-dihydro-1,2,3-triazine (2,5-DHT) series was developed by Butler *et al.* in 2006 [1]. These fluorophores have two absorbance bands at 310 nm and 400 nm and exhibit a bright green fluorescence centred at 520 nm. The fluorescence emission of the 2,5-DHT series is comprised of three bands when excited at 400 nm and four bands when excited at 310 nm and has a complex, multi-exponential lifetime decay. These bands are a result of three possible

geometrical arrangements (g0, g1, and g2), which are vibrationally accessible in the excited state. The fluorescence of the 2,5-DHT is quite different to that of the reported 1,3,5-, 1,2,4-, and 1,2,3-triazine fluorophores, which exhibit charge/proton transfer emission [63, 73, 77]. The structure of 5-methoxycarbonyl-5-(N-phenylformimidoyl)-2,4,6-triphenyl-2,5-dihydro-1,2,3-triazine (5MPFH-TDT) and its conformers are shown in Figure 18.

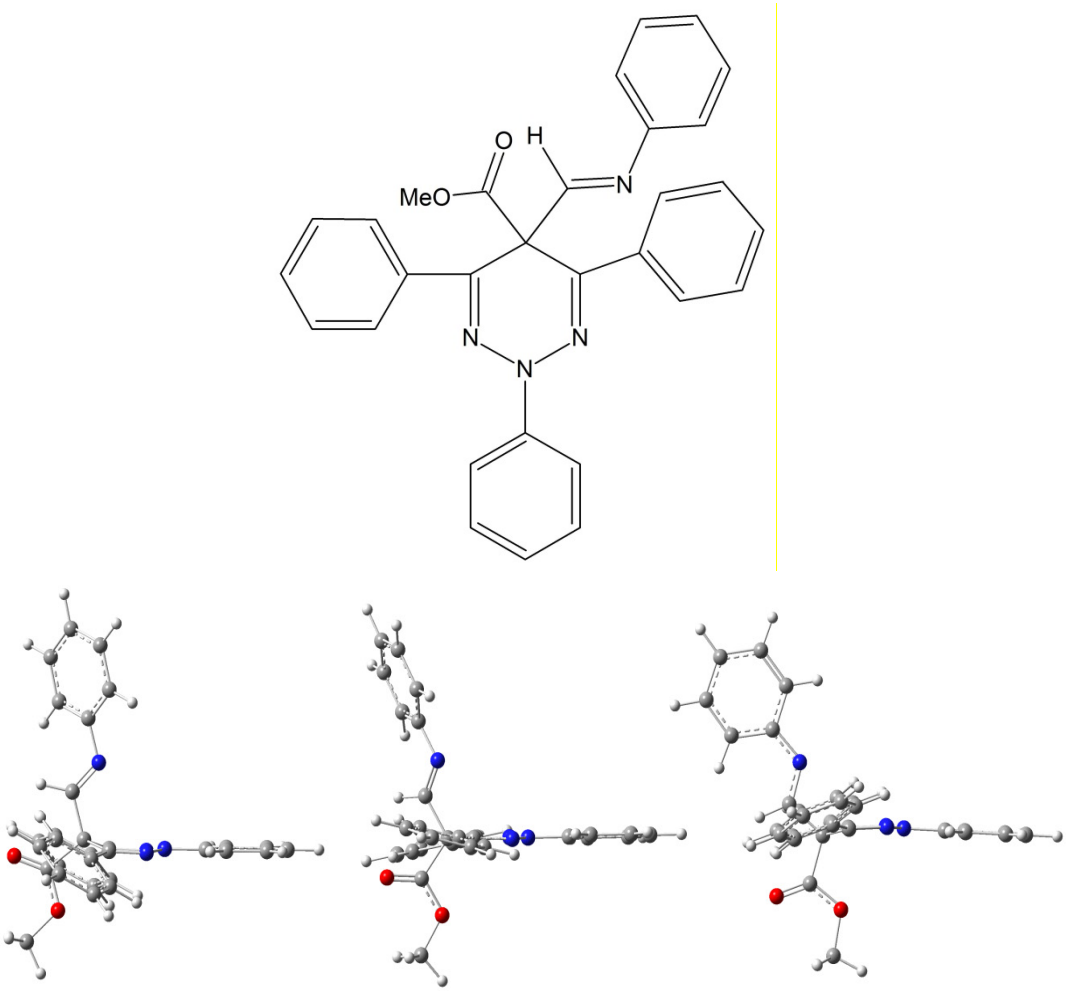

Figure 18: Structure of 5MPFH-TDT (above) and a side view of 5MPFH-TDT conformers: g0, g1, and g2 (below, left to right).

St. Mart *et al.* showed that these fluorophores exhibit exceptional photostability, and solvatochromism studies indicated that they are fairly insensitive to solvent polarity [78, 79]. Furthermore, dissolution of 5MPFH-TDT in methanol and deuterated methanol did not produce any band shifts in the UV-visible spectrum indicating that hydrogen bonding was not having any significant effect on the ground state. The

effect of substitution at the 4-position of the upper and lower phenyl rings was investigated using 5MPFH-TDT-Cl and 5MPFH-TDT-Br derivatives. They had very similar emission band properties (λ_{max}, FWHM, band area) as 5MPFH-TDT indicating that the molecular energy levels are unaffected by substitution at these positions.

Time-dependent density functional theory (TD-DFT) modelling, carried out by Professor Luke Burke, was used to resolve the photophysical behaviour of the triazine. Modelling was carried out on 5MPFH-TDT and a derivative in which the imine hydrogen was replaced by a methyl group. The g0, g1, and g2 conformers were optimised for S_0, S_1, and S_2 singlet states, respectively. For example, for the g0 structure S_0 was fixed and S_1, S_2, and S_3 are variable until local minima are determined. The same method was used to model the g1 and g2 structures. "*Using planarity of the dihydro-triazine ring as a motif, the three states for both 5MPFH-TDT and Me-5MPFH-TDT took the following forms: (g0) an envelope conformation with the ester equatorial and the imine axial giving a pseudo-plane of symmetry through the triazine; (g1) a flat ring with a coplanar N_2-phenyl and twisted C-4 and C-6 phenyls giving a pseudo-C_2 axis of symmetry; and (g2) an envelope with the ester axial and the imine equatorial giving total Cs symmetry"* [79]. There was only one stable envelope conformation for g0 and g2. In light of the modelling data and spectroscopic data for 310 nm and 400 nm excitation of 5MPFH-TDT and Me-5MPFH-TDT the photophysical model below was proposed.

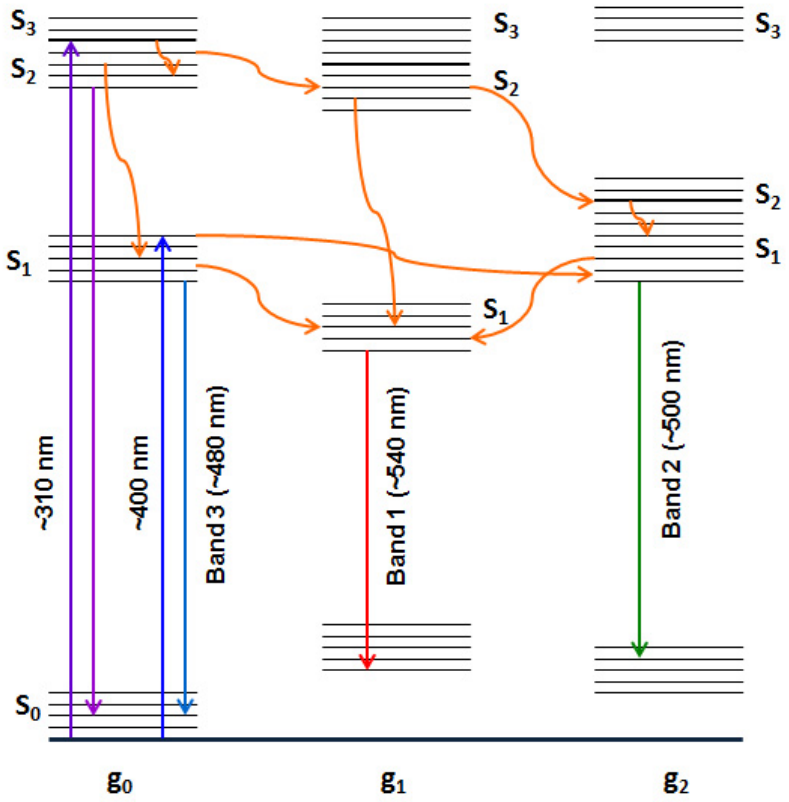

Figure 19: Photophysical model of 2,5-dihydro-1,2,3-triazine fluorescence.

It was found by comparison with the 5MPFH-TDT methyl derivative (a methyl group replaced the imine hydrogen) that the emission behaviour of the triazine was dramatically different. The major conformational difference between the g0 geometries of these two fluorophores was the alignment of the imine group. In the case of 5MPFH-TDT the C-H bond of the imine group is held within approximately 2° of the normal to the triazine pseudo-plane while the C-CH_3 group is twisted by approximately 70° to the normal. This rotation of the imine methyl group means the g1 and g2 states are vibrationally inaccessible from the g0 state. This explains the very different electronic properties reported for the 5MPFH-TDT methyl derivative compared to those of 5MPFH-TDT and emphasises the significance of the imine's position in space to the triazine's fluorescence.

Excitation of 5MPFH-TDT at 310 nm promotes the triazine to the S_3 or S_2 excited state of the g0 conformer. Since the predicted energies of S_3 and S_2 are very similar it is likely that internal conversion down to S_2 occurs. A very weak band at ~350 nm is

reported due to the transition between the S_2 excited state and the ground state but the emission is dominated by the band at ~520 nm. The excited molecule has five options for emission from the S_2 (g0) state: S_2 (g0) internally converts to S_1 (g0) and a photon is emitted due to the $S_{1\rightarrow0}$ (g0) transition; S_2 (g0) internally converts to S_2 (g1), and then internally converts down to the S_1 (g2) lowest energy level, followed by $S_{1\rightarrow0}$ (g2) emission. There are three pathways for emission corresponding to the long wavelength emission band: IC from S_2 (g0) down into the S_1 (g0) state occurs followed by IC across into S_1 (g1) followed by $S_{1\rightarrow0}$ (g1) emission; S_2 (g0) can internally convert to S_2 (g1) and then internally convert down to the lowest energy level of S_1 (g1) followed by $S_{1\rightarrow0}$ (g1) emission; IC from S_2 (g0) to S_2 (g1) occurs followed by IC down to the S_1 (g2) lowest energy level. Cross over into the lower energy S_1 (g1) state occurs to produce the third pathway for $S_{1\rightarrow0}$ (g1) emission.

Excitation at 400 nm is thought to promote 5MPFH-TDT from the ground state to the S_1 (g0) state. Since the S_1 (g1) and S_1 (g2) states are very close in energy there should be significant overlap of the vibronic bands and high rates of internal conversion. There are four options for emission after 400 nm excitation: S_1 (g0) vibrationally relaxes down to the lowest vibrational level and a photon is emitted due to the $S_{1\rightarrow0}$ (g0) transition. Since 400 nm is sufficient to promote 5MPFH-TDT to the upper vibrational levels of S_1 (g0) it is possible for IC to S_1 (g2) to occur followed by the $S_{1\rightarrow0}$ (g2) transition. S_1 (g0) may also internally convert to S_1 (g1) and return to the ground state with the emission of a photon. Finally, IC may also occur from S_1 (g2) to S_1 (g1) to produce a second pathway for g1 emission. Further details about the elucidation of the photophysical model are available in reference [80].

Surfactants and micelles

A surfactant is defined as a substance that lowers the surface tension of the medium in which it is dissolved [6]. Above a particular concentration point, called the critical micelle concentration (CMC), 50−100 surfactant molecules dynamically and spontaneously associate to form aggregates known as micelles [81]. The CMC is generally determined experimentally by measuring a particular physical parameter (surface tension [82], molar conductivity [83], fluorescence measurements [84]) as a function of concentration and determining the inflection point of the plot. In reality, the formation of a micellar solution occurs over a narrow range of concentration rather than a fixed point. The size of the range will vary depending on the physical parameter used to quantify the CMC. Dhar *et al.* determined the CMC of a number of Triton-X reverse micelles[4] in chloroform using three different techniques: absorption spectroscopy, fluorescence emission spectroscopy, and NMR. In the case of TX-114, CMCs of 1.89 mM, 1.77 mM, and 1.62 mM were determined by absorbance, fluorescence, and NMR techniques, respectively [85].

[4] In a reverse micelle the hydrophilic moiety of the surfactant is directed into the core of the micelle and the hydrophobic moiety is directed out into the bulk solution.

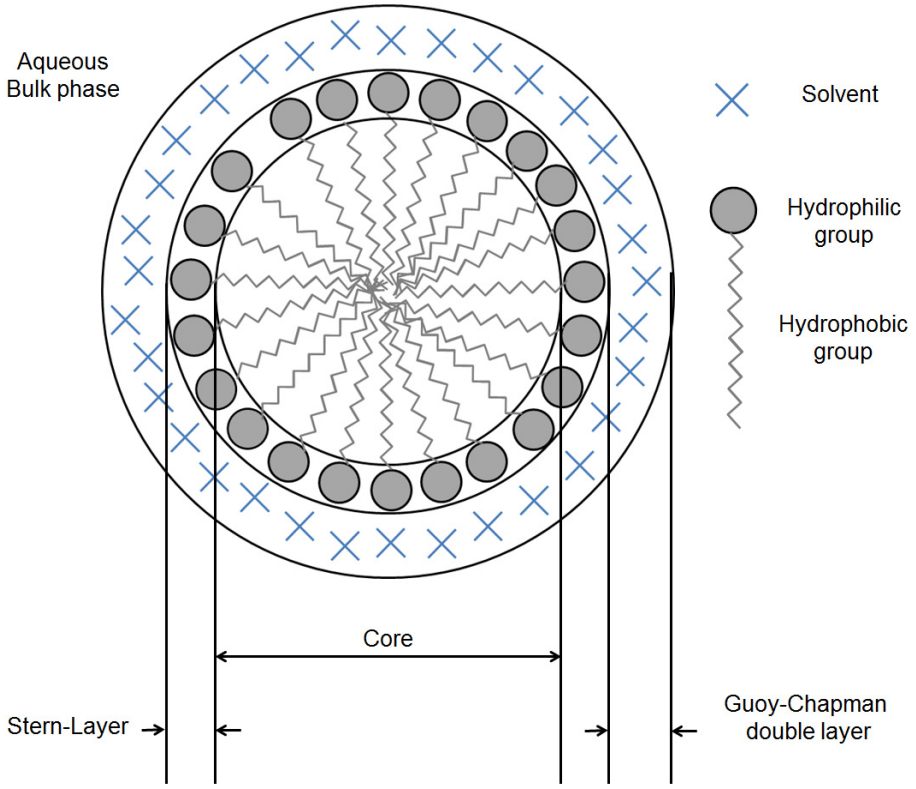

Figure 20: A surfactant is composed of a hydrophilic and a hydrophobic domain. When a micelle forms in aqueous solution the hydrophobic moiety is directed into the core of the micelle and the hydrophilic moiety is directed out into the bulk solution. The shell of the micelle, or the polar/charged component, is called the Stern layer, if the micelle is ionic, or the palisade layer, if the micelle is non-ionic.

A surfactant which can form a micelle consists of a hydrophobic and hydrophilic region. The hydrophilic region of the surfactant may be anionic, cationic, or non-ionic. The shell of the micelle, or the polar/charged component, is called the Stern layer, if the micelle is ionic, or the palisade layer, if the micelle is non-ionic. The non-polar moiety of the compound resides on the inside of the micelle while the polar moiety is directed out into the surrounding aqueous environment [86]. In this way, a species which is sparingly soluble in the bulk phase may be solubilised by the micelle. Micelle formation is thought to be driven by three intermolecular interactions: hydrophobic repulsion between the hydrocarbon chains and the aqueous environment, charge repulsion between the ionic head groups (if the surfactant is in fact ionic), and the Van der Waals attraction between the alkyl chains. A number of micelle

geometries have been observed, including ellipsoidal, cylindrical, and laminar, though spherical and globular are most common [87, 88].

Micelles are of particular interest in biomimetic studies since some of their properties—polarity, viscosity (η), permittivity (ε), refractive index (n), hydrogen bonding (α/β)— are comparable to those of proteins and membranes found in biological systems [81, 89]. Fluorophores are ideal candidates for the investigation of these environments since they can report on the micelle's microenvironment and fluorescence lifetime studies can reveal processes occurring at the nanosecond timescale. When a fluorophore interacts with a micelle it is expected that its emission properties will be altered in some way. This is because it is experiencing a different microenvironment from the bulk solution. The microheterogeneity of the micelle means the position of the fluorophore within the micelle must also be considered [90]. If the fluorophore resides between the hydrophobic tail and the hydrophilic head group it may be affected by any charged groups in the vicinity. Furthermore, if the fluorophore is fully encapsulated within the interior of the micelle the penetration depth will have a bearing on the viscosity experienced. The penetration depth is often a consequence of the thickness of the Stern/palisade layer. Panda *et al.* attribute the greater fluorescence intensity enhancement of epicocconone in TX-100 compared to SDS to the microviscosity of its location within the micelles. TX-100 has a much larger palisade layer (25 Å) than the Stern layer of SDS (6–9 Å). Therefore, the hydrophobic region of the TX-100 micelle is more compact than that of SDS and has a higher microviscosity [91].

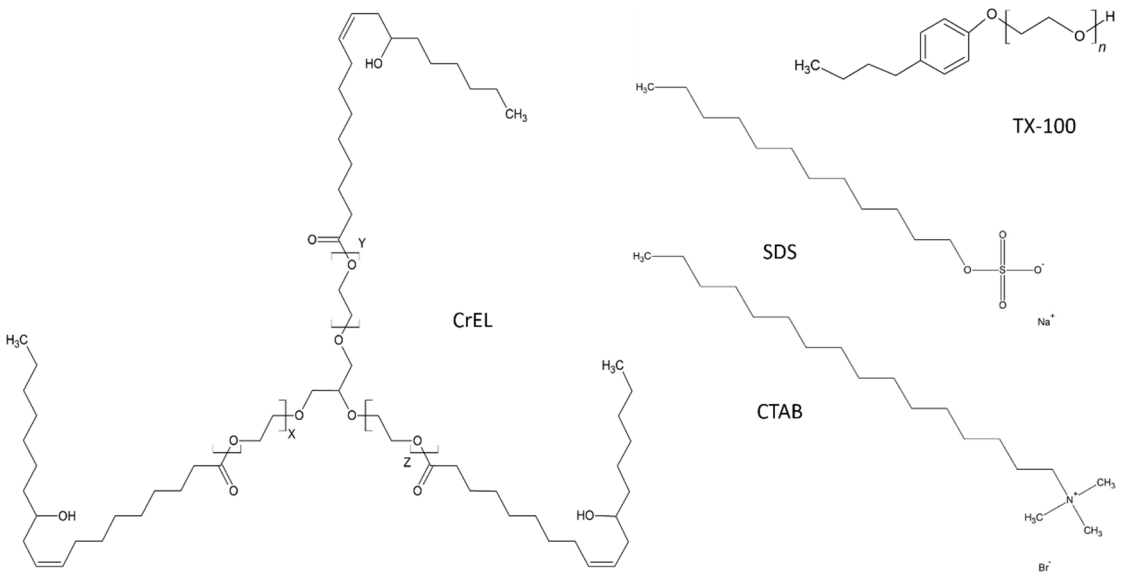

Figure 21: Chemical structures of Cremophor EL (CrEL), Triton X-100 (TX-100), sodium dodecyl sulfate (SDS), and cetyltrimethylammonium bromide (CTAB).

Zana found that at a given temperature, the microviscosity of a micelle increases with alkyl chain length, irrespective of the nature of the surfactant [92]. This study was carried out using the viscosity sensitive fluorophore 1,3-dipyrenylpropane (P3P). Zana also found that the microviscosity was dependent on the chemical structure of the surfactant: conventional surfactants consist of a long hydrophobic chain and a hydrophilic head group; bolaform surfactants have a hydrophobic chain that is terminated at either end by hydrophilic groups; dimeric/gemini surfactants consist of at least two conventional surfactant units joined by a spacer group either close to or at the hydrophilic head group. Zana investigated how the microviscosity of cationic surfactants that contained the same chain length and head group varied with surfactant structure. Conventional surfactants were found to have the lowest microviscosity while dimeric surfactants were found to have the greatest [92, 93].

The position of a fluorophore within a micelle depends on the relative hydrophobic or hydrophilic nature of the fluorophore itself [94]. For example, the hydrophobic moiety of the fluorophore interacts with the hydrocarbon chain of the micelle interior while the polar moiety is directed out toward the head group of the surfactant. Furthermore, like a monomer of the surfactant, the fluorophore is not fixed in the micelle; it is in constant dynamic equilibrium with the bulk phase. For surfactant

monomers the dissociation rate constant, which is dependent on the length of the hydrocarbon chains, is of the order of 10^5–10^9 s^{-1} and the association rate constant is near diffusion controlled; 10^8–10^9 M^{-1} s^{-1}. Since the amphiphilic character of the fluorophore may be quite different to the surfactant monomer, its dissociation and association rate constants may also be quite different. Almgren *et al.*, [94], proposed a method to quantify the affinity of a fluorophore for a micelle unit by calculating a value for the binding constant, K_{eq}, for the fluorophore-micelle interaction. According to this method,

$$\frac{(I_\infty - I_0)}{(I_t - I_0)} = 1 + \frac{1}{K_{eq}[M]} \qquad \textbf{Equation 24}$$

where, I_∞, I_0, and I_t are the fluorescence intensities of the fluorophore under conditions of complete micellisation, in the absence of surfactant, and at intermediate surfactant concentrations, respectively. The concentration of micelles, [M], is calculated from the following equation:

$$[M] = \frac{(S - CMC)}{N} \qquad \textbf{Equation 25}$$

where S is the surfactant concentration and N is the aggregation number. Almgren specifically investigated the kinetics of solubilisation of neutral arenes in ionic micelles. Binding constants of 2.7×10^7 M^{-1} and 9.1×10^4 M^{-1} were reported for perylene and naphthalene, respectively, in CTAB micelles. Pyrene interacts with CTAB micelles with a binding constant of 102.0×10^5 M, as reported by Almgren, while Piñeiro *et al.* report a binding constant of 33.0×10^5 M^{-1} for pyrene in TX-100 micelles.

1.7 Fluorophore labelling of proteins

The ability of a living system to assemble and organise a vast array of molecular components, each with a defined form and purpose, has long been a cornerstone of modern science. A wide range of experimental techniques have been employed to determine how these complex molecules self-assemble and behave *in-vitro* and *in-vivo*. One of the most highly investigated self-assembly processes is the folding of proteins into their three-dimensional structures [95]. A single living organism may

contain as many as 50,000 varieties of protein, each with a unique sequence, structure, and folding mechanism [96]. All of these steps must occur with accuracy and precision if the biological function of the organism is to be maintained. A better understanding of how these processes come to pass gives us an insight into the evolutionary development of the organism as well as making it easier to determine the origin of an inaccuracy when the organism does not function as it should [95].

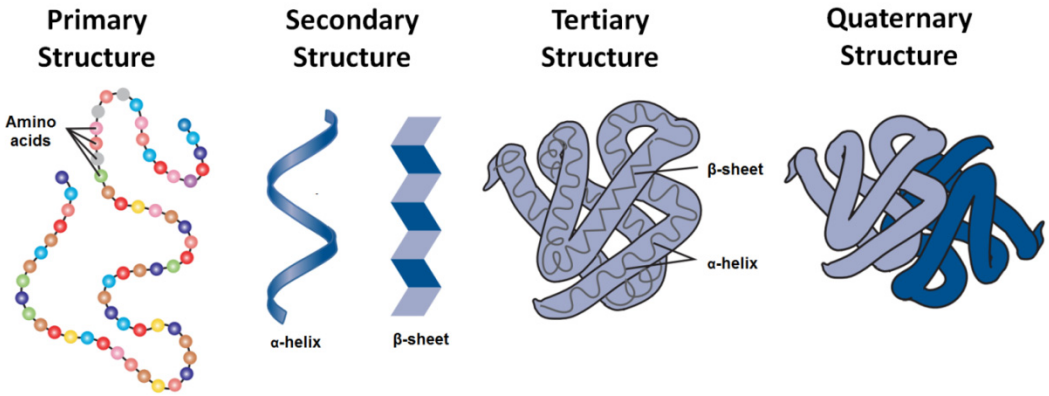

Figure 22: Primary protein structure is the sequence of amino acid residues in the polypeptide chain; secondary protein structure is the regular arrangement of regions of the polypeptide chain (alpha helices and beta sheets); tertiary protein structure is the arrangement of alpha helices and beta sheets in space; quaternary protein structure is the interaction of a protein molecule with other proteins to form a macromolecular assembly. Adapted from reference [97].

The structure of a protein is defined by four stages or levels. A protein's primary structure is the sequence of amino acid residues, of which there are twenty, joined together by polypeptide bonds. Its secondary structure forms when particular regions of the polypeptide develop into alpha-helices or beta-strands. Its tertiary structure is the arrangement of the alpha-helices and beta-strands in three-dimensional space. Finally, a protein's quaternary structure is the defined organisation of two or more protein molecules into a macrostructure that is able to carry out a specific biological function [6, 98]. A number of experimental techniques have been developed to measure and observe how proteins change from a random coiled sequence of amino acid residues into their functional native state. It was Perutz and Kendrew who developed the first static images of protein molecules, namely haemoglobin and myoglobin, by X-ray crystallography [99-101]. Multi-dimensional NMR spectroscopy is another standard technique employed to determine the molecular

structure of a protein molecule. Unfolded and partially-unfolded intermediates of a protein may be analysed and interpreted from the NMR spectra [102].

Equilibrium protein-folding studies generally present the denaturation of a protein as a two-state transition in which the protein is considered to exist in its native and unfolded forms only. This simplification arose due to the insensitivity of chosen experimental parameters to possible structural heterogeneity [103]. More recent theoretical and experimental progress indicates that various intermediates may exist before the final native conformation of the protein is achieved. It is believed that the energy landscape of protein folding is funnel-shaped, where-by the native protein is represented in the position of lowest free-energy. The protein's descent along the funnel—from the unfolded state to its native form—may consist of kinetic traps that lead to the population of partially folded, or misfolded sub-states. These sub-states may form in the course of reaching the native state directly or may represent a road-block of sorts whereby a reversal of protein folding must take place before further progress can be made [104]. Therefore, an ensemble of protein structure intermediates may exist *en route* to the native state. The detection of these heterogeneous sequences requires analytical techniques that avoid the inherent averaging of standard experimental methods [105].

Fluorescence spectroscopy is an important technique for the analysis of protein structure and dynamics due to its high-sensitivity and specificity. Fluorescence sampling techniques may be carried out *in-vivo* meaning the data is representative of the protein's behaviour in its native environment. Furthermore, since the time scale of fluorescence processes is on the order of nanoseconds many processes that are time averaged by other techniques can be resolved [106]. Intrinsic protein fluorescence[5], a naturally occurring phenomenon within these macromolecules, has proven useful for a myriad of biochemical applications. It is the three aromatic amino acid residues—tryptophan, tyrosine, and phenylalanine—that are responsible for most protein fluorescence. The excitation and fluorescence emission of all three residues occur in the ultraviolet spectral range. Energy absorbed by phenylalanine and tyrosine may be

[5] This property distinguishes proteins from other biopolymers, such as lipids and saccharides, which are non-fluorescent, and is superior to the intrinsic fluorescence possessed by DNA, which is much too weak to be considered useful [18].

transferred to a tryptophan residue in the same protein, if they are in close enough proximity, thus enhancing the fluorescence emission band of tryptophan. This along with its greater extinction coefficient explains why tryptophan emission dominates some protein fluorescence [7]. However, tryptophan fluorescence is often difficult to decipher, for example, multi-exponential lifetime decays are measured for proteins that contain only a single tryptophan residue. The number of decays therefore, cannot be related to the number of tryptophan residues [7].

A whole range of fluorescence techniques may be employed to investigate protein conformation and dynamics. Fluorescence anisotropy measurements are particularly valuable in studies of protein folding. This may be monitored by the intrinsic fluorescence of the protein or extrinsically using a fluorophore. FRET is also commonly employed to detect protein conformational changes. By labelling a protein with a donor and an acceptor fluorophore any conformational changes can be monitored on the nanosecond timescale.

Here we investigate the photophysical behaviour of 5MPFH-TDT in micelles and proteins to determine its viability as a probe or reporter of colloidal assemblies and biological molecules. The large Stokes shift, high quantum yield, and pronounced hydrophobicity of this fluorophore indicate that it may be suitable for these applications.

2 Materials and Methods

2.1 Materials

2.1.1 Fluorophores

The triazine fluorophores were obtained from Dr Dean St Mart of NUI Maynooth. These fluorophores were synthesised as previously described [1, 107], and were used as received without any further purification. The chemical structures of 5MPFH-TDT can be seen in Figure 18. Two methods were used to make up stock solutions of 5MPFH-TDT.

Method 1: 0.04725 g (10^{-4} moles) of the fluorophore were weighed out and dissolved in 10 ml of dichloromethane (DCM) to produce a 10^{-2} M solution. This was transferred to a 15 ml glass tube for storage in the –20 °C freezer. 0.1 ml of the 5MPFH-TDT/DCM solution was extracted and concentrated down to dryness. This was then made up to a volume of 1 ml with EtOH to produce a working solution with a concentration of 10^{-3} M.

Method 2: 0.0118 g (2.497×10^{-5} moles) of the fluorophore were weighed out and dissolved in a round-bottomed flask in a few millilitres of DCM. The DCM was evaporated by first placing the solution on a rotary evaporator and then leaving it under vacuum. The fluorophore was then re-dissolved in 25 ml of EtOH to produce a working solution with a concentration of 10^{-3} M.

Stock solutions of sulforhodamine 101 free acid (Fluka) and tetramethylrhodamine isothiocyanate, mixed isomers (Sigma-Aldrich), were made up in methanol and DMSO, respectively, to a concentration of 1 mM and were stored in the –20 °C freezer.

2.1.2 Buffers

Studies that required the use of buffer solutions were carried out using phosphate buffered saline (PBS) (Sigma-Aldrich), 3-(N-morpholino)propanesulfonic acid (MOPS) (Sigma, ≥99.5%), 4-(2-hydroxyethyl)piperazine-1-ethanesulfonic acid (HEPES) (Sigma, ≥99.5%). These buffers solutions were made up to a concentration

of 10 mM and the pH was adjusted to 7.4 using sodium hydroxide (NaOH) when required. Mixtures of sodium dihydrogen phosphate monohydrate, (98+% ACS reagent) and sodium phosphate dibasic heptahydrate (ACS Reagent 98.0−102.0%) were used for the protein labelling studies. Phosphate buffer was used as it is useful over much of the pH range due to its three pK_a values at 2.15, 7.2, and 12.33. 200 mM stock solutions of $Na_2HPO_4.7H_2O$ and $NaH_2PO_4.H_2O$ were made up by dissolving 13.4035 g and 6.8995 g, respectively, in 250 ml of high-purity water (HPW). A 50 ml volume of buffer mixture was measured out in different proportions to produce solutions of varying pH. Each buffer was made up to a volume of 100 ml to produce a buffer concentration of 100 mM. A constant ionic strength of 303 mM was maintained using sodium chloride (NaCl) as the background electrolyte. In order to produce buffer solutions of pH 9 and 10, only Na_2HPO_4 was required. A 100 mM stock solution of Na_2HPO_4 was made up by dissolving 2.6807 g in 80 ml. An appropriate amount of a 1 M solution of NaOH was added to produce the desired pH before making up to 100 ml.

Table 2: Phosphate buffer composition for a number of pH values.

pH	200 mM Na_2HPO_4 (ml)	200 mM NaH_2PO_4 (ml)	1 M NaCl (ml)
6	6.15	43.85	17.91
7	30.50	19.50	8.10
8	47.35	2.65	1.36

Solutions of variable ionic strength were made up at pH 9 using Na_2HPO_4. Sodium chloride was used as the background electrolyte. A 10 mM stock solution of Na_2HPO_4 has an ionic strength of 30 mM. This was made up by dissolving 0.2681 g in 100 ml of HPW. An appropriate amount of a 1 M solution of NaCl was added to subsequent samples to produce the desired ionic strength.

Table 3: Composition of phosphate buffer solutions of variable ionic strength.

Ionic Strength (mM)	1 M NaCl (ml)
30	0
50	2
100	7
150	12
200	17
250	22
300	27

2.1.3 Viscosity and microviscosity effects

Mixtures of ethylene glycol (EthGly) and EtOH were used to produce samples of varying viscosity. Sample volumes of 2 ml were made up. 20 µl of the 5MPFH-TDT/EtOH solution were concentrated down to dryness and 2 ml of an EtOH-EthGly solution of specified ratio was used to re-dissolve the fluorophore. This ratio determined the viscosity of the solution. Solvation was achieved using the vortex.

Table 4: Viscosity values of EtOH/EthGly mixtures.

w1	w2	$\ln\eta mix = \sum_{i}^{2} w\,i.\ln\eta i$	ηmix (mPa.s)
0.1	0.9	2.508	12.277
0.3	0.7	1.965	7.138
0.5	0.5	1.423	4.151
0.7	0.3	0.881	2.413
0.9	0.1	0.339	1.403

The fundamental anisotropy was determined by immobilising 5MPFH-TDT in a solid polymer thin-film. A 10% PMMA solution in DCM was made up. A 10^{-4} M solution of 5MPFH-TDT in the solution of PMMA was made up and this was used to cast the thin-films on quartz slides. The slides were left to dry under vacuum overnight. The fluorescence anisotropy was determined using a front-facing sampling orientation. In

order to eliminate any scatter from the detected emission an excitation wavelength of 370 nm was used while the anisotropy was detected at an emission wavelength of 470 nm. Since this excitation wavelength results in S_0 to S_1 excitation the anisotropy detected should match that which would be obtained using a 405 nm excitation wavelength. A fundamental anisotropy value of 0.3697 (±0.0012) was obtained. υ_h was determined as 403.8 $Å^3$ using the freeware programme Chimera 1.10.2. The rotational correlation time was determined for each emission wavelength. The corresponding microviscosity was subsequently calculated.

2.1.4 Micelles

20 µl of a 5MPFH-TDT stock solution were used to make up a single sample. The 5MPFH-TDT concentration was confirmed using a Beer-Lambert plot (λ_{abs} = 400 nm) of 5MPFH-TDT–surfactant solutions of variable fluorophore concentration (Table 5). Stock solutions of surfactant were made up in HPW prior to testing. Stock solutions of Cremophor EL (CrEL), Triton X-100 (TX100), sodium dodecyl sulfate (SDS), and cetyltrimethylammonium bromide (CTAB), (Sigma-Aldrich), had concentration values of 8 mM, 4 mM, 200 mM and 10 mM respectively. Sample volumes were made up to 2 ml.

Table 5: 5MPFH-TDT concentration calculated from Beer-Lambert plots for λ_{abs} 400 nm.

Surfactant	Absorbance	[5MPFH-TDT] (M)
CrEL	0.0867	1.65×10^{-5}
TX100	0.1063	2.05×10^{-5}
CTAB	0.1150	1.93×10^{-5}
SDS	0.0853	2.15×10^{-5}

Table 6: Surfactant concentration values and 5MPFH-TDT–surfactant ratio values.

	Stock Volume (µl)	Concentration (M)	5MPFH-TDT–CrEL Ratio
CrEL			
	2.5	1×10^{-5}	0.6
	5.0	2×10^{-5}	1.2
	7.5	3×10^{-5}	1.8
	10.0	4×10^{-5}	2.4
	12.5	5×10^{-5}	3.0
	25	1×10^{-4}	6.1
	50	2×10^{-4}	12.1
	100	4×10^{-4}	24.2
	150	6×10^{-4}	36.4
	200	8×10^{-4}	48.5
TX-100			
	50	1×10^{-4}	4.9
	100	2×10^{-4}	9.8
	200	4×10^{-4}	19.5
	300	6×10^{-4}	29.3
	400	8×10^{-4}	39.0
	500	1×10^{-3}	48.8
SDS			
	25	2.5×10^{-3}	116.3
	50	5.0×10^{-3}	232.6
	75	7.5×10^{-3}	348.8
	82	8.2×10^{-3}	381.4
	100	10.0×10^{-3}	465.1
	150	15.0×10^{-3}	697.7
	200	20.0×10^{-3}	930.2
CTAB			
	140	0.7×10^{-3}	36.3
	160	0.8×10^{-3}	41.5
	180	0.9×10^{-3}	46.6
	200	1.0×10^{-3}	51.8
	400	2.0×10^{-3}	103.6
	600	3.0×10^{-3}	155.4
	1000	5.0×10^{-3}	259.1
	1800	9.0×10^{-3}	466.3

2.1.5 Refractive index measurements of micelle solutions

The refractive index of each of the surfactant solutions was determined at a number of concentration values using an Abbe refractomer. A linear relationship was obtained between refractive index and surfactant concentration. The refractive index of the micelles was determined by extrapolating the line of best fit to a concentration value of 100%. All measurements were carried out in triplicate.

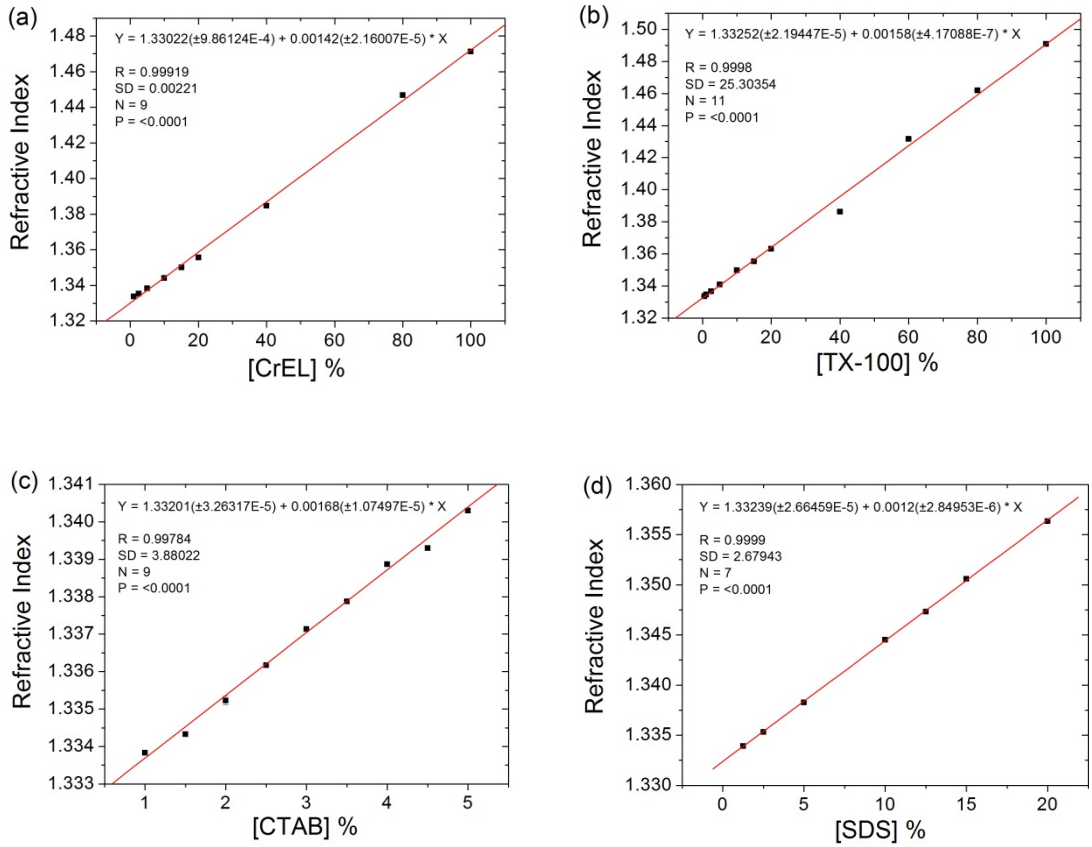

Figure 23: Refractive index versus concentration for solutions of (a) CrEL, (b) TX-100, (c) CTAB, and (d) SDS.

2.1.7 Protein Solutions

Bovine serum albumin (BSA) of purity ≥ 99% was purchased from Sigma (catalogue no. A7638) and was used without further purification. Protein solutions were made up as needed in phosphate buffer and kept in the refrigerator (4 °C) for no more than a week. Labelling of BSA with 5MPFH-TDT was carried out by adding a solution of the triazine in ethanol to the protein solution with stirring. The concentration of ethanol in the BSA–5MPFH-TDT solutions did not exceed 1%. The protein and fluorophore were left to interact at room temperature, in the dark, for several hours. Protein and fluorophore labelling concentrations are cited in Sections 6.2, and 6.3, and Appendices A.5, A.6, and A.7.

2.1.8 Removal of free fluorophore from BSA–5MPFH-TDT solutions

Free triazine was removed from the samples by passing the solutions through a Sephadex 50 size-exclusion column[6]. The column was made up by dissolving 2 g of Sephadex in 50 ml of HPW and sonicating this mixture for one minute or until the solution was homogeneous. Sephadex 50 separates molecules with a molecular weight exceeding 30,000 Da from molecules with a molecular weight less than 1,500 Da. Blue dextran (MW ~2000 kDa) and riboflavin (MW 376.63 Da) were employed to determine the void volume and elution volume of the column, respectively. The column was washed three times with a 100 mM phosphate buffer of pH 9 before loading the column with the sample to be separated. Unlabelled BSA was also passed through the column and the fractions in which BSA was present were recorded. The sample volume passed through the column was kept at 2.5% of the column volume to achieve the desired separation resolution. A 7 ml fraction was collected from the column and divided into seven eppendorfs. Following this they were placed in the concentrator for 90 minutes until a volume of 1 ml remained. The sample was finally filtered using 0.2 μm Nalgene™ syringe filters and placed in the –20 °C freezer.

[6] Gel filtration based on Sephadex enables the separation of large biomolecules that are above the exclusion limit of the medium from contaminants such as salts, fluorophores, and radioactive labels. It is prepared by cross-linking dextran with epichlorohydrin.

2.2 Instrumentation

All UV-Visible and steady-state fluorescence emission measurements were carried out using 4 mm × 10 mm quartz cuvettes (Lightpath Optical (UK) Ltd) while fluorescence lifetime measurements were carried out using front-surface excitation geometry in 1 mm pathlength quartz cuvettes.

2.2.1 UV-Visible Measurements

Absorption spectra were recorded using a Shimadzu UV-1601 spectrometer using a data interval of 0.1 nm and a pathlength of 10 mm. The pathlength was reduced to 4 mm when using the fluorophore SR101 in a FRET investigation due its large molar absorptivity coefficient. All measurements were carried out at 25 °C.

2.2.2 Steady-State Fluorescence Emission Measurements

Fluorescence emission spectra and anisotropy values were recorded using a Perkin Elmer LS50B spectrometer. It is fitted with a red-sensitive detector for the collection of emission data above 630 nm, above which the standard photomultiplier tube has little or no sensitivity. A polariser accessory (Part number L2250100), consisting of two filter wheels fitted with polarising elements were employed for all anisotropy measurements. The excitation and emission pathlengths were 4 mm and 10 mm respectively. All measurements were carried out at 25 °C. The emission spectra were normalised and converted from the nanometre to wavenumber scale and a three-band Gaussian fit was performed with Origin, ver. 7.0. Bands 1 (g1), 2 (g2), and 3 (g0) correspond to the long, intermediate, and short wavelength emission bands, respectively.

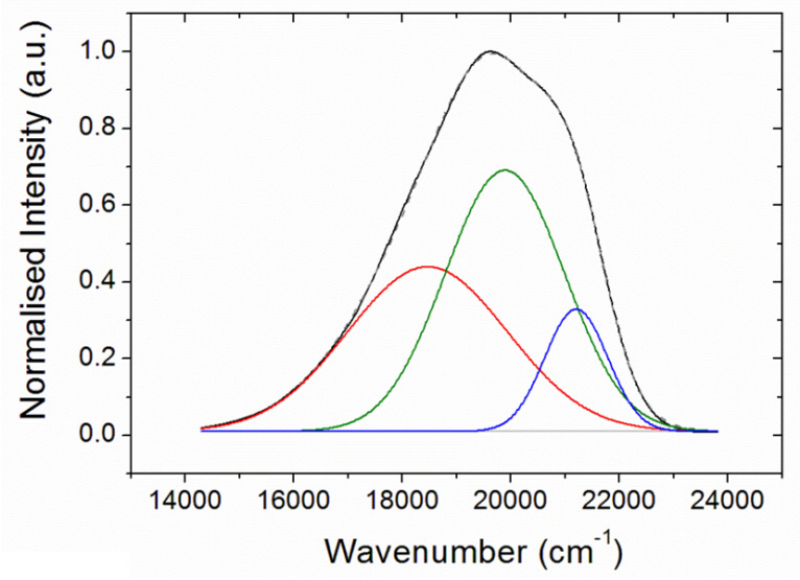

Figure 24: Band-fitted normalised emission spectrum of 5MPFH-TDT.

2.2.3 Fluorescence Lifetime Measurements

Fluorescence lifetime values were obtained using the PicoQuant FluoTime 200 system. Two sources of excitation were utilised throughout this study. A pulsed laser diode (PicoQuant GmbH) with a wavelength range of 390–420 nm was used to excite the 5MPFH-TDT fluorophore. The laser was run at 100% of maximum power, which corresponded to 431 μW at the sample. A 405 nm band-pass filter was placed in the path of the excitation beam to remove any spurious light. Fluorescence emission was detected over a spectral range of 470−570 nm. A 405 nm stop-line filter was placed in the emission pathway to prevent any scattered excitation light from reaching the detector. A sub-nanosecond pulsed LED (PicoQuant GmbH) with a wavelength centre at 295 nm was used to probe BSA fluorescence. In this case, fluorescence emission was recorded at 350 nm. A UV passing filter was fitted along the emission axis with a range of 325–385 nm to reduce the detection of any long wavelength emission. In both cases a repetition frequency of 10 MHz, delivered by the PDL 800-B (PicoQuant) driver, was selected.

A Sciencetech Model 9030 monochromator was used for emission wavelength selection. Settings for the zero cross level, constant fraction discriminator, and sync level were particular to the sample being tested. The FluoTime 200 spectrometer was connected to a nanosecond delay box (FAST ComTec, model 7800-7), which was used to compensate for any timing delays between the different channels. Samples

were contained in a 1 mm quartz cuvette placed at a 45° angle to the excitation beam. The fluorescence emission was collected at right angles to the excitation. Excitation and emission intensity were controlled using an adjustable iris and a combination of neutral density (ND) filters, respectively. Signal intensity, or the CFD rate, was always maintained at less than 1% of the excitation repetition rate. Data acquisition was controlled by TimeHarp 200 TCSPC software, and data was collected until there were either 20,000 or 10,000 counts in the channel of maximum intensity. It was recognised that this lower count rate could lead to greater uncertainty in the retrieved decay times. Fluorescence lifetimes were then extracted from the measured decay curves using FluoFit (ver. 4.1 PicoQuant).

The instrument response function (IRF) was generated by collecting the scattered light from a cuvette filled with EtOH or a solution of LUDOX® AS-40 colloidal silica. To ensure the system was in correct working order a standard solution of a fluorophore, with a mono-exponential decay and a λ_{ex} matching that of the excitation source, was tested. 8-Hydroxypyrene-1,3,6-trisulfonic acid (HPTS), with a concentration of 10^{-6} M, was used for 405 nm excitation. HPTS exhibits a mono-exponential lifetime of 5.4 ns. N-acetyl-L-Tryprophan Amide (NATA), with a concentration of 10^{-4} M and a mono-exponential lifetime of 2.98 ns, was used as the standard for 295 nm excitation.

3 Photophysical behaviour of 5MPFH-TDT in aqueous solutions

Since the overall objective of this research project was to employ 5MPFH-TDT as a label/reporter of protein molecules, an initial study of the triazine's photophysical behaviour in aqueous solutions was undertaken. However, the hydrophobicity of the triazine meant that the collection of reproducible data in simple aqueous solutions was impossible. The baseline scatter observed for the absorbance spectra of the triazine in buffer solutions indicated that the triazine may have been aggregating in aqueous solution (Figure 25). However, at the time there was no way to prove this hypothesis. Instead, the employment of surfactant solutions was considered as a means to learn more about the behaviour of the triazine in relatively simple aqueous solutions.

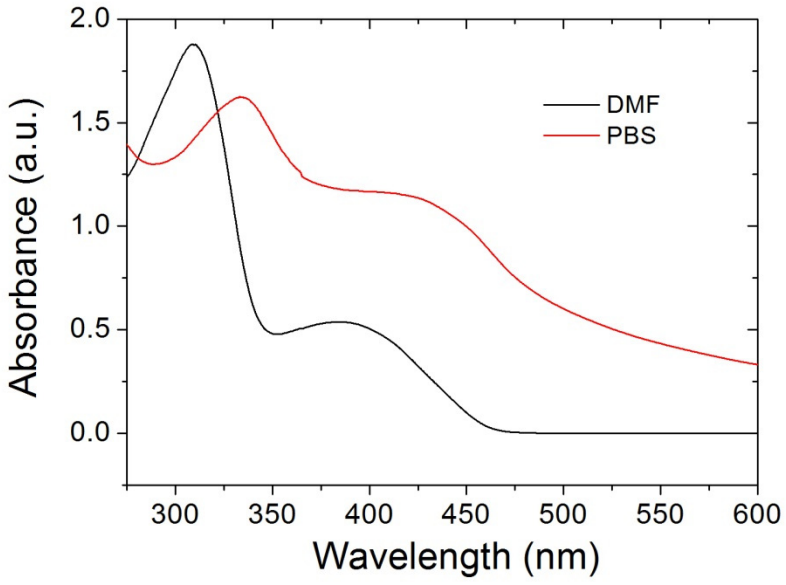

Figure 25: Absorbance spectra of 5MPFH-TDT (1×10^{-4} M) in DMF and PBS.

3.1 Absorbance and fluorescence emission properties of 5MPFH-TDT in aqueous solutions

A number of buffer solutions including HEPES, MOPS, and PBS were used in order to build up a reference data set of 5MPFH-TDT spectra, which could be compared with any subsequent protein labelling spectra (Figure 26). However, these measurements were not repeatable and large errors were recorded.

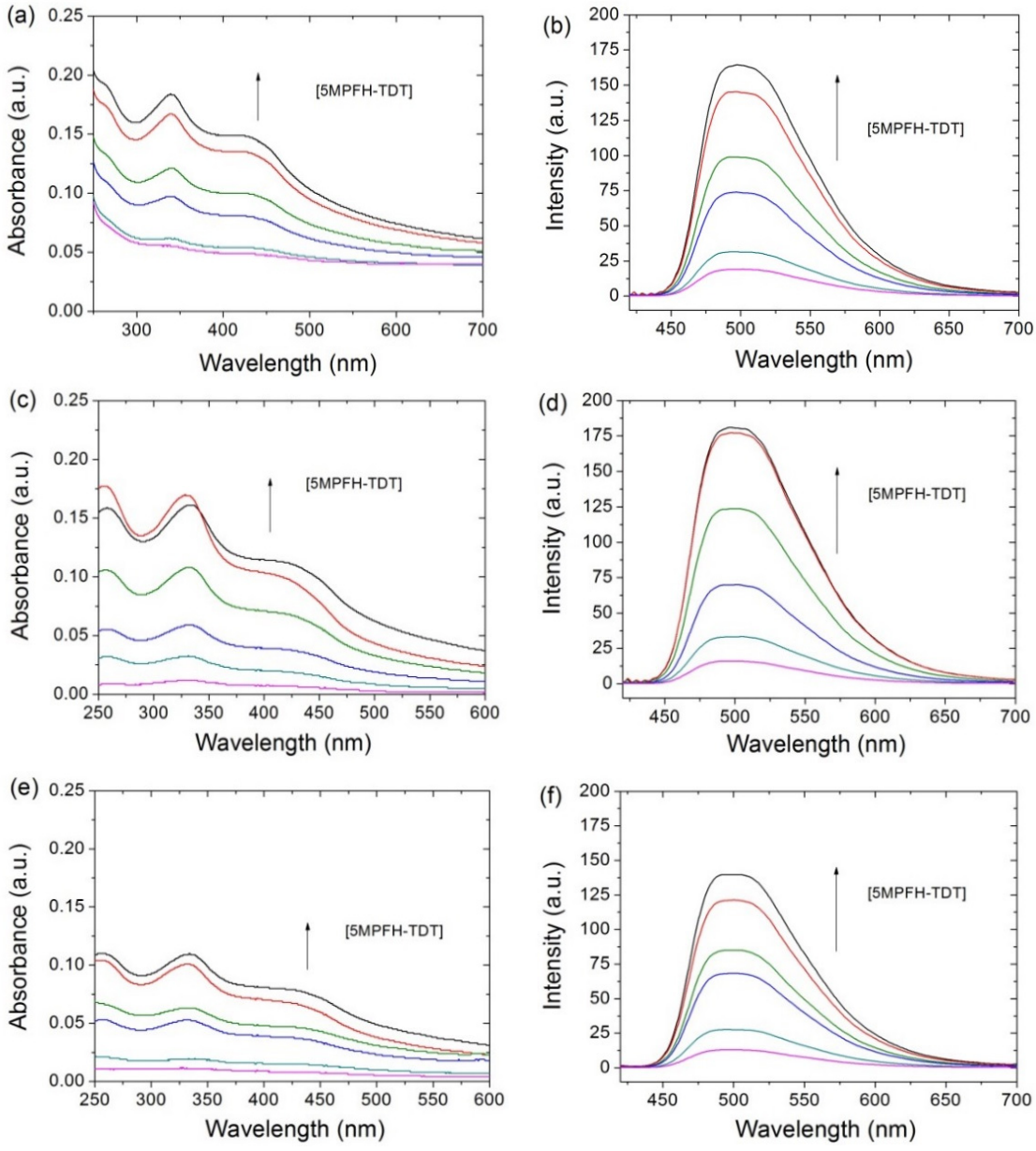

Figure 26: Absorbance and fluorescence emission spectra of 5MPFH-TDT in HEPES (a) and (b), MOPS (c) and (d), and PBS (e) and (f) buffer solutions. The concentration values of 5MPFH-TDT were 1 × 10^{-6} M, 2 × 10^{-6} M, 4 × 10^{-6} M, 6 × 10^{-6} M, 8 × 10^{-6} M, and 1 × 10^{-5} M. 1% DMSO was used as the co-solvent.

In the latter stages of this research project, a fluorescence correlation spectrometer was available to investigate the triazine's behaviour at the single molecule level. This investigation was carried out by Dr Dzmitry Melnikau. Fluorescence correlation spectroscopy (FCS) is a form of single molecule detection (SMD) that tracks freely diffusing molecules in solution. A very small volume, defined by a focused laser beam and a confocal aperture, is monitored and the intensity fluctuations that occur as a result of the translational diffusion of a fluorophore into the confocal volume are analysed [108]. The intensity at a particular time, F(t) is compared with the intensity at a slightly later time, F(t + τ) and the correlation between F(t) and F(t + τ) is determined for a range of decay times. The size and shape of the observed volume, which is an ellipsoid that is elongated along the optical axis, may be determined using a fluorescence standard of known diffusion coefficient. The correlation function for three-dimensional diffusion is given as,

$$G(\tau) = G(0)\left(1 + \frac{4D\tau}{s^2}\right)^{-1}\left(1 + \frac{4D\tau}{\mu^2}\right)^{-1/2} \qquad \textbf{Equation 26}$$

where D is the diffusion coefficient of the fluorophore, s is the ellipsoid radius and μ is the ellipsoid half-length.

The number of fluorophores in the observed volume (N) can also be determined from the autocorrelation function and the bulk fluorophore concentration ($\bar{C}$) can subsequently be determined. This is due to the relationship between N and the effective volume,

$$N = \bar{C}V_{eff} \qquad \textbf{Equation 27}$$

Solutions of CrEL, TX-100, and CTAB micellar solutions of varying concentration were used. The results of this study indicated that the triazine was forming large, bright aggregates at low surfactant concentrations. The fluorescence intensity of 5MPFH-TDT dropped consistently with decreasing surfactant concentration and at a surfactant concentration well below the CMC the fluorescence intensity of the triazine was at a minimum. This was to be expected as we observed this behaviour in the ensemble fluorescence data. Interestingly, as well as a drop in 5MPFH-TDT fluorescence intensity with decreasing surfactant concentration we also observed a significant drop in the apparent concentration of the triazine fluorophore. This coupled with the intermittent sharp peaks observed at the lowest surfactant concentration point indicated that large, bright aggregates of the triazine fluorophore were forming. This demonstrated that 5MPFH-TDT does not exist in its monomeric form in aqueous solution, which explains why it was difficult to obtain reproducible ensemble absorbance and fluorescence emission data for the triazine in the buffer solutions.

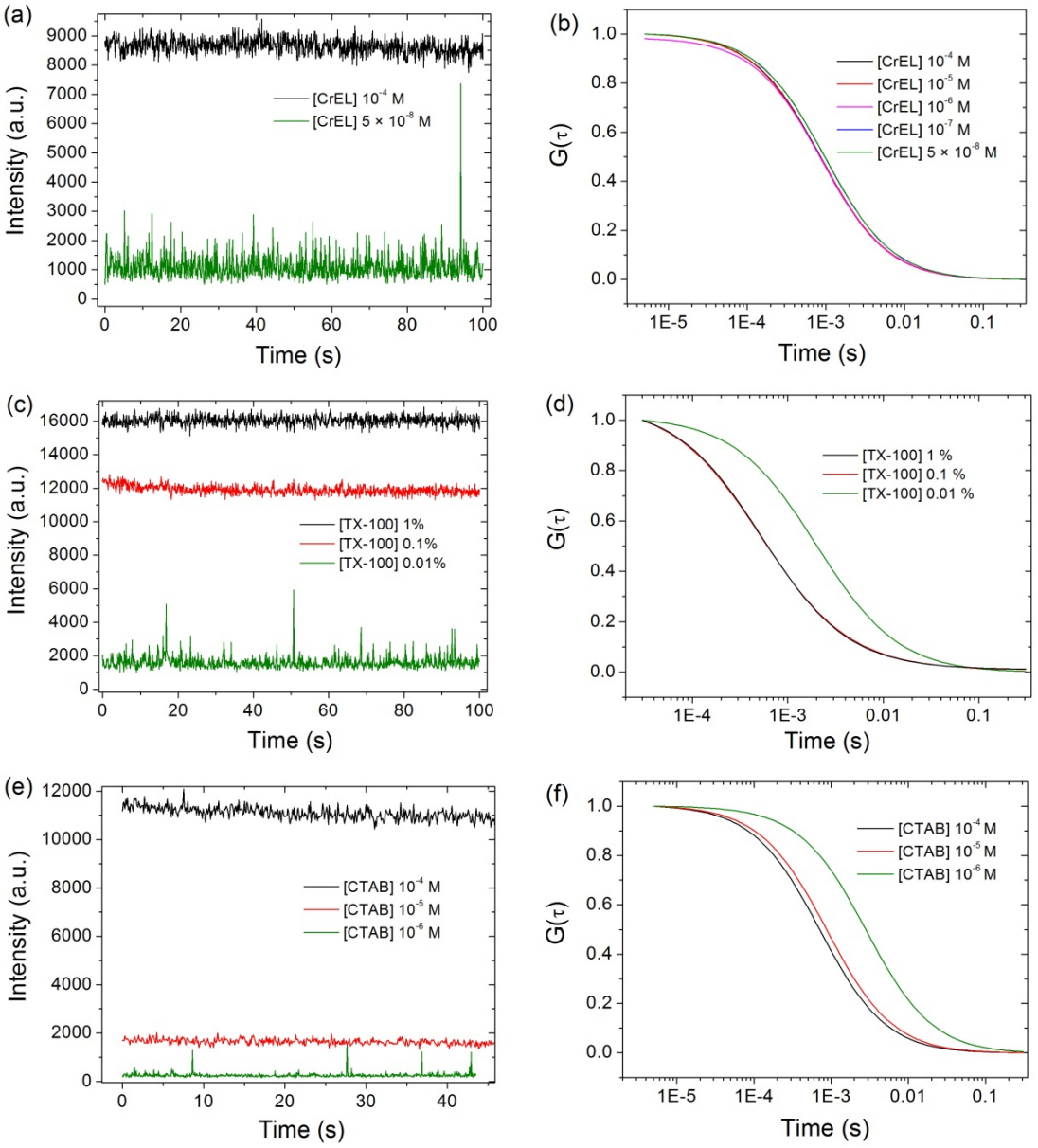

Figure 27: FCS intensity profile and autocorrelation function plots for 5MPFH-TDT (50 nM) in CrEL solutions (10^{-4}, 10^{-5}, 10^{-6}, 10^{-7}, 5×10^{-8} M) (a and b), and for 5MPFH-TDT (100 nM) in TX-100 solutions (1%, 0.1% and 0.01%) (c and d), and CTAB solutions (10^{-4} M, 10^{-5} M, and 10^{-6} M) (e and f).

3.2 Effect of viscosity on the fluorescence emission of 5MPFH-TDT

Since the origin of 5MPFH-TDT fluorescence is due to its three vibrationally accessible conformers we expected that the viscosity of its environment might have a systematic effect on its emission properties. It was also necessary to collect a

reference anisotropy data set that would help with the evaluation of micellar and BSA data. This was carried out using EtOH-EthGly solvent mixtures. The band profile was unaffected by the changing solvent composition but systematic changes to the fluorescence lifetime and fluorescence anisotropy data were observed. As the EthGly content was increased the fluorescence lifetime of 5MPFH-TDT decreased. This effect was more marked for Bands 1 and 2 while the fluorescence lifetime of Band 3 remained mostly unchanged. This appeared to indicate that the g1 and g2 conformers were more susceptible to non-radiative decay in solutions of higher viscosity.

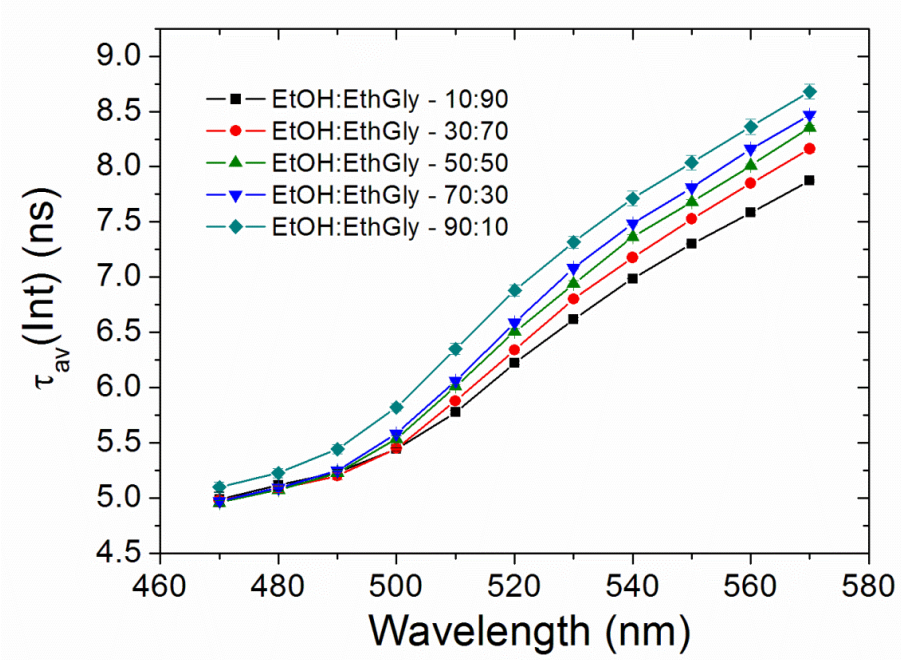

Figure 28: Intensity weighted average fluorescence lifetime, τ_{av} (Int), (λ_{ex} 405 nm) of 5MPFH-TDT in EtOH/EthGly solutions for the emission wavelength range of 470−570 nm.

However, it seemed more likely that the shortening of the fluorescence lifetime of 5MPFH-TDT with increasing EthGly was due to the increase in the refractive index[7]. The relationship between the refractive index and the fluorescence lifetime of a fluorophore is described by the Strickler-Berg equation (Equation 5) in Section 1.3.2. The fluorescence anisotropy increased from close to zero in 90% EtOH solutions to

[7] EtOH and EthGly have refractive indices of 1.3611 and 1.4318, respectively [37].

0.067 in 10% EtOH solutions in EthGly. The anisotropy of each fluorescence emission band has a linear dependence on the viscosity of the solution.

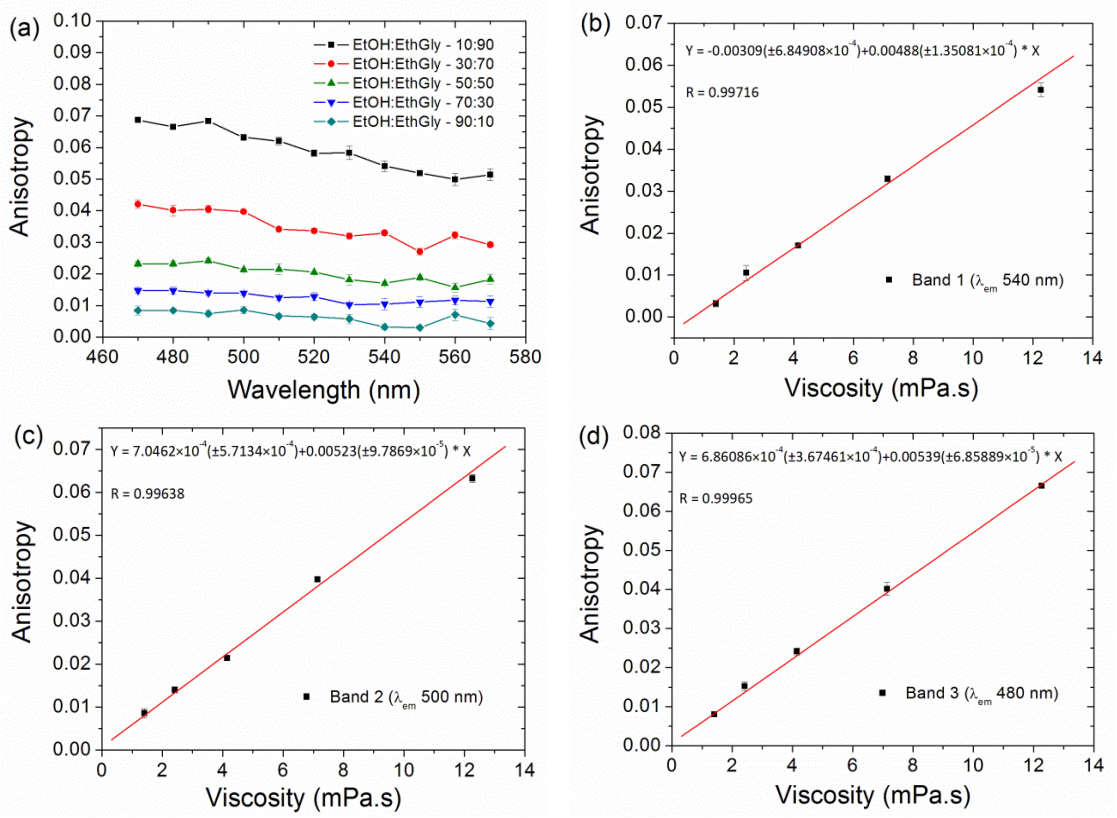

Figure 29: (a) Fluorescence anisotropy (λ_{ex} 405 nm) of 5MPFH-TDT in EtOH/EthGly solutions for the emission wavelength range of 470−570 nm. Fluorescence anisotropy versus viscosity for (b) Band 1, (c) Band 2, and (d) Band 3.

4 Photophysical behaviour of 5MPFH-TDT in micellar solutions

4.1 Introduction

Surfactants play a role in environmental medicine, material sciences, industrial chemistry, biological analysis and pharmaceuticals. Various experimental methods, including x-ray diffraction, dynamic light scattering, and NMR, have been utilised to determine the size and shape of the micelles formed by surfactant molecules [109]. Due to the luminescence enhancement effect of micelles, a number of fluorometric assays have been developed for the detection of environmental pollutants, tumour markers, and various pharmaceuticals [109]. However, micelle solutions have been used in this investigation as semi-analogous models of protein molecules. As with protein molecules, properties like polarity, viscosity and diffusion of water molecules towards the core of a micelle are different from the bulk phase [89]. This study investigated how the photophysical behaviour of the triazine changed due to inclusion within the micelle's microenvironment rather than that of the bulk medium. Similar microenvironments of interest could then be investigated based on well-characterised photophysical transitions. These assemblies also helped to deal with the poor water solubility of the triazine, which was discovered in the initial period of this research study. The spectral variation of 5MPFH-TDT that occurs above and below the critical micelle concentration (CMC) of a number of surfactants was monitored. Cremophor EL (CrEL), Triton X-100 (TX-100), sodium dodecyl sulfate (SDS) and cetyltrimethylammonium bromide (CTAB) were used as examples of neutral, anionic, and cationic surfactants.

Table 7: Physical properties of surfactants employed.

Surfactant	M.W. (g/mol)	CMC (mM)	Radius (Å)	Stern layer/Palisade layer (Å)	Charge
CrEL	~2500	0.036	56.5 [110] 65.25 [111]	—	Neutral
TX-100	647.00	0.25 [84]	51 [112]	25 [91]	Neutral
SDS	288.37	5.89 [113], 6.00 [84]	21.6 [114]	6–9 [91]	Anionic
SDBS	348.48	2.30 [113]	22.4 [114]	—	Anionic
CTAB	364.45	0.88. 0.9 [84]	50[115]	10 [115]	Cationic

4.2 Absorbance and band position variation of 5MPFH-TDT in micellar solutions

The baseline scatter that was evident in all of the aqueous buffer solutions was eliminated upon the introduction of surfactant (Figure 30e). The absorption data of 5MPFH-TDT in CrEL solutions of varying concentration indicated a small change to the chemical environment of the fluorophore at a CrEL concentration of approximately 0.05 mM. At this concentration, a 5MPFH-TDT−CrEL ratio of one-to-three was achieved. The band position at ~400 nm was blue-shifted by 3–4 nm when the CrEL concentration was increased from 0.01 mM to 0.1 mM.

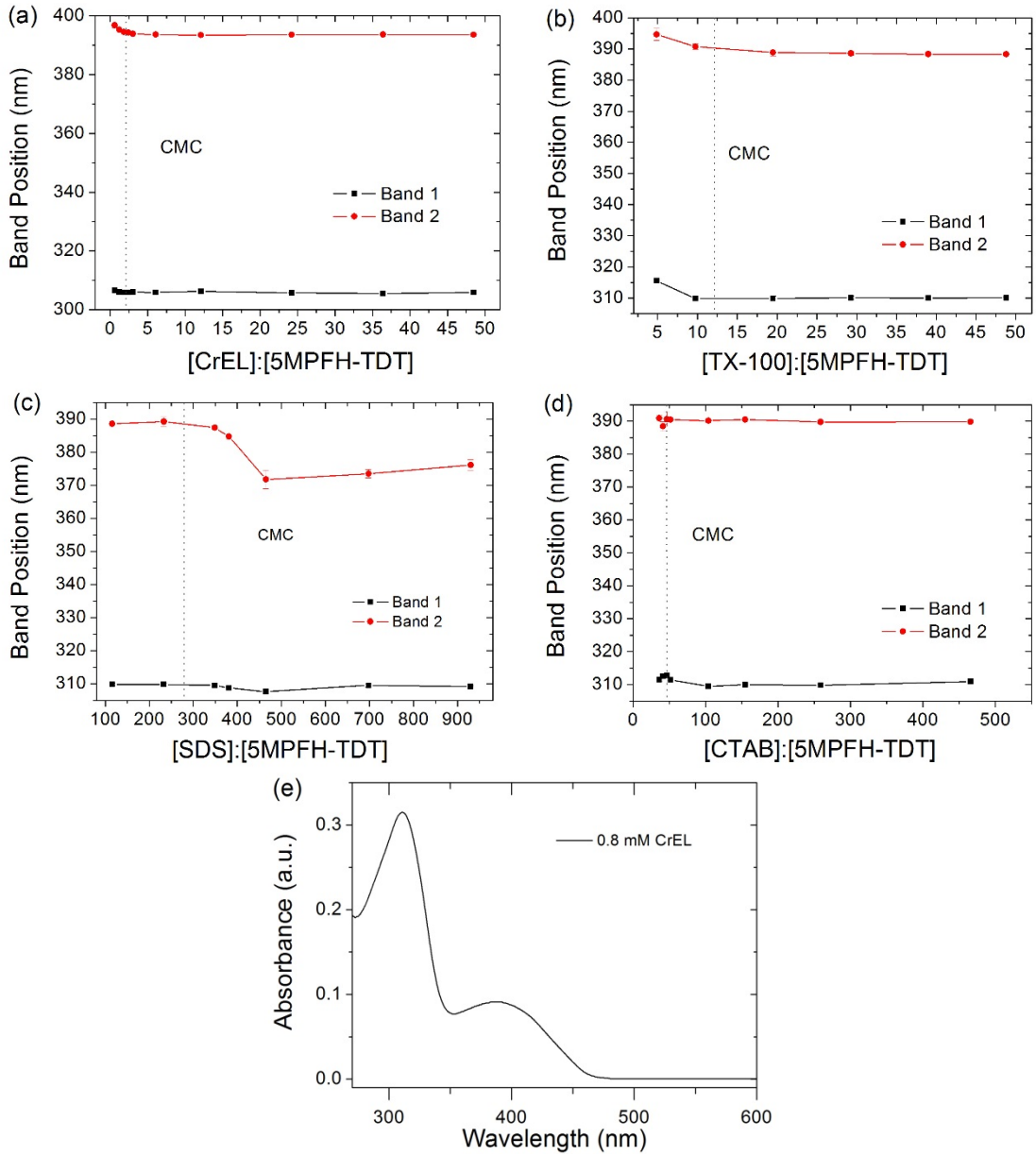

Figure 30: Positions of λ_{max} for absorption bands 1 and 2 versus 5MPFH-TDT–surfactant concentration ratio in solutions of (a) CrEL, (b) TX-100, (c) SDS, and (d) CTAB. (e) Absorbance spectrum of 5MPFH-TDT in a 0.8 mM solution of CrEL.

This hypsochromic shift observed indicated that the new chemical environment of the fluorophore had stabilised its electronic ground state with respect to the Franck-Condon excited state. In the case of TX-100, a similar trend was detected. The absorption data showed that on increasing the non-ionic surfactant concentration to above the CMC (0.23 mM) a hypsochromic shift occurred. A stabilisation of the ground state of the triazine relative to its excited state was also observed for above the

CMC of the anionic surfactant, SDS, while in the case of CTAB, the band position of the triazine remained fairly unchanged.

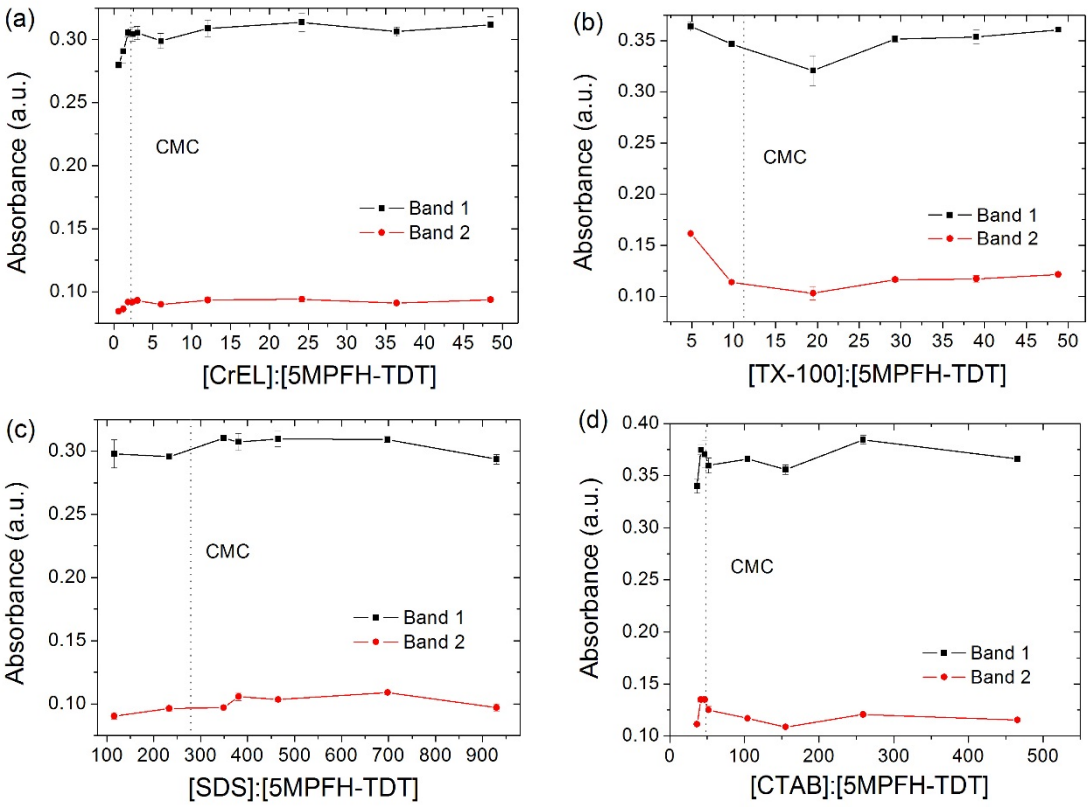

Figure 31: Change in absorbance of bands 1 and 2 versus 5MPFH-TDT–surfactant concentration ratio in solutions of (a) CrEL, (b) TX-100, (c) SDS, and (d) CTAB.

Although a marginal enhancement of the triazine's absorbance was observed with increasing CrEL concentration, no clear trend can be applied to the behaviour of the triazine's absorbance in the other surfactants investigated. These fluctuations in absorbance values could be due to a variation in the concentration of 5MPFH-TDT as a consequence of the formation of small quantities of aggregates in solution.

4.3 Quantum yield of 5MPFH-TDT in micellar solutions

The quantum yield of 5MPFH-TDT in each of the micelle environments was determined by comparison with Coumarin 153 using the following equation:

$$\varphi = \varphi_R \left(\frac{m}{m_R}\right)\left(\frac{n^2}{{n^2}_R}\right) \qquad \textbf{Equation 28}$$

where φ is the quantum yield, m is the slope of the integrated intensity versus the absorbance, and n is the refractive index. Coumarin 153 has a fluorescence quantum yield of 0.544 (±0.028) in EtOH for an excitation range of 360–470 nm and an emission range of 485–635 nm [116]. The quantum yield of the reference and the unknown were determined using the exact same experimental conditions. An excitation wavelength of 400 nm was used for excitation and fluorescence emission was collected over the range 420–750 nm. Excitation and emission slit widths were both set at 7.5 nm and a scan speed of 500 nm/min was used. Absorbance values were likewise determined at 400 nm. 5MPFH-TDT–surfactant samples were prepared as before but the concentration of 5MPFH-TDT was varied between 1×10^{-5} M and 2×10^{-6} M while the concentration of each surfactant was maintained at a constant value above the CMC. All samples were tested in triplicate.

Table 8: Critical micelle concentration and sampling concentration of each surfactant employed.

Surfactant	M.W. (g/mol)	CMC (mM)	Concentration (mM)
CrEL	~2500	0.036	0.05
TX-100	647.00	0.25 [84]	0.6
SDS	288.37	5.89 [113], 6.00 [84]	10.0
CTAB	364.45	0.88. 0.9 [84]	2.0

The refractive index of each of the surfactant solutions was determined at a number of concentration values using an Abbe refractometer. A linear relationship was obtained between refractive index and surfactant concentration. The refractive index of the micelles was determined by extrapolating the line of best fit to a concentration value of 100%. The concentration of the surfactant solutions exceeded each of their

respective CMC values. The quantum yield values for 5MPFH-TDT in CrEL, TX-100, CTAB, and SDS are listed in Table 9. The recorded quantum yield was greatest in the cases of CrEL and TX-100.

Table 9: Quantum yield values of 5MPFH-TDT in various micelles calculated by comparison with the standard fluorophore Coumarin 153 in EtOH.

Fluorophore	Solvent	Slope	n	Φ (±SE)
Coumarin 153	EtOH	1.29×10^6	1.36	0.54 ± 0.03
5MPFH-TDT	CrEL	1.76×10^6	1.47	0.86 ± 0.06
5MPFH-TDT	TX-100	1.67×10^6	1.49	0.84 ± 0.04
5MPFH-TDT	CTAB	1.52×10^6	1.50	0.78 ± 0.05
5MPFH-TDT	SDS	7.52×10^5	1.45	0.36 ± 0.02

The high quantum yield calculated for CrEL was indicative of a strong interaction between this surfactant and 5MPFH-TDT. The larger size of this surfactant molecule and its three-chain structure could explain why the quantum efficiency of the triazine increases in its presence. The quantum yield of 5MPFH-TDT was also slightly greater in the presence of TX-100 than CTAB. A subsequent comparison between the binding constant of 5MPFH-TDT in these micelles also indicated that it was bound more strongly to micelles of TX-100 (Section 4.6). These micelles have an almost identical radius of approximately 50 Å so their relative sizes cannot explain the disparity in binding constant values. However, the palisade layer of TX-100 (25 Å) was much greater than the Stern layer of CTAB (10 Å). This could mean that a larger palisade/Stern layer slows the rate of disassociation of the fluorophore-micelle complex resulting in a greater quantum yield and binding constant.

4.4 Fluorescence emission of 5MPFH-TDT in micellar solutions

4.4.1 Fluorescence emission of 5MPFH-TDT in Cremophor EL solutions

The raw fluorescence emission data showed an increase in the fluorescence intensity with increasing surfactant concentration as well as an overall shift to shorter wavelengths/higher wavenumbers. This is more clearly visible from the normalised data (Figure 32b). A three-band Guassian fit was performed with Origin, ver. 7.0, and

the data extracted was plotted against CrEL concentration. The % integrated area plot (Figure 32c) demonstrates how little the population of Band 3 changed across the CrEL concentration range. This represented the transition from the S_1 excited state to the ground state for the g0 conformer. However, the populations of Bands 1 and 2 showed some variation, particularly between CrEL concentrations of 0.02 and 0.03 mM. The population of the $S_1 \rightarrow S_0$ (g1) transition (Band 1) increased with increasing concentration while the population of the $S_1 \rightarrow S_0$ (g2) transition (Band 2) decreased. Similarly, a variation was observed for the maximum band intensity between the CrEL concentration points of 0.02 mM and 0.03 mM. The intensity of Band 1 increased by 4.44% while that of Band 2 decreased by 4.91%. Band 3 followed a gradual increase in intensity over the CrEL concentration range of 0.01 to 0.1 mM.

The band position plot (Figure 32e) shows the variation of the energetic states with CrEL concentration. On increasing the concentration from 0.01 to 0.1 mM a definite blue shift occurred for Band 1 with a wavelength change of 6.8 nm. A wavelength change of 5.0 and 5.5 nm was observed for Bands 2 and 3, respectively. The maximum shift was reached at approximately 0.02 mM. The Full-Width Half-Maxima (FWHM) data remains fairly constant across the CrEL concentration range. Bands 2 and 3 became slightly narrower upon the addition of surfactant molecules. This implied that the microheterogeneity of the triazine's immediate environment decreased and this had a particular influence on the emission from the g2 and g0 conformers.

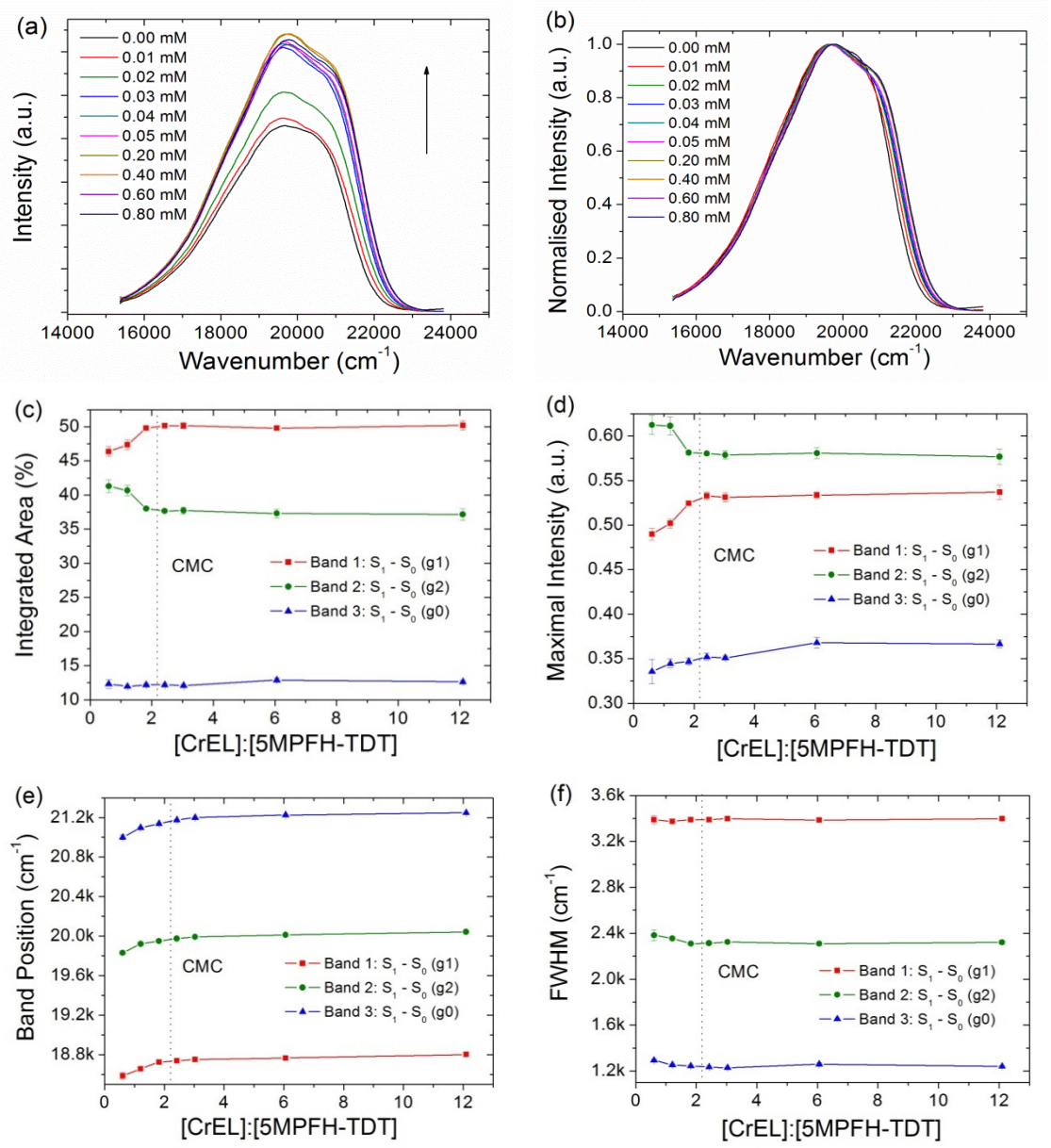

Figure 32: Raw (a) and normalised (b) fluorescence emission spectra of 5MPFH-TDT (1.65×10^{-5} M) in solutions of CrEL of varying concentration. (c) % Integrated area, (d) intensity maximum and, (e) band position, and (f) FWHM of the three fluorescence emission bands of 5MPFH-TDT versus the 5MPFH-TDT–surfactant concentration ratio.

A correlation was drawn between the integrated area of Band 1, which corresponds to the transition from the S_1 excited state to the ground state for the g1 conformer, and the intensity weighted average fluorescence lifetime, τ_{av} (Int) (Figure 33). Both of these parameters increased with increasing surfactant concentration. The integrated area of Band 1 increased by 15% and the lifetime more than doubled on going from an aqueous solution to a 0.8 mM solution of CrEL. This is in line with the

photophysical model, which shows that the S_1 (g0) and S_1 (g2) excited states may both internally convert to the S_1 (g1) state if fluorescence emission does not first occur [79]. The longer average fluorescence lifetime values reported for CrEL micellar solutions of higher concentration meant that population of the S_1 excited state of the g1 conformer was favoured under these conditions. According to the photophysical model of 5MPFH-TDT, this is the final state to be populated following excitation. Internal conversion from the S_1 (g0) excited state to the S_1 (g1) and S_1 (g2) states, and also from the S_1 (g2) state to the S_1 (g1) state, occurred to a larger extent at these higher surfactant concentrations.

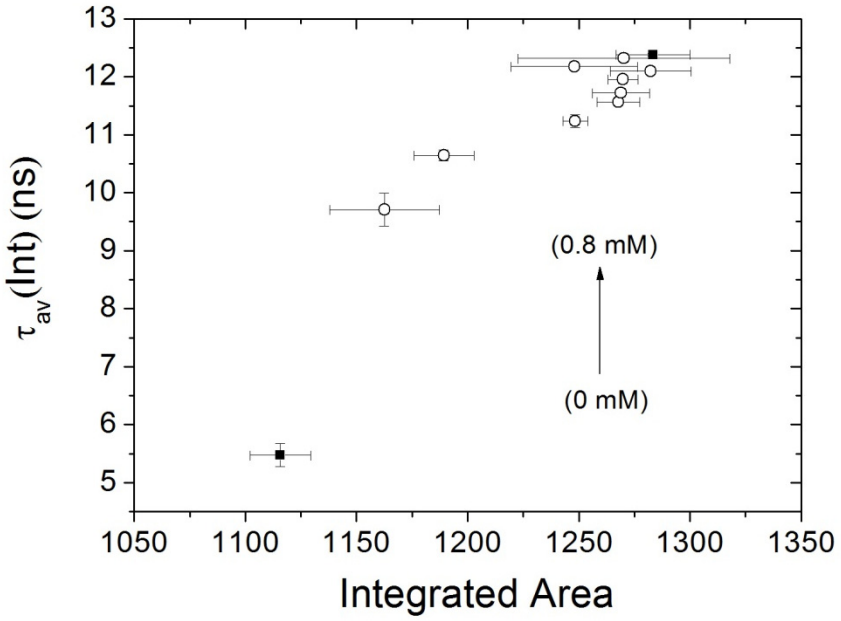

Figure 33: Intensity weighted average fluorescence lifetime, τ_{av} (Int), versus integrated area for Band 1. Data markers correspond to CrEL concentration values of 0, 0.01, 0.02, 0.03, 0.04, 0.05, 0.1, 0.2, 0.4, 0.6, 0.8 mM. Lowest and highest CrEL concentration points are indicated by filled squares.

Plots of intensity weighted average fluorescence lifetime versus band position (Figure 34) demonstrate that an increasing fluorescence lifetime could be correlated to the reported hypsochromic shift with increasing surfactant concentration for each of the three bands. The increasing surfactant concentration resulted in a longer fluorescence lifetime (Figure 35b) but this effect was offset by the increase in the refractive index as the band shifted to longer wavenumbers (Equation 5).

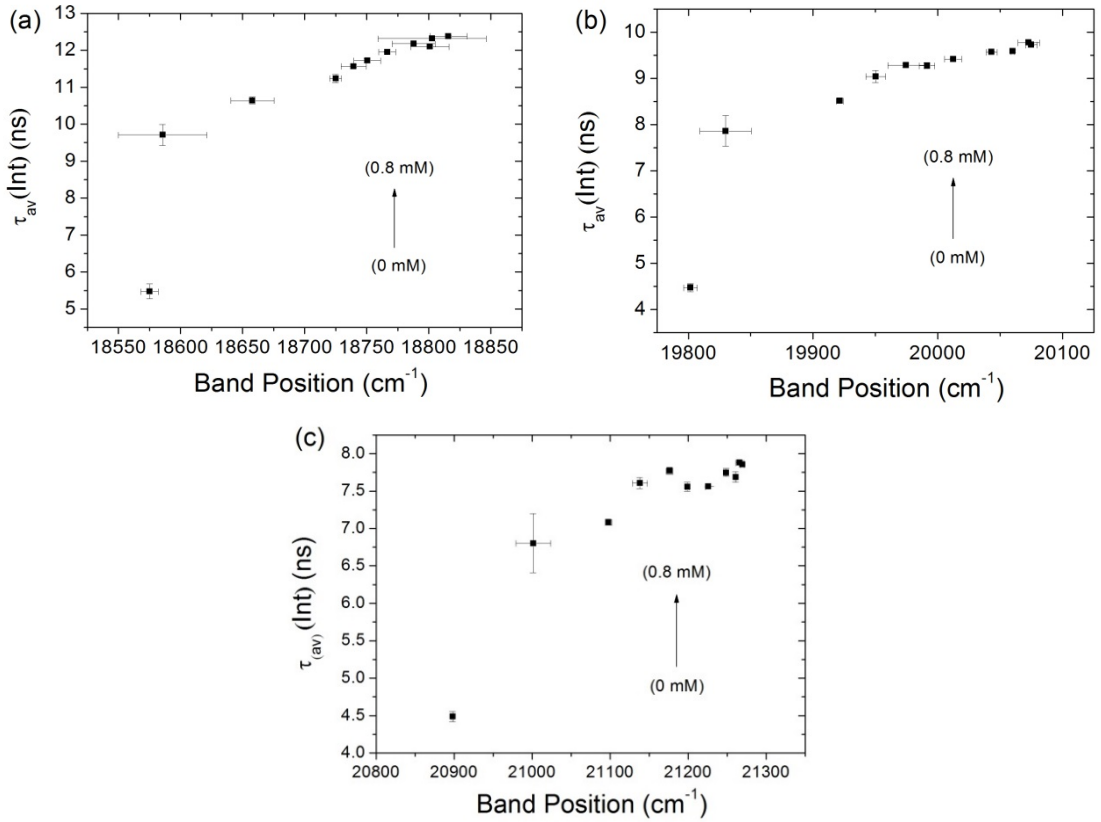

Figure 34: τ_{av} (Int) versus band position for (a) Band 1, (b) Band 2, and (c) Band 3. Data markers correspond to CrEL concentration values of 0, 0.01, 0.02, 0.03, 0.04, 0.05, 0.1, 0.2, 0.4, 0.6, 0.8 mM.

A steady rise in fluorescence anisotropy was observed for the triazine as the concentration of CrEL increased. Very low anisotropy values were observed for 5MPFH-TDT free in solution. As the surfactant solution became more concentrated some of the triazine molecules began to interact with surfactant molecules in solution and the extent of rotational diffusion was diminished. As the concentration increased more of the triazine was bound to the CrEL and the net fluorescence anisotropy approached a maximum of 0.134 (±0.69%) at 470 nm (Figure 35a). It is probable that all of the triazine had migrated into the CrEL micelle structure at this point and the anisotropy only increased minimally at higher CrEL concentrations.

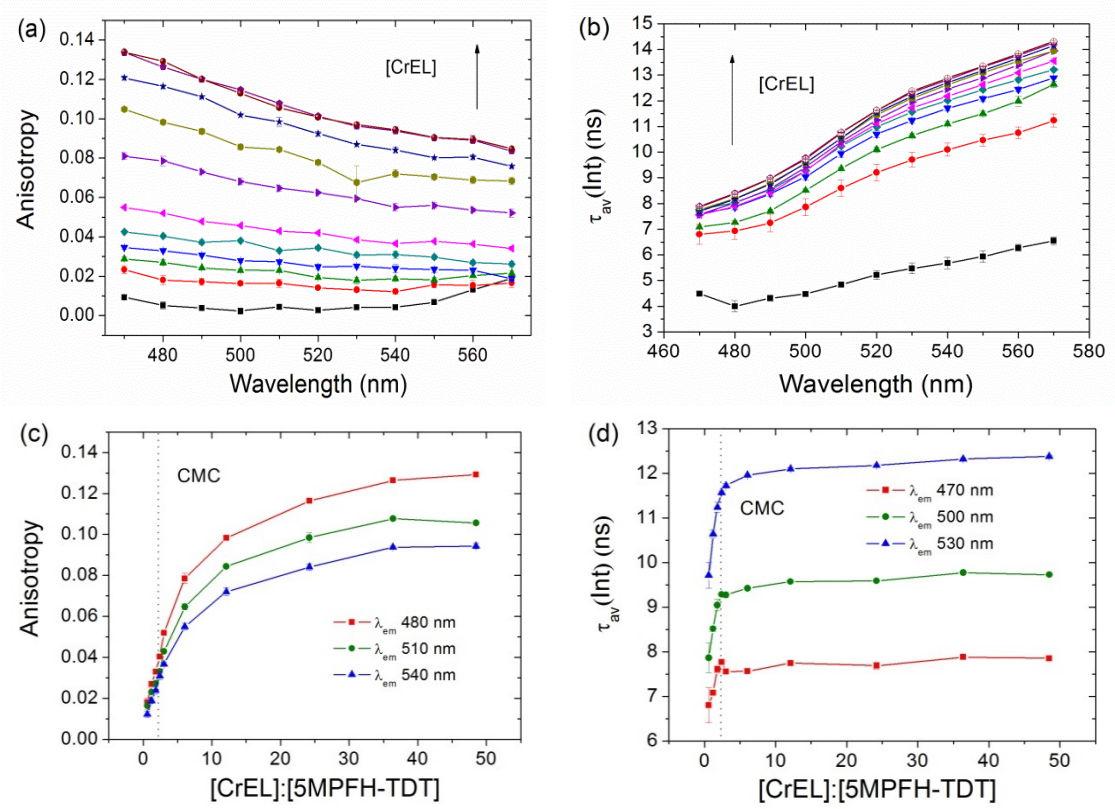

Figure 35: (a) Fluorescence anisotropy and (b) intensity weighted average fluorescence lifetime, τ_{av} (Int), of 5MPFH-TDT (1.65×10^{-5} M) in solutions of CrEL of varying concentration (0–0.8 mM) for the emission wavelength range of 470−570 nm. (c) Anisotropy and (d) fluorescence lifetime data was extracted and plotted against the 5MPFH-TDT–surfactant concentration ratio.

The fluorescence lifetime data of 5MPFH-TDT in solutions of CrEL showed a gradual increase in all three lifetime components until a maximum was reached at 0.2 mM. This lengthening of the fluorophore's lifetime was indicative of its stabilisation in the excited state. The longest lifetime was reached at a much lower concentration for the lifetime data in comparison to the steady-state fluorescence anisotropy. This indicated that the triazine interacted with CrEL at quite low surfactant concentrations but the micellar structures continued to grow to produce larger assemblies with greater rotational correlation times. The fluorescence lifetime data across the entire emission wavelength range (Figure 35b) also demonstrated the relationship between the fluorescence lifetime of the fluorophore and the refractive index of the medium. This relationship is given by the Strickler-Berg equation (Equation 5). A plot of the average fluorescence lifetime versus the emission wavelength for a CrEL concentration of 0.05 mM (Figure 36a), shows some deviation

from linearity. This can be explained by the dependence of the refractive index on the wavelength of light. Since each emission band spanned a very different wavelength range there was a significant variation in refractive index. The plots in Figure 36 show that there is a slightly different relationship between τ_{av} (Int) and wavelength/refractive index, presumably because of the different emission processes. This trend is also observed for equivalent fluorescence anisotropy plots due to the dependence of the anisotropy on the fluorescence lifetime of a fluorophore (Appendix A.1).

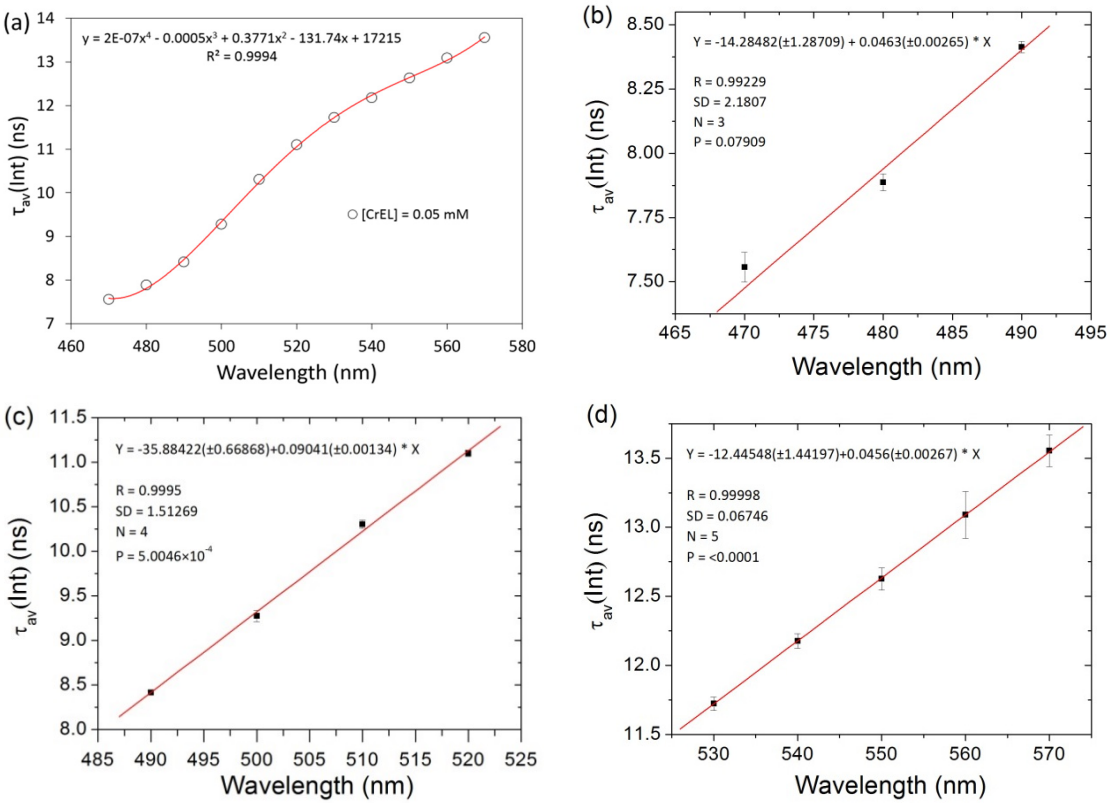

Figure 36: Intensity weighted average fluorescence lifetime data of 5MPFH-TDT in a 0.05 mM solution of CrEL versus fluorescence emission wavelength. (a) 470−570 nm. (b) 470–490 nm (g0). (c) 490−520 nm (g2). (d) 530−570 nm (g1).

4.4.2 Fluorescence emission of 5MPFH-TDT in Triton X-100 solutions

Like CrEL, TX-100 is a non-ionic surfactant. However, it has a much smaller average molecular weight than CrEL. As well as an increase in fluorescence intensity (the fluorescence intensity increased by approximately 170% on going from a TX-100 concentration of 0.1 to 1.0 mM) the slightly changing profiles of the raw fluorescence emission spectra (Figure 37b) indicated that the environment of the fluorophore was

changing with increasing surfactant concentration. As before, a three-band Guassian fit was performed and the data extracted was plotted against TX-100 concentration. The % integrated area of each fluorescence emission band versus surfactant concentration indicated the point at which the individual electronic transitions of the triazine were affected by the presence of surfactant molecules. At a TX-100 concentration of 0.4 mM an inversion of the % integrated area of Band 1 and Band 2 occurred. From this it was inferred that the $S_1 \rightarrow S_0$ (g1) transition became more favoured than that of the g2 conformer as the micelle structure formed around the triazine fluorophore. Band 3, which represented the $S_1 \rightarrow S_0$ (g0) transition, remained fairly unchanged with only a slight decrease in area being reported.

Plots of maximum intensity (Figure 37d) and band position (Figure 37e) versus TX-100 concentration also describe a transition in the triazine's environment between 0.2 and 0.4 mM. A trend echoing that observed for the % integrated area plot could be seen in a plot comparing the maximum intensity with surfactant concentration. The intensity of the most prominent peak, that of Band 2, dropped off somewhat but that of Band 1 increased concomitantly. This outcome, coupled with the trend observed for the % integrated area plot suggested that the transition from the excited state to the ground state for g1 of the triazine became more favoured as the triazine was secured within the hydrophobic core of the micelle. As before, with CrEL solutions, the band positon of 5MPFH-TDT was shifted to shorter wavelengths (~7 nm shift) with increasing surfactant concentration for all three fluorescence emission bands indicating an overall stabilisation of the ground state relative to the excited state. This was most likely due to the lower polarity of the micelle interior compared to the bulk solution. Although the dipole moments of each of the conformers of 5MPFH-TDT are only slightly greater in the excited state compared to the ground state, this difference seemed to be sufficient to produce the observed blue-shift. Bhattacharya *et al.* observed this trend for the fluorophore Dapsone in a number of surfactant solutions. However, the blue shift was much more pronounced in the case of this fluorophore [117].

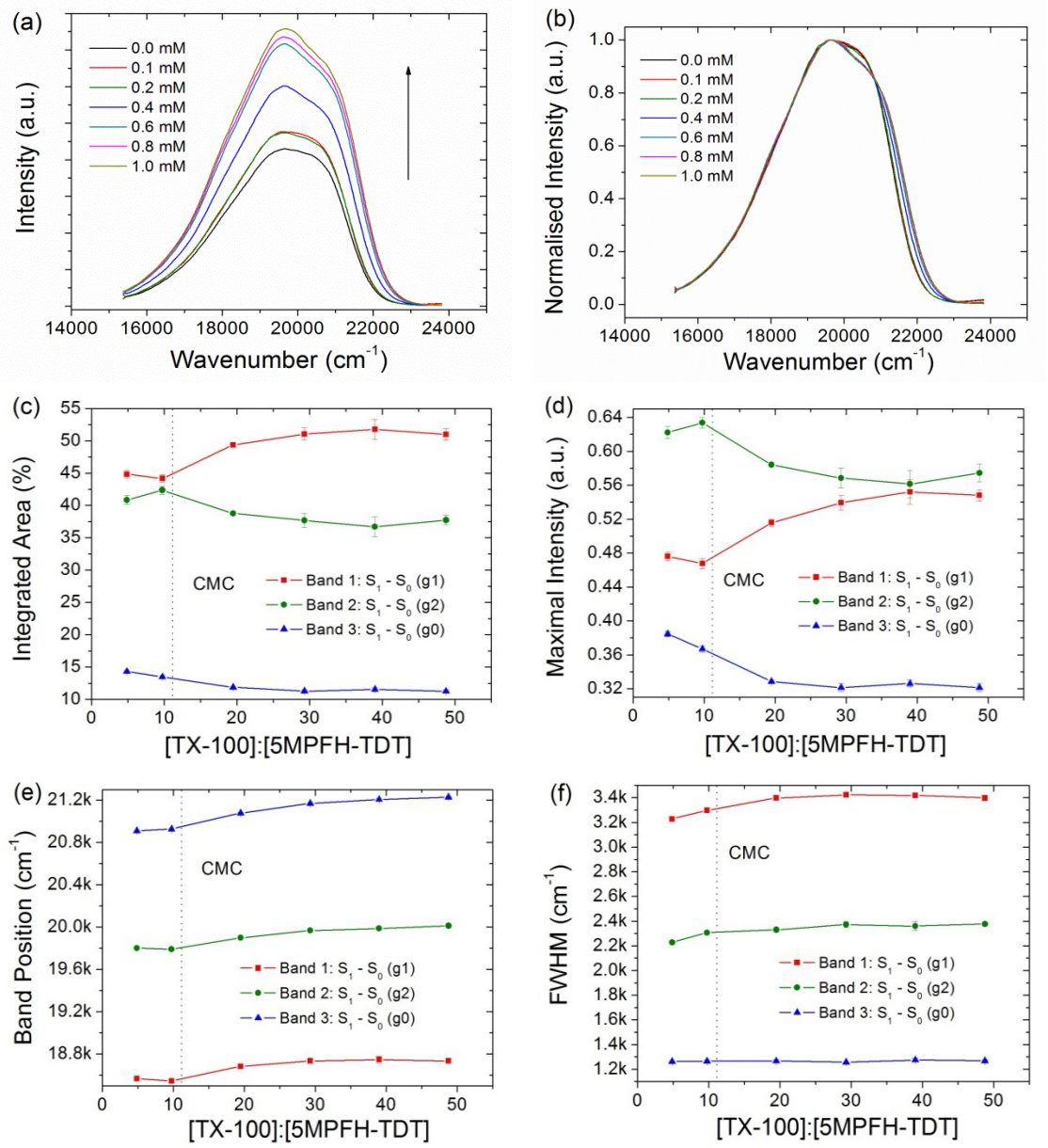

Figure 37: (a) Raw and (b) normalised fluorescence emission spectra of 5MPFH-TDT (2.05×10^{-5} M) in solutions of TX-100 of varying concentration. (c) % Integrated area, (d) maximum intensity, (e) band position, and (f) FWHM of the normalised fluorescence emission bands of 5MPFH-TDT versus the 5MPFH-TDT–surfactant concentration ratio.

A rise in fluorescence anisotropy with increasing surfactant concentration confirmed the interaction between the triazine and TX-100. The anisotropy increased from a value close to zero to a value approaching 0.1. This was lower than the maximum anisotropy reported for 5MPFH-TDT in micelles of CrEL (Figure 35a) and was probably due to the smaller size of the TX-100 micelles (Table 7). The three-chain structure of the CrEL molecule can also explain why the rotational motion of the

triazine was more restricted in this particular micelle than that of TX-100. The intensity weighted average fluorescence lifetime of 5MPFH-TDT in TX-100 solutions of increasing concentration followed a very similar pattern to that observed for CrEL. The average lifetime for each emission band seemed to reach a maximum above a concentration of 0.6 mM. Again, this is a lower maximum point than that suggested by the anisotropy data. This suggested that the maximum lifetime was reached once the surfactant concentration reached the point at which all of the triazine had been encapsulated within the micelles while the anisotropy data continued to increase as the size of the micelles increased.

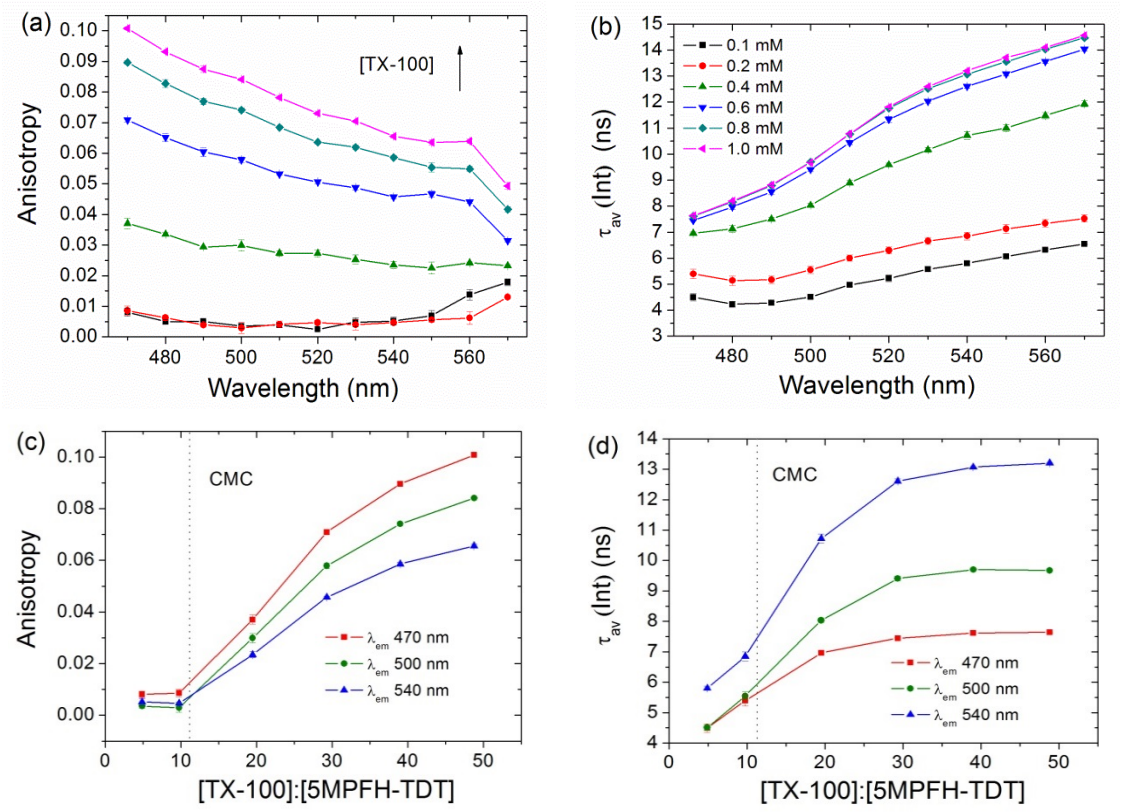

Figure 38: (a) Fluorescence anisotropy and (b) intensity weighted average fluorescence lifetime, τ_{av} (Int), of 5MPFH-TDT (2.05×10^{-5} M) in solutions of TX-100 of varying concentration for the emission wavelength range of 470−570 nm. (c) Anisotropy and (d) fluorescence lifetime data was extracted and plotted against the 5MPFH-TDT–surfactant concentration ratio.

Once again the linear relationship between the fluorescence lifetime and the emission wavelength (Figure 39) was very suggestive of a strong refractive index effect, similar to that observed for CrEL. For a constant TX-100 concentration (1.0 mM) three

linear regions for fluorescence lifetime versus the emission wavelength were observed (Figure 39). The slopes reported for these three linear regions in the two non-ionic surfactants investigated, CrEL (Figure 36) and TX-100, were very close in value. This indicated that the processes that govern the fluorescence emission of 5MPFH-TDT were influenced to a similar extent by the local chemical environment of each micelle.

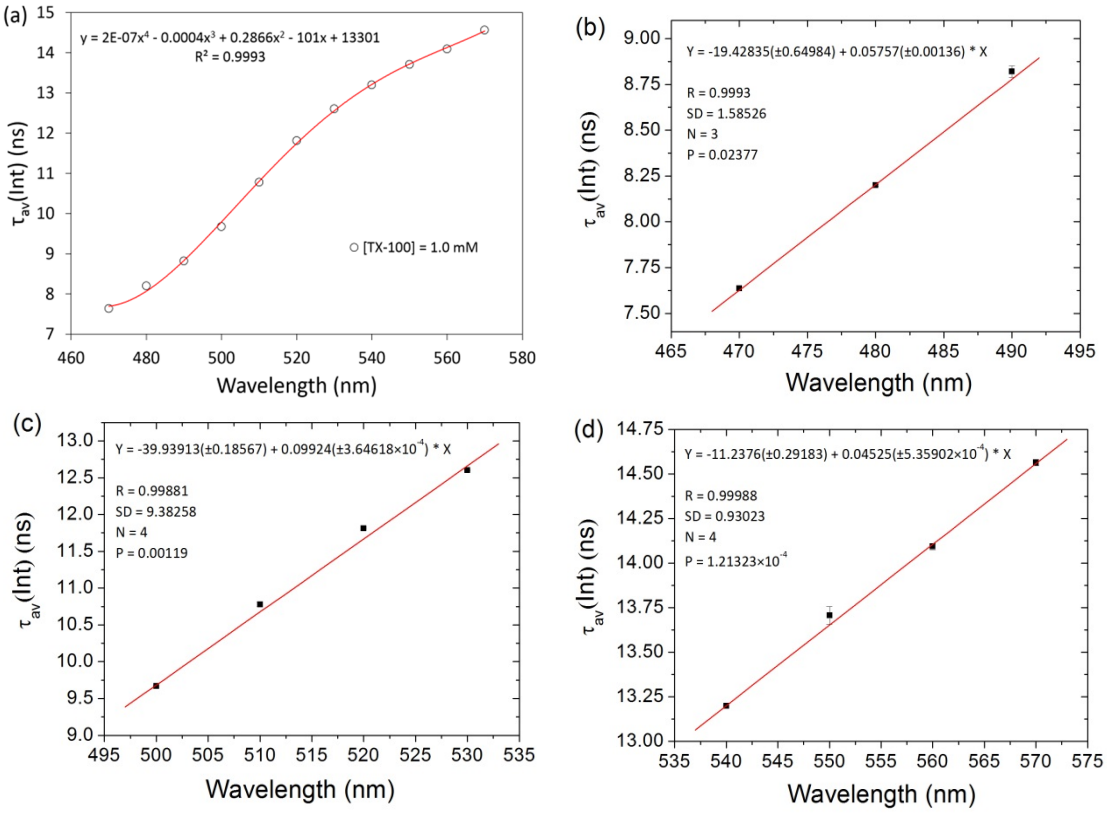

Figure 39: Intensity weighted average fluorescence lifetime of 5MPFH-TDT in a 1.0 mM solution of TX-100 versus fluorescence emission wavelength.
(a) 470−570 nm. (b) 470–490 nm (g0). (c) 490−530 nm (g2). (d) 540−570 nm (g1).

4.4.3 Fluorescence emission of 5MPFH-TDT in sodium dodecyl sulfate solutions

Contrary to the trend observed for non-ionic surfactants, a decrease in triazine fluorescence intensity was observed for sodium dodecyl sulfate solutions. When the concentration exceeded the CMC of 8.2 mM the intensity dropped to about 65% of its maximum. This implied that the triazine fluorophore was being quenched by the anionic surfactant. However, it still seemed to favour its position within the micelle over the bulk solution as the shape of the fluorescence band changed somewhat and its band position was red-shifted (Figure 40a). Band 3 was shifted to the greatest extent with a 9 nm jump on exceeding the CMC of SDS.

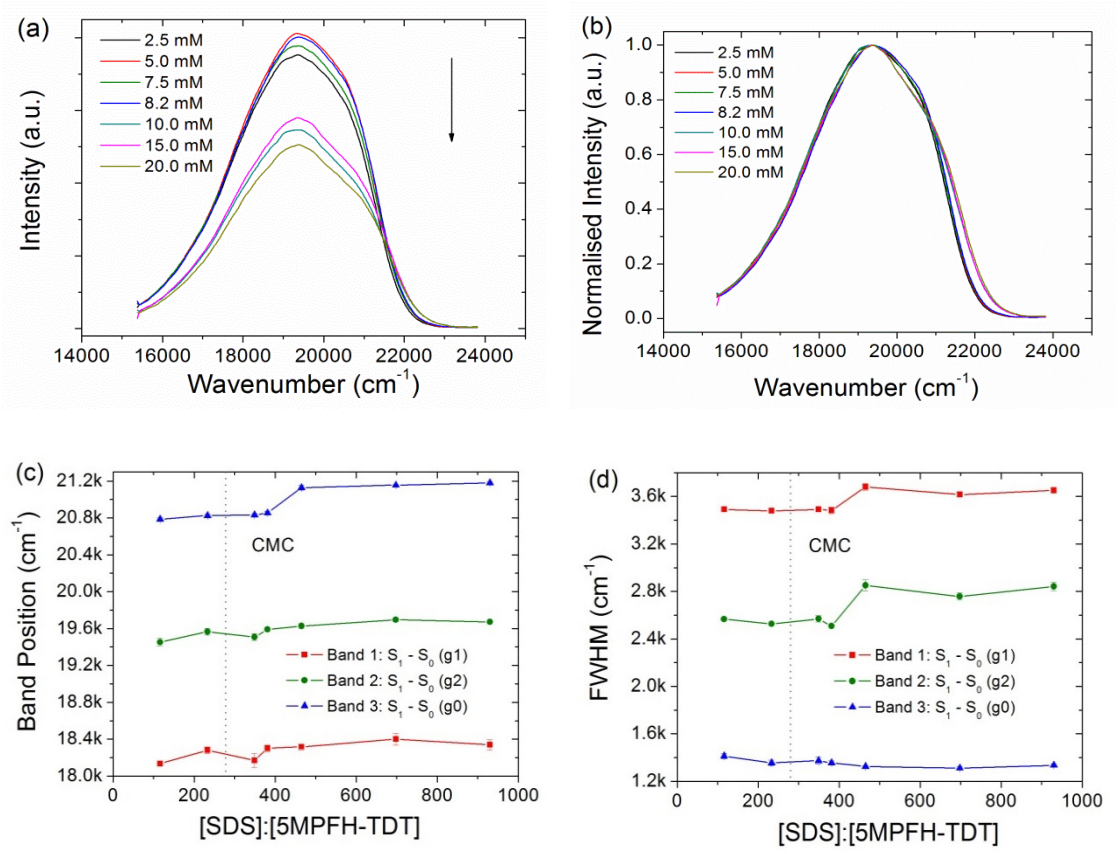

Figure 40: (a) Raw and (b) normalised fluorescence emission spectra of 5MPFH-TDT (2.15×10^{-5} M) in solutions of SDS of varying concentration. (c) Band position and (d) FWHM of the three normalised fluorescence emission bands of 5MPFH-TDT versus the 5MPFH-TDT–surfactant concentration ratio.

Despite having the highest fluorophore–surfactant ratio, the anisotropy of 5MPFH-TDT remained quite low over the SDS concentration range. However, a

notable increase in the anisotropy occurred above the CMC indicating that the triazine had been incorporated into the SDS micelle. The intensity weighted average fluorescence lifetime of 5MPFH-TDT in SDS was fairly non-reproducible and no particular trend was observed in this case. This implied that the solvation of the triazine within the SDS micelle was either unstable or incomplete. Values did not approach those observed in the cases of the other surfactants employed but the average lifetime did increase beyond the values recorded for the fluorophore in water alone.

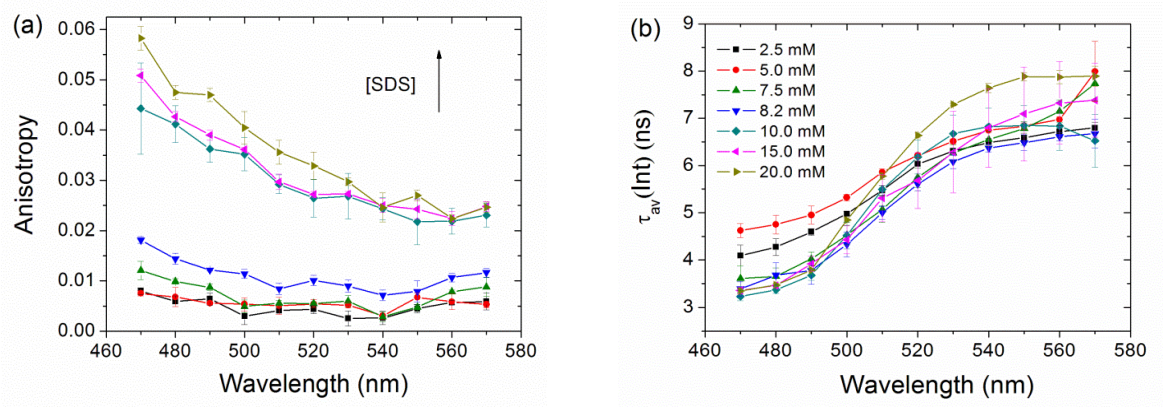

Figure 41: (a) Fluorescence anisotropy and (b) intensity weighted average fluorescence lifetime, τ_{av} (Int), of 5MPFH-TDT (2.15×10^{-5} M) in solutions of SDS of varying concentration for the emission wavelength range of 470−570 nm.

4.4.4 Fluorescence emission of 5MPFH-TDT in sodium dodecylbenzene sulphonate solutions

The fluorescence emission intensity of 5MPFH-TDT in SDBS did not follow a regular trend. It increased for SDBS concentrations of up to 4.0 mM, and then decreased. The integrated area plot showed that as the concentration of SDBS was increased beyond 4.0 mM the population of Band 1 increased while that of Band 2 decreased. Band 3 was mostly unaffected. This meant that a greater concentration of SDBS inhibited internal conversion into S_1 of the g2 conformer while internal conversion into S_1 of the g1 conformer was supported. The FWHM data showed that all of the bands became broader up to an SDBS concentration of 5.0 mM. This showed that the SDBS created a more heterogeneous environment for 5MPFH-TDT. This broadening effect was not present at an SDBS concentration of 20.0 mM. In fact, Bands 2 and 3 became narrower at this point. A blue shift with increasing SDBS

was observed for all three bands indicating a stabilisation of the ground state relative to the excited state with increasing surfactant concentration.

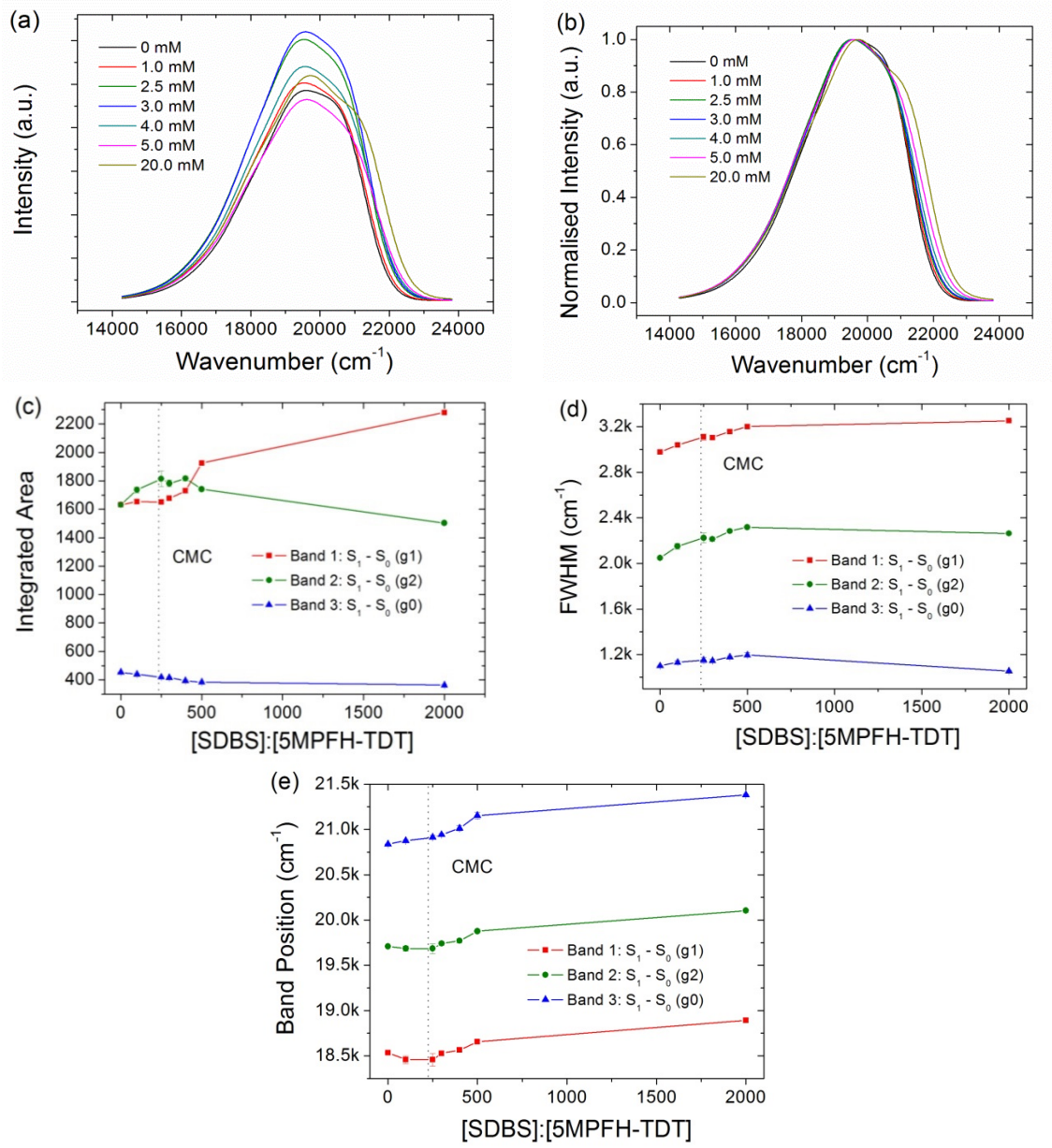

Figure 42: (a) Raw and (b) normalised fluorescence emission spectra of 5MPFH-TDT (10^{-5} M) in solutions of SDBS of varying concentration. (c) Integrated area, (d) FWHM, and (e) band position of the three fluorescence emission bands of 5MPFH-TDT versus SDBS concentration.

4.4.5 Fluorescence emission of 5MPFH-TDT in cetyltrimethylammonium bromide solutions

The cationic surfactant, CTAB, produced similar trends to those observed for both non-ionic surfactants with the intensity increasing with increasing CTAB concentration. The % integrated area versus surfactant concentration plot mimicked the behaviour observed for the non-ionic surfactants, CrEL and TX-100: an increase in the % integrated area of Band 1 was accompanied by a decrease for Band 2 while Band 3 was mostly unaltered. Again, a hypsochromic shift occurred for all three fluorescence emission bands with increasing surfactant concentration. This indicated that the electronic behaviour of the triazine is consistent across the range of surfactants investigated. The same trend was also observed for the FWHM versus surfactant concentration—Bands 1 and 2 became slightly broader. As previously stated, this described an increase in the microheterogeneity of the fluorophore's chemical environment.

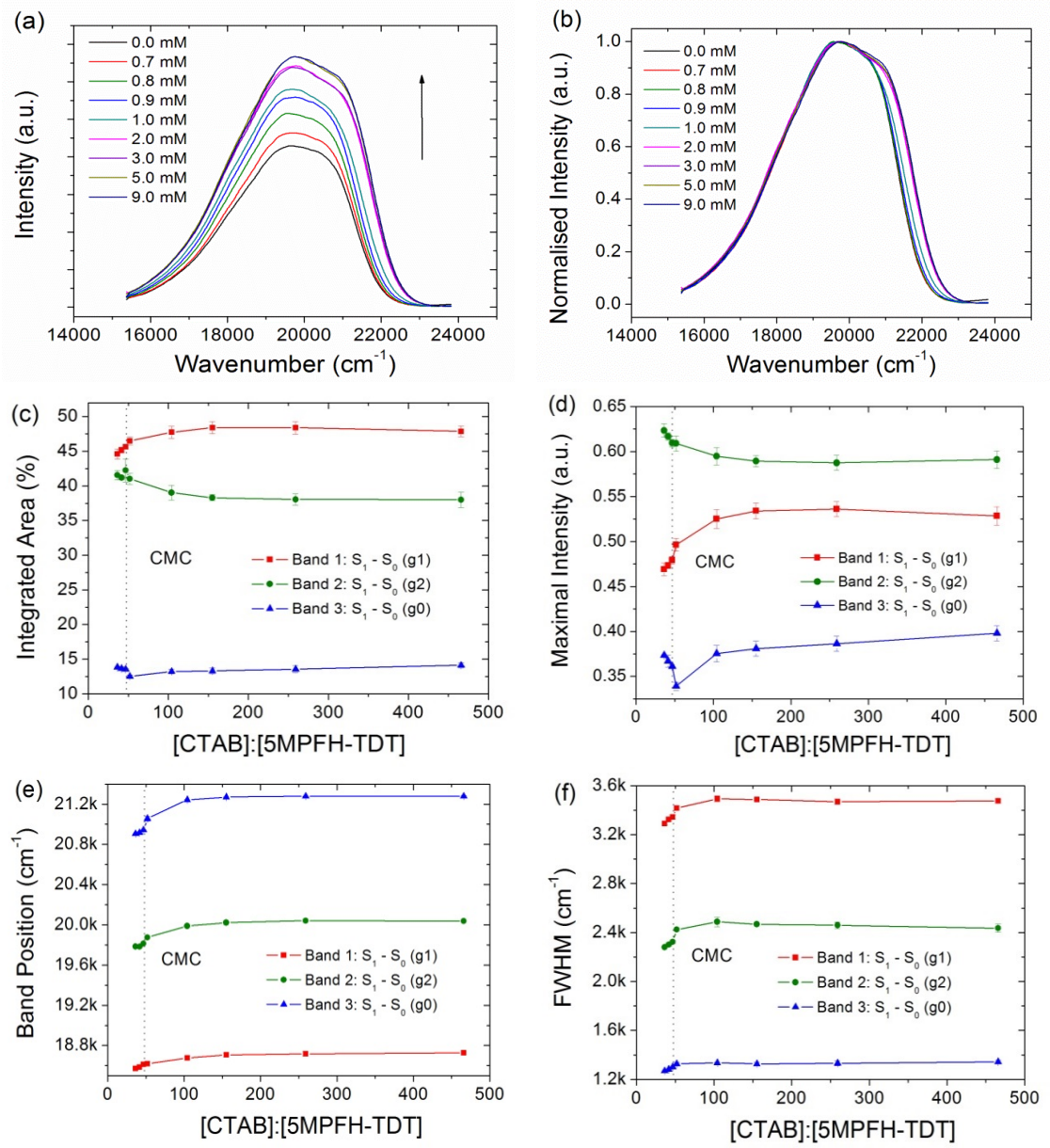

Figure 43: (a) Raw and (b) normalised fluorescence emission spectra of 5MPFH-TDT (1.93×10^{-5} M) in solutions of CTAB of varying concentration. (c) % Integrated area, (d) maximum intensity, and (e) band position, and (f) FWHM of the three normalised fluorescence emission bands of 5MPFH-TDT versus the 5MPFH-TDT–surfactant concentration ratio.

The fluorescence anisotropy increased substantially when the CMC point of 0.9 mM was exceeded. A tenfold increase in the concentration did not produce much of an increase in the fluorescence anisotropy beyond this point indicating that most of the triazine molecules had interacted with CTAB at fairly low micellar concentrations. This same trend was reflected in the fluorescence lifetime data.

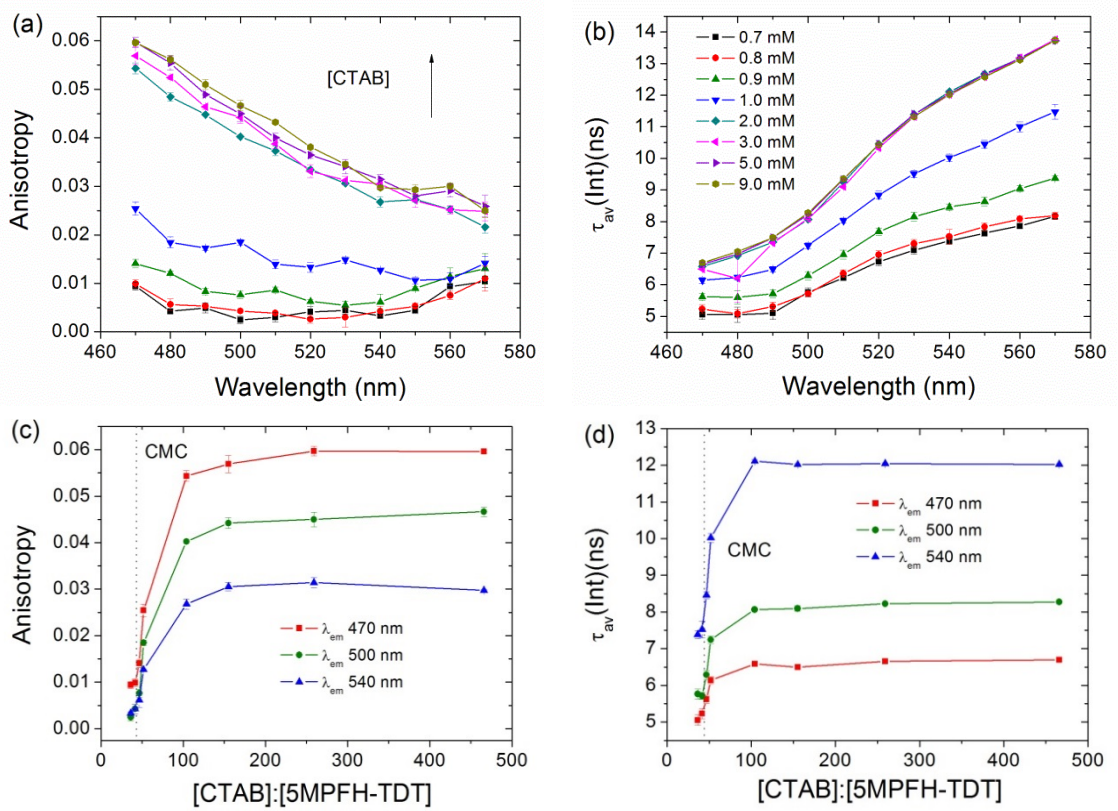

Figure 44: (a) Fluorescence anisotropy and (b) intensity weighted average fluorescence lifetime, τ_{av} (Int), of 5MPFH-TDT (1.93×10^{-5} M) in solutions of CTAB of varying concentration for the emission wavelength range of 470−570 nm. (c) Anisotropy and (d) fluorescence lifetime data was extracted and plotted against the 5MPFH-TDT–surfactant concentration ratio.

Table 10: Spectroscopic characteristics of 5MPFH-TDT in four different surfactant solutions. UV/Vis-absorption (λ_{abs}), fluorescence emission (λ_{em}), fluorescence anisotropy (λ_{em} 480 nm), and average intensity weighted fluorescence lifetime, (τ_{av}) (λ_{em} 480 nm).

[S] (mM)	[5MPFH-TDT]/ [S]	λ_{abs} (nm)		λ_{em} (nm)			r	τ_{av} (Int)(ns)
		Band 1	Band 2	Band 1	Band 2	Band 3	λ_{em} 480 nm	λ_{em} 480 nm
CrEL								
0		310.0	404.0	538.4	505.0	478.5	0.005	4.0
0.01	0.61	306.5	396.7	538.1	504.3	476.2	0.018	6.9
0.02	1.21	306.0	395.2	536.0	502.0	474.0	0.027	7.3
0.03	1.82	305.9	394.5	534.0	501.2	473.1	0.033	7.9
0.04	2.42	305.9	394.3	533.6	500.6	472.2	0.040	8.0
0.05	3.03	306.0	393.8	533.3	500.2	471.7	0.052	7.9
0.1	6.06	305.9	393.6	532.9	499.7	471.1	0.079	8.0
0.2	12.10	306.2	393.4	531.9	498.9	470.6	0.098	8.2
0.4	24.20	305.8	393.6	532.3	498.5	470.3	0.116	8.2
0.6	36.40	305.6	393.6	531.8	498.2	470.2	0.126	8.4
0.8	48.50	305.9	393.5	531.5	498.1	470.2	0.129	8.4
TX-100								
0.1	4.88	315.6	394.7	538.6	505.1	478.3	0.005	4.2
0.2	9.76	309.8	390.7	539.3	505.3	477.9	0.006	5.1
0.4	19.50	310.0	389.0	535.2	502.5	474.4	0.034	7.1
0.6	29.30	310.1	388.6	533.8	500.8	472.4	0.065	8.0
0.8	39.00	310.1	388.3	533.4	500.3	471.6	0.083	8.2
1.0	48.80	310.1	388.3	533.8	499.7	471.1	0.093	8.2
CTAB								
0.7	36.30	311.5	390.8	538.5	505.4	478.3	0.004	5.1
0.8	41.50	312.5	388.4	538.1	505.5	478.1	0.006	5.1
0.9	46.60	312.8	390.6	537.3	504.7	477.5	0.012	5.6
1.0	51.80	311.4	390.4	537.1	503.2	474.9	0.018	6.2
2.0	104.00	309.5	390.1	535.5	500.3	470.7	0.048	6.9
3.0	155.00	310.0	390.5	534.6	499.4	470.1	0.052	6.2
5.0	259.00	309.8	389.7	534.3	499.0	469.9	0.055	7.0
9.0	466.00	310.9	389.8	534.0	499.1	469.9	0.056	7.0
SDS								
2.5	116.00	309.8	388.6	551.4	514.1	481.1	0.006	4.3
5.0	233.00	309.8	389.9	547.1	511.1	480.2	0.007	4.8
7.5	349.00	309.5	387.4	550.3	512.6	480.0	0.010	3.7
8.2	381.00	308.8	384.8	546.4	510.5	479.5	0.014	3.7
10.0	465.00	307.6	371.7	545.9	509.5	473.3	0.041	3.4
15.0	698.00	309.5	373.5	543.5	507.8	472.7	0.043	3.5
20.0	930.00	309.2	376.1	545.3	508.4	472.1	0.047	3.5

5MPFH-TDT was found to interact with a selection of non-ionic, cationic, and anionic micelles. The use of these surfactant solutions meant it was possible to obtain reproducible fluorescence emission data for this highly hydrophobic fluorophore. These surfactant molecules inhibited, to some extent, the formation of triazine aggregates in aqueous solution (Figure 27). 5MPFH-TDT behaved quite similarly in CrEL, TX-100, and CTAB: its emission bands were blue-shifted and its fluorescence intensity was increased. The blue shift observed with increasing non-ionic and cationic surfactants was due to the slightly greater dipole moment of the triazine in the excited state [79]. Binding of the fluorophore to the less polar interior of the micelle stabilised the ground state to a greater extent than the excited state resulting in a hypsochromic shift across the entire emission band [84, 118].

An increase in the fluorescence intensity of a fluorophore in the presence of micelles has been reported elsewhere in the literature [84, 117]. This phenomenon can occur for a number of reasons. Generally, encapsulation of a fluorophore within a micelle may act to enhance the emissive state of a fluorophore or inhibit the formation of a less emissive state [91]. For example, 4,4'-diaminodiphenyl sulfone (Dapsone) has both LE and TICT states but only the LE state is fluorescent. Therefore, inhibition of the formation of the TICT state, in the restrictive environment of a micelle for instance, can increase the fluorescence intensity from the LE state [117]. Interacting with the non-polar core of a micelle or simply being shielded from specific interactions which may result in de-excitation by non-radiative pathways may also result in an increase in the fluorescence intensity of a fluorophore [91]. However, based on the photophysical model of 5MPFH-TDT [79] and its behaviour in aqueous solution it seemed most likely that the increase in fluorescence intensity was due to a reduction in the formation of triazine aggregates evidenced by single-molecule investigations discussed in Section 3.1.

4.5 Fluorescence quenching of 5MPFH-TDT in mixed micellar solutions

Since the fluorescence intensity of 5MPFH-TDT was reduced following the addition of SDS and SDBS surfactants it was thought that the triazine was being quenched by the surfactant molecules. SDBS closely resembles the structure of SDS except a

phenyl sulfonate group replaces the sulfate group of SDS and it is marginally larger. Quenching in SDS and SDBS most likely occurs due to the smaller size of these anionic micelles (Table 7). When 5MPFH-TDT is incorporated into the micelles the fluorophore may be quite close to the charged group of the surfactants' hydrophilic component. Anion-induced quenching [119] seems to be the obvious answer and the process is based on a radiationless charge transfer mechanism between anion and excited states. RET and electron exchange quenching mechanisms were considered. RET is a through-space interaction which requires spectral overlap between the fluorescence emission of the donor and the absorbance of the acceptor. Typical Förster distances are within the range of 15 to 60 Å [7]. An electron exchange/Dexter interaction also requires spectral overlap. However, it only occurs over small distances when the electron clouds are in close enough proximity for electron exchange to occur (<< 30 Å). Since RET may occur over greater distances this mechanism dominates over electron exchange. However, when the spectral overlap is very small, the rate of electron exchange becomes more significant [120]. Since the Stern layer of an SDS micelle is 6–9 Å [91] and its radius is 21.6 Å [114] the micelle-encapsulated fluorophore is in close enough proximity to the charged sulfate head group for a Dexter interaction to occur.

However, the reduction in fluorescence intensity and fluorescence lifetime in aqueous SDS and SDBS solutions cannot be described either by a static or a dynamic quenching mechanism, using the Stern-Volmer equation (Equation 10 and Equation 11), and the modified form of the Stern-Volmer equation (Equation 13) does not improve the fit. Following a single molecule investigation of 5MPFH-TDT in micellar solutions (Figure 27) it was clear that it aggregates in aqueous solution making it difficult to obtain reproducible data. This meant it was impossible to determine the mechanism of quenching from this data alone. Therefore, the triazine was first stabilised in micelles of TX-100 before the introduction of the anionic quencher [53]. The concentrations of 5MPFH-TDT and TX-100 were kept constant at 10^{-6} M and 10^{-3} M, respectively, and solutions were spiked with a concentrated stock solution of SDS. The decrease in 5MPFH-TDT fluorescence emission intensity (Figure 45) was almost linear with increasing SDS concentration but there were two domains present (Figure 45b). The value of the slope for domain 1 (Figure 44c) was less than that calculated for domain 2 (Figure 44d) (Table 11).

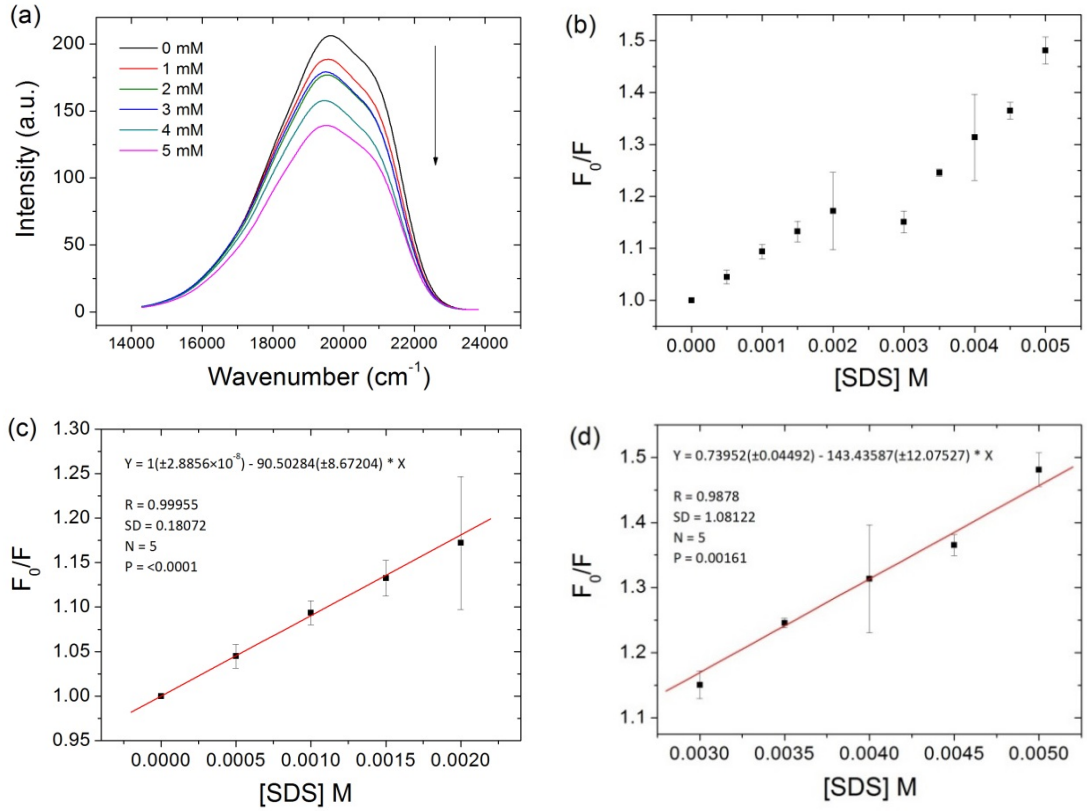

Figure 45: (a) Raw fluorescence emission spectra of 5MPFH-TDT in 10^{-3} M TX-100 solutions of varying SDS concentration. (b) A Stern-Volmer plot describes the fluorescence quenching of 5MPFH-TDT by SDS. (c) The first linear region describes a lower quenching efficiency. (d) The second linear region indicates a binding interaction between the fluorophore and quencher.

The bimolecular quenching constant indicates the efficiency of quenching or the accessibility of fluorophores to the quencher. Diffusion controlled quenching typically results in values of k_q of about 1×10^{10} $M^{-1}s^{-1}$. This value was determined from the quenching of tryptophan by oxygen and is considered to be the largest bimolecular quenching constant possible in water. However, as the diffusion coefficients of fluorophore and quencher decrease the bimolecular quenching constant decreases. Generally speaking, values of k_q less than this indicate steric shielding of the fluorophore or a low quenching efficiency and values of k_q greater than this indicate a binding interaction between the fluorophore and quencher [121]. Bimolecular quenching constants for the three emission bands of 5MPFH-TDT in the presence of SDS, up to concentrations of 2.0 mM, indicated a diffusion controlled quenching mechanism. However, for SDS concentration values within the range of 3.0 and 5.0 mM the bimolecular quenching constant increased indicating a more

efficient quenching mechanism than diffusion. It is likely that a mixed micelle unit consisting of both TX-100 and SDS had formed. The fluorescence of 5MPFH-TDT was thereby quenched more efficiently due to a binding interaction between the quencher and fluorophore.

Table 11: Stern-Volmer quenching constant and bimolecular quenching constant for 5MPFH-TDT in 10^{-3} M TX-100 solutions of varying SDS concentration.

		τ_0 (ns) ± SE	K_{SV} (M^{-1}) ± SE	k_q ($M^{-1}.s^{-1}$) ± RSE
Diffusion	**Band 1 (g_1)**	14.11 ± 0.01	90.50 ± 8.67	0.64×10^{10} ± 0.05%
	Band 2 (g_2)	10.96 ± 0.02		0.83×10^{10} ± 0.14%
	Band 3 (g_0)	8.17 ± 0.02		1.11×10^{10} ± 0.24%
Binding interaction	**Band 1 (g_1)**	14.11 ± 0.01	143.44 ± 12.08	1.02×10^{10} ± 0.06%
	Band 2 (g_2)	10.96 ± 0.02		1.31×10^{10} ± 0.14%
	Band 3 (g_0)	8.17 ± 0.02		1.76×10^{10} ± 0.25%

A reduction in the fluorescence lifetime with increasing SDS concentration was also observed. However the clear two domain quenching process that was observed from the steady-state fluorescence data was not evident from the dynamic Stern-Volmer quenching plots (Figure 46). However, the data followed a cubic polynomial trend quite well, indicating that a number of dynamic quenching processes were responsible for the reduction in 5MPFH-TDT fluorescence intensity. This was most likely due to the changing SDS-mole fraction of the mixed micelle [122]. Dynamic quenching dominates for lower SDS concentrations but as the mole fraction of SDS increased the rate of static quenching increased and dynamic quenching became less prominent. The slight increase in quenching efficiency (Figure 46d) at an SDS concentration of 5 mM is less easy to explain. It's possible that the composition of the micelles changed significantly at this concentration point so that dynamic quenching became more efficient relative to static quenching.

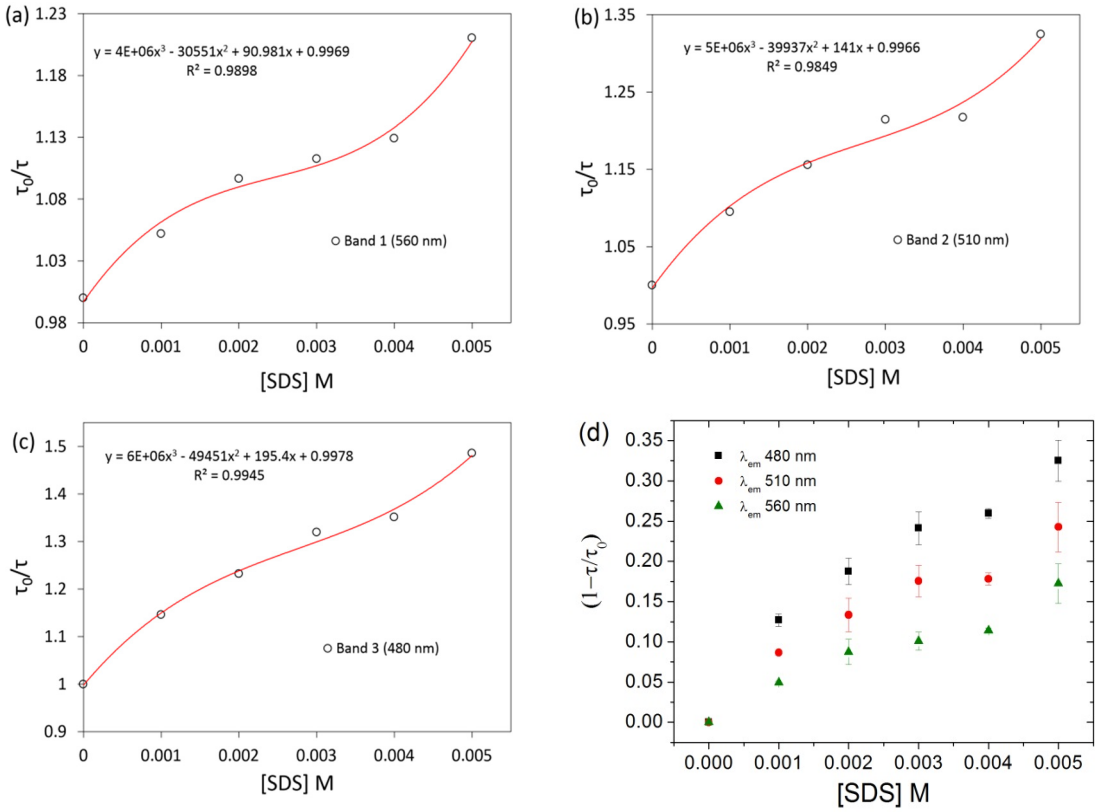

Figure 46: Dynamic quenching Stern-Volmer plots of 5MPFH-TDT in TX-100 solutions (10^{-3} M) spiked with SDS for (a) Band 1, (b) Band 2, and (c) Band 3 and (d) energy transfer efficiency of 5MPFH-TDT versus SDS concentration.

4.6 Binding constant determination of 5MPFH-TDT in micelles

Fluorophore-micelle binding constants were determined for the 5MPFH-TDT–micelle interactions. This was accomplished using the method proposed by Almgren *et al.* in 1979 [94]. Since the fluorescence intensity and anisotropy of 5MPFH-TDT were altered considerably upon the introduction of the non-ionic surfactants CrEL and TX-100 and the cationic surfactant CTAB (Figure 47) it was possible to approximate their CMC values from the steady-state data. However, multiple inflection points were evident from some of these plots.

In the case of TX-100, inflection points at a concentration of 3.25×10^{-4} M were evident in the fluorescence intensity and anisotropy plots. Another point occurred at the lower concentration point of 1.75×10^{-4} M for the fluorescence intensity data. This was most likely due to the existence of triazine aggregates in surfactant solutions below the CMC, which were detected by FCS measurements in the latter stages of

this project (Figure 27). These aggregates were very bright and diffused slowly in solution. Therefore the anisotropy data of 5MPFH-TDT in TX-100 solutions with a concentration below the CMC was representative of a molecule with a greater molecular weight than a monomer triazine unit. It can be seen from Equation 7 that the molecular weight of a molecule has a direct effect on its rotational correlation time. However, the interaction of a triazine aggregate with a monomer of TX-100 would not increase the molecular weight of the triazine aggregate to a great enough extent to strongly influence the rotational correlation time and fluorescence anisotropy of the fluorophore. This explains why we did not see a significant increase in the anisotropy until the concentration had exceeded the CMC and the formation of aggregates was reduced due to the inclusion of the fluorophore within the micelle units.

Two break points were also evident from the plot of fluorescence intensity versus CTAB concentration. The first derivative of this plot indicates an inflection point at a CTAB concentration of 10^{-4} M while the second point occurs at 10^{-3} M. This is the same behaviour we observed for 5MPFH-TDT in TX-100 solutions and can also be explained by the presence of large, bright triazine aggregates in CTAB solutions below the CMC. On the other hand, the fluorescence anisotropy data of 5MPFH-TDT in CrEL solutions indicated two inflection points at 3.0×10^{-6} M and 3.6×10^{-5} M while only the lower concentration inflection point (4.0×10^{-6} M) was evident from the fluorescence intensity data. The larger size of CrEL meant the anisotropy was more sensitive to the formation of pre-micellar aggregates (5MPFH-TDT–CrEL unimer). The lack of an inflection point at the higher concentration point for the intensity data indicated that a unimer of CrEL was capable of producing the increase in fluorescence. This was possibly due to the larger size and three-chain structure of this surfactant.

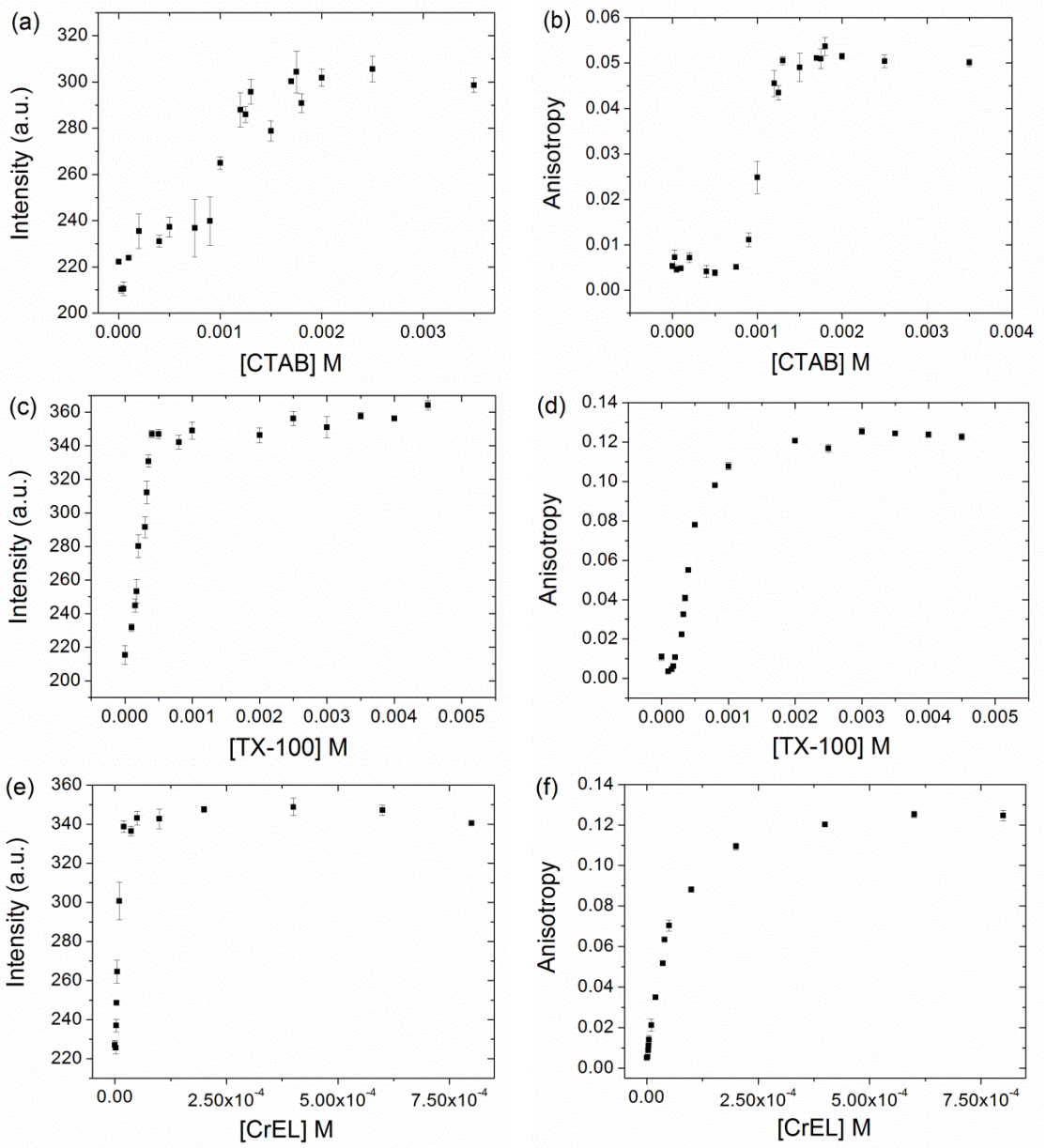

Figure 47: Variation of fluorescence intensity and anisotropy of 5MPFH-TDT (10^{-5} M) as a function of CTAB (a and b), TX-100 (c and d), and CrEL (e and f) concentration.

According to the method proposed by Almgren,

$$(I_{\propto} - I_0)/(I_t - I_0) = 1 + (K[M])^{-1} \qquad \textbf{Equation 29}$$

where I_0, I_t, and I_α are the fluorescence intensities in the absence of surfactant, at an intermediate surfactant concentration, and under conditions of complete micellisation, respectively. K is the binding constant and [M] is the micellar concentration. The micellar concentration may be determined by

$$[M] = (S - CMC)/N \qquad \textbf{Equation 30}$$

Where S is the surfactant concentration and N is the aggregation number. Aggregation numbers of 60 [94] and 143 [123] were used for CTAB and TX-100, respectively.

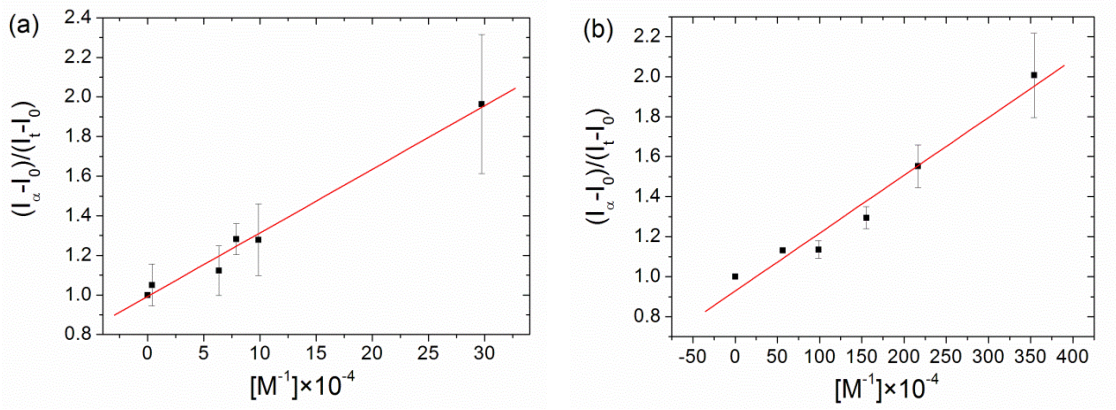

Figure 48: Binding constant plots for 5MPFH-TDT in micelles of (a) CTAB and (b) TX-100.

Binding constant values for the interaction between 5MPFH-TDT and micelles of both TX-100 and CTAB are presented in the table below. The binding interaction between 5MPFH-TDT and the non-ionic surfactant TX-100 was found to be approximately ten times stronger than its interaction with the cationic CTAB micelles. The strength of the triazine's interaction with these micelles was already indicated by the fluorescence anisotropy data in Figure 38a and Figure 44a, which showed maximum anisotropy values of 0.093 in TX-100 micelles and 0.056 in CTAB micelles ($\lambda_{ex}/\lambda_{em}$ 405/480 nm). As stated previously (Section 4.3) the larger palisade layer of the TX-100 micelle (25 Å) compared to the Stern layer of CTAB (10 Å) was most likely responsible for the disparity in binding constant and anisotropy values for these similarly sized micelles.

Table 12: Binding constant values for 5MPFH-TDT and a number of well-known fluorophores in TX-100 and CTAB micelles.

Fluorophore	Binding Constant (M^{-1})
CTAB	
5MPFH-TDT	3.11×10^5
Pyrene	102.0×10^5 [94]
Anthracene	26.0×10^5 [94]
Naphthalene	9.1×10^4 [94]
TX-100	
5MPFH-TDT	34.58×10^5
Pyrene	33.0×10^5 [124]
1-anilino-8-naphthalene sulfonate	0.9×10^5 [125]

The binding constant for a number of different fluorophores in CTAB and TX-100 micelles are presented in Table 12. The binding constant of a naphthalene–CTAB complex is comparable to the value reported for 5MPFH-TDT in Table 12. This is surprising considering the size and structural differences between these two molecules. The binding constant values reported for fluorophores in CTAB micelles increase with increasing molecular weight (pyrene > anthracene > naphthalene) but the triazine, which is the largest of all four fluorophores listed, does not fit in with this trend. However, the triazine lacks the planarity of the other fluorophores. Its L-shaped conformation could explain its slightly lower binding constant (Figure 18). Dapsone (Figure 49), a fluorophore which has a greater structural similarity with 5MPFH-TDT due to its V-shape, has a much lower binding constant in CTAB micelles (669 M^{-1}). The hydrophobicity which seemed to drive the triazine's interaction with micelles is possibly less prominent in the case of the Dapsone–CTAB interaction.

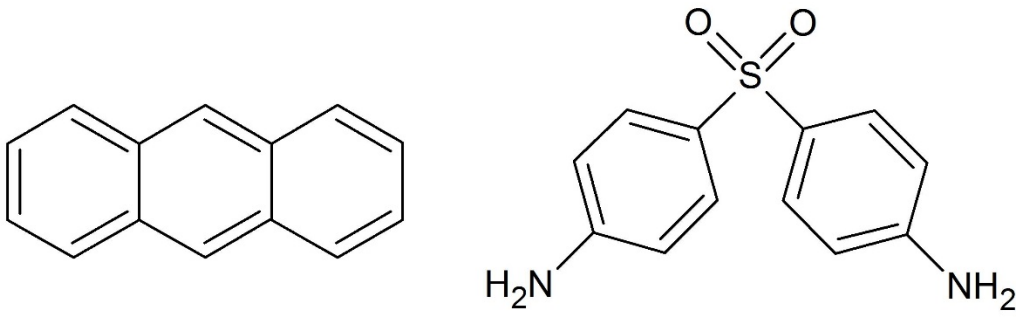

Figure 49: Anthracene has a planar geometry while Dapsone is V-shaped.

4.7 Microviscosity determination of micelles using 5MPFH-TDT

The relationship between the fluorescence anisotropy of 5MPFH-TDT and the viscosity could be used to estimate the position of the fluorophore in the micellar assemblies. The microviscosity, η_m, can be calculated from the Debye-Stokes-Einstein relation,

$$\eta_m = kT\theta/v_h \qquad \textbf{Equation 31}$$

where υ_h is the hydrodynamic volume of the fluorophore, k is the Boltzmann constant, T is the temperature, and θ is the rotational correlation time of the fluorophore. The rotational correlation time can be determined from the following equation:

$$\theta = \tau_f \left(\frac{r_0}{r} - 1\right)^{-1} \qquad \textbf{Equation 32}$$

where r_0 is the fundamental anisotropy, τ_f is the fluorescence lifetime, and r is the anisotropy of the fluorophore in the micelle.

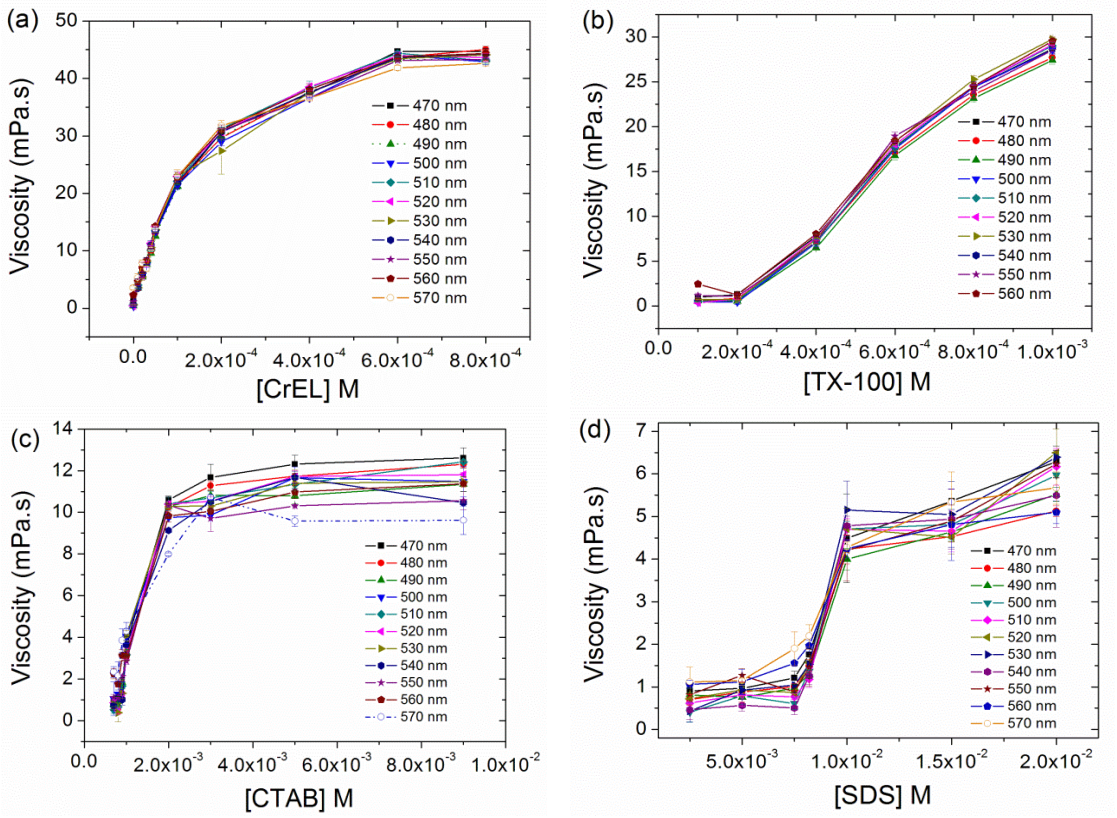

Figure 50: Microviscosity reported by 5MPFH-TDT in micelles of (a) CrEL, (b) TX-100, (c) CTAB, and (d) SDS.

The microviscosity values reported by 5MPFH-TDT in micelles of TX-100, and CTAB were close to those values reported in the literature (Table 13) [126, 127]. Since the fluorescence of 5MPFH-TDT was quenched in micelles of SDS we could not rely on the microviscosity value determined by our fluorophore for this micelle. Viscosity values of 29.00 and 11.85 mPa.s were reported by 5MPFH-TDT for TX-100 and CTAB, respectively. This result helped to explain the micelle binding constant values reported for 5MPFH-TDT in Section 4.6. The greater viscosity values reported for TX-100 indicated that the triazine was more restricted in this micelle than in a micelle of CTAB. This was most likely due to the longer hydrophilic head group of TX-100 (25 Å) compared to that of CTAB (10 Å). Since these micelles both have a radius of about 50 Å, the TX-100 has a much more compact hydrophobic interior than CTAB [91]. These viscosity values are lower than those reported by Roy *et al.* (39.81 and 17.77 mPa.s) using 1,6-diphenyl-1,3,5-hexatriene (DPH). This variance was most likely due to the difference in geometry between the two fluorophores. DPH has been shown to locate itself close to the acyl chains within a dipalmitoylphosphatidylcholine (DPPC) bilayer, orientated in the direction of the

membrane normal [126, 128]. The rod-like shape of DPH (Figure 51a) is less bulky than 5MPFH-TDT and therefore may align quite closely with the hydrophobic chains. The L-shaped geometry of 5MPFH-TDT means it is held less rigidly in place by the linear, hydrocarbon tails.

(a) (b)

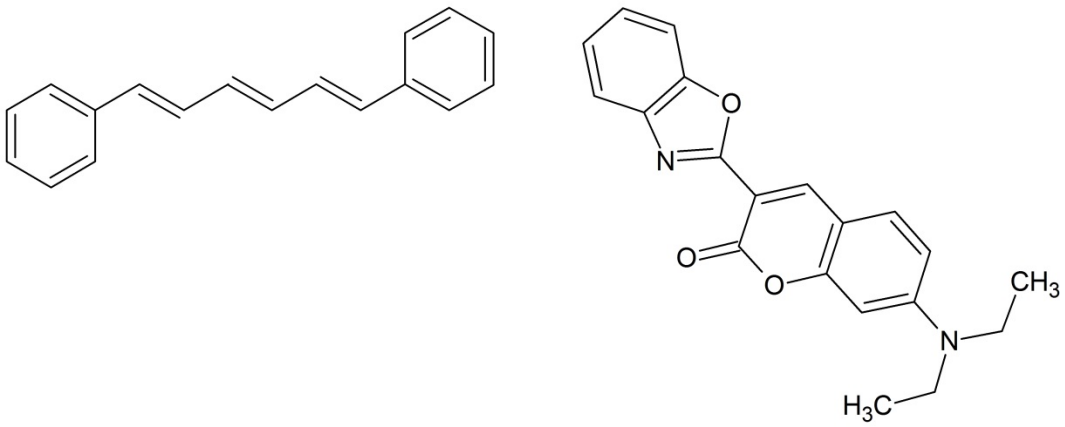

Figure 51: Microviscosity fluorophores (a) DPH, and (b) 3-benzoxazol-2-yl-7-(N,N-diethylamino)-chromen-2-one.

Conversely, the fluorophore used by De Paula *et al.*, 3-benzoxazol-2-yl-7-(N,N-diethylamino)-chromen-2-one (Figure 51b), reports a slightly lower value of microviscosity than 5MPFH-TDT. This is probably because this fluorophore is bulkier than DPH and cannot align as closely with the hydrophobic chains of the micelle.

Table 13: Rotational correlation times, τ_R, and microviscosity values, η_m, for 5MPFH-TDT in micelles of CrEL, TX-100, CTAB, and SDS for Band 1 (λ_{em} 530 nm), Band 2 (λ_{em} 500 nm), and Band 3 (λ_{em} 470 nm).

S	Band	r	τ_f (ns)	τ_R (ns)	η_m (mPa.s) ± SE	Ref. η_m (mPa.s)
CrEL (0.08 mM)	Band 1	0.097	12.38	4.40	44.1 ± 0.8	
	Band 2	0.113	9.73	4.28	42.9 ± 0.5	
	Band 3	0.134	7.85	4.46	44.7 ± 0.6	
TX-100 (1.0mM)	Band 1	0.071	12.52	2.97	28.7 ± 0.2	39.81 [126]
	Band 2	0.084	9.70	2.85	28.6 ± 0.2	
	Band 3	0.101	7.62	2.86	29.8 ± 0.1	
CTAB 9.0 mM)	Band 1	0.047	11.32	1.14	11.5 ± 0.2	17.77 [126], 6.78 [127]
	Band 2	0.035	8.27	1.15	11.5 ± 0.7	
	Band 3	0.060	6.70	1.26	12.6 ± 0.5	
SDS (20.0 mM)	Band 1	0.030	7.29	0.64	6.4 ± 0.2	16.33 [126], 7.4 [127]
	Band 2	0.040	4.85	0.60	6.0 ± 0.5	
	Band 3	0.058	3.35	0.63	6.3 ± 0.4	

4.8 Conclusion

The fluorescence emission properties of 5MPFH-TDT were investigated in non-ionic, cationic, and anionic micelles in aqueous solution. The addition of surfactants to an aqueous solution of the triazine reduces the formation of triazine aggregates, which results in an increase in the fluorescence intensity. However, changes to the emission band properties were minimal across a range of surfactant concentrations. In the case of SDS micelles, it was found that 5MPFH-TDT was subject to anionic quenching by a Dexter interaction. A considerable increase in the fluorescence anisotropy with increasing surfactant concentration was observed. Simultaneously, the fluorescence lifetime increased dramatically. This meant that the recorded anisotropy data was underestimating the extent of the interaction between 5MPFH-TDT and the micelles. A binding study assessed quantitatively the interaction between 5MPFH-TDT and micelles of both TX-100 and CTAB. Binding constant values were on the scale of those recorded for the well-known fluorophores, pyrene and naphthalene. It was also noted that each of the three fluorescence lifetime components associated with the triazine's three emission bands increased linearly with emission wavelength. This trend is ascribed to the Strickler-Berg defined relationship between the fluorescence lifetime and the refractive index.

5 Förster Resonance Energy Transfer of triazine fluorophores

5.1 Introduction

Organising fluorophores in fixed assemblies for the purposes of energy transfer processes is of interest due to the development of devices that exploit this phenomenon [129]. However, since covalently linked FRET assemblies can be time-consuming and costly to develop, systems in which the donor and acceptor are covalently linked to a scaffold are not always economical. Self-assembling systems that rely on non-covalent interactions are thought to provide an alternative scaffold for energy transfer networks. Micelles provide a suitable model system due to their ability to co-solubilise donor-acceptor fluorophores at fixed distances. Furthermore, their reliance on non-covalent interactions such as hydrogen bonding, and dipole-dipole, van der Waals, and hydrophobic interactions is biomimetic in nature [130]. If the energy transfer process between a donor and acceptor pair in a particular assembly is well-understood, the assembly may be fine-tuned for altered functionality.

The fluorescence data discussed in Chapter 3 indicated that the triazine was interacting with the micelles in solution. In order to confirm 5MPFH-TDT's position within the micelles, and to assess its suitability as a FRET donor, an energy transfer study was carried out. FRET may be employed for such a study due to its distance-dependence. Both a water-soluble and a non-water soluble fluorophore were used in the case of CTAB micelles. Sulforhodamine 101 (SR101) and tetramethylrhodamine isothiocyanate (TRITC) were selected as FRET acceptors since they absorb at the emission band of 5MPFH-TDT (λ_{abs} SR101 = 590 nm and λ_{abs} TRITC = 550 nm) (Figure 52a and b).

It can be seen from these figures that the absorbance of SR101 in the CTAB solution spanned from ~500–620 nm while its emission began at ~570 nm. TRITC, on the other hand, had an absorbance profile spanning ~470−590 nm and its emission band began at ~540 nm. SR101 had a very low molar extinction coefficient at an excitation wavelength of 400 nm (1333.33 M^{-1} cm^{-1} in CTAB solution), and it is highly soluble in water [131]. A fluorescence lifetime of 4.12 ± 0.01 ns (λ_{ex} 580 nm) has been

reported by Ishizaka *et al.* for SR101 in aqueous solution [132]. TRITC, on the other hand, is a very hydrophobic fluorophore with limited solubility in water [133]. However, its molar extinction coefficient at 400 nm (3660.0 M^{-1} cm^{-1} in CTAB solution) is not negligible. A preliminary investigation found TRITC to be less suitable as a FRET acceptor for the triazine donor (Appendix A.2). The following equation was used to correct for any absorbance by the acceptor fluorophores [38].

$$F_{corr} = F_{obs} antilog\left(\frac{OD_{ex} + OD_{em}}{2}\right) \qquad \textbf{Equation 33}$$

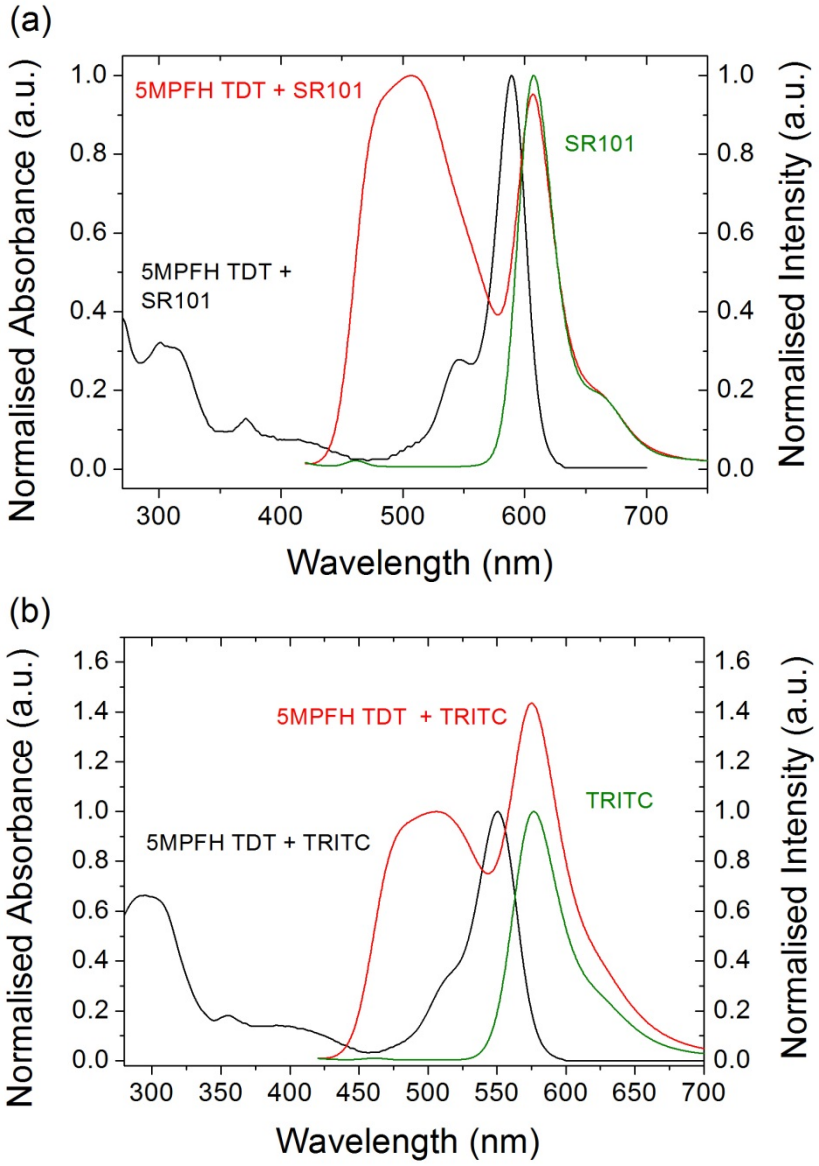

Figure 52: Overlaid normalised absorbance and fluorescence emission spectra of 5MPFH-TDT (10^{-6} M) in 2.0 mM CTAB solutions along with an equal concentration of the FRET acceptor (a) SR101 (10^{-6} M) and (b) TRITC (10^{-6} M).

5.2 Förster Resonance Energy Transfer for the FRET pair 5MPFH-TDT and SR101 in CTAB micelles

The overlap integral[8] was determined for the overall emission band and each of the triazine's individual emission bands (Figure 53a). The overlap integral was greatest for Band 1, the longest wavelength emission band (Table 14). This was important to note because the visual impression of overlap (Figure 53b), could be misleading since the overlap integral, J(λ), depends on λ^4 (Equation 17) [19]. Therefore, as the fluorescence emission wavelength tends to longer wavelengths, J(λ) should increase significantly.

Table 14: The overlap integral of SR101 absorbance and 5MPFH-TDT fluorescence emission for each of the three individual emission bands. Relative standard error is indicated.

Micelle	Band 1 (±RSE)	Band 2 (±RSE)	Band 3 (±RSE)	Total (±RSE)
CTAB	3.0×10^{15} (±0.3%)	8.1×10^{14} (±1.3%)	3.4×10^{14} (±6.0%)	1.6×10^{15} (±1.5%)

[8] a|e—UV-Vis-IR Spectral Software 1.2 (http://www.fluortools.com/software/ae).

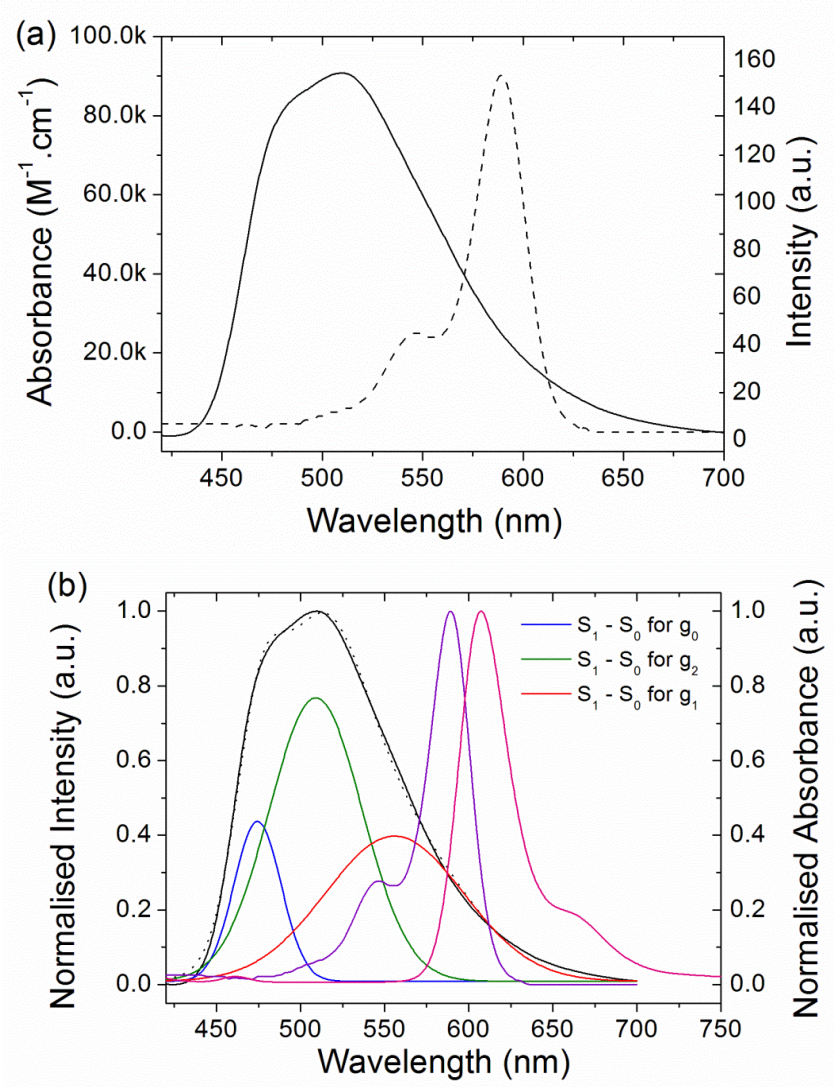

Figure 53: 5MPFH-TDT (10^{-6} M) and SR101 (10^{-6} M) in 2.0 mM CTAB solutions: (a) spectral overlap of 5MPFH-TDT fluorescence emission (λ_{ex} 400 nm) and SR101 absorbance; (b) normalised band-fitted fluorescence emission spectrum of 5MPFH-TDT overlaid with the absorbance and emission spectra of SR101.

In this energy transfer study it was assumed that all the 5MPFH-TDT fluorophores were associated with CTAB micelles. The concentration of 5MPFH-TDT was maintained well below the micellar concentration to remove the likelihood of self-quenching. The effect of increasing acceptor concentration on the fluorescence of 5MPFH-TDT was assessed and modelled according to a number of quenching mechanisms to assess the most likely scenario by which energy transfer takes place.

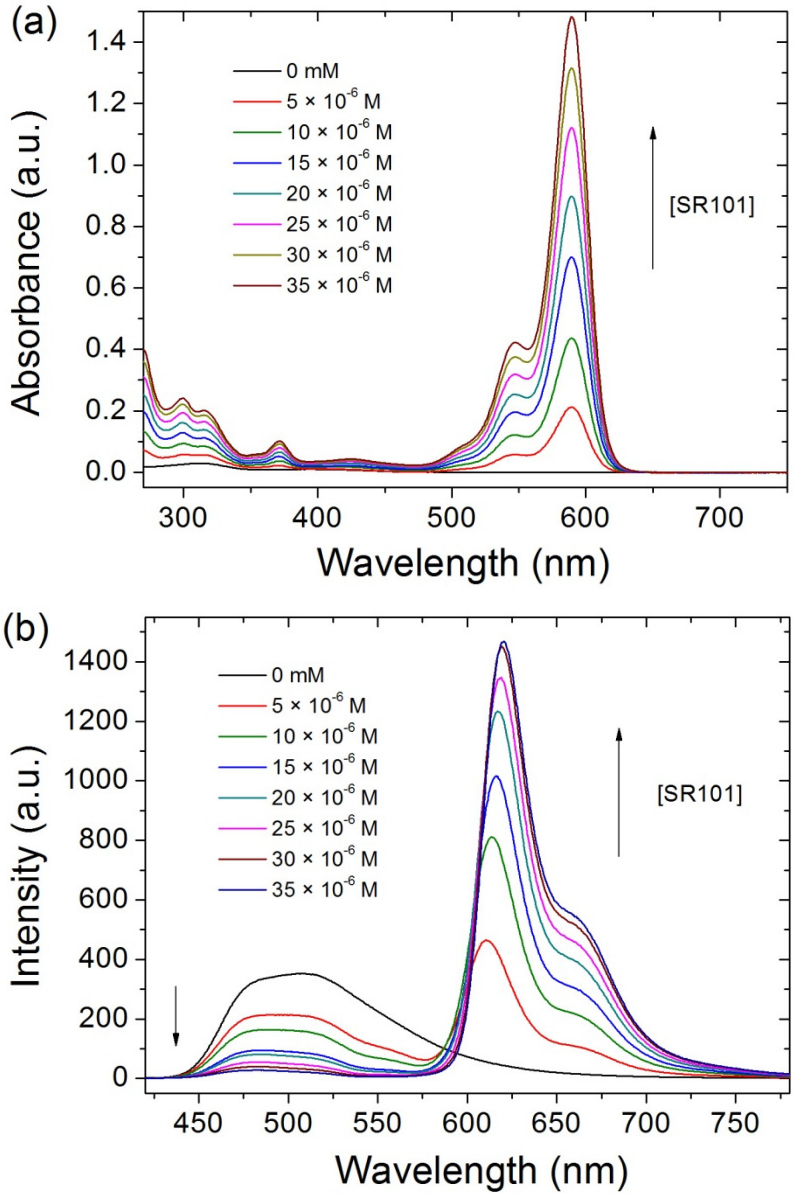

Figure 54: (a) Absorbance and (b) fluorescence emission spectra of 5MPFH-TDT (5×10^{-6} M) in the presence of increasing quantities of the FRET acceptor SR101 in 2.0 mM CTAB solutions.

The fluorescence emission spectra (Figure 54b) show the reduction in the fluorescence intensity of 5MPFH-TDT upon the introduction of SR101. Even at a donor-acceptor ratio of only one-to-one, when the likelihood of co-localisation was relatively low, the reduction of triazine fluorescence was marked and the inner-filter effect was only responsible for a small fraction of this reduction of fluorescence intensity (Table 15). We also observed the appearance of the sensitised fluorescence emission of SR101. This sensitised emission is red-shifted with increasing SR101

concentration and is probably due to self-absorption of co-localised acceptor fluorophores in the same micelle.

Table 15: Fluorescence intensity of 5MPFH-TDT in the presence of increasing quantities of the FRET acceptor SR101 corrected for the inner-filter effect. Standard error is indicated.

[SR101] µM	F_{obs} (±SE)	OD_{ex}	OD_{em}	F_{corr} (±SE)
0	351.5 ± 15.3	0.01	0.00	355.5 ± 15.3
5	209.5 ± 3.4	0.01	0.01	214.9 ± 3.5
10	157.8 ± 3.5	0.02	0.03	165.7 ± 3.6
15	85.5 ± 2.4	0.02	0.04	91.7 ± 2.6
20	71.2 ± 0.4	0.03	0.06	78.1 ± 0.5
25	45.5 ± 1.0	0.03	0.07	51.0 ± 1.1
30	31.6 ± 1.5	0.03	0.08	36.1 ± 1.5
35	21.4 ± 0.7	0.04	0.09	24.7 ± 0.8

A Stern-Volmer plot and a Perrin plot (Figure 55a) were used to model the fluorescence quenching of 5MPFH-TDT and SR101 in CTAB micelles. The upward curvature of the Stern-Volmer plot indicated that more than one mechanism was responsible for the fluorescence quenching observed. The modified Stern-Volmer plot (Figure 55b), which models quenching by a ground-state complex, static mechanism and a collisional mechanism, did not adequately describe the data either. However, good-linearity was observed for the Perrin-plot, which describes a type of static quenching where the donor and acceptor molecules are adjacent at the time of excitation. Quenching is said to take place in a "sphere-of-action" where the probability of quenching is unity [121]. The modified form of the Stern-Volmer equation in this case takes the following form,

$$\frac{\mathbf{F_0}}{\mathbf{F}} = (\mathbf{1} + \mathbf{K_D}[\mathbf{Q}])\mathbf{exp}(\mathbf{V_M}[\mathbf{Q}]) \qquad \textbf{Equation 34}$$

where V_M is the molar volume in which quenching may take place. The fit of Equation 34 indicated a V_M of 72,332 $dm^3\ mol^{-1}$, which corresponds to a "sphere-of-action" of radius 306.08 Å. This is several times the radius of the CTAB micelle and suggests that several CTAB micelles had aggregated in solution. This behaviour is

reported for SDS micelles in the presence of silver nitrate ($AgNO_3$). Garden *et al.* reported that the addition of $AgNO_3$ to SDS micelles led to the formation of aggregate structures of diameter 52.5–68.4 nm as measured by dynamic light scattering and scanning electron microscopy. The aggregates in this case were ascribed to a reduction in the thickness of the electrical double layer upon $AgNO_3$ addition. [134].

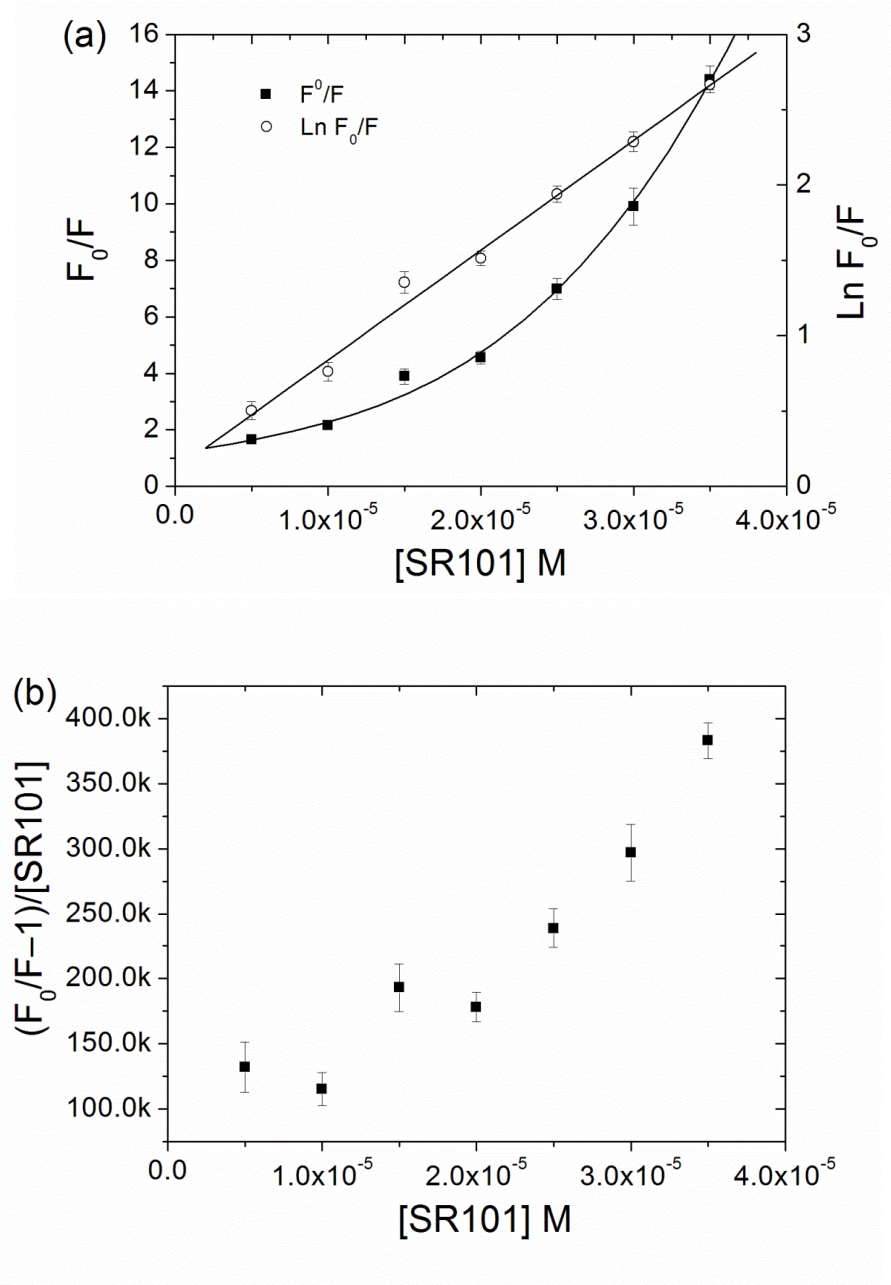

Figure 55: (a) Stern-Volmer plot (■) and Perrin plot (○) of 5MPFH-TDT quenching by SR101 in CTAB micelles and (b) modified Stern-Volmer plot.

Dynamic quenching also played a role in the reduction of 5MPFH-TDT fluorescence, which was demonstrated by the marked decrease in the triazine's fluorescence

lifetime with increasing SR101 concentration (Figure 56a). The fit data for some of these lifetime measurements can be found in Table 24 and Appendix A.2. The Stern-Volmer plot (Figure 56b) also exhibits an upward curvature that is concave towards the y-axis. It fits well to a second order polynomial indicating that the mechanism of quenching is altered with changing acceptor fluorophore concentration.

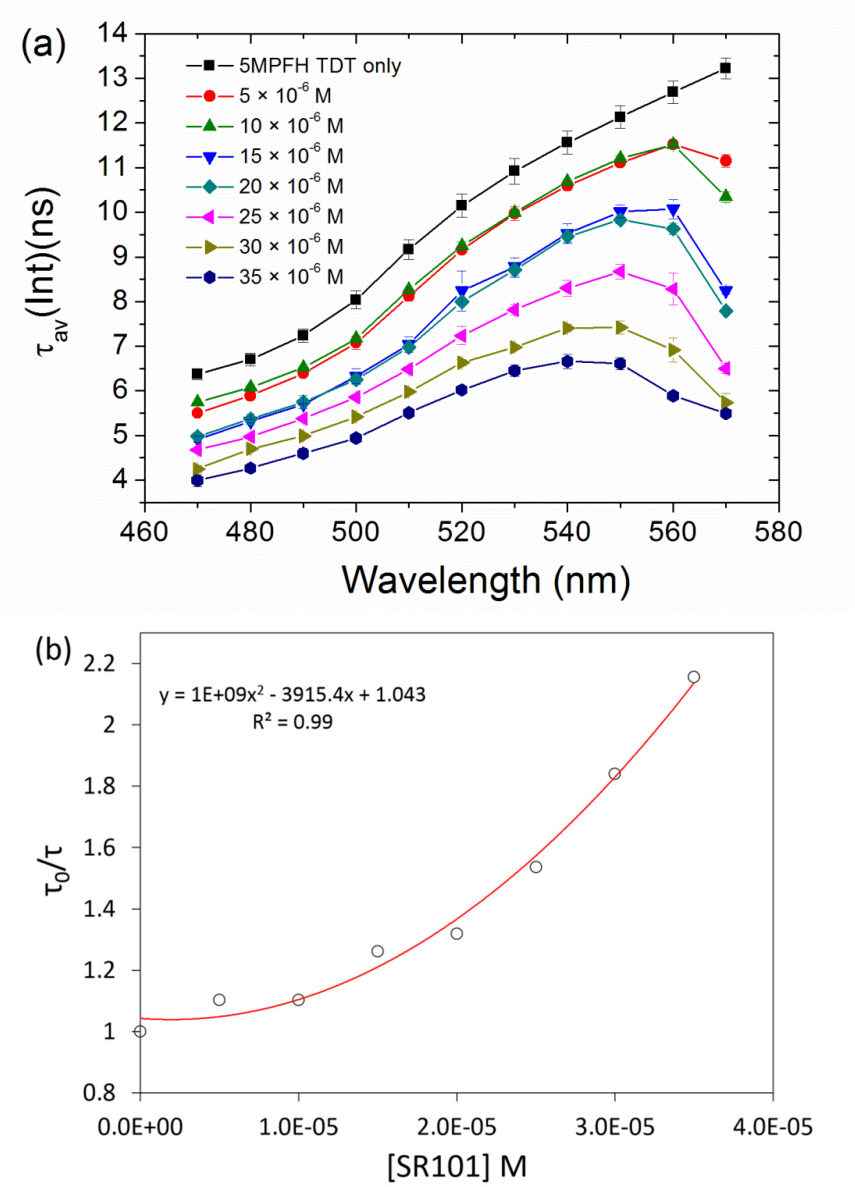

Figure 56: (a) Average intensity weighted fluorescence lifetime, (τ_{av}) (λ_{ex} 405 nm) of 5MPFH-TDT (5×10^{-6} M) in the presence of increasing quantities of the FRET acceptor SR101 in 2.0 mM CTAB solutions. (b) Stern-Volmer plot of 5MPFH-TDT quenching by SR101 in CTAB micelles (λ_{em} 560 nm).

Since dynamic quenching contributed to the quenching of 5MPFH-TDT it was necessary to determine if energy transfer occurred between donor and acceptor fluorophores in neighbouring micelles. Quenching that occurs on an intramicelle level is only dependent on the likelihood that an acceptor fluorophore exists in the same micelle as the donor fluorophore. Therefore, the probability of energy transfer is directly related to the probability of finding acceptor fluorophores in micelles. The distribution of acceptor fluorophores in micelles obeys Poisson statistics,

$$P_n^A = \frac{x^n e^{-x}}{n!} \qquad \textbf{Equation 35}$$

where P_n^A is the probability that a micelle contains n acceptor fluorophores, and x is the mean number of acceptor fluorophores per micelle. The number of surfactant molecules which form a micelle must be known to determine the micelle concentration (Equation 30). For the purposes of this calculation, CTAB aggregation numbers of 60 [94], 90 [135], and 104 [136] were used.

$$x = \frac{[Acceptor]}{[Micelle]} \qquad \textbf{Equation 36}$$

Therefore, the probability that a micelle contained at least one acceptor fluorophore was equal to $1\text{-}P_0^A$. The energy transfer efficiency and the probability of a micelle containing an acceptor were plotted against acceptor concentration and compared (Figure 57). The energy transfer efficiency reported by this quenching study was greater than $1\text{-}P_0^A$, which indicated that energy transfer was not completely dependent upon co-localisation of donor and acceptor fluorophores within the same micelle and a certain degree of inter-micelle energy transfer occurred.

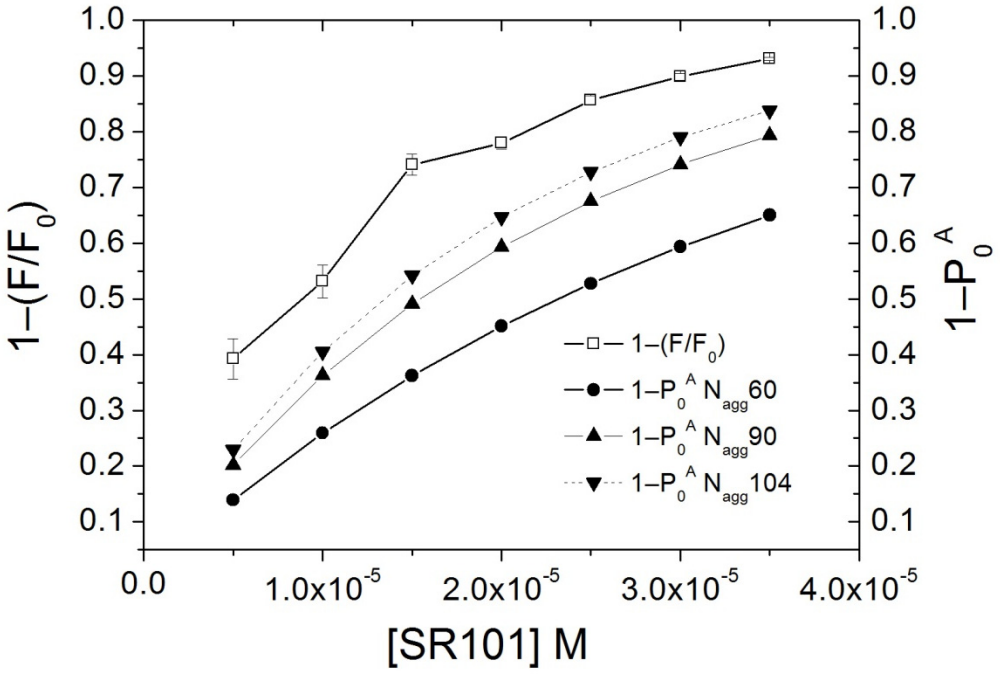

Figure 57: Energy transfer efficiency (□) as a function of SR101 concentration and the probability of finding SR101 in micelles for a number of CTAB aggregation numbers of 60 (●), 90 (▲), and 104 (▼).

Table 16: Fluorescence lifetime (λ_{ex} 405 nm) decay parameters of 5MPFH-TDT (5×10^{-6} M) in the presence of the FRET acceptor SR101 (35×10^{-6} M) in 2.0 mM CTAB solutions. Standard error is indicated.

λ (nm)	a_1	a_2	a_3	τ_1 (ns)	τ_2 (ns)	τ_3 (ns)	τ_{av} (ns)	χ^2 (red)
470	483.1 ± 69.9	1036.0 ± 93.6	3653.0 ± 150.8	6.7 ± 0.5	1.7 ± 0.3	0.35 ± 0.04	4.0 ± 0.1	1.212
480	577.4 ± 38.3	1118.8 ± 38.3	3210.5 ± 53.5	6.7 ± 0.1	1.6 ± 0.1	0.36 ± 0.01	4.3 ± 0.0	1.152
490	602.6 ± 36.3	1163.6 ± 62.2	3082.0 ± 157.6	7.1 ± 0.2	1.7 ± 0.1	0.37 ± 0.02	4.6 ± 0.1	1.237
500	614.7 ± 12.8	1200.9 ± 19.3	3129.5 ± 134.3	7.5 ± 0.1	1.7 ± 0.1	0.38 ± 0.02	4.9 ± 0.1	1.203
510	616.4 ± 32.8	1200.3 ± 39.2	2969.9 ± 84.5	8.2 ± 0.1	1.8 ± 0.1	0.38 ± 0.01	5.5 ± 0.0	1.157
520	630.0 ± 12.0	1221.0 ± 14.0	2864.4 ± 71.7	8.8 ± 0.1	1.8 ± 0.1	0.39 ± 0.01	6.0 ± 0.1	1.239
530	638.9 ± 13.2	1255.1 ± 46.2	2702.7 ± 135.7	9.3 ± 0.2	1.8 ± 0.1	0.38 ± 0.02	6.5 ± 0.1	1.245
540	659.2 ± 8.9	1300.9 ± 26.6	2894.7 ± 171.8	9.6 ± 0.2	1.8 ± 0.1	0.38 ± 0.02	6.7 ± 0.2	1.201
550	729.1 ± 16.6	1301.2 ± 39.6	2849.7 ± 57.2	9.3 ± 0.2	1.9 ± 0.1	0.38 ± 0.01	6.6 ± 0.1	1.204
560	1061.1 ± 11.3	1205.7 ± 10.7	2560.1 ± 15.5	7.8 ± 0.1	2.2 ± 0.0	0.39 ± 0.00	5.9 ± 0.1	1.238
570	415.9 ± 47.4	2362.8 ± 43.5	1313.3 ± 70.2	9.2 ± 0.4	4.5 ± 0.1	0.49 ± 0.02	5.5 ± 0.1	1.255

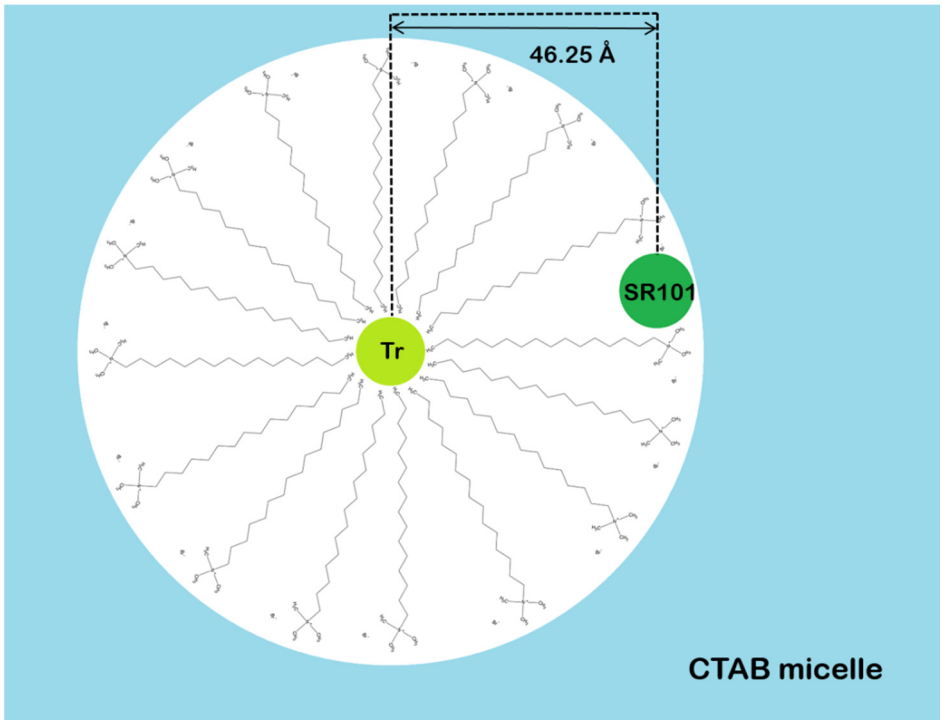

Figure 58: Förster distance of the 5MPFH-TDT–SR101 FRET pair in a CTAB micelle.

All of the FRET parameters are tabulated in Table 17. A donor-acceptor distance of 46.25 (±0.32) Å was calculated, which is less than the reported value for the radius of CTAB micelles. This could mean that one of the fluorophores was positioned in the very centre of the micelle while the other fluorophore was interacting with the Stern layer. The hydrophobic nature of 5MPFH-TDT suggests that it was located in the non-polar, central region of the micelle while SR101, which is known for being highly surface active, was most likely located in the Stern layer [132]. The presence of the charged SR101 fluorophore in the Stern layer could have produced a reduction in the electrical double layer of the micelle resulting in the formation of CTAB micelle aggregates. This would explain the larger "sphere of action" determined from the Perrin plot (Figure 55a).

Table 17: The Förster distance, overlap integral, transfer efficiency, and the donor-acceptor distance for 5MPFH-TDT (10^{-6} M) and SR101 (35×10^{-6} M) in CTAB micelles. Relative standard error is indicated.

$J(\lambda)$ (M^{-1} cm^{-1})	τ_{DA} (ns) (560 nm)	τ_{D} (ns) (560 nm)	E	R_0 (Å)	R_{DA} (Å)	Radius (Å)
1.6×10^{15} (±1.6%)	5.9 (±1.2%)	12.7 (±2.0)	0.536 (±1.6%)	47.4 (±0.3%)	46.3 (±0.3%)	50.0 [115]

5.3 Conclusion

Herein it was found that 5MPFH-TDT may be used as a donor fluorophore, alongside the acceptor fluorophore, SR101, for RET investigations of micelle size and solution behaviour. The triazine and rhodamine fluorophores colocalised in micelles of CTAB and a donor–acceptor distance of 46.25 (±0.32%) Å was determined. As SR101 is known to be a highly surface active fluorophore it was concluded that it interacted at the periphery of the micelle while 5MPFH-TDT was located in the micelle core. A fluorescence quenching investigation revealed that quenching was taking place by a "sphere-of-action" mechanism. However, this model indicated a quenching volume with a radius several times the size of a single CTAB micelle. Micellar aggregation was believed to be the cause of this larger than expected volume and it was thought that this came about due to the presence of the charged SR101 fluorophore at the surfactant-water boundary.

6 Fluorescence emission properties of 5MPFH-TDT in BSA

6.1 Introduction

Following a biomolecule's behaviour in solution requires the use of a reporter or sensor. A number of methods are in use for this application including radioactive tracers, electrochemical sensors, and fluorescent labels. Fluorescent labelling is generally considered preferable due to its non-destructive nature and high sensitivity. Fluorescent labelling is often accomplished by conjugation of the fluorophore to a specific site on the target molecule [137]. However, sometimes the fluorophore is non-covalently bound to the biomolecule. This can be favourable as it may produce minimal interference to the molecule's unlabelled solution behaviour. Although this type of labelling may be less stable, it occurs at a faster rate and purification steps may be unnecessary [138].

A well-characterised and extensively studied protein is most useful for the purposes of investigating a new fluorophore whose binding characteristics are not well-understood. Serum albumin proteins are some of the most widely studied proteins in science[9]. This is partly due to their ease of availability and low cost. These proteins bind and transport a wide range of ligands including fatty acids, amino acids, Cu^{2+}, Ni^{2+}, and a range of pharmaceuticals. Molecular forces such as hydrogen bonding, and electrostatic and hydrophobic interactions at the various binding sites contribute to its binding characteristics [139, 140]. The predominantly helical structure of serum albumin is composed of three similar domains which are arranged in an overall heart-shaped conformation. Seventeen disulphide bridges confer a high degree of stability to this conformation. Each homologous domain is composed of two subdomains, A and B, which are composed of six and four helical structures, respectively. It has been revealed by extensive crystallographic studies that ligands are primarily bound to subdomains IIA and IIIA [141, 142].

[9] A Google Scholar search of 'serum albumin' returns 2,440,000 results and a Science Citation Index search returns 81,323 publications.

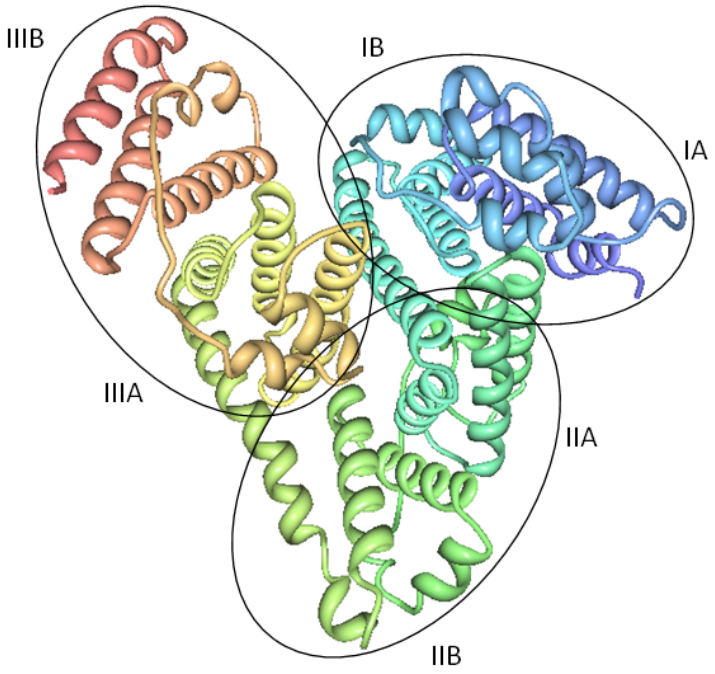

Figure 59: Crystal structure of bovine serum albumin (2.47 Å resolution) from the protein data bank (PDB ID: 4F5S). The three domains and subdomains of bovine serum albumin are indicated [143].

Up until recently, human serum albumin (HSA) was the primary focus of structural investigations of serum albumins with about seventy structures of HSA complexes deposited in the protein data bank[10]. This was most likely due to crystallisation and diffraction difficulties associated with other species of serum albumin. Since all mammalian serum albumins exhibit fairly high sequence homology they are often studied with the structure of HSA as a template [139]. However, since 2012 a number of crystal structures of bovine serum albumin (BSA) and BSA complexes have been deposited in the protein data bank [143-146]. BSA, which is one of the most widely used proteins in laboratory practise, is often used as a replacement of HSA in kinetic and affinity drug tests [143, 145], as a molecular-weight standard [140], and in immunological tests including ELISAs [147].

As discussed in Section 1.7, a protein may exhibit intrinsic fluorescence if it contains the aromatic amino acids. The fluorescence emission of tryptophan, which is particularly sensitive to its environment, often changes in response to conformational

[10] This refers to a PDB search carried out in July 2016.

transitions, substrate binding, or denaturation. However, these amino acids are relatively rare in protein molecules and it is often necessary to introduce an extrinsic fluorophore to investigate a protein using fluorescence based methodologies [18]. 1-Anilinonaphthalene-8-sulfonate (ANS) is a well-known, hydrophobic fluorophore that was found to exhibit a weak, green fluorescence emission band in aqueous solution while in BSA an intense blue emission band was observed [148]. This makes them particularly useful as the background fluorescence from unbound fluorophore is minimal [149]. Togashi *et al.* reported a binding ratio of 1:5 for an BSA–ANS complex [139]. This relatively large ratio is useful if a strong fluorescence signal is important. However, fluorescent labelling of fluorophores is known to affect the solution behaviour of some proteins and a larger fluorophore–protein ratio may exacerbate this problem [150]. Gajraj *et al.* reported that the ratio of a BSA–FITC complex had a significant effect on the diffusion coefficient of BSA in solution. This was attributed to the greater degree of surface hydrophobicity that was conferred to BSA at higher fluorophore–protein ratios [151]. Low fluorophore–protein ratios may give a truer assessment of the solution behaviour of the protein of interest.

6.2 Binding stoichiometry of a BSA−5MPFH-TDT complex

The binding stoichiometry of 5MPFH-TDT and BSA was determined using a Job plot analysis [152]. In this method the molar fractions of the ligand and the protein are varied while their total concentration is kept constant. A measureable parameter, which is altered significantly upon binding, is monitored. In the case of 5MPFH-TDT and BSA both the anisotropy and the band position of 5MPFH-TDT were monitored and plotted against 5MPFH-TDT mole fraction. Linear regressions were performed on the two extreme ends of the curve. The crossing point of these linear regions indicated the concentration of 5MPFH-TDT at which the binding stoichiometry had been reached. The intercept of the two straight lines in the anisotropy plot occurred at a 5MPFH-TDT mole fraction of 0.329 while the intercept in the band position plot occurred at 0.326. This corresponded to a BSA−5MPFH-TDT binding stoichiometry of 2:1. A variety of different labelling strategies for 5MPFH-TDT and BSA were attempted. The conditions under which these binding studies were carried out were chosen based on experiments outlined in Appendices A.5, A.6, and A.7. These samples were made up using a 100 mM phosphate buffer of pH 9 with an ionic

strength of 300 mM and the total concentration of 5MPFH-TDT and BSA was maintained at 2×10^{-5} M.

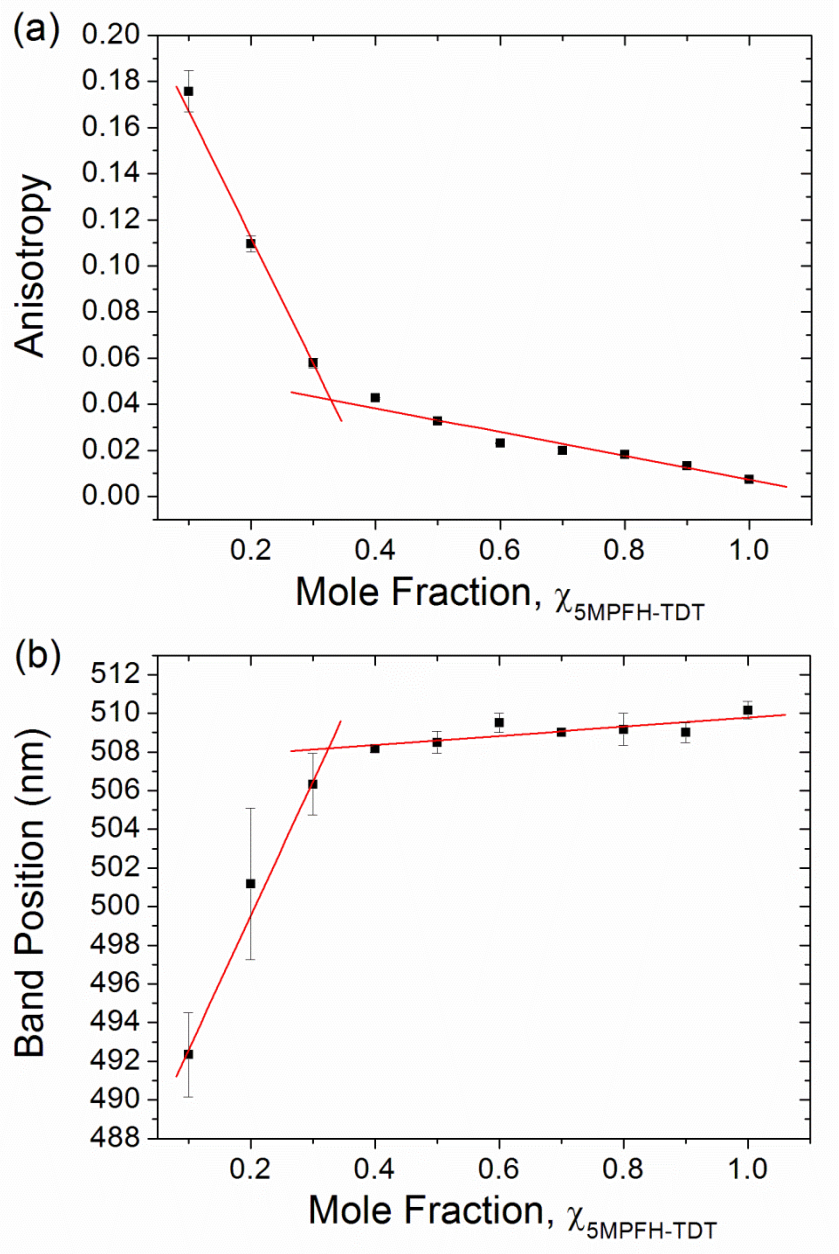

Figure 60: Job plots for BSA−5MPFH-TDT fluorescence (a) anisotropy ($\lambda_{ex}/\lambda_{em}$ 405/480 nm), and (b) band position (λ_{ex} 400) for a total concentration [5MPFH-TDT] + [BSA] = 2×10^{-5} M.

The BSA−5MPFH-TDT binding stoichiometry of 2:1 suggested that dimers of BSA had formed as a consequence of labelling. Though BSA is a monomeric protein, the presence of the triazine on its surface may have resulted in a larger than usual hydrophobic patch. Quinn *et al.* estimate the hydrophobic patch that arises due to the

binding of a fluorophore to a protein to be 3–4 times larger than a hydrophobic amino acid [150]. When the triazine interacted with the surface of BSA it is possible that it acted as a locus for aggregation. As stated previously, fluorescent labelling of a protein molecule, and in particular the alteration of its surface chemistry, has been shown to influence its solution behaviour [151]. James *et al.* state that the interaction between two particles in solution is characterised by the net-interaction potential between those two particles. The forces that contribute to this net-interaction potential include long-range repulsive electrostatic interactions, short-range attractive van der Waals interactions, attractive hydrophobic interactions, hydrogen bonding and repulsive hydration effects [153]. Proteins have been described as patchy particles due to their heterogeneous surface chemistry. This is conferred, on the molecular level, by a diverse range of surface-exposed amino acids. Since this net-interaction potential is affected, to varying extents, by each surface-exposed amino acid, any alteration to the surface composition of a protein will affect the net-interaction potential [150]. If a fluorophore binds to the surface of a protein it will confer a higher degree of hydrophobicity to that patch. This conclusion is based on the fact that most fluorophores have a larger molecular weight and a higher degree of aromaticity than any of the aromatic amino acids [150].

6.3 Purified BSA−5MPFH-TDT complex

Since the Job plot analysis reported in Section 6.2 indicated that the level of BSA−5MPFH-TDT labelling was 2:1 it was very important to ensure that any free triazine was removed from the BSA−5MPFH-TDT solutions. Size-exclusion chromatography (SEC) was employed to separate the free fluorophore from the labelled protein solutions. When assessing the fluorescence emission data of the BSA−5MPFH-TDT solutions, both before and after purification, it was supposed that there were three possible environments in which the triazine may be located: free in aqueous solution; bound to the surface of BSA; and/or bound in a hydrophobic cavity of BSA. The binding stoichiometry also indicated that the triazine may have interacted with a hydrophobic surface patch on the BSA, and subsequently acted as a locus for BSA dimer formation [150]. Fluorophore-protein solutions were made up in two different ratios, 1:1 and 4:1. In the case of the 1:1 BSA−5MPFH-TDT solutions a concentration of triazine above the binding stoichiometry was used while for the 4:1

BSA−5MPFH-TDT solutions the triazine concentration was kept below the binding stoichiometry. The labelling concentration of BSA was kept constant at 3×10^{-5} M. BSA−5MPFH-TDT solutions with ratios of 1:1 and 4:1 were made up in 100 mM phosphate buffer with a pH of 9 and an ionic strength of 300 mM. Samples were left to mix for 5–6 hours at room temperature before being passed through the Sephadex column. A portion of the non-purified sample was kept for comparison.

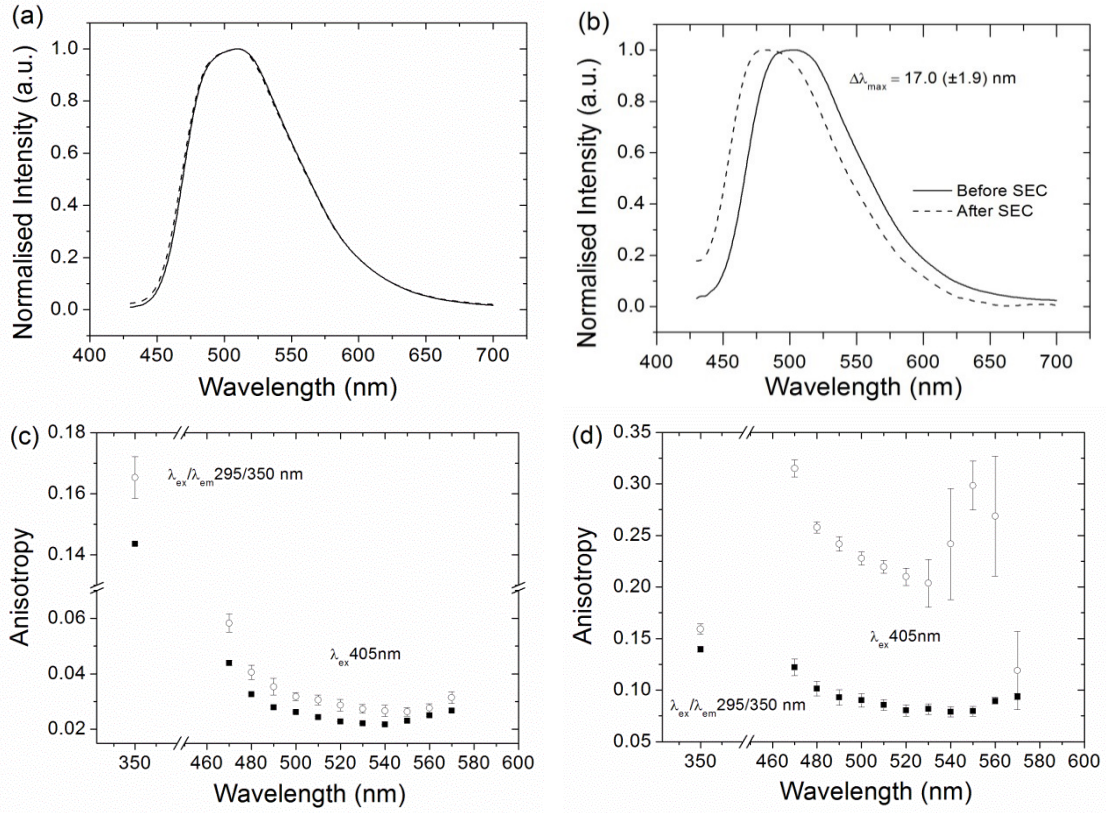

Figure 61: Normalised fluorescence emission spectra (λ_{ex} 400 nm) of BSA−5MPFH-TDT mixtures at pH 9 before (—) and after (- - -) purification by SEC at a ratio of (a) 1:1 and (b) 4:1. Fluorescence anisotropy ($\lambda_{ex}/\lambda_{em}$ 405 nm/470−570 nm) of (c) 1:1 and (d) 4:1 BSA−5MPFH-TDT mixtures at pH 9 before (■) and after (○) purification by SEC.

In Figure 61a, the fluorescence emission spectra of 5MPFH-TDT in the 1:1 BSA−5MPFH-TDT mixture before and after purification by SEC are shown. It could be seen that the steady-state emission was not altered in this case. However, a clear hypsochromic shift of 17.0 (±1.9) nm was evident following purification of the 4:1 BSA−5MPFH-TDT mixture (Figure 61b). This blue shift of 5MPFH-TDT fluorescence was also observed for the non-ionic and cationic micelles. It can be seen

from the band fitting parameters (Table 18) that this shift was primarily due to Band 3 shifting towards the blue with a small contribution from Band 2, while Band 1 remained mostly unchanged. This indicated an increase in the energy difference between the first excited singlet state and the ground state of the g0 conformer. This blue shift represented the transition of the triazine from a polar environment to a more non-polar region and so was indicative of a hydrophobic interaction between the triazine and BSA. Furthermore, there was a drop in the FWHM of Bands 1 and 2 with each of the bands decreasing by 376.11 cm^{-1} and 482.84 cm^{-1}, respectively, while Band 3 was broadened by 422.74 cm^{-1}. Sharper bands are an indicator of a less heterogeneous environment and signify the removal of free fluorophore from solution. Since the FWHM of Band 3 was increased and its band position was been significantly blue-shifted this indicated that the g0 conformer may have been active in a fluctuating interaction with BSA.

The fluorescence anisotropy data of the 1:1 mixture (Figure 61c) was not altered significantly following SEC, indicating that binding was inefficient at this ratio and purification was inadequate. However, a large increase in the anisotropy of the 4:1 mixture (Figure 61d) was observed after SEC. An average rotational correlation time of 15.51 (±7.07%) ns was determined from the triazine fluorescence of the BSA−5MPFH-TDT complex. This was much less than the observed rotational correlation time of 41.7 ns reported for serum albumin [3]. This shorter rotational correlation time was probably due to the segmental motion of the triazine within the BSA−5MPFH-TDT complex.

Table 18: Band fitting parameters of (4:1) BSA−5MPFH-TDT fluorescence before and after purification. The concentration of BSA was kept constant at 3×10^{-5} M. Standard error is indicated.

	Impure BSA−5MPFH-TDT solution			Purifed BSA−5MPFH-TDT complex		
	Band 1	**Band 2**	**Band 3**	**Band 1**	**Band 2**	**Band 3**
Band Area	821.0 ± 159.2	1307.6 ± 146.6	277.2 ± 10.9	652.5 ± 32.8	1069.0 ± 87.2	896.8 ± 54.5
Total Area		2405.7 ± 11.2			2618.3 ± 8.6	
BP (cm^{-1})	18398.6 ± 216.3	19879.7 ± 41.9	20939.1 ± 7.9	18396.5 ± 67.3 (-2.2)	19948.1 ± 14.9 (+68.4)	21428.1 ± 22.9 (+489.1)
FWHM (cm^{-1})	3033.5 ± 180.1	2567.2 ± 46.5	1342.5 ± 17.8	2657.6 ± 49.7	2084.4 ± 64.4	1765.2 ± 27.2
Max. Int. (a.u.)	0.38 ± 0.06	0.72 ± 0.07	0.29 ± 0.01	0.35 ± 0.01	0.72 ± 0.04	0.72 ± 0.03

Overall, there was a decrease in the fluorescence lifetime of 5MPFH-TDT following purification (Figure 62). Although the fluorescence lifetime of the triazine was already quite short in aqueous solution, a further reduction in the lifetime indicated that binding had a quenching effect. A reported isoelectric point of 5.4 confers a net negative charge on BSA at pH 9 [154], which could mean that 5MPFH-TDT was located close to an anionic quenching species (Section 4.5). A radius of 2.55 (±2.17%) nm was determined from the rotational correlation time and the fluorescence lifetime data[11]. This was much smaller than the reported Stokes radius for BSA of 3.48 nm [156]. An underestimation of the Stokes radius indicates that the mobility of the triazine is not completely inhibited by the protein.

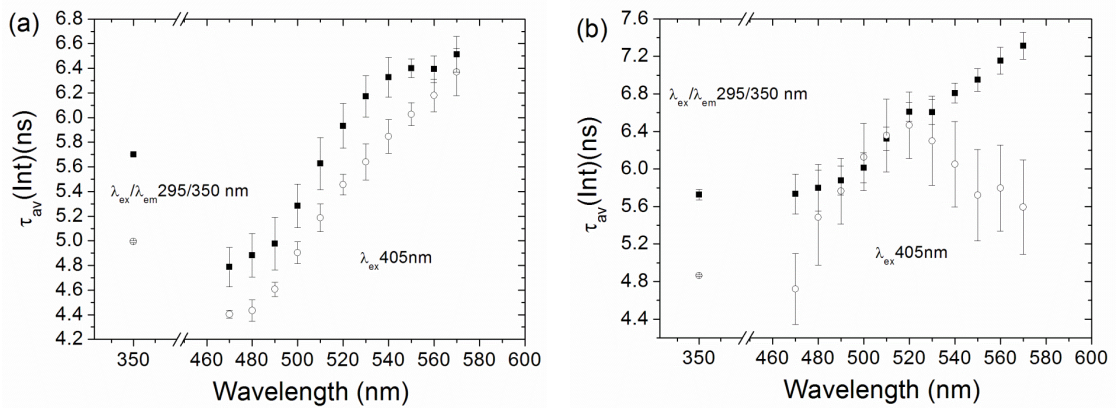

Figure 62: Intensity weighted average fluorescence lifetime, τ_{av} (Int), ($\lambda_{ex}/\lambda_{em}$ 405 nm/470−570 nm) of (a) 1:1 and (b) 4:1 BSA−5MPFH-TDT mixtures at pH 9 before (■) and after (○) purification by SEC. The concentration of BSA was kept constant at 3×10^{-5} M.

In Table 19, the band positons of the impure and purified 4:1 BSA−5MPFH-TDT solutions are compared to those observed in each of the micelles and water. In the non-purified BSA−5MPFH-TDT solution the positions of Bands 2 and 3 were very close to those observed in water while Band 1 was slightly red-shifted. However, following purification, Bands 2 and 3 became quite blue-shifted relative to water (Band 1 remained unchanged). This indicated that fluorophores free in solution were removed successfully by SEC and only those fluorophores taking part in a hydrophobic interaction with BSA remained.

[11] Calculations carried out using T = 298.15 and η = 0.89 mPa.s [155].

Table 19: Band positions of 5MPFH-TDT conformers in water, micelles, and BSA (4:1).

	Band 1 (nm)	Band 2 (nm)	Band 3 (nm)
Water	538.4	505.01	478.51
CrEL	531.5 (−6.9)	498.1 (−6.9)	470.2 (−8.4)
TX-100	533.4 (−4.9)	500.3 (−4.7)	471.6 (−7.0)
CTAB	534.3 (−4.1)	499.0 (−6.0)	469.9 (−8.6)
SDS	543.5 (+5.1)	507.8 (+2.8)	472.7 (+5.8)
Impure 5MPFH-TDT−BSA	543.5 (+5.2)	503.0 (−2.0)	477.6 (−0.9)
Purifed 5MPFH-TDT−BSA	543.6 (+5.2)	501.3 (−3.7)	466.7 (−11.8)

The difference between the average fluorescence lifetime of tryptophan in 1:1 and 4:1 BSA−5MPFH-TDT mixtures, before and after purification, are shown in Table 20. The fluorescence lifetime decreases by 0.71 ns and 0.87 ns, respectively. This indicated that the fluorescence lifetime was being quenched in the purified solutions. This could mean that the 5MPFH-TDT binding site was in close proximity to one of the two tryptophan residues or binding of the 5MPFH-TDT caused some rearrangement of BSA which resulted in solvent quenching of tryptophan fluorescence.

The interaction between 5MPFH-TDT and BSA was quite difficult to determine using typical protein labelling procedures due to the triazine's propensity to aggregate in aqueous solution. Although a binding stoichiometry of 2:1 was determined for the BSA–5MPFH-TDT complex, a molar ratio of 4:1 was employed for the labelling protocol to minimise the likelihood of triazine aggregation. The use of BSA in excess as well as SEC meant it was possible to obtain a fluorescence signal from only the BSA–5MPFH-TDT complex. This fluorescence emission was blue-shifted relative to the triazine's emission in water and there was a significant increase in the fluorescence anisotropy. These observations indicated that an interaction between the triazine and BSA had taken place. However, the rotational correlation time of the triazine (15.51 (±7%) ns) was considerably less than the value reported in the literature for BSA [3]. This implied that the mobility of the triazine, as part of the BSA–5MPFH-TDT complex, was not overly restricted [157]. The 2:1 binding

stoichiometry calculated by the Job plot suggested that the triazine was initiating the formation of BSA dimers. This might occur due to the increased hydrophobicity that a fluorophore can confer to a protein surface [150]. The location of 5MPFH-TDT on the protein surface would explain the greater level of mobility indicated by the rotational correlation time calculated.

Table 20: Intensity weighted average lifetime, τ_{av} (Int) (ns), of 5MPFH-TDT in micelle solutions and solutions of BSA before and after SEC. The standard error is indicated.

λ_{em} (nm)	Water	CrEL	TX-100	SDS	CTAB	BSA−5MPFH-TDT = 4:1	
						Impure	Purified
350						*5.73 ± 0.06*	*4.86 ± 0.01*
470	4.49 ± 0.06	7.85 ± 0.02	7.64 ± 0.01	3.35 ± 0.05	6.70 ± 0.03	5.73 ± 0.21	4.72 ± 0.38
480	4.00 ± 0.21	8.36 ± 0.03	8.20 ± 0.01	3.47 ± 0.04	7.04 ± 0.03	5.80 ± 0.25	5.48 ± 0.51
490	4.31 ± 0.11	8.96 ± 0.02	8.82 ± 0.03	3.79 ± 0.03	7.49 ± 0.03	5.88 ± 0.16	5.76 ± 0.35
500	4.47 ± 0.09	9.73 ± 0.01	9.67 ± 0.01	4.85 ± 0.05	8.27 ± 0.02	6.01 ± 0.16	6.13 ± 0.36
510	4.84 ± 0.09	10.75 ± 0.02	10.78 ± 0.03	5.78 ± 0.06	9.36 ± 0.01	6.32 ± 0.12	6.36 ± 0.39
520	5.22 ± 0.16	11.62 ± 0.01	11.81 ± 0.01	6.64 ± 0.06	10.43 ± 0.02	6.61 ± 0.10	6.47 ± 0.35
530	5.47 ± 0.20	12.38 ± 0.02	12.60 ± 0.01	7.29 ± 0.03	11.32 ± 0.01	6.61 ± 0.13	6.30 ± 0.48
540	5.67 ± 0.22	12.88 ± 0.02	13.20 ± 0.01	7.64 ± 0.10	12.02 ± 0.01	6.81 ± 0.11	6.05 ± 0.46
550	5.93 ± 0.23	13.35 ± 0.01	13.71 ± 0.05	7.88 ± 0.09	12.58 ± 0.01	6.95 ± 0.12	5.72 ± 0.49
560	6.27 ± 0.14	13.83 ± 0.01	14.09 ± 0.02	7.87 ± 0.14	13.12 ± 0.01	7.15 ± 0.14	5.80 ± 0.46
570	6.54 ± 0.15	14.31 ± 0.04	14.56 ± 0.02	7.89 ± 0.21	13.74 ± 0.02	7.31 ± 0.14	5.59 ± 0.50

6.4 Conclusion

5MPFH-TDT was found to interact with BSA with a 2:1 binding stoichiometry. This low binding ratio implied that dimers of BSA may have formed in solution as a result of the triazine's presence. Quinn *et al.* describe how the presence of a fluorophore on the surface of a protein can produce a patch of increased hydrophobicity, which leads to an increase in the net interaction potential of the protein solution [150]. The rotational correlation time of the triazine in the purified BSA–5MPFH-TDT complex indicated that the triazine was not being completely immobilised by BSA, which was consistent with the idea of the triazine interacting at the protein's surface rather than a more enclosed hydrophobic pocket.

7 Summary and Conclusion

We have investigated the spectroscopic properties of 5MPFH-TDT in micelle and protein solutions. The hydrophobicity of the triazine fluorophore meant it was difficult to obtain reproducible data in buffer solutions. This was due to the tendency of the triazine to aggregate in aqueous solutions, as demonstrated by FCS measurements (Figure 27). Micelle solutions were used as an alternative method to study the behaviour of 5MPFH-TDT in relatively simple aqueous solutions prior to carrying out any protein labelling experiments. The introduction of micelles seemed to reduce the formation of triazine aggregates, which resulted in a fluorescence signal of increased intensity and a longer average fluorescence lifetime. A 5MPFH-TDT–micelle interaction was also characterised by a hypsochromic shift. This was ascribed to the hydrophobic interaction between the fluorophore and the micelle interior [117]. The transition of a fluorophore to a more non-polar environment is often associated with an increase in the energy difference between the ground state and the excited state. This is because the dipole moment of the ground state is usually less than that of the excited state resulting in a greater stabilisation of the ground state species [84]. It was also noted that each of the three fluorescence lifetime components associated with the triazine's three emission bands increased linearly with emission wavelength. This trend was ascribed to the Strickler-Berg defined relationship between the fluorescence lifetime and the refractive index [12].

The strength of the interaction between the triazine and the micelles showed a dependence on the size of the Stern/palisade later. 5MPFH-TDT was bound more strongly to micelles of TX-100 (25 Å palisade later [91]) than micelles of CTAB (10 Å Stern later [115]). The fluorescence anisotropy data also showed that the rotational motion of the triazine was inhibited to a greater extent in TX-100. Since the lipophilic region of TX-100 has a smaller radius than that of CTAB, 5MPFH-TDT was more deeply embedded in these micelles. The microviscosity of these environments was determined from this anisotropy data and agreed quite well with other values reported in the literature [126, 127]. Contrary to its behaviour in non-ionic and cationic micelles, the fluorescence intensity of 5MPFH-TDT was reduced in the presence of anionic micelles. A quenching mechanism was in operation but this was difficult to demonstrate in aqueous solutions spiked with the quencher due to the

aggregation of the triazine. The formation of aggregates was inhibited by first stabilising the triazine in TX-100 micelles and following this the quenching species, SDS, was added to the samples. Two bimolecular quenching constants were determined due to the shielding effect of the TX-100 micelles. The mechanism of quenching was thought to be electron exchange between the anionic head group of SDS and the fluorophore [120, 158].

The high binding constant of 5MPFH-TDT in micelles of TX-100 and CTAB meant it was a good candidate for the assessment of micelle size by Förster resonance energy transfer. 5MPFH-TDT was used as a FRET donor and the surface active fluorophore SR101 [132] was the FRET acceptor in an investigation of CTAB micelle size. A Förster distance of 46.25 (±0.32) Å was determined for this FRET pair, which was quite close to the reported radius of CTAB micelles. A quenching investigation using 5MPFH-TDT and increasing quantities of SR101 revealed that quenching took place by a "sphere-of-action" mechanism with a radius of 306.08 Å. Of course this was too large to explain purely intramicellar quenching since it is several times the radius of the CTAB micelle. This seemed to suggest that several CTAB micelles had aggregated in solution [134].

The interaction between 5MPFH-TDT and micelles seemed to be driven by the fluorophore's hydrophobicity. Therefore, it seemed probable that 5MPFH-TDT would also interact hydrophobically with a protein molecule. An investigation of a BSA–5MPFH-TDT complex revealed a binding stoichiometry of 2:1. This implied that the triazine was acting as a locus for the formation of BSA dimers. A large hypsochromic shift of 17.00 (±1.89) nm, which was observed when purified samples of BSA–5MPFH-TDT were analysed, suggested that the triazine was involved in a hydrophobic interaction with BSA. The calculated rotational correlation time of 15.51 (±7.07%) ns was much less than the rotational correlation time of serum albumin [3]. This indicated that the mobility of the BSA–bound triazine was not completely restricted and the binding site of the triazine was probably not particularly confined. The location of 5MPFH-TDT on the protein surface would explain the greater level of mobility indicated by the rotational correlation time calculated.

Overall we have assessed the photophysical behaviour of the new 2,5-dihydro-1,2,3-triazine, 5MPFH-TDT in micellar and protein solutions. The marked hydrophobicity

of this fluorophore and its proclivity to aggregate, particularly in aqueous solutions, was a dominant feature of this investigation. In many ways the presence of these aggregates defined the direction of this study, even though evidence for their existence was not obtained until towards the end of the project.

8 Appendices

A.1 Fluorescence anisotropy of 5MPFH-TDT in Cremophor EL solutions

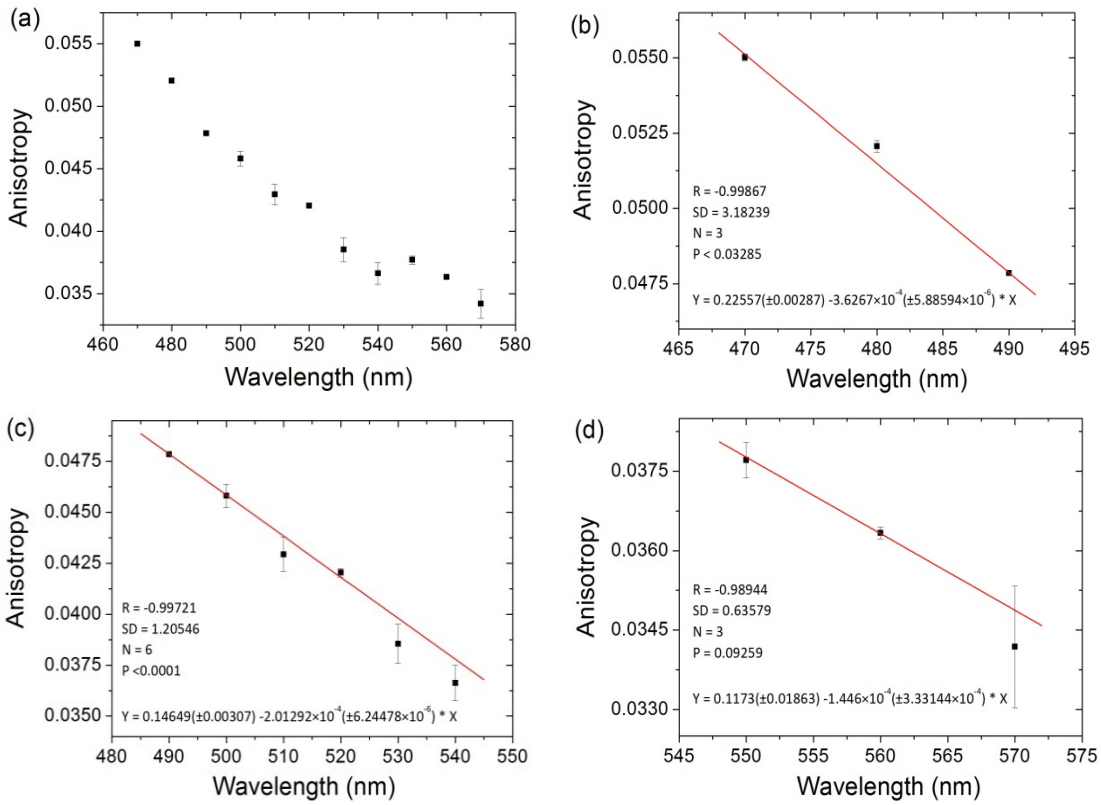

Figure 63: Fitted anisotropy data for the 0.05 mM solution of CrEL versus fluorescence emission wavelength. (a) 470−570. (b) 470–490 nm (g0). (c) 490−540 nm (g2). (d) 550−570 nm (g1).

A.2 Fluorescence lifetime of 5MPFH-TDT in cetyltrimethylammonium bromide solutions

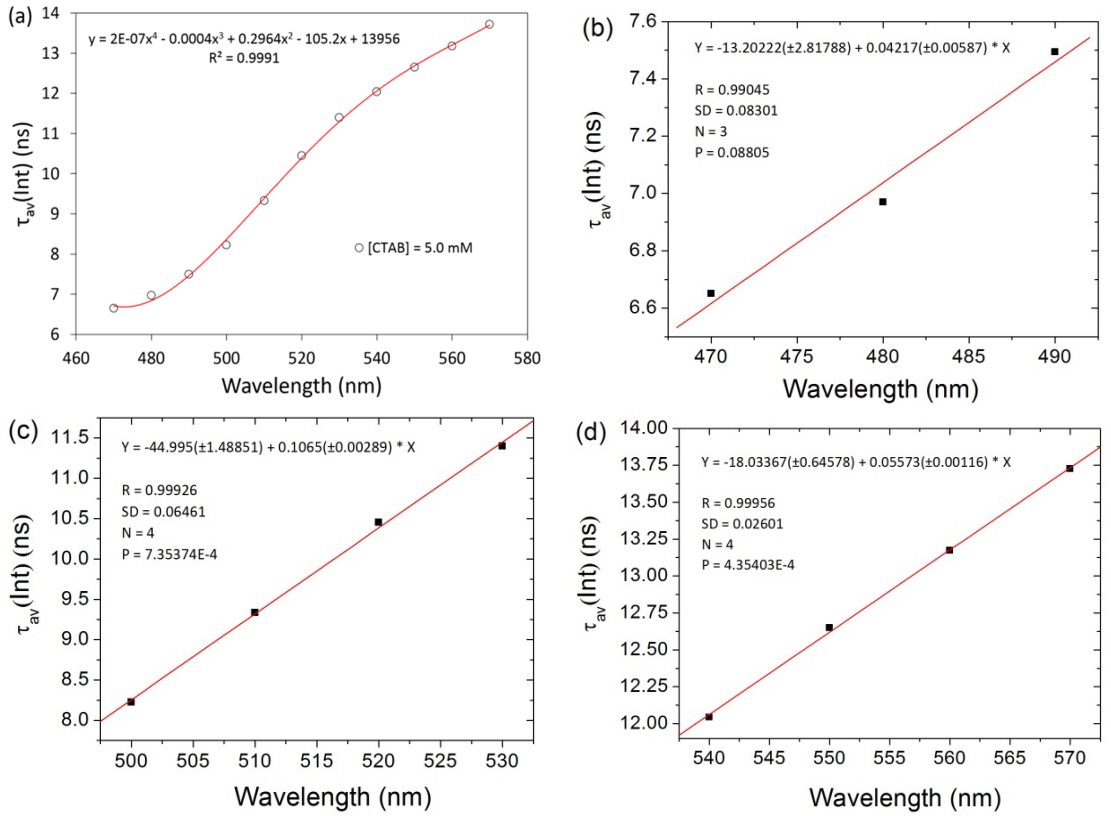

Figure 64: Intensity weighted average fluorescence lifetime data of 5MPFH-TDT in a 5.0 mM solution of CTAB versus fluorescence emission wavelength. (a) 470−570 nm. (b) 470–490 nm (g0). (c) 490−520 nm (g2). (d) 530−570 nm (g1).

A.3 Förster Resonance Energy Transfer for the FRET pair 5MPFH-TDT and TRITC

The absorbance and fluorescence emission spectra of 5MPFH-TDT, TRITC, and mixtures of 5MPFH-TDT and TRITC in 2.0 mM CTAB solutions are shown in Figure 65a and Figure 67b. Although λ_{max} for TRITC is at 550 nm (Figure 65a), it also absorbs to a small extent at 400 nm. This means that we expected a small degree of direct excitation of the FRET acceptor. However, since fluorescence quenching of 5MPFH-TDT was the effect of interest this did not pose too much of an issue. It can

be seen in Figure 65b, that the fluorescence intensity of 5MPFH-TDT in the presence of TRITC was only slightly diminished.

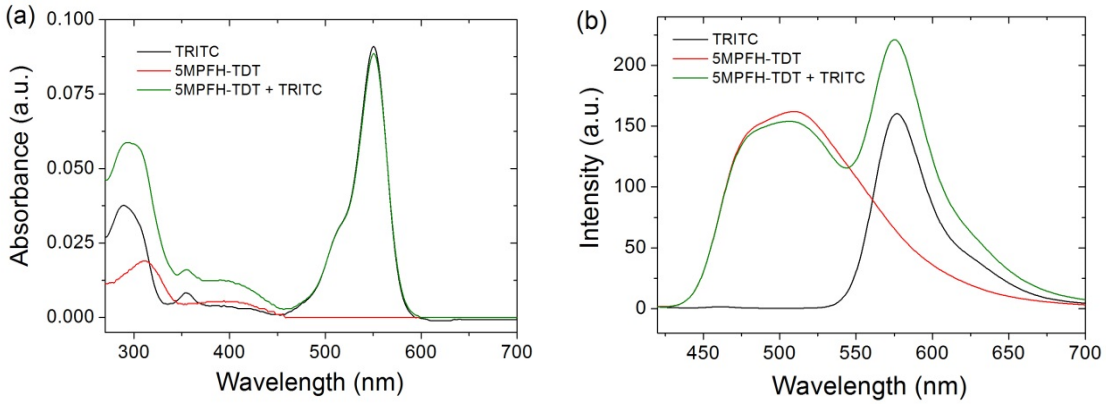

Figure 65: 5MPFH-TDT (10^{-6} M) and TRITC (10^{-6} M) in 2.0 mM CTAB solutions. (a) Absorbance spectra. (b) Fluorescence emission spectra (λ_{ex} 400 nm).

The spectral overlap integral of 5MPFH-TDT emission and TRITC absorbance is shown in Figure 66a. The overlaid spectra in Figure 66b show the normalised fluorescence emission (band fitted) of 5MPFH-TDT and the normalised absorbance and fluorescence emission of TRITC in a 2.0 mM CTAB solution. It can be seen that the greatest degree of overlap between the donor's emission and the acceptor's absorption occurred for the long wavelength emission band of 5MPFH-TDT (Band 1). However, the overlap integral for Band 2 was more pronounced in the case of 5MPFH-TDT and TRITC than for 5MPFH-TDT and SR101. If the fluorophores are in close enough proximity than we expect that FRET will be evident for the middle band.

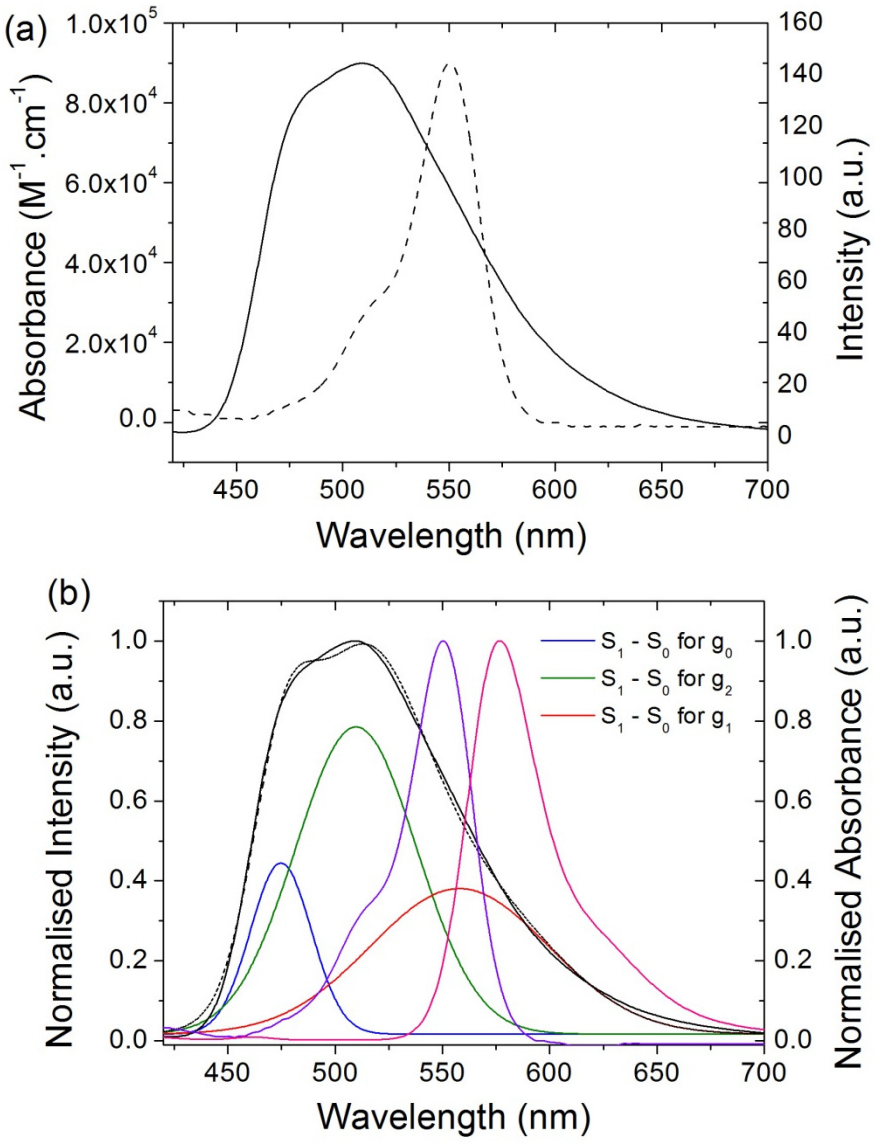

Figure 66: 5MPFH-TDT (10^{-6} M) and TRITC (10^{-6} M) in 2.0 mM CTAB solutions. (a) Spectral overlap of 5MPFH-TDT fluorescence emission (λ_{ex} 400 nm) and TRITC absorbance. (b) Normalised band-fitted fluorescence emission spectrum of 5MPFH-TDT overlaid with the absorbance and emission spectra of TRITC.

The corrected fluorescence intensity values (Table 21) show that the drop in 5MPFH-TDT fluorescence intensity was not due to FRET but was rather a consequence of the absorbance of TRITC at the excitation wavelength.

Table 21: Fluorescence intensity of 10^{-6} M 5MPFH-TDT in the presence of 10^{-6} M TRITC in a CTAB solution corrected for inner filter effects.

$F_{DA\text{-}obs}$ (± SE)	OD_{ex}	OD_{em}	$F_{DA\text{-}corr}$ (± SE)	F_D (± SE)
153.7 (±4.3)	0.01	0.0271	160.8 (±4.4)	162.1 (±13.0)

Furthermore, the presence of TRITC did not cause any changes to the fluorescence lifetime of 5MPFH-TDT for the emission wavelengths in the range 470−530 nm (Figure 67). A drop in the lifetime was first detected at 540 nm. In the absence of the TRITC acceptor the fluorescence lifetime (λ_{em} = 540 nm) of a 10^{-6} M 5MPFH-TDT solution is 11.99 ns. The fluorescence lifetime of 5MPFH-TDT drops to 11.31 ns when the donor and acceptor fluorophores are present in a one-to-one ratio. However, this is most likely due to the shorter fluorescence lifetime of TRITC.

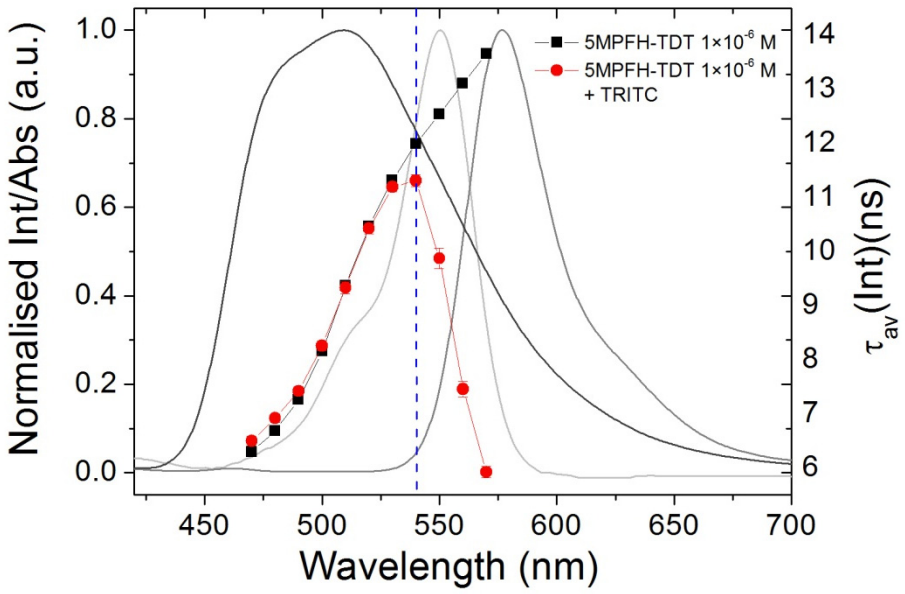

Figure 67: Intensity weighted average fluorescence lifetime (λ_{ex} 405 nm) of 5MPFH-TDT (10^{-6} M) in the presence of the acceptor TRITC (10^{-6} M) in 2.0 mM CTAB solutions. The normalised fluorescence emission spectrum of 5MPFH-TDT and the normalised absorbance and fluorescence emission spectra of TRITC are overlaid on the graph.

There was a dramatic drop in the fluorescence lifetime of 5MPFH-TDT at emission wavelengths longer than 550 nm. In the absence of the TRITC acceptor the

fluorescence lifetime ($\lambda_{em} = 570$ nm) of a 10^{-6} M 5MPFH-TDT solution is 13.66 (±0.04) ns. The fluorescence lifetime of 5MPFH-TDT drops to 5.92 (±0.11) ns when the donor and acceptor fluorophores are present in a one-to-one ratio. This also includes the emission spectrum of TRITC and contributes to the reduction in the average fluorescence lifetime observed[12].

[12] A fluorescence lifetime of 2.3 ± 0.3 ns (λ_{ex} 550 nm) has been reported for TRITC in buffer solution of pH ~7.1 [159].

Table 22: Decay parameters of multi-exponential fit of 5MPFH-TDT in a 2.0 mM CTAB solution containing the FRET acceptor TRITC. The concentrations of 5MPFH-TDT and TRITC were maintained at 10^{-6} M. Standard error is indicated.

λ (nm)	a_1	a_2	a_3	τ_1 (ns)	τ_2 (ns)	τ_3 (ns)	τ_{av} (ns)	χ^2 (red)
470	1055.6 ± 31.9	1746.9 ± 59.0	930.0 ± 46.7	8.63 ± 0.15	4.43 ± 0.14	0.63 ± 0.03	6.50 ± 0.09	1.216
480	861.8 ± 78.2	1995.1 ± 51.8	661.0 ± 43.7	9.62 ± 0.12	5.02 ± 0.01	0.78 ± 0.06	6.92 ± 0.08	1.243
490	894.9 ± 73.0	2083.1 ± 52.0	610.3 ± 33.1	10.38 ± 0.13	5.18 ± 0.01	0.77 ± 0.06	7.42 ± 0.08	1.285
500	727.6 ± 30.8	2209.9 ± 17.1	534.0 ± 43.1	12.30 ± 0.10	5.66 ± 0.08	0.93 ± 0.09	8.26 ± 0.09	1.285
510	833.9 ± 13.5	2180.8 ± 21.9	521.5 ± 47.7	13.61 ± 0.12	5.77 ± 0.12	0.83 ± 0.03	9.33 ± 0.11	1.302
520	983.1 ± 17.6	2028.7 ± 16.8	421.1 ± 33.3	14.49 ± 0.07	5.86 ± 0.13	0.88 ± 0.01	10.43 ± 0.10	1.325
530	1118.9 ± 22.4	1894.2 ± 4.8	443.5 ± 30.1	14.98 ± 0.03	5.90 ± 0.11	0.95 ± 0.02	11.19 ± 0.08	1.314
540	1159.9 ± 30.3	1670.0 ± 24.9	586.5 ± 37.1	14.87 ± 0.02	5.44 ± 0.09	1.35 ± 0.09	11.31 ± 0.11	1.319
550	825.5 ± 34.1	1680.2 ± 127.5	1069.0 ± 144.0	14.46 ± 0.07	4.11 ± 0.18	1.69 ± 0.16	9.87 ± 0.19	1.250
560	417.1 ± 19.2	2263.0 ± 482.2	884.4 ± 456.0	14.21 ± 0.11	3.13 ± 0.17	1.76 ± 0.29	7.45 ± 0.15	1.189
570	237.6 ± 10.5	3315.7 ± 5.8		14.39 ± 0.01	2.73 ± 0.01		5.92 ± 0.11	1.189

A.4 Fluorescence lifetime decay parameters of 5MPFH-TDT in the presence of SR101 in CTAB micelles

Table 23: Fluorescence lifetime (λ_{ex} 405 nm) decay parameters of 5MPFH-TDT (5×10^{-6} M) in 2.0 mM CTAB solutions. Standard error is indicated.

λ (nm)	a_1	a_2	a_3	τ_1 (ns)	τ_2 (ns)	τ_3 (ns)	τ_{av} (ns)	χ^2 (red)
470	1096.9 ± 27.7	2010.1 ± 94.3	1206.8 ± 246.3	8.65 ± 0.19	4.34 ± 0.21	0.57 ± 0.06	6.37 ± 0.12	1.209
480	1048.7 ± 77.8	2092.1 ± 108.8	872.2 ± 83.2	9.19 ± 0.34	4.57 ± 0.25	0.64 ± 0.03	6.70 ± 0.14	1.269
490	886.8 ± 59.8	2298.0 ± 62.5	814.8 ± 45.1	10.45 ± 0.30	4.96 ± 0.18	0.66 ± 0.09	7.24 ± 0.15	1.278
500	916.2 ± 16.2	2321.0 ± 48.2	734.8 ± 67.7	11.63 ± 0.34	5.13 ± 0.19	0.65 ± 0.01	8.04 ± 0.20	1.288
510	957.9 ± 45.8	2285.0 ± 54.5	664.3 ± 62.3	13.19 ± 0.25	5.36 ± 0.13	0.74 ± 0.07	9.17 ± 0.22	1.303
520	1135.1 ± 49.6	2110.1 ± 43.9	682.5 ± 44.6	13.83 ± 0.29	5.37 ± 0.18	0.53 ± 0.08	10.15 ± 0.26	1.266
530	1266.0 ± 45.3	1985.2 ± 18.2	600.5 ± 48.4	14.38 ± 0.24	5.46 ± 0.17	0.61 ± 0.10	10.92 ± 0.29	1.287
540	1406.6 ± 57.9	1866.0 ± 9.1	582.3 ± 55.5	14.73 ± 0.20	5.52 ± 0.19	0.54 ± 0.04	11.56 ± 0.26	1.285
550	1531.0 ± 62.3	1743.7 ± 35.2	499.1 ± 44.7	15.06 ± 0.16	5.67 ± 0.20	0.63 ± 0.09	12.13 ± 0.25	1.284
560	1709.4 ± 66.2	1560.0 ± 36.8	665.3 ± 89.9	15.21 ± 0.16	5.64 ± 0.17	0.45 ± 0.11	12.69 ± 0.25	1.335
570	1886.5 ± 65.4	1366.6 ± 41.1	610.7 ± 94.9	15.36 ± 0.17	5.69 ± 0.22	0.45 ± 0.11	13.22 ± 0.23	1.355

Table 24: Fluorescence lifetime (λ_{ex} 405 nm) decay parameters of 5MPFH-TDT (5×10^{-6} M) in the presence of the FRET acceptor SR101 (5×10^{-6} M) in 2.0 mM CTAB solutions. Standard error is indicated.

λ (nm)	a_1	a_2	a_3	τ_1 (ns)	τ_2 (ns)	τ_3 (ns)	τ_{av} (ns)	χ^2 (red)
470	1192.1 ± 181.0	1544.2 ± 119.6	1544.9 ± 106.6	7.31 ± 0.34	3.18 ± 0.34	0.53 ± 0.06	5.50 ± 0.06	1.269
480	1049.4 ± 173.3	1668.6 ± 142.8	1319.5 ± 46.9	8.09 ± 0.42	3.66 ± 0.28	0.62 ± 0.05	5.89 ± 0.05	1.234
490	956.9 ± 42.1	1773.6 ± 9.1	1245.5 ± 42.3	8.92 ± 0.12	3.99 ± 0.06	0.65 ± 0.02	6.39 ± 0.02	1.256
500	942.1 ± 159.6	1808.9 ± 123.3	1221.8 ± 79.0	10.14 ± 0.74	4.15 ± 0.28	0.70 ± 0.06	7.08 ± 0.15	1.297
510	887.6 ± 56.3	1862.1 ± 41.9	1168.1 ± 73.5	11.68 ± 0.36	4.43 ± 0.09	0.71 ± 0.02	8.12 ± 0.11	1.297
520	902.1 ± 30.2	1844.0 ± 43.9	1097.3 ± 27.3	13.04 ± 0.26	4.63 ± 0.06	0.75 ± 0.02	9.16 ± 0.06	1.282
530	978.9 ± 76.7	1753.6 ± 59.3	1010.8 ± 12.8	13.76 ± 0.55	4.67 ± 0.22	0.72 ± 0.06	9.97 ± 0.15	1.270
540	1042.4 ± 36.4	1699.1 ± 17.1	1060.5 ± 26.3	14.30 ± 0.24	4.78 ± 0.09	0.75 ± 0.01	10.59 ± 0.10	1.302
550	1153.0 ± 17.9	1607.8 ± 9.8	969.5 ± 18.8	14.44 ± 0.10	4.71 ± 0.06	0.68 ± 0.04	11.11 ± 0.03	1.283
560	1207.1 ± 15.4	1579.4 ± 22.8	1029.9 ± 63.7	14.77 ± 0.16	4.70 ± 0.08	0.67 ± 0.03	11.52 ± 0.05	1.281
570	1095.4 ± 35.4	1829.7 ± 39.0	794.6 ± 54.6	14.88 ± 0.33	4.69 ± 0.11	0.64 ± 0.04	11.15 ± 0.14	1.266

Table 25: Fluorescence lifetime (λ_{ex} 405 nm) decay parameters of 5MPFH-TDT (5×10^{-6} M) in the presence of the FRET acceptor SR101 (10×10^{-6} M) in 2.0 mM CTAB solutions. Standard error is indicated.

λ (nm)	a_1	a_2	a_2	τ_1 (ns)	τ_2 (ns)	τ_3 (ns)	τ_{av} (ns)	χ^2 (red)
470	1196.9 ± 93.1	1277.5 ± 34.5	1925.8 ± 34.4	7.52 ± 0.16	3.09 ± 0.16	0.53 ± 0.02	5.75 ± 0.01	1.247
480	1260.2 ± 96.8	1275.5 ± 55.0	1693.5 ± 99.3	7.82 ± 0.19	3.20 ± 0.20	0.56 ± 0.01	6.08 ± 0.04	1.256
490	1217.7 ± 65.3	1292.7 ± 39.2	1593.1 ± 81.6	8.42 ± 0.13	3.47 ± 0.10	0.60 ± 0.02	6.52 ± 0.02	1.253
500	1157.4 ± 56.1	1345.3 ± 46.8	1526.7 ± 70.7	9.36 ± 0.17	3.74 ± 0.14	0.64 ± 0.01	7.17 ± 0.04	1.266
510	987.5 ± 25.3	1481.4 ± 27.8	1533.1 ± 57.2	11.26 ± 0.13	4.29 ± 0.09	0.68 ± 0.02	8.27 ± 0.03	1.320
520	1018.1 ± 28.4	1447.4 ± 41.6	1469.1 ± 47.5	12.41 ± 0.25	4.44 ± 0.12	0.70 ± 0.02	9.25 ± 0.09	1.299
530	1114.0 ± 14.8	1375.0 ± 22.9	1420.7 ± 33.2	12.97 ± 0.12	4.44 ± 0.07	0.70 ± 0.02	9.99 ± 0.07	1.313
540	1124.8 ± 18.3	1360.4 ± 13.3	1446.2 ± 43.9	13.81 ± 0.02	4.64 ± 0.03	0.70 ± 0.01	10.69 ± 0.02	1.312
550	1202.6 ± 21.8	1304.1 ± 20.3	1421.6 ± 27.9	14.14 ± 0.05	4.56 ± 0.03	0.68 ± 0.00	11.21 ± 0.06	1.251
560	1205.2 ± 28.3	1353.8 ± 19.9	1435.2 ± 53.5	14.53 ± 0.05	4.58 ± 0.02	0.64 ± 0.02	11.51 ± 0.08	1.272
570	869.1 ± 25.3	1978.4 ± 20.7	1003.9 ± 57.3	14.85 ± 0.13	4.74 ± 0.04	0.58 ± 0.02	10.34 ± 0.12	1.269

Table 26: Fluorescence lifetime (λ_{ex} 405 nm) decay parameters of 5MPFH-TDT (5×10^{-6} M) in the presence of the FRET acceptor SR101 (15×10^{-6} M) in 2.0 mM CTAB solutions. Standard error is indicated.

λ (nm)	a_1	a_2	a_3	τ_1 (ns)	τ_2 (ns)	τ_3 (ns)	τ_{av} (ns)	χ^2 (red)
470	1051.0 ± 140.7	1078.5 ± 91.8	2870.3 ± 195.8	6.56 ± 0.09	1.98 ± 0.06	0.37 ± 0.02	4.92 ± 0.07	1.220
480	1145.6 ± 82.0	1140.8 ± 33.3	2472.8 ± 138.5	6.98 ± 0.11	2.27 ± 0.14	0.44 ± 0.02	5.32 ± 0.03	1.256
490	1202.3 ± 72.3	1175.4 ± 38.4	2334.2 ± 77.8	7.32 ± 0.08	2.25 ± 0.10	0.41 ± 0.02	5.70 ± 0.02	1.243
500	1057.4 ± 123.8	1205.1 ± 57.4	2224.6 ± 201.2	8.43 ± 0.53	2.77 ± 0.43	0.50 ± 0.05	6.33 ± 0.17	1.280
510	1093.2 ± 82.3	1212.1 ± 5.0	2163.5 ± 140.9	9.20 ± 0.41	2.78 ± 0.35	0.51 ± 0.06	7.04 ± 0.17	1.264
520	893.2 ± 169.3	1310.6 ± 43.7	2140.9 ± 152.2	11.50 ± 1.26	3.50 ± 0.70	0.58 ± 0.10	8.24 ± 0.45	1.268
530	977.6 ± 26.9	1228.3 ± 19.4	2168.6 ± 165.2	11.62 ± 0.37	3.37 ± 0.25	0.56 ± 0.04	8.78 ± 0.20	1.310
540	958.1 ± 52.9	1190.4 ± 39.2	2082.5 ± 93.9	12.58 ± 0.47	3.65 ± 0.28	0.60 ± 0.04	9.52 ± 0.22	1.336
550	952.7 ± 43.4	1175.9 ± 30.0	2038.9 ± 47.2	13.16 ± 0.30	3.79 ± 0.19	0.61 ± 0.03	10.02 ± 0.14	1.320
560	896.5 ± 78.5	1313.4 ± 35.7	1958.1 ± 89.8	13.62 ± 0.55	4.00 ± 0.23	0.58 ± 0.03	10.07 ± 0.21	1.273
570	577.5 ± 17.4	2108.0 ± 47.0	1214.8 ± 54.0	13.43 ± 0.21	4.55 ± 0.02	0.52 ± 0.01	8.24 ± 0.07	1.276

Table 27: Fluorescence lifetime (λ_{ex} 405 nm) decay parameters of 5MPFH-TDT (5×10^{-6} M) in the presence of the FRET acceptor SR101 (20×10^{-6} M) in 2.0 mM CTAB solutions. Standard error is indicated.

λ (nm)	a_1	a_2	a_3	τ_1 (ns)	τ_2 (ns)	τ_3 (ns)	τ_{av} (ns)	χ^2 (red)
470	1011.8 ± 46.6	1097.2 ± 17.2	2953.1 ± 69.2	6.71 ± 0.07	2.00 ± 0.09	0.38 ± 0.02	4.98 ± 0.03	1.254
480	1039.1 ± 47.3	1098.3 ± 36.6	2595.7 ± 149.7	7.17 ± 0.20	2.31 ± 0.22	0.45 ± 0.04	5.37 ± 0.11	1.246
490	1019.2 ± 99.8	1148.5 ± 25.1	2540.3 ± 103.8	7.75 ± 0.40	2.57 ± 0.42	0.48 ± 0.05	5.75 ± 0.15	1.241
500	1129.3 ± 106.6	1162.0 ± 22.5	2361.3 ± 78.1	8.07 ± 0.33	2.24 ± 0.30	0.44 ± 0.05	6.25 ± 0.11	1.233
510	1133.7 ± 17.0	1127.2 ± 17.0	2330.8 ± 50.3	8.91 ± 0.04	2.36 ± 0.04	0.47 ± 0.01	6.98 ± 0.06	1.267
520	1012.7 ± 97.8	1128.7 ± 18.9	2253.6 ± 113.7	10.46 ± 0.40	2.92 ± 0.31	0.52 ± 0.03	8.00 ± 0.07	1.281
530	1008.6 ± 135.3	1148.7 ± 22.4	2285.7 ± 12.4	11.39 ± 0.63	3.05 ± 0.46	0.54 ± 0.05	8.71 ± 0.17	1.307
540	942.6 ± 18.6	1104.1 ± 8.8	2297.2 ± 18.1	12.43 ± 0.11	3.49 ± 0.07	0.58 ± 0.01	9.46 ± 0.13	1.309
550	952.0 ± 51.0	1110.8 ± 28.7	2240.1 ± 85.2	12.85 ± 0.14	3.55 ± 0.06	0.58 ± 0.01	9.83 ± 0.09	1.292
560	901.4 ± 62.6	1273.6 ± 18.9	2108.6 ± 38.7	13.00 ± 0.35	3.81 ± 0.12	0.56 ± 0.00	9.63 ± 0.13	1.286
570	510.3 ± 25.4	2203.0 ± 22.6	1250.0 ± 52.5	13.28 ± 0.18	4.66 ± 0.01	0.54 ± 0.01	7.79 ± 0.05	1.244

Table 28: Fluorescence lifetime (λ_{ex} 405 nm) decay parameters of 5MPFH-TDT (5×10^{-6} M) in the presence of the FRET acceptor SR101 (25×10^{-6} M) in 2.0 mM CTAB solutions. Standard error is indicated.

λ (nm)	a_1	a_2	a_3	τ_1 (ns)	τ_2 (ns)	τ_3 (ns)	τ_{av} (ns)	χ^2 (red)
470	779.1 ± 18.4	1081.0 ± 10.6	3124.5 ± 75.7	6.72 ± 0.06	1.89 ± 0.03	0.37 ± 0.01	4.68 ± 0.02	1.188
480	872.8 ± 21.3	1125.9 ± 10.1	2885.1 ± 31.3	6.92 ± 0.10	1.91 ± 0.08	0.39 ± 0.01	4.97 ± 0.04	1.164
490	862.4 ± 15.4	1117.2 ± 31.2	2756.7 ± 62.1	7.50 ± 0.08	2.16 ± 0.07	0.44 ± 0.01	5.38 ± 0.04	1.170
500	902.5 ± 8.0	1173.7 ± 16.6	2554.1 ± 61.1	7.95 ± 0.04	2.04 ± 0.01	0.42 ± 0.00	5.86 ± 0.01	1.233
510	906.1 ± 5.5	1168.7 ± 31.6	2653.2 ± 74.6	8.73 ± 0.06	2.13 ± 0.05	0.44 ± 0.01	6.48 ± 0.06	1.211
520	870.1 ± 55.8	1174.5 ± 68.0	2669.6 ± 55.2	9.82 ± 0.43	2.39 ± 0.29	0.47 ± 0.05	7.24 ± 0.20	1.234
530	899.4 ± 15.1	1187.8 ± 28.8	2575.8 ± 47.6	10.38 ± 0.21	2.32 ± 0.12	0.46 ± 0.01	7.82 ± 0.12	1.266
540	894.5 ± 29.8	1178.3 ± 34.4	2545.5 ± 34.2	10.96 ± 0.35	2.42 ± 0.19	0.47 ± 0.03	8.30 ± 0.18	1.284
550	846.5 ± 46.8	1145.7 ± 18.3	2477.8 ± 29.4	11.64 ± 0.40	2.79 ± 0.21	0.51 ± 0.02	8.67 ± 0.17	1.298
560	821.7 ± 120.9	1290.2 ± 44.0	2220.8 ± 59.4	11.64 ± 0.95	3.38 ± 0.41	0.53 ± 0.05	8.28 ± 0.36	1.324
570	524.3 ± 66.0	2259.3 ± 52.0	1356.2 ± 31.5	10.90 ± 0.62	4.48 ± 0.10	0.48 ± 0.00	6.50 ± 0.12	1.287

Table 29: Fluorescence lifetime (λ_{ex} 405 nm) decay parameters of 5MPFH-TDT (5×10^{-6} M) in the presence of the FRET acceptor SR101 (30×10^{-6} M) in 2.0 mM CTAB solutions. Standard error is indicated.

λ (nm)	a_1	a_2	a_3	τ_1 (ns)	τ_2 (ns)	τ_3 (ns)	τ_{av} (ns)	χ^2 (red)
470	622.4 ± 33.8	1100.8 ± 43.7	3603.4 ± 216.8	6.50 ± 0.04	1.55 ± 0.06	0.32 ± 0.01	4.25 ± 0.08	1.256
480	649.6 ± 47.7	1050.2 ± 68.8	3039.2 ± 141.4	7.05 ± 0.16	1.89 ± 0.13	0.40 ± 0.02	4.70 ± 0.06	1.157
490	712.8 ± 22.5	1129.4 ± 10.5	2949.9 ± 125.3	7.30 ± 0.12	1.84 ± 0.06	0.40 ± 0.01	4.99 ± 0.05	1.135
500	707.2 ± 37.4	1145.7 ± 10.2	2996.7 ± 118.9	7.91 ± 0.11	1.96 ± 0.05	0.41 ± 0.01	5.42 ± 0.04	1.175
510	740.8 ± 30.6	1221.5 ± 25.8	2725.5 ± 91.4	8.43 ± 0.11	1.84 ± 0.07	0.39 ± 0.00	5.98 ± 0.04	1.247
520	714.1 ± 53.8	1174.2 ± 33.5	2685.6 ± 198.8	9.35 ± 0.27	2.02 ± 0.13	0.42 ± 0.02	6.63 ± 0.07	1.227
530	752.4 ± 37.3	1231.6 ± 30.4	2743.6 ± 44.2	9.63 ± 0.15	1.91 ± 0.08	0.40 ± 0.02	6.98 ± 0.04	1.218
540	741.7 ± 43.1	1185.8 ± 18.7	2610.0 ± 91.6	10.17 ± 0.30	2.05 ± 0.14	0.42 ± 0.02	7.41 ± 0.09	1.216
550	789.4 ± 14.3	1178.0 ± 20.3	2501.7 ± 86.3	10.04 ± 0.13	2.13 ± 0.07	0.43 ± 0.02	7.42 ± 0.15	1.251
560	821.7 ± 63.7	1226.4 ± 26.6	2295.3 ± 21.3	9.66 ± 0.60	2.93 ± 0.23	0.47 ± 0.03	6.92 ± 0.27	1.258
570	868.1 ± 306.0	1905.7 ± 270.0	1306.6 ± 83.4	8.58 ± 1.26	4.07 ± 0.32	0.46 ± 0.03	5.74 ± 0.20	1.259

A.5 Fluorescence emission properties of 5MPFH TDT in BSA at varying pH

A study was carried out to determine how the fluorescence emission of 5MPFH-TDT varies in BSA solutions of varying pH. The labelling concentration of BSA was 3×10^{-6} M and that of 5MPFH-TDT was 7.5×10^{-7} M. The intrinsic fluorescence anisotropy of BSA did not vary much over the pH range investigated [160]. It can be seen from the absorbance data (Figure 68a) that either the concentration or molar absorptivity of the triazine was different in solutions of pH 7 than in solutions of pH 6, 8, 9, or 10. The raw fluorescence emission data (Figure 68b) showed that the fluorescence intensity of 5MPFH-TDT was somewhat reduced in the two solutions of most extreme pH, particularly at pH 6. However, when the normalised spectra (Figure 69c) were overlaid it was apparent that the shapes of the bands had been mostly conserved indicating that it was unlikely that acid hydrolysis of the triazine had occurred [80]. This implied that the pH of the buffer solution and/or the conformation of BSA in solution influenced the fluorescence emission of the triazine fluorophore to some extent. All samples were made up using 100 mM phosphate buffers of variable pH while the ionic strength was kept constant at 303 mM using NaCl as the background electrolyte.

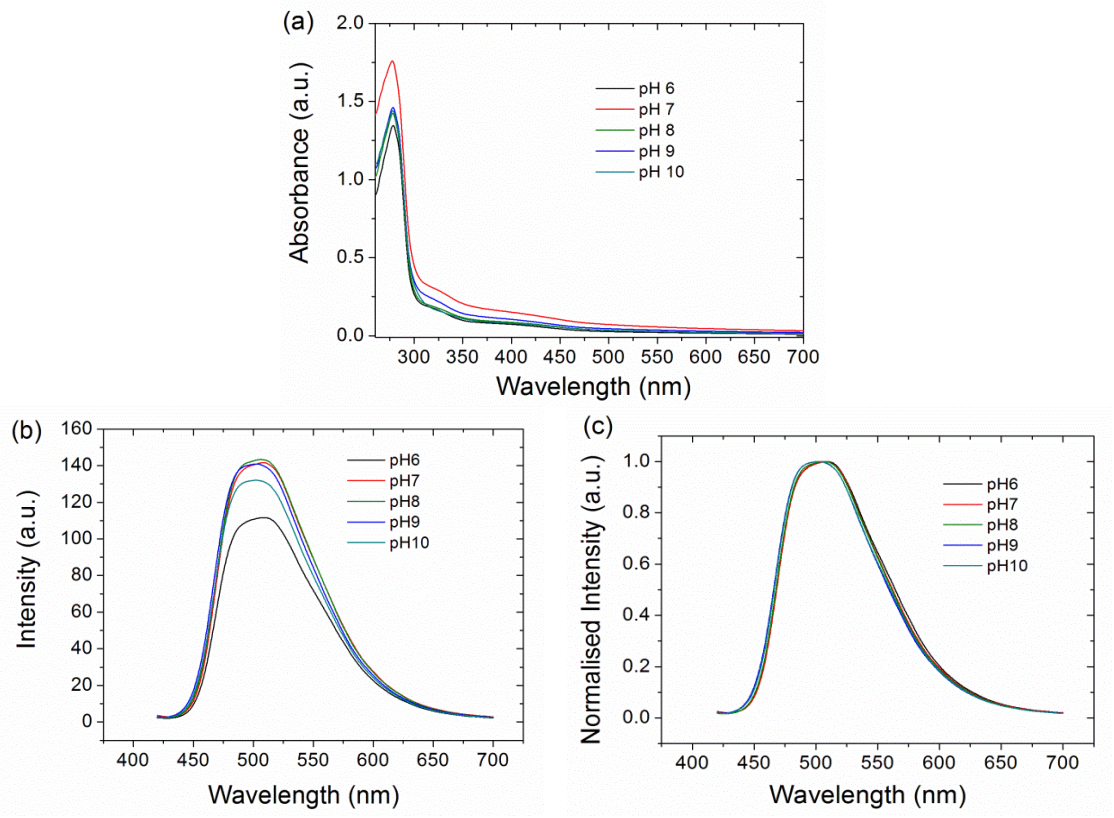

Figure 68: (a) Absorbance spectra, and (b) raw and (c) normalised fluorescence emission spectra of 4:1 BSA−5MPFH-TDT solutions in phosphate buffer of variable pH. [BSA] = 3 × 10^{-5} M and [5MPFH-TDT] = 7.5 × 10^{-6} M.

After band-fitting, the integrated area, band position, and FWHM were plotted against the solution pH (Figure 69). Little variation was seen across the pH range for the band position and FWHM. The absence of any significant change meant that the energies of the ground and excited states were not affected, nor was the environment of the fluorophore. However, the relative areas of Bands 1 and 2 did change. The population of the $S_1 \rightarrow S_0$ (g1) transition was reduced while the population of the $S_1 \rightarrow S_0$ (g2) transition increased. This could mean that internal conversion from the S_1 state of the g2 conformer to the g1 conformer was inhibited to some extent. It was also thought that the observed band changes could have been due to acid hydrolysis since the hydrolysed triazine (λ_{em} 480 nm) was blue-shifted relative to 5MPFH-TDT [78]. This would mean that the fluorescence emission was a combination of the hydrolysed and non-hydrolysed triazine fluorophores. The introduction of the hydrolysed triazine would produce an increase in the population of the shorter wavelength bands i.e. Bands 2 and 3. While the population of Band 2 (λ_{em} 520 nm) increased, the population of Band 3 (λ_{em} 480 nm) was unchanged, suggesting that the

band variations were due to environmental variations of 5MPFH-TDT rather than acid hydrolysis.

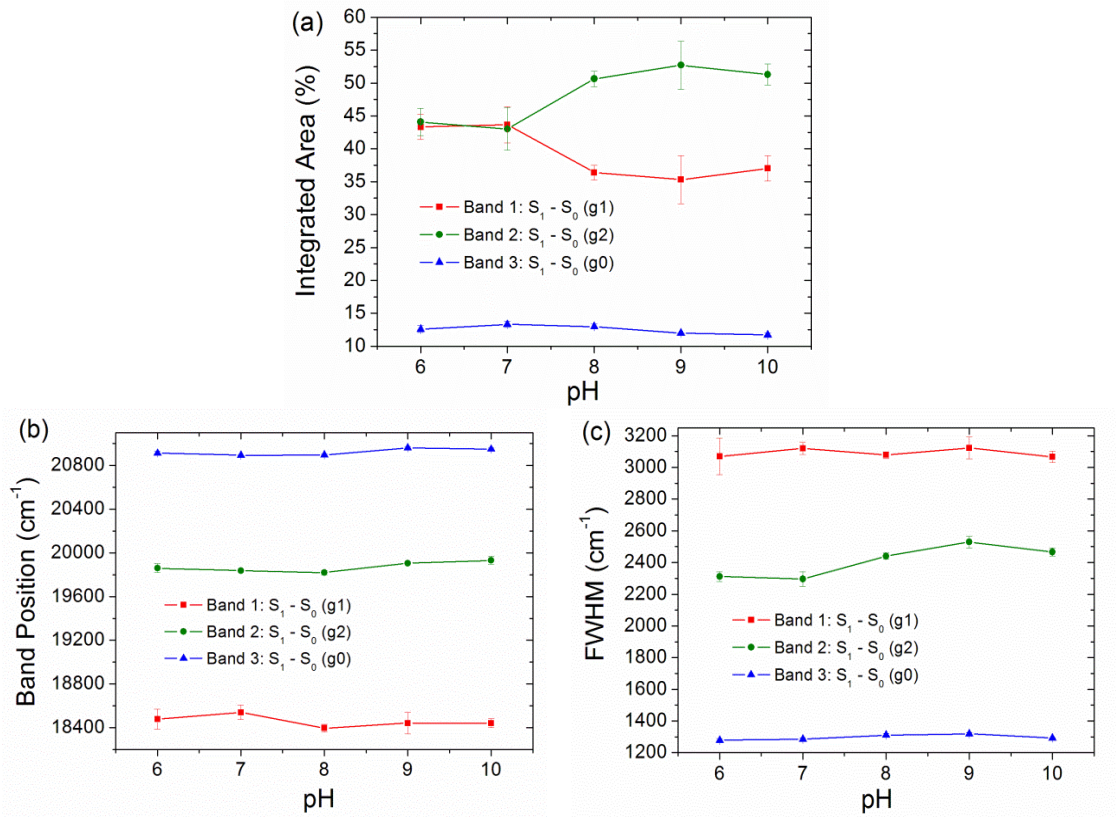

Figure 69: (a) Integrated area, (b) % integrated area, (c) band position, and (d) FWHM of the three fluorescence emission bands of BSA/5MPFH-TDT solutions in phosphate buffer of variable pH. [BSA] = 3×10^{-5} M and [5MPFH-TDT] = 7.5×10^{-6} M.

The anisotropy data of 5MPFH-TDT in BSA solutions of varying pH illustrates the variability of the triazine's mobility with the conformation of BSA. The pH appears to affect the degree to which the triazine is held in place by the protein molecule. The anisotropy reaches a maximum of 0.114 at pH 9 (λ_{em} 480 nm). This could mean that binding of the triazine to BSA is most efficient at this hydrogen ion concentration or that the conformation of BSA at this pH tumbles more slowly in solution.

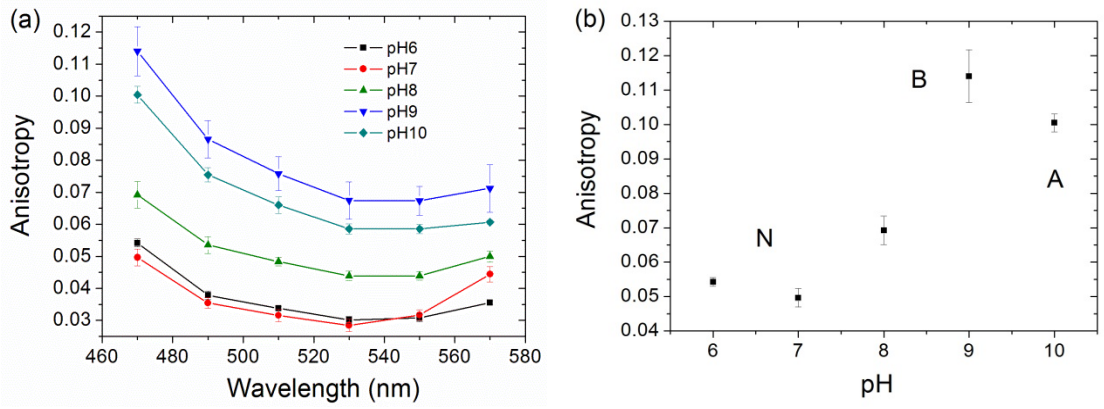

Figure 70: Steady-state fluorescence anisotropy of 4:1 BSA−5MPFH-TDT solutions in phosphate buffer of variable pH versus (a) emission wavelength and (b) pH. [BSA] = 3 × 10^{-5} M and [5MPFH-TDT] = 7.5 × 10^{-6} M.

Four conformational isomers of the normal form (N) of BSA have been identified: the fast (F) form occurs at pH 4; the extended (E) form exists at pH values below 3; the basic (B) form occurs near pH 8; and the aged (A) form is present at pH values near 10. These conformational isomers must be considered when carrying out *in-vitro* solution studies on BSA in which the pH is adjusted, particularly when measuring a parameter that is influenced by the rate of rotational diffusion. However, for the purposes of this study it is only necessary to consider the N, B, and A forms of BSA.

Figure 71: The pH of the buffer used to make up a solution of BSA has a direct influence on its conformation, which is described as its normal (N) form at physiological pH. When the pH is increased its basic (B) form is present and over time its aged (A) form occurs. When the pH drops to slightly acidic and very acidic conditions its fast (F) and extended (E) forms appear, respectively. Image reproduced from reference [140].

Leonard *et al.* detected a drop in the specific rotation, α_{313}, of BSA between pH 8 and 9. This was put down to a conformational change of the BSA molecule [161]. Aoki and Sogami describe this conformational change as a loosening of the molecule, most notably at the N-terminus. Ligand binding studies have found that structural changes

occurring in serum albumin due to a basic transition are concentrated around domain 2, with a contribution from domain 1, while domain 3 remains largely unchanged [140]. The aged form occurs as a consequence of a sulfhydryl-catalysed disulphide interchange reaction. The reaction does not occur if the thiol is blocked unless low molecular weight thiol groups are added in catalytic amounts [162].

A.6 Fluorescence emission properties of 5MPFH TDT in BSA at varying molar ratios

Mixtures of 5MPFH-TDT and BSA with different molar ratios were prepared in phosphate buffer of pH 9 and allowed to interact overnight at a temperature of 2–8 °C. All samples were made up using a 100 mM phosphate buffer of pH 9 while the ionic strength was kept constant at 303 mM using NaCl as the background electrolyte. The concentration of BSA was kept constant at 3×10^{-5} M while the concentration of 5MPFH-TDT was varied. BSA was present in excess in all cases to ensure that any alterations to the fluorescence emission of the fluorophore would not be obscured by the presence of free triazine. When the fluorescence emission spectra were normalised (Figure 72b) and analysed it was clear that there were no significant changes to the emission of 5MPFH-TDT. The lack of any band shifts (Figure 72d) indicates that 5MPFH-TDT is located in a very different environment compared to the micelles, where hypsochromic shifts were observed. Similarly, the band areas (Figure 72c) and FWHMs (Figure 72e) of the triazine's emission bands do not exhibit any significant changes like those observed in the 5MPFH-TDT–micelle studies. This implies that the triazine is not located in one of the hydrophobic binding sites of BSA, where water accessibility is restricted, but rather is located on the surface of the protein or in solution.

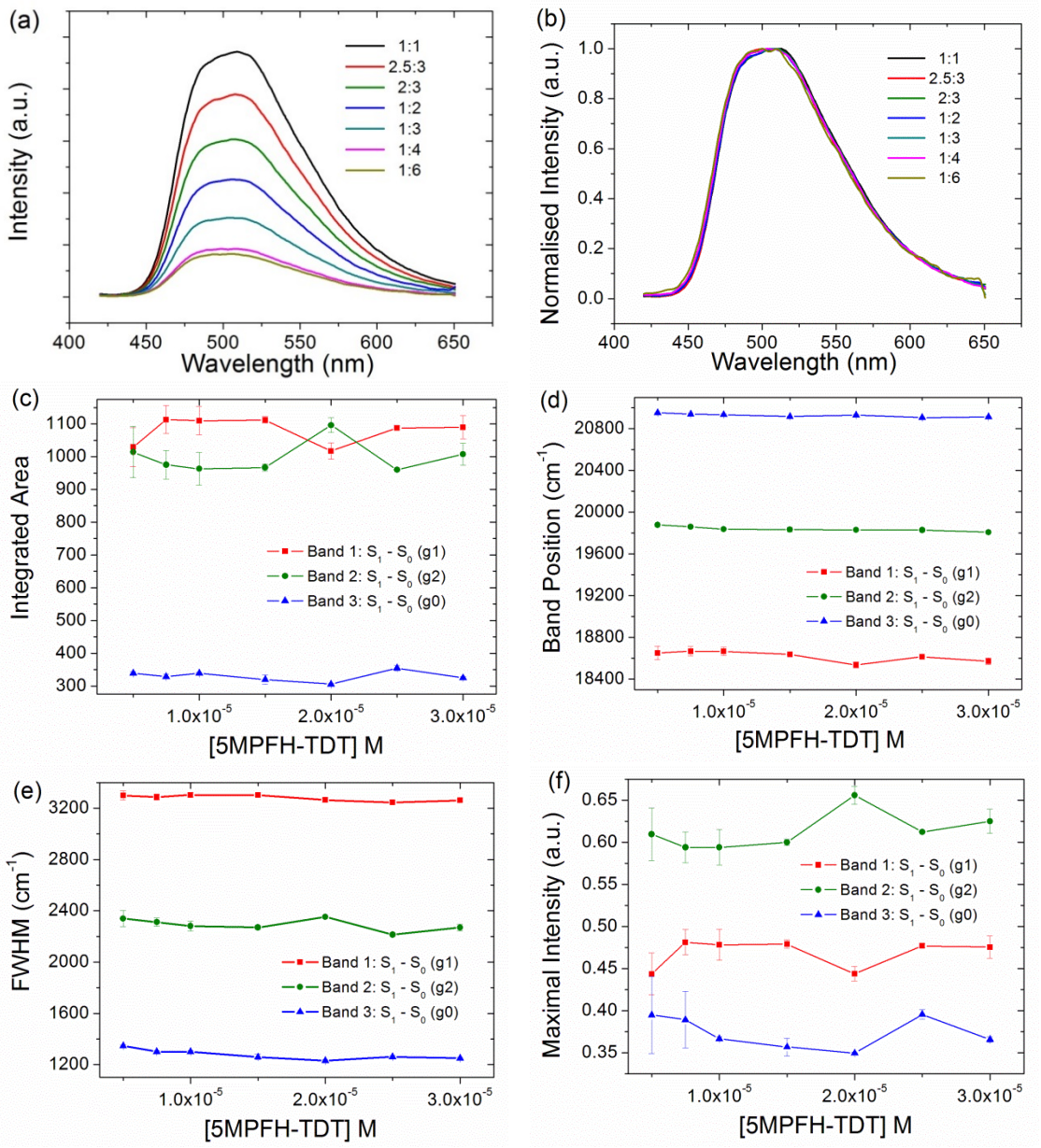

Figure 72: (a) Raw and (b) normalised fluorescence emission spectra (λ_{ex} 400 nm) and (c) integrated area, (d) band position, (e) FWHM, (f) maximum intensity of the normalised fluorescence emission bands of 5MPFH-TDT in BSA solutions of pH 9 versus 5MPFH-TDT concentration. [BSA] = 3 × 10^{-5} M.

As demonstrated by the Job plot analysis in Section 6.2, the fluorescence anisotropy of 5MPFH-TDT can be used to monitor binding in the case of this fluorophore–protein pair. It is evident from Figure 73 that the fluorescence anisotropy of 5MPFH-TDT increases as the relative concentration of BSA to triazine increases. This indicates that some of the triazine is in a less restrictive environment at low

BSA−5MPFH-TDT ratios and contributes to a loss in the overall polarisation of the fluorescence emission.

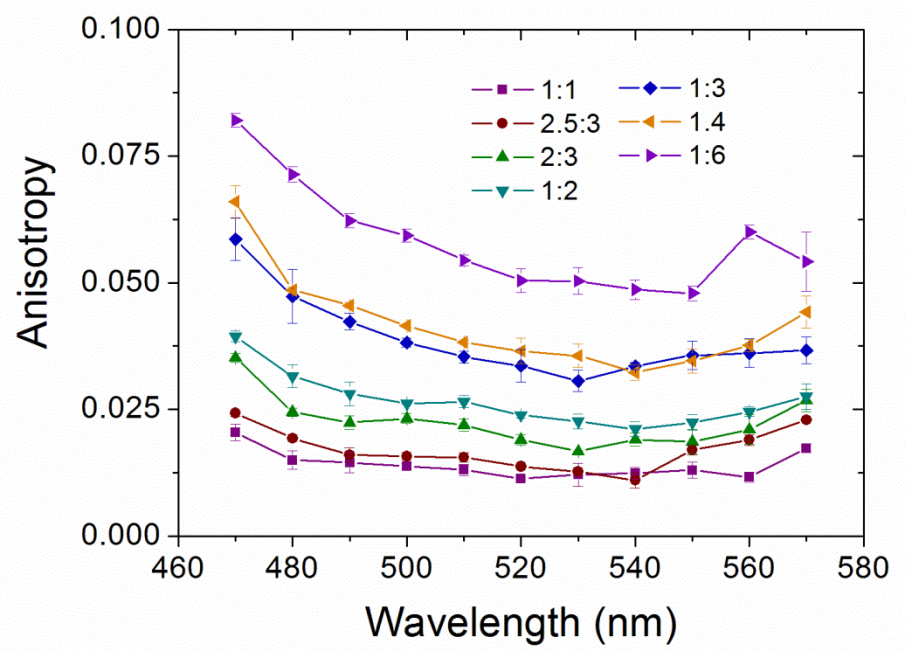

Figure 73: Steady-state fluorescence anisotropy of BSA−5MPFH-TDT mixtures of varying ratios at pH 9. The concentration of BSA was kept constant at 3×10^{-5} M.

A.7 Time course study of the interaction of 5MPFH-TDT with BSA

The fluorescence anisotropy increases to a maximum after a period of approximately 30 minutes. Some variation for the anisotropy values was observed across a triplicate data set. Preparation of the BSA solution was investigated to account for this variation. The force used for mixing the solutions was controlled but the anisotropy proved to be somewhat variable regardless of the technique employed. This variability was probably due to the formation of triazine aggregates before the interaction of the triazine and BSA could take place.

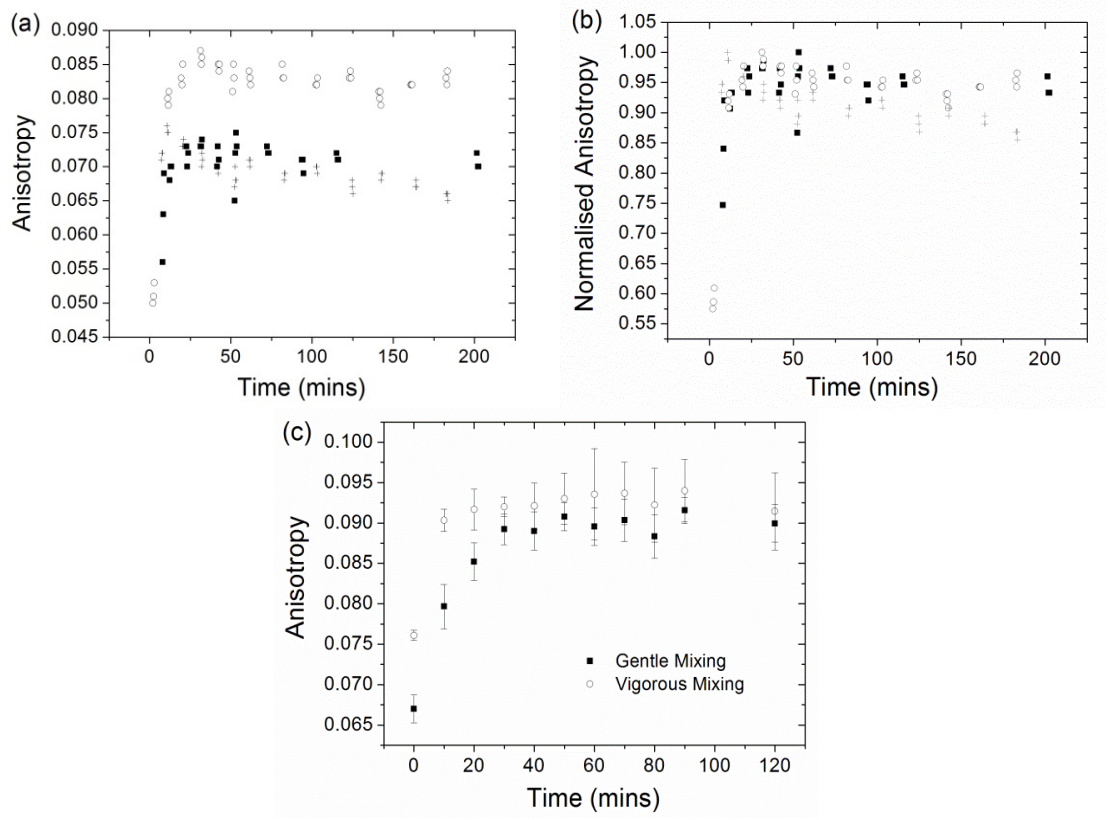

Figure 74: (a) Raw and (b) normalised steady-state fluorescence anisotropy (λ_{ex} 405, λ_{em} 500 nm) of a BSA−5MPFH-TDT complex (4:1) versus time (pH 9, ionic strength 300 mM). Symbols represent triplicate data points. (c) Effect of varying mixing conditions on the fluorescence anisotropy (λ_{ex} 405, λ_{em} 480 nm) of a BSA−5MPFH-TDT complex (4:1) versus time. [BSA] = 3 × 10^{-5} M.

In order to determine if there were any changes to either the triazine or the intrinsic fluorescence of BSA during the early stages of incubation the entire fluorescence emission range was measured at intervals over 3 hours (Figure 75). Spectra were collected for excitation wavelengths of 290 and 400 nm. The steady-state emission data for λ_{ex} 290 nm and λ_{ex} 400 nm provides no proof that the triazine has been incorporated into BSA.

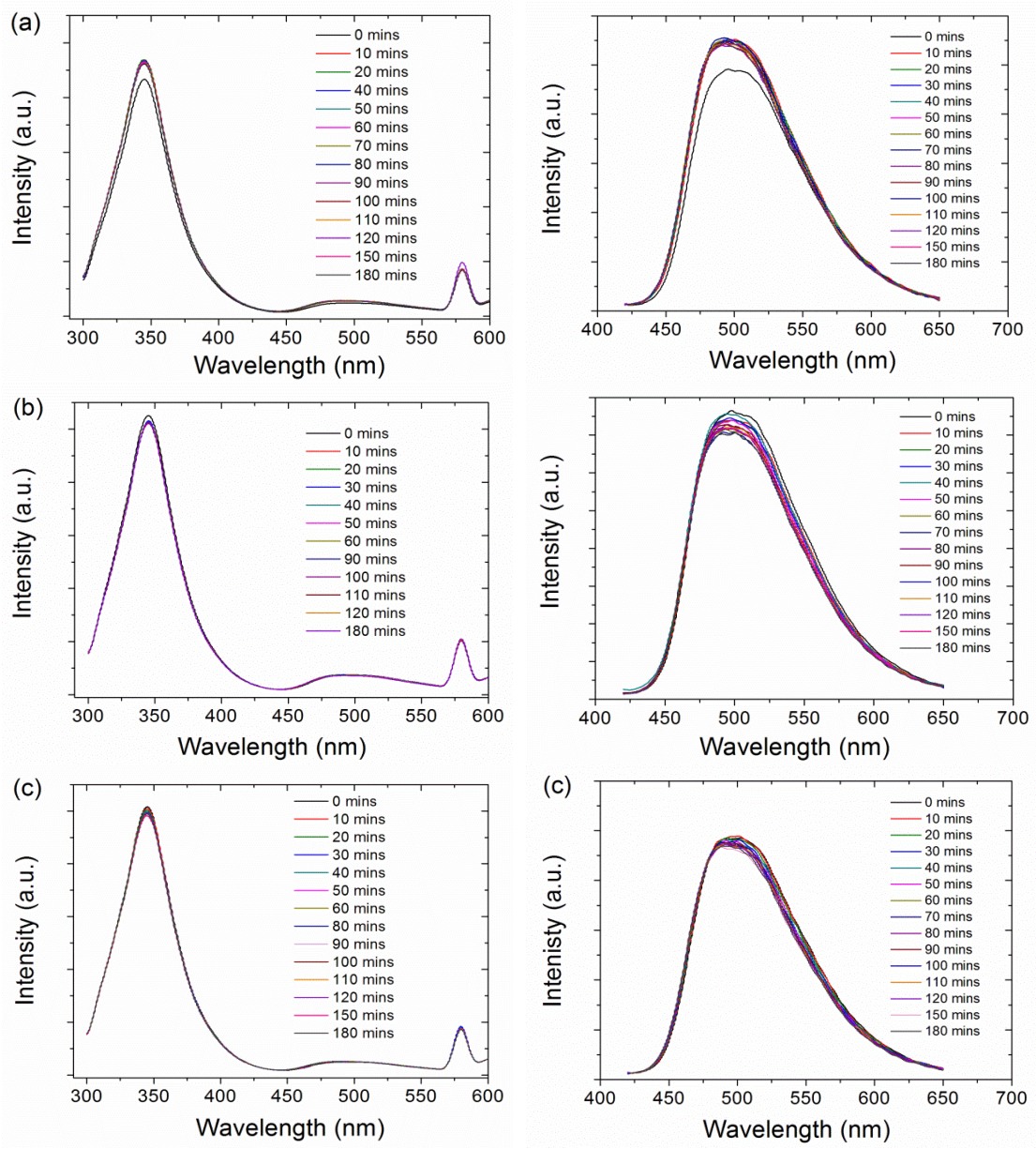

Figure 75: Raw fluorescence emission spectra (λ_{ex} 290 nm and 400 nm) of a BSA−5MPFH-TDT complex (4:1/pH 9) over a time period of 180 minutes. Test performed in triplicate. [BSA] = 3×10^{-5} M.

Fluorescence lifetime emission spectra were recorded over a period of three hours for samples made up using phosphate buffer of pH 9. The intrinsic fluorescence lifetime of BSA was monitored at 350 nm using a 295 nm LED, while a 405 nm laser was used to excite the triazine and the fluorescence lifetime was monitored at 480 nm. The average fluorescence lifetime of the triazine and the intrinsic fluorescence lifetime of BSA did not change over the three hour period. This indicated that the triazine was not in close enough proximity to Trp–134 or Trp–213 for FRET to occur.

Table 30: Decay parameters of a 4:1 BSA−5MPFH-TDT mixture at the beginning and end of complexation. A triple exponential fit was performed for intrinsic BSA fluorescence ($295_{ex}/350_{em}$) and 5MPFH-TDT fluorescence emission ($405_{ex}/480_{em}$). Phosphate buffer of pH 9 was used for dissolution of the protein. [BSA] $= 3 \times 10^{-5}$ M. Standard error is indicated.

Time (hrs)	τ1 (ns)	τ2 (ns)	τ3 (ns)	a1	a2	a3	τ_{av} (Int)(ns)	χ^2
				$295_{ex}/350_{em}$				
0	7.38 ± 0.10	3.82 ± 0.09	0.87 ± 0.09	778.5 ± 37.0	966.5 ± 33.1	314.5 ± 15.7	5.84 ± 0.02	1.123
3	7.62 ± 0.19	4.00 ± 0.13	1.01 ± 0.11	695.1 ± 70.8	1031.6 ± 50.9	318.2 ± 16.6	5.86 ± 0.02	1.079
				$405_{ex}/480_{em}$				
0	8.18 ± 0.37	2.79 ± 0.11	0.53 ± 0.03	899.2 ± 9.6	1932.8 ± 65.2	1899.2 ± 38.9	5.52 ± 0.30	1.260
3	7.73 ± 0.22	2.64 ± 0.04	0.48 ± 0.02	950.3 ± 22.5	1936.7 ± 23.0	1883.6 ± 46.1	5.29 ± 0.20	1.247

9 References

1. Butler, R.N., et al., *New reactive fluorophores in the 1,2,3-triazine series.* Tetrahedron Letters, 2006. **47**(11): p. 1721-1724.

2. St. Mart, D., *Design, synthesis and fluorescent characterisation of 2,5-dihydro-1,2,3-triazines*, in *Chemistry*. 2013, National University of Ireland Maynooth: Maynooth, Co. Kildare, Ireland.

3. Yguerabide, J., Epstein, H.F., and Stryer, L., *Segmental flexibility in an antibody molecule.* Journal of molecular biology, 1970. **51**(3): p. 573-590.

4. Jones, L., Hoeger, C., Atkins, P.W., and Schoenfield-Tacher, R., *Chemistry: Molecules, Matter, and Change Media Activities Book: Integrating Media in Learning*. Vol. 2. 2000: Macmillan.

5. Valeur, B., *Molecular Fluorescence: Principles and Applications*. WCH, Weinheim, Germany. 2001. p. 20-33.

6. McNaught, A.D. and Wilkinson, A. *IUPAC. Compendium of Chemical Terminology*. 1997; 2nd ed. :[Available from: http://goldbook.iupac.org

7. Lakowicz, J.R., *Principles of Fluorescence Spectroscopy*. 3rd ed. 2006: Springer. p. 1-26.

8. Valeur, B., *Molecular Fluorescence: Principles and Applications*. WCH, Weinheim, Germany. 2001. p. 34-70.

9. Turro, N.J., *Modern Molecular Photochemistry*. 1991: University Science Books. p. 65.

10. Atkins, P. and Friedman, R., *Molecular quantum mechanics*. 1997: Oxford : Oxford University Press p. 545.

11. Klán, P. and Wirz, J., *Photochemistry of organic compounds: From concepts to practice*. 2009: John Wiley & Sons. p. 40.

12. Strickler, S.J. and Berg, R.A., *Relationship between Absorption Intensity and Fluorescence Lifetime of Molecules.* The Journal of Chemical Physics, 1962. **37**(4): p. 814-822.

13. Lakowicz, J.R., *Principles of Fluorescence Spectroscopy*. 3rd ed. 2006: Springer. p. 353-382.

14. Lakowicz, J.R., *Principles of Fluorescence Spectroscopy*. 3rd ed. 2006: Springer. p. 353-381.

15. Valeur, B., *Molecular Fluorescence: Principles and Applications*. WCH, Weinheim, Germany. 2001. p. 125-154.

16. Rule, G.S. and Hitchens, T.K., *Fundamentals of protein NMR spectroscopy*. Vol. 5. 2006: Springer Science & Business Media.

17. Zhang, X., Jackson, J.K., and Burt, H.M., *Determination of surfactant critical micelle concentration by a novel fluorescence depolarization technique.* Journal of Biochemical and Biophysical Methods, 1996. **31**(3): p. 145-150.

18. Lakowicz, J.R., *Principles of Fluorescence Spectroscopy*. 3rd ed. 2006: Springer. p. 529-577.

19. Lakowicz, J.R., *Principles of Fluorescence Spectroscopy*. 3rd ed. 2006: Springer. p. 443-476.

20. Valeur, B., *Molecular Fluorescence: Principles and Applications*. WCH, Weinheim, Germany. 2001. p. 72-123.

21. Kosk-Kosicka, D., Bzdega, T., and Wawrzynow, A., *Fluorescence energy transfer studies of purified erythrocyte Ca2+-ATPase. Ca2+-regulated activation by oligomerization.* Journal of Biological Chemistry, 1989. **264**(33): p. 19495-19499.

22. Patterson, G.H., Piston, D.W., and Barisas, B.G., *Förster Distances between Green Fluorescent Protein Pairs.* Analytical biochemistry, 2000. **284**(2): p. 438-440.

23. Selvin, P.R. and Hearst, J.E., *Luminescence energy transfer using a terbium chelate: improvements on fluorescence energy transfer.* Proceedings of the National Academy of Sciences, 1994. **91**(21): p. 10024-10028.

24. Aydın, B.M., Acar, M., Arık, M., and Onganer, Y., *The fluorescence resonance energy transfer between dye compounds in micellar media.* Dyes and Pigments, 2009. **81**(2): p. 156-160.

25. Chatterjee, S., Nandi, S., and Bhattacharya, S.C., *Fluorescence resonance energy transfer from Fluorescein to Safranine T in solutions and in micellar medium.* Journal of Photochemistry and Photobiology A: Chemistry, 2005. **173**(2): p. 221-227.

26. Moyá, M.L., Rodríguez, A., del Mar Graciani, M., and Fernández, G., *Role of the solvophobic effect on micellization.* Journal of Colloid and Interface Science, 2007. **316**(2): p. 787-795.

27. Tummino, P.J. and Gafni, A., *Determination of the aggregation number of detergent micelles using steady-state fluorescence quenching.* Biophysical journal. **64**(5): p. 1580-1587.

28. Tummino, P.J. and Gafni, A., *Determination of the aggregation number of detergent micelles using steady-state fluorescence quenching.* Biophysical journal, 1993. **64**(5): p. 1580.

29. Sánchez, F.G. and Ruiz, C.C., *Intramicellar energy transfer in aqueous CTAB solutions.* Journal of Luminescence, 1996. **69**(4): p. 179-186.

30. Valeur, B., *Molecular Fluorescence: Principles and Applications*. WCH, Weinheim, Germany. 2001. p. 200-225.

31. Haidekker, M.A. and Theodorakis, E.A., *Environment-sensitive behavior of fluorescent molecular rotors.* Journal of biological engineering, 2010. **4**(1): p. 1.

32. Zhou, F., et al., *Molecular Rotors as Fluorescent Viscosity Sensors: Molecular Design, Polarity Sensitivity, Dipole Moments Changes, Screening Solvents, and Deactivation Channel of the Excited States.* European Journal of Organic Chemistry, 2011. **2011**(25): p. 4773-4787.

33. Lakowicz, J.R., *Principles of Fluorescence Spectroscopy*. 3rd ed. 2006: Springer. p. 205-236.

34. Brand, L., Seliskar, C.J., and Turner, D.C., *THE EFFECTS OF CHEMICAL ENVIRONMENT ON FLUORESCENCE PROBES**, in *Probes and Membrane Function*, B. Chance, C.-p. Lee, and J.K. Blasie, Editors. 1971, Academic Press. p. 17-31.

35. Hecht, E., *Optics, 4th.* International edition, Addison-Wesley, San Francisco, 2002: p. 467-473.

36. Dereniak, E.L. and Dereniak, T.D., *Geometrical and trigonometric optics*. 2008: Cambridge University Press.

37. David, R.L., *CRC Handbook of Chemistry and Physics, Internet Version 2005*. 2005, CRC Press, Boca Raton, FL.

38. Lakowicz, J.R., *Principles of Fluorescence Spectroscopy*. 3rd ed. 2006: Springer. p. 27-62.

39. Toptygin, D., *Effects of the Solvent Refractive Index and Its Dispersion on the Radiative Decay Rate and Extinction Coefficient of a Fluorescent Solute.* Journal of fluorescence, 2003. **13**(3): p. 201-219.

40. Kaufman, T.S. and Rúveda, E.A., *The Quest for Quinine: Those Who Won the Battles and Those Who Won the War.* Angewandte Chemie International Edition, 2005. **44**(6): p. 854-885.

41. Lavis, L.D. and Raines, R.T., *Bright Ideas for Chemical Biology.* ACS Chemical Biology, 2008. **3**(3): p. 142-155.

42. Herschel, J.F.W., *No. I. On a Case of Superficial Colour Presented by a Homogeneous Liquid Internally Colourless.* Philosophical Transactions of the Royal Society of London, 1845. **135**: p. 143-145.

43. Stokes, G.G., *On the Change of Refrangibility of Light.* Philosophical Transactions of the Royal Society of London, 1852. **142**: p. 463-562.

44. Boens, N., Leen, V., and Dehaen, W., *Fluorescent indicators based on BODIPY.* Chemical Society Reviews, 2012. **41**(3): p. 1130-1172.

45. Lakowicz, J.R., *Principles of Fluorescence Spectroscopy*. 3rd ed. 2006: Springer. p. 63-97.

46. Scott, T.G., Spencer, R.D., Leonard, N.J., and Weber, G., *Synthetic spectroscopic models related to coenzymes and base pairs. V. Emission properties of NADH. Studies of fluorescence lifetimes and quantum efficiencies of NADH, AcPyADH, [reduced acetylpyridineadenine dinucleotide] and simplified synthetic models.* Journal of the American Chemical Society, 1970. **92**(3): p. 687-695.

47. Honikel, K.O. and Madsen, N.B., *Comparison of the absorbance spectra and fluorescence behavior of phosphorylase b with that of model pyridoxal phosphate derivatives in various solvents.* Journal of Biological Chemistry, 1972. **247**(4): p. 1057-1064.

48. Teale, F.W. and Weber, G., *Ultraviolet fluorescence of the aromatic amino acids.* Biochemical Journal, 1957 **65**: p. 476-482.

49. Beechem, J.M. and Brand, L., *Time-Resolved Fluorescence of Proteins.* Annual Review of Biochemistry, 1985. **54**(1): p. 43-71.

50. Lakowicz, J.R., *Principles of Fluorescence Spectroscopy*. 3rd ed. 2006: Springer. p. 623-674.

51. Schäferling, M., *The Art of Fluorescence Imaging with Chemical Sensors.* Angewandte Chemie International Edition, 2012. **51**(15): p. 3532-3554.

52. Mahato, P., et al., *Ratiometric Detection of Cr3+ and Hg2+ by a Naphthalimide-Rhodamine Based Fluorescent Probe.* Inorganic Chemistry, 2012. **51**(3): p. 1769-1777.

53. Zhu, C., Zheng, H., Li, D., Li, S., and Xu, J., *Fluorescence quenching method for the determination of sodium dodecyl sulphate with near-infrared hydrophobic dye in the presence of Triton X-100.* Spectrochimica Acta Part A: Molecular and Biomolecular Spectroscopy, 2004. **60**(13): p. 3173-3179.

54. Lakowicz, J.R., Gryczynski, I., Gryczynski, Z., and Dattelbaum, J.D., *Anisotropy-Based Sensing with Reference Fluorophores.* Analytical biochemistry, 1999. **267**(2): p. 397-405.

55. Jablonski, A., *On the notion of emission anisotropy.* Bull. Acad. Pol. Sci, 1960. **8**: p. 259-264.

56. Ryder, A.G., Power, S., Glynn, T.J., and Morrison, J.J. *Time-domain measurement of fluorescence lifetime variation with pH*. in *BiOS 2001 The International Symposium on Biomedical Optics*. 2001. International Society for Optics and Photonics.

57. Baleizão, C., Nagl, S., Schäferling, M., Berberan-Santos, M.N., and Wolfbeis, O.S., *Dual Fluorescence Sensor for Trace Oxygen and Temperature with Unmatched Range and Sensitivity.* Analytical Chemistry, 2008. **80**(16): p. 6449-6457.

58. Kumar, R., et al., *1, 2, 3-Triazine Scaffold as a Potent Biologically Active Moiety: A Mini Review.* Mini reviews in medicinal chemistry, 2014. **14**(1): p. 72-83.

59. Fulscher, M.P., Andersson, K., and Roos, B.O., *Toward an accurate molecular orbital theory for excited states: The azabenzenes.* The Journal of Physical Chemistry, 1992. **96**(23): p. 9204-9212.

60. Mason, S.F., *245. The electronic spectra of N-heteroaromatic systems. Part I. The n[rightward arrow][small pi] transitions of monocyclic azines.* Journal of the Chemical Society (Resumed), 1959(0): p. 1240-1246.

61. MacColl, A., *137. The light absorption and resonance energies of some heterocyclic molecules.* Journal of the Chemical Society (Resumed), 1946: p. 670-672.

62. Qi, X., et al., *New BODIPY–triazine based tripod fluorescent systems.* Tetrahedron Letters, 2008. **49**(2): p. 261-264.

63. Stueber, G.J., et al., *Ultraviolet Stabilizers of the 2-(2'-Hydroxyphenyl)-1,3,5-triazine Class: Structural and Spectroscopic Characterization.* The Journal of Physical Chemistry, 1995. **99**(25): p. 10097-10109.

64. Elbe, F., et al., *Photochemical and Photophysical Deactivation of 2,4,6-Triaryl-1,3,5-triazines.* The Journal of Physical Chemistry A, 2000. **104**(35): p. 8296-8306.

65. Fink, R., et al., *Synthesis and Application of Dimeric 1,3,5-Triazine Ethers as Hole-Blocking Materials in Electroluminescent Devices.* Chemistry of Materials, 1998. **10**(11): p. 3620-3625.

66. Keck, J., Stüber, G.J., and Kramer, H.E.A., *Deactivation processes of 2-hydroxyphenyl-1,3,5-triazines — polymeric and monomeric UV absorbers of the benzotriazole and triazine class.* Die Angewandte Makromolekulare Chemie, 1997. **252**(1): p. 119-138.

67. Kim, J.Y.H., et al., *Combinatorial Solid-Phase Synthesis of 4,6-Diaryl and 4-Aryl, 6-Alkyl-1,3,5-triazines and Their Application to Efficient Biofuel Production.* ACS Combinatorial Science, 2012. **14**(7): p. 395-398.

68. Jung, D.-W., et al., *A Triazine Compound S06 Inhibits Proinvasive Crosstalk between Carcinoma Cells and Stromal Fibroblasts via Binding to Heat Shock Protein 90.* Chemistry & Biology, 2011. **18**(12): p. 1581-1590.

69. Jung, D.-W., Ha, H.-H., Zheng, X., Chang, Y.-T., and Williams, D.R., *Novel use of fluorescent glucose analogues to identify a new class of triazine-based insulin mimetics possessing useful secondary effects.* Molecular BioSystems, 2011. **7**(2): p. 346-358.

70. Shaykhalishahi, H., Yazdanparast, R., Ha, H.-H., and Chang, Y.-T., *Inhibition of H2O2-induced neuroblastoma cell cytotoxicity by a triazine derivative, AA3E2.* European Journal of Pharmacology, 2009. **622**(1–3): p. 1-6.

71. Zhou, C., et al., *Synthesis and biological evaluation of novel 1,3,5-triazine derivatives as antimicrobial agents.* Bioorganic & Medicinal Chemistry Letters, 2008. **18**(4): p. 1308-1311.

72. Li, N.-K., et al., *Triazine-based tyrosinase inhibitors identified by chemical genetic screening.* Pigment Cell Research, 2005. **18**(6): p. 447-453.

73. Sun, Y.-F., Huang, W., Lu, C.-G., and Cui, Y.-P., *The synthesis, two-photon absorption and blue upconversion fluorescence of novel, nitrogen-containing heterocyclic chromophores.* Dyes and Pigments, 2009. **81**(1): p. 10-17.

74. Neunhoeffer, H. and Wiley, P.F., *The Chemistry of Heterocyclic Compounds, Chemistry of 1 2 3-Triazines and 1 2 4-Triazines, Tetrazines, and Pentazin*. Vol. 33. 2009: Wiley-Interscience.

75. Ohsawa, A., Arai, H., Ohnishi, H., and Igeta, H., *1,2,3-Triazine.* Journal of the Chemical Society, Chemical Communications, 1981(22): p. 1174-1174.

76. Henriksen, L. and Autrup, H., *Chemistry of 1,1-dithiolates. 2. Thieno-1,2,3-triazines by diazotization of 3-aminothiophene-2- and -4-carboxamide.* ACTA CHEMICA SCANDINAVICA, 1972. **26**(8): p. 3342-3346.

77. Zhu, L., Becker, H.-C., Henriksen, L., and Kilså, K., *A class of fluorescent heterocyclic dyes revisited: Photophysics, structure, and solvent effects.* Spectrochimica Acta Part A: Molecular and Biomolecular Spectroscopy, 2009. **73**(4): p. 757-763.

78. St. Mart, D., *Design, synthesis and fluorescent characterisation of 2,5-dihydro-1,2,3-triazines*, in *Chemistry*. 2013, National University of Ireland Maynooth: Maynooth, Co. Kildare, Ireland.

79. St. Mart, D., Togashi, D.M., Stephens, J., Burke, L.A., and Ryder, A.G., *An interesting class of fluorophores: the 2,5-Dihydro-1,2,3-Triazine.* In preparation.

80. St. Mart, D., *Design, synthesis and fluorescent characterisation of 2,5-dihydro-1,2,3-triazines*, in *Chemistry*. 2013, National University of Ireland Maynooth: Maynooth, Co. Kildare, Ireland.

81. Fendler, J.H., *Atomic and molecular clusters in membrane mimetic chemistry.* Chemical Reviews, 1987. **87**(5): p. 877-899.

82. Sulthana, S.B., Rao, P.V.C., Bhat, S.G.T., and Rakshit, A.K., *Interfacial and Thermodynamic Properties of SDBS−C12E10 Mixed Micelles in Aqueous Media: Effect of Additives.* The Journal of Physical Chemistry B, 1998. **102**(48): p. 9653-9660.

83. Alawi, S.M. and Akhter, M.S., *Effect of N,N-dimethyl acetamide on the critical micelle concentration of aqueous solutions of sodium surfactants.* Journal of Molecular Liquids, 2011. **160**(2): p. 63-66.

84. Fayed, T.A., *Probing of micellar and biological systems using 2-(p-dimethylaminostyryl)benzoxazole: An intramolecular charge transfer fluorescent probe.* Colloids and Surfaces A: Physicochemical and Engineering Aspects, 2004. **236**(1–3): p. 171-177.

85. Dhar, S., et al., *Physicochemical characterization of reverse micelles of Triton X using 1-anthracene sulphonate as fluorescent probe: A spectroscopic study.* Colloids and Surfaces A: Physicochemical and Engineering Aspects, 2009. **349**(1–3): p. 117-124.

86. Clint, J.H., *Surfactant aggregation*. 2012: Springer Science & Business Media.

87. Reichardt, C. and Welton, T., *Solvents and solvent effects in organic chemistry*. 2011: John Wiley & Sons.

88. Mallick, A., Purkayastha, P., and Chattopadhyay, N., *Photoprocesses of excited molecules in confined liquid environments: An overview.* Journal of Photochemistry and Photobiology C: Photochemistry Reviews, 2007. **8**(3): p. 109-127.

89. Mallick, A., Haldar, B., Maiti, S., and Chattopadhyay, N., *Constrained photophysics of 3-acetyl-4-oxo-6,7-dihydro-12H indolo-[2,3-a] quinolizine in micellar*

environments: a spectrofluorometric study. Journal of Colloid and Interface Science, 2004. **278**(1): p. 215-223.

90. Fayed, T.A., El-morsi, M.A., and El-Nahass, M.N., *Fluorescence Characteristics and Inclusion of ICT Fluorescent Probe in Organized Assemblies.* Journal of fluorescence, 2012. **22**(4): p. 1101-1111.

91. Panda, D., Khatua, S., and Datta, A., *Enhanced Fluorescence of Epicocconone in Surfactant Assemblies as a Consequence of Depth-Dependent Microviscosity.* The Journal of Physical Chemistry B, 2007. **111**(7): p. 1648-1656.

92. Zana, R., *Microviscosity of Aqueous Surfactant Micelles: Effect of Various Parameters.* The Journal of Physical Chemistry B, 1999. **103**(43): p. 9117-9125.

93. Sekhon, B., *Gemini (dimeric) surfactants.* Resonance, 2004. **9**(3): p. 42-49.

94. Almgren, M., Grieser, F., and Thomas, J.K., *Dynamic and static aspects of solubilization of neutral arenes in ionic micellar solutions.* Journal of the American Chemical Society, 1979. **101**(2): p. 279-291.

95. Dobson, C.M., *Protein folding and misfolding.* Nature, 2003. **426**(6968): p. 884-890.

96. Dobson, C.M. *Protein folding and its links with human disease*. in *Biochemical Society Symposia*. 2001. London; Portland on behalf of The Biochemical Society; 1999.

97. Brody, L.C. and Leja, D. *Talking Glossary of Genetic Terms*. [cited 2016 13th of July]; Available from: https://www.genome.gov/glossary/resources/protein.pdf.

98. Branden, C. and Tooze, J., *Introduction to protein structure*. Vol. 2. 1991: Garland New York.

99. Perutz, M. *Structure of hemoglobin*. in *Brookhaven Symp Biol*. 1960.

100. Kendrew, J.C., *Architecture of a protein molecule.* Nature, 1958. **182**: p. 764-767.

101. Michalet, X., Weiss, S., and Jäger, M., *Single-Molecule Fluorescence Studies of Protein Folding and Conformational Dynamics.* Chemical reviews, 2006. **106**(5): p. 1785-1813.

102. Keinan, E. and Schechter, I., *Chemistry for the 21st Century*. 2008: John Wiley & Sons.

103. Saxena, A.M., Krishnamoorthy, G., Udgaonkar, J.B., and Periasamy, N., *Identification of intermediate species in protein-folding by quantitative analysis of amplitudes in time-domain fluorescence spectroscopy.* Journal of Chemical Sciences, 2007. **119**(2): p. 61-69.

104. Lindhoud, S., Westphal, A.H., Visser, A.J.W.G., Borst, J.W., and van Mierlo, C.P.M., *Fluorescence of Alexa Fluor Dye Tracks Protein Folding.* PloS one, 2012. **7**(10): p. 1-8.

105. Gilad, H., *Single-molecule fluorescence spectroscopy of biomolecular folding.* Journal of Physics: Condensed Matter, 2003. **15**(32): p. R1291.

106. Wu, P.G. and Brand, L., *Resonance Energy Transfer: Methods and Applications.* Analytical biochemistry, 1994. **218**(1): p. 1-13.

107. Butler, R.N., et al., *One-Pot Synthesis of Fluorescent 2,5-Dihydro-1,2,3-triazine Derivatives from a Cascade Rearrangement Sequence in the Reactions of 1,2,3-Triazolium-1-aminide 1,3-Dipoles with Propiolate Esters.* The Journal of Organic Chemistry, 2006. **71**(15): p. 5679-5687.

108. Lakowicz, J.R., *Principles of Fluorescence Spectroscopy*. 3rd ed. 2006: Springer. p. 797-840.

109. Alarfaj, N.A. and El-Tohamy, M.F., *Applications of micelle enhancement in luminescence-based analysis.* Luminescence, 2015. **30**(1): p. 3-11.

110. Aliabadi, H.M., Mahmud, A., Sharifabadi, A.D., and Lavasanifar, A., *Micelles of methoxy poly(ethylene oxide)-b-poly(ε-caprolactone) as vehicles for the solubilization and controlled delivery of cyclosporine A.* Journal of Controlled Release, 2005. **104**(2): p. 301-311.

111. Weiszhár, Z., et al., *Complement activation by polyethoxylated pharmaceutical surfactants: Cremophor-EL, Tween-80 and Tween-20.* European Journal of Pharmaceutical Sciences, 2012. **45**(4): p. 492-498.

112. Paradies, H.H., *Shape and size of a nonionic surfactant micelle. Triton X-100 in aqueous solution.* The Journal of Physical Chemistry, 1980. **84**(6): p. 599-607.

113. Bystrzejewski, M., et al., *Dispersion and diameter separation of multi-wall carbon nanotubes in aqueous solutions.* Journal of Colloid and Interface Science, 2010. **345**(2): p. 138-142.

114. Palazzesi, F., Calvaresi, M., and Zerbetto, F., *A molecular dynamics investigation of structure and dynamics of SDS and SDBS micelles.* Soft Matter, 2011. **7**(19): p. 9148-9156.

115. Sarkar, R., Shaw, A.K., Ghosh, M., and Pal, S.K., *Ultrafast photoinduced deligation and ligation dynamics: DCM in micelle and micelle-enzyme complex.* Journal of Photochemistry and Photobiology B: Biology, 2006. **83**(3): p. 213-222.

116. Rurack, K. and Spieles, M., *Fluorescence Quantum Yields of a Series of Red and Near-Infrared Dyes Emitting at 600−1000 nm.* Analytical Chemistry, 2011. **83**(4): p. 1232-1242.

117. Bhattacharya, P., Sahoo, D., and Chakravorti, S., *Photophysical properties of 4,4-diaminodiphenyl sulfone in micelles and the role of BF-anion on micellar aggregation.* Journal of Photochemistry and Photobiology A: Chemistry, 2012. **250**(0): p. 25-32.

118. Samanta, A., Paul, B., and Guchhait, N., *Modulation of Intramolecular Charge Transfer Emission Inside Micelles: A Fluorescence Probe for Studying Microenvironment of Micellar Assemblies.* Journal of fluorescence, 2012. **22**(1): p. 289-301.

119. Shizuka, H., Nakamura, M., and Morita, T., *Anion-Induced Fluorescence Quenching of Aromatic-Molecules.* Journal of Physical Chemistry, 1980. **84**(9): p. 989-994.

120. Lakowicz, J.R., *Principles of Fluorescence Spectroscopy*. 3rd ed. 2006: Springer. p. 331-352.

121. Lakowicz, J.R., *Principles of Fluorescence Spectroscopy*. 3rd ed. 2006: Springer. p. 278-330.

122. Denkova, P.S., Van Lokeren, L., and Willem, R., *Mixed Micelles of Triton X-100, Sodium Dodecyl Dioxyethylene Sulfate, and Synperonic L61 Investigated by NOESY and Diffusion Ordered NMR Spectroscopy.* The Journal of Physical Chemistry B, 2009. **113**(19): p. 6703-6709.

123. Robson, R.J. and Dennis, E.A., *The size, shape, and hydration of nonionic surfactant micelles. Triton X-100.* The Journal of Physical Chemistry, 1977. **81**(11): p. 1075-1078.

124. Piñeiro, L., Novo, M., and Al-Soufi, W., *Fluorescence emission of pyrene in surfactant solutions.* Advances in Colloid and Interface Science, 2015. **215**: p. 1-12.

125. Biaselle, C.J. and Millar, D.B., *Studies on triton X-100 detergent micelles.* Biophysical chemistry, 1975. **3**(4): p. 355-361.

126. Roy, S., Mohanty, A., and Dey, J., *Microviscosity of bilayer membranes of some N-acylamino acid surfactants determined by fluorescence probe method.* Chemical Physics Letters, 2005. **414**(1–3): p. 23-27.

127. De Paula, R., da Hora Machado, A.E., and de Miranda, J.A., *3-Benzoxazol-2-yl-7-(N,N-diethylamino)-chromen-2-one as a fluorescence probe for the investigation of micellar microenvironments.* Journal of Photochemistry and Photobiology A: Chemistry, 2004. **165**(1–3): p. 109-114.

128. Repáková, J., Čapková, P., Holopainen, J.M., and Vattulainen, I., *Distribution, Orientation, and Dynamics of DPH Probes in DPPC Bilayer.* The Journal of Physical Chemistry B, 2004. **108**(35): p. 13438-13448.

129. Claussen, J.C., et al., *Biophotonic logic devices based on quantum dots and temporally-staggered Forster energy transfer relays.* Nanoscale, 2013. **5**(24): p. 12156-12170.

130. Bhat, P.A., Chat, O.A., and Dar, A.A., *Exploiting Co-solubilization of Warfarin, Curcumin, and Rhodamine B for Modulation of Energy Transfer: A Micelle FRET On/Off Switch.* ChemPhysChem, 2016. **17**(15): p. 2360-2372.

131. Kang, J., et al., *Sulforhodamine 101 induces long-term potentiation of intrinsic excitability and synaptic efficacy in hippocampal CA1 pyramidal neurons.* Neuroscience, 2010. **169**(4): p. 1601-1609.

132. Ishizaka, S., Habuchi, S., Kim, H.-B., and Kitamura, N., *Excitation Energy Transfer from Sulforhodamine 101 to Acid Blue 1 at a Liquid/Liquid Interface: Experimental Approach To Estimate Interfacial Roughness.* Analytical Chemistry, 1999. **71**(16): p. 3382-3389.

133. Goding, J.W., *Monoclonal antibodies: principles and practice*. 1996: Academic Press. p. 352-399.

134. Garden, A.L., Scholz, K., Schwass, D.R., and Meledandri, C.J., *Optimized colloidal chemistry for micelle-templated synthesis and assembly of silver nanocomposite materials.* Colloids and Surfaces A: Physicochemical and Engineering Aspects, 2014. **441**: p. 367-377.

135. Berthod, A., Girard, I., and Gonnet, C., *Additive effects on surfactant adsorption and ionic solute retention in micellar liquid chromatography.* Analytical Chemistry, 1986. **58**(7): p. 1362-1367.

136. Roelants, E. and De Schryver, F., *Parameters affecting aqueous micelles of CTAC, TTAC, and DTAC probed by fluorescence quenching.* Langmuir, 1987. **3**(2): p. 209-214.

137. Sahoo, H., *Fluorescent Labeling Techniques in Biomolecules: A Flashback.* RSC Adv., 2012.

138. Patonay, G., Salon, J., Sowell, J., and Strekowski, L., *Noncovalent Labeling of Biomolecules with Red and Near- Infrared Dyes.* Molecules, 2004. **9**(3): p. 40.

139. Togashi, D.M. and Ryder, A.G., *A fluorescence analysis of ANS bound to bovine serum albumin: binding properties revisited by using energy transfer.* Journal of fluorescence, 2008. **18**(2): p. 519-526.

140. Peters Jr, T., *All about albumin: biochemistry, genetics, and medical applications*. 1995: Academic press. p. 54-62.

141. Togashi, D. and Ryder, A., *Time-Resolved Fluorescence Studies on Bovine Serum Albumin Denaturation Process.* Journal of fluorescence, 2006. **16**(2): p. 153-160.

142. Carter, D.C., Chang, B., Ho, J.X., Keeling, K., and Krishnasami, Z., *Preliminary crystallographic studies of four crystal forms of serum albumin.* European Journal of Biochemistry, 1994. **226**(3): p. 1049-1052.

143. Sohl, J.L. and Splittgerber, A.G., *The binding of Coomassie brilliant blue to Bovine Serum Albumin: A physical biochemistry experiment.* Journal of Chemical Education, 1991. **68**(3): p. 262.

144. Majorek, K.A., et al., *Structural and immunologic characterization of bovine, horse, and rabbit serum albumins.* Mol Immunol, 2012. **52**(3-4): p. 174-182.

145. Sekula, B., Zielinski, K., and Bujacz, A., *Crystallographic studies of the complexes of bovine and equine serum albumin with 3,5-diiodosalicylic acid.* International Journal of Biological Macromolecules, 2013. **60**: p. 316-324.

146. Bujacz, A., Zielinski, K., and Sekula, B., *Structural studies of bovine, equine, and leporine serum albumin complexes with naproxen.* Proteins: Structure, Function, and Bioinformatics, 2014. **82**(9): p. 2199-2208.

147. Hertzog, P.J., Shaw, A., Smith, J.R.L., and Garner, R.C., *Improved conditions for the production of monoclonal antibodies to carcinogen-modified DNA, for use in enzyme-linked immunosorbent assays (ELISA).* Journal of Immunological Methods, 1983. **62**(1): p. 49-58.

148. Brand, L. and Gohlke, J.R., *Fluorescence probes for structure.* Annual review of biochemistry, 1972. **41**(1): p. 843-868.

149. Edelman, G.M. and McClure, W.O., *Fluorescent probes and the conformation of proteins.* Accounts of Chemical Research, 1968. **1**(3): p. 65-70.

150. Quinn, M., et al., *How fluorescent labelling alters the solution behaviour of proteins.* Physical Chemistry Chemical Physics, 2015. **17**(46): p. 31177-31187.

151. Gajraj, A. and Ofoli, R.Y., *Effect of Extrinsic Fluorescent Labels on Diffusion and Adsorption Kinetics of Proteins at the Liquid−Liquid Interface.* Langmuir, 2000. **16**(21): p. 8085-8094.

152. Huang, C.Y., *Determination of binding stoichiometry by the continuous variation method: the Job plot.* Methods in enzymology, 1982. **87**: p. 509-525.

153. James, S. and McManus, J.J., *Thermal and Solution Stability of Lysozyme in the Presence of Sucrose, Glucose, and Trehalose.* The Journal of Physical Chemistry B, 2012. **116**(34): p. 10182-10188.

154. Shi, Q., Zhou, Y., and Sun, Y., *Influence of pH and Ionic Strength on the Steric Mass-Action Model Parameters around the Isoelectric Point of Protein.* Biotechnology Progress, 2005. **21**(2): p. 516-523.

155. David, R.L., *CRC Handbook of Chemistry and Physics, Internet Version 2005*. 2005, CRC Press, Boca Raton, FL.

156. Axelsson, I., *Characterization of proteins and other macromolecules by agarose gel chromatography.* Journal of Chromatography A, 1978. **152**(1): p. 21-32.

157. Ferguson, B.Q. and Yang, D.C.H., *Methionyl-tRNA synthetase induced 3'-terminal and delocalized conformational transition in tRNAfMet: steady-state fluorescence of tRNA with a single fluorophore.* Biochemistry, 1986. **25**(3): p. 529-539.

158. Shizuka, H., Nakamura, M., and Morita, T., *Anion-Induced Fluorescence Quenching of Aromatic-Molecules.* Journal of Physical Chemistry, 1980. **84**(9): p. 989-994.

159. Chang, K. and Forcé, R.K., *Time-Resolved Laser-Induced Fluorescence Study on Dyes Used in DNA Sequencing.* Applied Spectroscopy, 1993. **47**(1): p. 24-29.

160. Bhattacharya, M., Jain, N., Bhasne, K., Kumari, V., and Mukhopadhyay, S., *pH-induced Conformational Isomerization of Bovine Serum Albumin Studied by Extrinsic and Intrinsic Protein Fluorescence.* Journal of fluorescence, 2011. **21**(3): p. 1083-1090.

161. Leonard, W.J., Vijai, K.K., and Foster, J.F., *A structural transformation in bovine and human plasma albumins in alkaline solution as revealed by rotatory dispersion studies.* Journal of Biological Chemistry, 1963. **238**(6): p. 1984-1988.

162. Rosenoer, V.M., Oratz, M., and Rothschild, M.A., *Albumin: Structure, Function and Uses*. 2014: Elsevier Science. p. 78.